LIVING UNDER FAR-RED LIGHT :

Adaptation Of Photosynthetic Machinery Of *Stanieria cyanosphaera*, *Vitrella brassicaformis*, And *Euglena gracilis*.

Thesis Submitted By

TOM FELLER

In Fulfillment Of The Requirements For The Degree Of

Doctor In Science

UNIVERSITY OF LIEGE

FACULTY OF SCIENCE – LIFE SCIENCE DEPARTMENT

LABORATORY OF GENETICS AND PHYSIOLOGY OF MICROALGAE

THESIS SUPERVISOR: DR. PIERRE CARDOL

THESIS CO-SUPERVISOR : DR. EMMANUELLE JAVAUX

ACADEMIC YEAR: 2024 - 2025

LIÈGE université Sciences

belspo

Remerciement

Tout d'abord, je tiens à remercier Pierre, qui m'a donné l'opportunité de réaliser cette thèse, et qui m'a permis de voyager au Japon, dans les îles Canaries, en Italie et en France. Ces voyages, plus qu'instructifs, ont aussi été très amusants et enrichissants. Je garderai en mémoire ces nombreux souvenirs ; manger comme des ogres, refaire le monde autour d'une bière, visiter les temples japonais ; serpenter dans les étroites rues de Venise, siroter des spritz et déguster la meilleure glace du monde avec Edmée ; vivre la dolce vita au bord de la piscine avec Yannick lors du congrès à La Palma, visiter les plus grands télescopes, puis partir randonner dans les volcans avec Julie ; passer des journées sur la plage à Roscoff à chercher ces satanés vers, se balader sur la côte, se régaler de crustacés et de crêpes bretonnes à volonté… et j'en passe ! Tous ces moments ont embelli ma thèse et m'ont permis de garder la motivation jusqu'au bout.

Un énorme merci à tous les copains du labo pour cette ambiance plus qu'exceptionnelle ! Les nombreuses bières au soleil, au bord de l'eau, sur le toit, ou même juste à table quand le temps ne le permettait pas. On n'attendait évidemment pas les beaux jours pour prendre l'apéro ! Une ambiance inégalable, qui sera difficile à retrouver.

Edmée et Pablo, mes deux acolytes avec qui nous avons commencé cette thèse ensemble (et presque fini ensemble !). Évidemment, mes « collègues » plus que préférés : vous avez été très précieux à mes yeux, pour se confier, s'encourager, et surtout rigoler. Cette amitié tissée au fil de quatre années de presque colocation est magnifique, et j'espère qu'elle durera encore très longtemps.

Merci à mes parents, qui ont toujours été aux petits soins pour m'apporter tout ce dont j'avais besoin et beaucoup plus. Vous êtes parfaits.

Merci à Julie, qui m'a soutenu, surtout durant cette dernière année. Aussi aux petits soins, mais surtout là pour m'encourager, me consoler, et me motiver jusqu'au bout pour y arriver.

Robin, mon Bro, cette thèse est pour toi.

Abstract of the thesis

Photosynthesis is a fundamental biological process that converts light energy into chemical energy. Over billions of years, photosynthetic organisms have evolved diverse adaptations to optimize light capture and energy conversion, enabling their survival across a broad range of environmental conditions. Among these adaptations, the ability to utilize far-red light (FRL, 700–750 nm) has emerged as a critical strategy for photosynthetic organisms inhabiting shaded environments such as microbial mats, dense forests, and aquatic ecosystems. This thesis investigates the diversity, mechanisms, and evolutionary significance of FRL acclimation in eukaryotic microalgae and cyanobacteria, with implications for astrobiology and the potential for phototrophy under infrared-rich exoplanetary conditions.

As part of the interdisciplinary PORTAL project, this study explores the habitability of temperate rocky exoplanets orbiting very low-mass (VLM) stars, which primarily emit in the infrared spectrum. Since conventional oxygenic photosynthesis is adapted to visible light, understanding how certain organisms harvest long-wavelength photons is essential for assessing the feasibility of extraterrestrial photosynthetic life. To this end, this research examines the physiological, molecular, and genomic basis of FRL adaptation in diverse phototrophic taxa, focusing on newly identified eukaryotic microalgae exhibiting red-shifted chlorophyll absorption.

The first part of this thesis presents a large-scale screening of 120 microalgal strains across 14 phylogenetic lineages to assess their ability to acclimate to FRL. Spectroscopic analyses revealed that several species exhibited distinct absorption shifts in the 700–720 nm range under FRL conditions, suggesting the presence of modified pigment-protein complexes enabling long-wavelength light utilization. Notably, *Vitrella brassicaformis* has been identified as the first eukaryotic organism to constitutively absorb FRL, a trait previously observed only in cyanobacteria. Unlike the facultative adaptations of many phototrophs, *V. brassicaformis* appears to have developed a light-harvesting system intrinsically optimized for FRL utilization, suggesting a unique evolutionary specialization among eukaryotes. This discovery provides new insights into the diversity of FRL adaptation and opens avenues for understanding the evolutionary and ecological constraints associated with photon absorption in environments with limited visible light.

The second part of this work investigates the molecular and biochemical basis of FRL acclimation in *Stanieria cyanosphaera*, a cyanobacterium demonstrating complementary chromatic acclimation (CCA), low-light photoacclimation (LoLiP), and far-red light photoacclimation (FaRLiP) mechanisms. Genomic and transcriptomic analyses revealed the presence of canonical LoLiP and FaRLiP gene clusters, which orchestrate pigment biosynthesis, photosystem remodeling, and redox regulation under FRL conditions. Structural and spectroscopic characterization of its photosystems indicated a significant enhancement in antenna size and photosynthetic efficiency under FRL exposure.

Further investigations focused on *Euglena gracilis*, revealing the involvement of a unique light-harvesting complex (LHCE) in FRL absorption and state transition-like mechanisms. This pentameric LHCE is genetically regulated by the light environment, this regulation is dynamic and influence the state transition. These findings expand our understanding of the evolutionary pathways leading to specialized light-harvesting adaptations in eukaryotes.

Collectively, this research highlights the widespread occurrence of FRL adaptation across phototrophic lineages and sheds light on the underlying genetic, structural, and physiological mechanisms governing this process. The ability of eukaryotic microalgae and cyanobacteria to thrive under FRL conditions suggests that similar adaptations could enable photosynthetic life on exoplanets orbiting M-dwarf stars. By integrating astrophysical, microbiological, and ecological perspectives, this thesis contributes to the broader discourse on life's potential diversity beyond Earth and provides essential constraints for future biosignature detection efforts.

Résumé de la thèse

La photosynthèse est un processus biologique fondamental qui convertit l'énergie lumineuse en énergie chimique. Au fil de milliards d'années, les organismes photosynthétiques ont développé diverses adaptations optimisant la capture de la lumière et la conversion de l'énergie, leur permettant de survivre dans une large gamme de conditions environnementales. Parmi ces adaptations, la capacité à utiliser la lumière rouge lointaine (FRL, 700–750 nm) est apparue comme une stratégie essentielle pour les organismes vivant dans des environnements ombragés, tels que les tapis microbiens, les forêts denses et les écosystèmes aquatiques. Cette thèse explore la diversité, les mécanismes et la signification évolutive de l'acclimatation à la FRL chez les microalgues eucaryotes et les cyanobactéries, avec des implications pour l'astrobiologie et la possibilité d'une phototrophie sous des conditions exoplanétaires riches en infrarouge.

Dans le cadre du projet interdisciplinaire PORTAL, cette étude examine l'habitabilité des exoplanètes rocheuses tempérées en orbite autour d'étoiles de très faible masse, dont l'émission est principalement située dans le spectre infrarouge. Étant donné que la photosynthèse oxygénique conventionnelle est adaptée à la lumière visible, comprendre comment certains organismes exploitent les photons de grande longueur d'onde est essentiel pour évaluer la faisabilité d'une vie photosynthétique extraterrestre. À cette fin, cette recherche examine les bases physiologiques, moléculaires et génomiques de l'adaptation à la FRL chez divers taxons phototrophes, en mettant l'accent sur de nouvelles microalgues eucaryotes identifiées présentant une absorption de la chlorophylle décalée vers le rouge.

La première partie de cette thèse présente un criblage de 120 souches de microalgues appartenant à 14 lignées phylogénétiques afin d'évaluer leur capacité à s'acclimater à la FRL. Les analyses spectroscopiques ont révélé que plusieurs espèces présentaient un décalage distinct d'absorption dans la gamme 700–720 nm sous des conditions de FRL, suggérant la présence de complexes pigment-protéine modifiés permettant l'utilisation de la lumière de grande longueur d'onde. Notamment, *Vitrella brassicaformis* a été identifiée comme le premier organisme eucaryote à absorber constitutivement la FRL, un trait jusque-là uniquement observé chez les cyanobactéries. Contrairement aux adaptations facultatives de nombreux phototrophes, *V. brassicaformis* semble avoir développé un système de récolte de la lumière intrinsèquement optimisé pour l'utilisation de la FRL, ce qui suggère une spécialisation évolutive unique parmi les eucaryotes. Cette découverte apporte de nouvelles perspectives sur la diversité de l'adaptation à la FRL et ouvre des pistes pour la compréhension des contraintes évolutives et

écologiques liées à l'absorption des photons dans des environnements limités en lumière visible.

La deuxième partie de ce travail explore les bases moléculaires et biochimiques de l'acclimatation à la FRL chez *Stanieria cyanosphaera*, une cyanobactérie démontrant des mécanismes d'acclimatation chromatique complémentaire (CCA), d'acclimatation à la faible luminosité (LoLiP) et de photoacclimatation à la FRL (FaRLiP). Les analyses génomiques et transcriptomiques ont révélé la présence de clusters de gènes LoLiP et FaRLiP canoniques, orchestrant la biosynthèse des pigments, la restructuration des photosystèmes et la régulation redox sous conditions de FRL. La caractérisation structurale et spectroscopique de ses photosystèmes a mis en évidence une augmentation significative de la taille de l'antenne et de l'efficacité photosynthétique en réponse à l'exposition à la FRL.

D'autres investigations ont porté sur *Euglena gracilis*, révélant l'implication d'un complexe unique de récolte de la lumière (LHCE) dans l'absorption de la FRL et des mécanismes similaires aux transitions d'état. Cette antenne pentamérique LHCE est génétiquement régulée en fonction de l'environnement lumineux, cette régulation est dynamique et influence la transition d'état. Ces résultats élargissent notre compréhension des voies évolutives ayant conduit à des adaptations spécialisées pour la récolte de la lumière chez les eucaryotes.

Collectivement, cette recherche met en évidence l'occurrence généralisée de l'adaptation à la FRL chez les phototrophes et éclaire les mécanismes génétiques, structuraux et physiologiques sous-jacents à ce processus. La capacité des microalgues eucaryotes et des cyanobactéries à prospérer sous des conditions de FRL suggère que des adaptations similaires pourraient permettre l'existence d'une vie photosynthétique sur des exoplanètes en orbite autour d'étoiles naines M. En intégrant des perspectives astrophysiques, microbiologiques et écologiques, cette thèse contribue au débat plus large sur la diversité potentielle de la vie au-delà de la Terre et fournit des contraintes essentielles pour les futures recherches de biosignatures.

List of Abbreviations :

AAT	Average Arrival Time
AA	Amino Acid
ACKS	Strain or collection code
BBM	Bold's Basal Medium
BM-I to **BM-VII**	Subtypes of LhcbM proteins
BRH	Best Reciprocal Hit
CAP3	Sequence Assembly Software
CCA	Complementary Chromatic Acclimation
CCM	Carbon-concentration Mechanism
CD-HIT	Cluster Database at High Identity with Tolerance
CEF	Cyclic Electron Flow
Chl	Chlorophyll
CN-PAGE	Clear Native Polyacrylamide Gel Electrophoresis
CP24, **CP26**, **CP29**	PSII Minor Antenna Complexes
DDM	Dodecyl Maltoside
ETR	Electron Transport Rate
FaRLiP	Far-Red Light Photoacclimation
FLIM	Fluorescence Lifetime Imaging Microscopy
FRL	Far-Red Light
GTDB	Genome Taxonomy Database
HL	High Light
HPLC	High-Performance Liquid Chromatography
hrCN	High-Resolution Clear-Native electrophoresis
ISI	Iron-Stress-Induced protein (e.g., isiX)
JTS	Joliot Type Spectrophotometer
LC-MS/MS	Liquid Chromatography–Tandem Mass Spectrometry
LC-ESI-Q-TOF-MS	Liquid Chromatography-Electrospray Ionization-Quadrupole Time-of-Flight Mass Spectrometry
LHCBM	Major light-harvesting chlorophyll-binding proteins
LHCE	Euglena-specific LHC clade
LHCII	Light-Harvesting Complex II

LHC	Light-Harvesting Complex
LL	Low Light
LoLiP	Low-Light Photoacclimation
ML	Medium Light
MS	Mass Spectrometry
NPQ	Non-Photochemical Quenching
OCP	Orange Carotenoid Protein
ORF	Open Reading Frame
PAL	Present Atmospheric Level
PBS	Phycobilisome
PC	Phycocyanin
PE	Phycoerythrin
PPFD	Photosynthetic Photon Flux Density
PQ	Plastoquinone
PQH_2	Reduced Plastoquinone
PSSM	Position-Specific Scoring Matrix
PSI	Photosystem I
PSII	Photosystem II
RFP	Response Regulators (e.g., rfpA/B/C)
RNAi	RNA interference
RT	Room Temperature
SRA-STEMA	ULiege research support program
STK-STN	Kinases and phosphatases
TMP	Tris Minimal Phosphate
ULg	Université de Liège
UnLOC	ULiege research initiative
VLL	Very Low Light
WL	White Light
WT	Wild Type

Content Table

Introduction

1.1 Portal Project

Starlight is an inexhaustible and highly efficient energy source, central to Earth's trophic systems and widely utilized by terrestrial life forms. It is reasonable to posit that starlight could also play a crucial role in sustaining extraterrestrial biospheres across the cosmos. Investigating the universality and diversity of phototrophic metabolisms is, therefore, essential to understanding life on a cosmic scale—a core goal of astrobiology. In the past three decades, scientists have identified thousands of exoplanets, with several deemed potentially habitable. For a few of these, atmospheric analyses are possible with the James Webb Space Telescope (JWTS) but will be even more detailed with the advent of next-generation giant telescopes. Assessing the habitability of planets around late-type M-dwarfs is crucial to deepening our understanding of life's universality and constraints. These small and cool stars primarily emit in the near-infrared spectrum (around 1000 nm). Due to their low luminosity, rocky planets must orbit near these stars to maintain habitability (defined here as the possibility of having surface liquid water), resulting in potentially high exposure to XUV radiation and stellar winds, which may impact their surfaces far more intensively than Earth's environment. Consequently, the apparition of photosynthetic life on such planets may depend on how effectively phototrophic organisms can harvest infrared photons and withstand X-ray and UV radiation as well as high-speed charged particles.

The "PhOtotrophy on Rocky habiTAble pLanets" (PORTAL) project, founded by BELSPO BRAIN 2.0 (B2/212/P1/PORTAL), aims to explore the habitability of temperate rocky exoplanets orbiting very low-mass (VLM; <0.2 Msun) stars and the detectability of potential biosignatures on these worlds. This interdisciplinary endeavor integrates astrophysics, internal geophysics, atmospheric and planetary dynamics, geology, paleobiology, and microbiology. The primary goals are: (1) to define observational constraints on the physical and irradiative conditions on planets in the habitable zone of the nearby dwarf star TRAPPIST-1, and (2) to apply these constraints to assess the potential for infrared phototrophy and to evaluate detectable biosignatures, including analyses of early-Earth and extreme modern habitats, simulations under exoplanet conditions in the new TRAPPIST biodome, and conditions on rocky exoplanets orbiting VLM stars. (modified from unpublished report 2021 for Belgian Research Action through Interdisciplinary Networks)

1.2 Objectives pursued within the framework of the 'PORTAL' project.

The objective of the PORTAL project is to investigate whether life, relying on photosynthesis similar to that observed on Earth, could emerge or could have emerged under red dwarf stars, whose light emission is almost exclusively in the infrared range. On Earth, shaded habitats exhibit low levels of visible light but are enriched in far-red radiation. This enrichment arises because visible wavelengths are readily filtered by even minor obstructions, whereas the longer wavelengths of far-red light can penetrate these barriers. Such environments (including mangroves, shaded forest canopies, microbial mats, cave entrances, and others) host species capable of thriving under these specific light conditions.

Although several studies aim to elucidate the mechanisms of far-red light-harvesting antennas, many aspects remain poorly understood (Kotabová et al., 2014; Wolf & Blankenship, 2019). As part of the PORTAL project, this thesis primarily focuses on investigating organisms that grow under far-red light conditions and understanding the diverse mechanisms enabling them to harvest long-wavelength photons.

1.3 Overview of Photosynthesis

1.3.1 Prelude

Our biosphere is dynamic, sustained by the energy generated through photosynthesis. This is reflected in the spectral characteristics of Earth (Kiang et al., 2007), shaped by the pigments responsible for capturing sunlight. Additionally, the coexistence of high concentrations of oxygen with large quantities of complex organic molecules in the atmosphere (Lovelock, J.E. 1965) serves as another indicator of a planet with potential life. Over billions of years, photosynthetic organisms have profoundly transformed the planet and its biosphere (Cavalier-Smith, 2006).

The molecular oxygen from Earth's atmosphere is almost entirely a product of oxygenic photosynthesis. However, for much of Earth's history, oxygen was scarce in the atmosphere, which primarily consisted of diverse gases such as methane, ammonia, carbon dioxide, and dinitrogen, in variable conditions (Kasting, 1993). Early life forms thrived in strictly anaerobic conditions, relying on biochemistry independent of the oxygen–water cycle. The emergence of permanent oxygenation at a planetary scale, around 2.4 billion years ago (Gya), dramatically

disrupted the planet's redox balance and opened new ecological niches where complex cells later evolved (Lyons et al. , 2021; Lyons et al., 2024). Organisms were forced to adapt to oxygen, retreat to anaerobic habitats, or face extinction. Those that evolved tolerance to oxygen, and later the ability to harness its energy as a terminal oxidant, significantly diversified their metabolic pathways (Canfield et al., 2006, Raymond & Segre, 2006).

The intricate relationship between oxygenic photosynthesis and the evolution of Earth, along with the life it supports, makes exploring the evolutionary history of photosynthesis a compelling area of research. This field integrates experimental evidence with theoretical insights, bridging multiple scientific disciplines.

1.3.2 Evolution of photosynthesis

Photosynthesis likely began in the early Archean, around 3.4 billion years ago (Ga) where anoxygenic and oxygenic photosynthesis evolved (Tice & Lowe, 2004). Anoxygenic photosynthetic organisms utilize primitive energy sources—such as geothermal heat, molecular hydrogen (H_2), and reduced inorganic compounds (e.g., ferrous iron or hydrogen sulfide) to drive their metabolic processes. In contrast, oxygenic photosynthesizers evolved the capacity to oxidize water (H_2O), splitting its molecules to extract electrons and protons, thereby releasing oxygen (O_2) as a byproduct. The extracted hydrogen equivalents are then used to reduce inorganic carbon (CO_2) into organic matter (Martin & Russell, 2003).

It was assumed that these two photosynthetic systems originated from ancestral anoxygenic phototrophs (Hohmann-Marriott & Blankenship, 2011) but the idea that anoxygenic reaction centers are more ancient than those found in oxygenic photosystems is not corroborated by phylogenetic or structural data which show that PSII's ability to split water predates cyanobacteria (Cardona 2015; Cardona, 2019).

Among bacterial phototrophs, Cyanobacteria stands out as the only group possessing two distinct photosynthetic reaction centers: RCI, which uses iron-sulfur clusters as secondary electron acceptors, and RCII, which relies on quinones for electron transfer. By contrast, anoxygenic bacteria only have one type of reaction center, either the Fe–S or quinone-based variant. Several hypotheses have been put forward to explain the coexistence of both reaction centers in modern Cyanobacteria. Two of these suggest that an ancestral anoxygenic phototroph already contained both RC types. According to the first hypothesis, both RCs originated in the common ancestor of all bacterial phototrophs but were selectively lost in different anoxygenic lineages, while Cyanobacteria retained both (Olson & Pierson, 1987; Xiong and Bauer 2002).

The second hypothesis proposes that RCI and RCII arose via duplication of a single ancestral RC in a protocyanobacterial lineage, followed by lateral transfer of one type to progenitors of modern anoxygenic phototrophs (Allen & Martin, 2007). Evidence supporting the existence of an anoxygenic cyanobacterial ancestor includes the retention of genes associated with anoxygenic photosynthesis, such as among others BchE, PscA, PufLM, in common contemporary cyanobacterial genomes (Mulkidjanian et al., 2006), as well as the parallel occurrence of both anoxygenic and oxygenic photosynthesis within certain cyanobacterial clades (Klatt et al., 2016). The third hypothesis, commonly called the "fusion hypothesis," posits that RCI and RCII evolved independently in separate anoxygenic phototroph lineages and were later transferred together into a protocyanobacterial ancestor (Mathis, 1990). Notably, in purple bacteria, genes for RCII are often grouped within a photosynthesis gene cluster, sometimes residing on large plasmids, which facilitates the horizontal transfer of entire photosystems. Recent observations in *Rhodobacteraceae* further support the plausibility of such transfers (Brinkmann et al., 2018).

Recently phylogenetic analyses consistently indicate that all modern phototrophic organisms inherited their light-based metabolic capabilities from a single ancestral bacterium, referred to as the Last Phototrophic Common Ancestor (LPCA). This ancestral organism was an anoxygenic phototroph, already equipped with carbon fixation pathways and two types of photosynthetic reaction centers—one resembling present-day Type I systems and a more ancestral version of Type II. Furthermore, the data suggest that the emergence of chlorophototrophy predated the LPCA (Nishihara et al. 2024).

Even the evolution of RC remains uncertain, the apparition of oxygenic photosynthetis had transformative effects on Earth's environment, shifting the atmosphere from reducing to oxidizing and facilitating the evolution of aerobic bacteria and eukaryotes (Raymond & Blankenship, 2008) (Figure 1). With the rise of mitochondria-bearing protists and chloroplast-containing microalgae (eucaryotic and prokaryotic microalgae), multicellular organisms such as animals, plants, and fungi eventually dominated terrestrial ecosystems (Knoll, 2003).

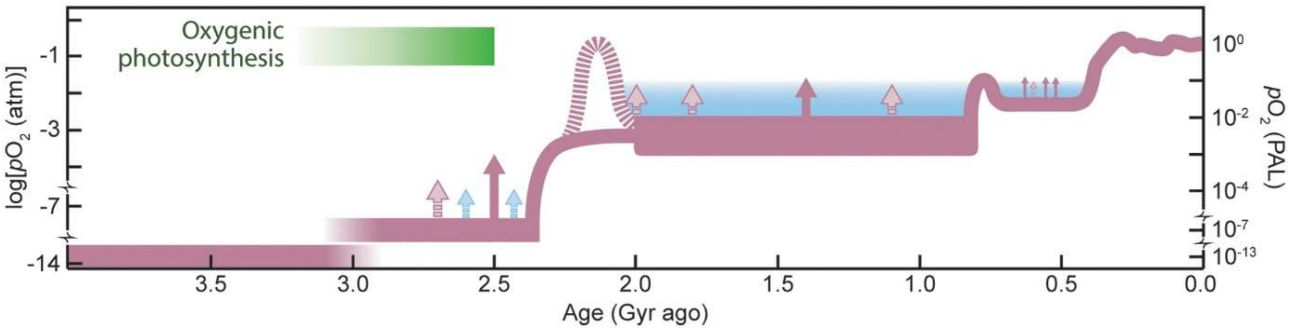

Figure 1. Representation of the oxygenation of the Earth.

The light red curve in the figure represents the "classical two-step" model for atmospheric oxygen evolution, whereas the blue-shaded area indicates alternative interpretations derived from numerical models, which suggest that O_2 remains stable only above certain partial pressures (Daines et al., 2017). The solid red arrows mark possible transient oxygen increases supported by geochemical evidence, while the pink dashed arrows denote events with lower levels of certainty. In the late Archean, the blue arrows illustrate hypothetical short-lived "whiffs" of O_2, conceptually indicating the oscillatory behavior expected during transitions between different steady states. "PAL" denotes the present atmospheric level (Lyons et al., 2021).

1.4 Diversity of Photosynthetic Microalgae

1.4.1 Cyanobacteria

Cyanobacteria constitute a remarkably diverse phylum of oxygen-producing prokaryotes, although there are anoxygenic cyanobacteria, distinguished by their extensive evolutionary history and ability to inhabit a broad range of ecological niches. Their notable contributions to carbon and nitrogen fixation, as well as phosphorus accumulation underline their fundamental role in shaping Earth's atmosphere. (Stal, 2007; Shestakov, 2017). Further investigations into these organisms indicate they play an integral role in ecosystem productivity and resilience, from polar regions (Makhalanyane et al., 2015) to hot springs and other underexplored environments (Cantonati et al., 2015).Their presence in extreme settings, including hot springs, hypersaline waters, frozen Antarctic lakes, and hot desert highlights their ecological versatility and evolutionary significance (Stal, 2007).

These prokaryotes occur both as free-living populations and in symbiotic associations within terrestrial and aquatic ecosystems. In marine environments, they commonly pair with diatoms and dinoflagellates but also with corals, sponges, and tunicates (Carpenter, 2002), while on land, they can partner with fungi, bryophytes, and even angiosperms such as *Gunnera*. Their capacity to persist under oligotrophic or otherwise demanding conditions, including polar zones and mangrove ecosystems, underscores their remarkable survival mechanisms (Makhalanyane, 2015). For example, *Gloeocapsa*, a colonial unicellular genus characterized by thick gelatinous sheaths, can endure vacuum exposure, extreme temperature shifts, ultraviolet and intense radiation, thus exemplifying cyanobacteria's resilience in habitats that test the limits of life (Budel, 1999; Lara et al., 2022).

Often labeled "blue-green algae", cyanobacteria present notable morphological breadth, including unicellular spherical, ovoid, or cylindrical forms, as well as multicellular colonies and branching and non-branching filaments (Figure 2). These differences in shape, size, and cell organization have prompted the emphasis on morphology as a primary basis for classifying these organisms. For example, taxa like *Synechococcus* represent unicellular forms, while *Gloeocapsa* illustrates colonial structures, and filamentous varieties range from simple threads (*Scytonema*) to truly branched filaments (*Stigonema*) (Geitler, 1932). This extensive morphological variation has historically positioned cyanobacteria as a group of significant interest to both microbiologists and phycologists.

Since Stanier et al., (1978) proposed to follow the International Code of Nomenclature for Bacteria, cyanobacteria were categorized cyanobacteria into five subclasses: I—unicellular cyanobacteria undergoing binary fission; II—unicellular cyanobacteria reproducing through multiple fission that generates small daughter cells called baeocytes; III—multicellular cyanobacteria that divide linearly within a single plane; IV—multicellular filamentous cyanobacteria with specialized cells (vegetative cells, heterocyst, and akinetes); and V—multicellular filamentous cyanobacteria with branched structures (Rippka et al., 1979). However, species with distinct physiological, environmental, and genetic traits were grouped within the same sections. This grouping hindered the ability to uncover relationships that accurately represent the phylogeny of the taxa (Shestakov and Karbysheva, 2016). Since then, taxonomy classification is in constant evolution. In 2014, Komarek et al., introduced a taxonomic framework for cyanobacteria, utilizing a comprehensive polyphasic approach incorporating molecular-genetic, morphological, physiological, and ecological criteria

(Komarek et al., 2016). Thus, Cyanobacteria were reclassified in 9 orders: Gloeobacterales, Synechococcales, Oscillatoriales, Chroococcales, Pleurocapsales, Spirulinales, Rudibacter, Halothece, Chroococcidiopsidales, Nostocales. It was the last current classification until nowadays when an update taxonomic system was proposed. It is based on a robust multigene phylogenetic tree constructed from 120 concatenated genes, serving as a scaffold for a less robust but better sampled 16S rRNA gene phylogeny leading to an original table of classification (Strunecký et al., 2023). However, misname still occur depending on the knowledge and taxonomic concept of the isolator.

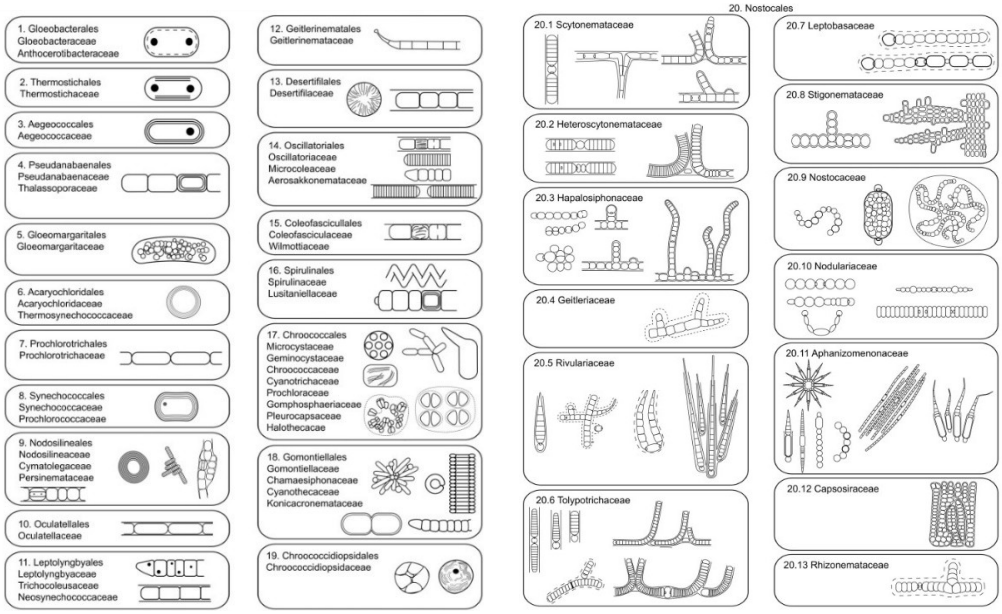

Figure 2. Schematic view of cyanobacterial orders and families. Some of the important taxonomic characters used to distinguish them. From Strunecký et al., 2023.

1.4.2 Eukaryotic Microalgae

1.4.2.1 Endosymbiosis

In the past, following the singular development of the Last Eukaryotic Common Ancestor (LECA), a remarkable event occurred: the endosymbiosis. Plastids, the photosynthetic organelles in eukaryotes, originated through a primary endosymbiotic event over a billion years ago, where a cyanobacterium was engulfed by a non-photosynthetic eukaryotic host (Margulis, 1971; Archibald , 2015) (Figure 3A). This integration facilitated the evolution of three major photosynthetic lineages: green microalgae and land plants, red microalgae, and glaucophyte microalgae (Rockwell et al., 2014). During primary endosymbiosis, DNA was transferred from the cyanobacterial endosymbiont to the host genome, and a protein import system evolved.

Primary plastids are surrounded by two membranes, with the cyanobacterial peptidoglycan layer retained in glaucophytes but lost in red and green microalgae. Secondary endosymbiosis occurred when non-photosynthetic eukaryotes engulfed primary plastid-bearing microalgae (Figure 3B). This process involved further gene transfers from the endosymbiont to the host nucleus, resulting in plastids surrounded by three or four membranes (Sibbald & Archibald, 2020). In cryptophyte and chlorarachniophyte microalgae, the nucleus of the engulfed microalgae persists as a nucleomorph within the periplastidial compartment, although nucleomorphs have been lost in other secondary plastid-bearing microalgae. Through secondary and even tertiary endosymbiosis, plastids were horizontally transferred across diverse eukaryotic lineages, leading to the patchy distribution of photosynthetic capabilities among modern eukaryotes (Keeling, 2010). Consequently, microalgae are a polyphyletic group, and understanding the frequency and mechanisms of plastid transfer remains a crucial challenge in evolutionary cell biology (Sibbald & Archibald, 2020).

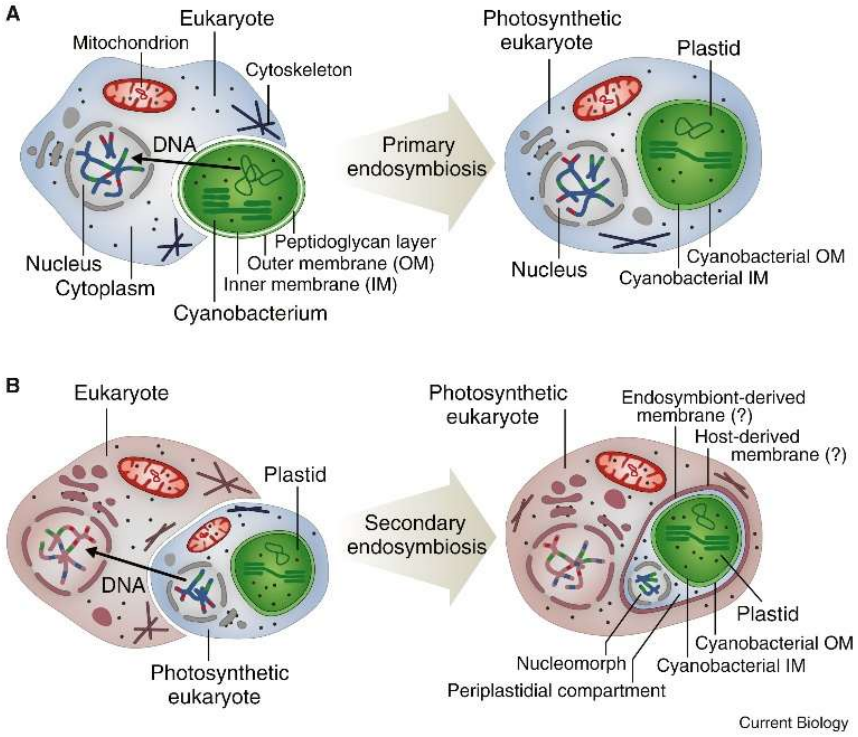

Figure 3. Schematic representation of primary endosymbiosis

(A) in which a eukaryotic organism engulfs a cyanobacteria and secondary endosymbiosis (B) where a eukaryotic organism engulfs a photosynthetic eukaryotic organism. Scheme from Archibald (2015).

1.4.2.2 Diversity of Eukaryotic Microalgae

Due to the vast potential for endosymbiotic events and adaptation, eukaryotes exhibit remarkable diversity encompassing organisms ranging from unicellular protists to complex multicellular forms like plants, animals, and fungi (Figure 4). While much research has focused on multicellular groups, most of the eukaryotic diversity lies within predominantly unicellular lineages, which remain poorly characterized despite their ecological and biological importance. These microorganisms are critical for understanding the fundamental principles of biology, as they often challenge conventional rules and provide insights into cellular complexity and evolution (Archibald, 2015).

Eukaryotic cells are inherently complex, possessing features such as nuclei with structured chromatin, spliceosomal introns, and highly organized cytoplasm supported by cytoskeletons (Cavalier-Smith, 2002). Organelles like mitochondria and chloroplasts play essential roles in energy transformation. Photosynthetic eukaryotes, particularly within the Archaeplastida, highlight the evolutionary significance of these organelles which originated from primary endosymbiosis and later spread through secondary and tertiary endosymbiotic events (Reyes-Prieto et al., 2007; Archibald, 2009).

Eukaryotes are broadly classified into several major lineages; Amorphea, CRuMs, Archaeplastida, Cryptista, Haptista, TSAR, Discoba and Hemimastigophora, each representing significant evolutionary traits and ecological diversity (Burki et al., 2020).

Amorphea includes Obazoa (animals, fungi, and their relatives) and Amoebozoa, distinguished by a single posterior flagellum (Cavalier-Smith, 2002). Amoebozoa, such as free-living amoebas and slime molds, feature lobose pseudopodia and tubular mitochondrial cristae (Smirnov et al., 2005). Multicellularity evolved independently in Obazoa (Medina et al., 2003).

Archaeplastida originated eukaryotic photosynthesis through primary endosymbiosis with cyanobacteria (Archibald, 2015). This group includes red microalgae, green microalgae (and land plants), and glaucophytes, with plastids that are monophyletic with cyanobacteria. Red and green microalgae plastids have been transferred to other lineages through secondary and tertiary endosymbiosis, spreading photosynthetic capabilities across the eukaryotic tree (Rodriguez-Ezpeleta et al., 2005). Glaucophytes are unique in retaining the peptidoglycan layer of their cyanobacterial ancestor (Bhattacharya et al., 2014). Cryptista, including cryptophytes, is closely associated with Archaeplastida. Cryptophytes acquired red algal plastids through secondary

endosymbiosis, retaining a nucleomorph, a remnant of the engulfed algal nucleus (Gentil et al., 2017).

The **TSAR** supergroup (an acronym for telonemids, stramenopiles, alveolates, and rhizaria, Haptista, Cryptista, Archaeplastida, Amorphea) unites highly diverse taxa; Rhizaria includes Chlorarachniophytes which acquired photosynthesis through secondary endosymbiosis with green microalgae (Archibald, 2009). Alveolates include some dinoflagellates and apicomplexans have plastids of red algal origin, acquired through secondary endosymbiosis. Apicomplexans retain non-photosynthetic plastids, or apicoplasts, for metabolic functions (Waller & McFadden, 2005). Stramenopiles include photosynthetic members include diatoms and brown microalgae, both critical for primary production in marine ecosystems (Moreira & López-García, 2002). Their plastids also derive from red microalgae through secondary endosymbiosis (Hackett et al., 2007). Haptista, encompassing haptophytes, is often associated with the RAS group. Haptophytes obtained red algal plastids via secondary endosymbiosis and are crucial for carbon cycling, notably through coccolithophores (Tsuji & Yoshida, 2017) The sister group to SAR was previously uncertain, but strong evidence now points to the enigmatic free-living flagellate taxon Telonemia.

Cryptista encompasses the cryptomonads (formerly classified among the chromalveolates), a group pivotal to research on plastid origins across eukaryotes. In addition, Cryptista includes katablepharids and the more recently identified which are enigmatic heterotrophic flagellates. Phylogenomic investigations consistently confirm the monophyly of Cryptista (Burki et al., 2012).

Haptista encompasses both the haptophyte microalgae (previously placed within the chromalveolates and the centrohelids. Haptophytes, notably the calcifying coccolithophorids, play key ecological roles in marine environments and significantly influence global biogeochemical cycles. Centrohelids, on the other hand, are free-living protozoa characterized by sphere-like cells bearing microtubule-supported, ray-shaped pseudopodia (axopodia) (Burki et al., 2016).

Similar to TSAR, **CRuMs** is a recently proposed supergroup named by combining its three constituent lineages—collodictyonids (also referred to as diphylleids), Rigifilida, and Mantamonas. Despite having distinct core morphologies (flagellates, amoeboid cells with threadlike projections, and small gliding forms, respectively) and previously being classified as

"orphan taxa," new phylogenomic evidence robustly supports their grouping into a single clade of non-photosynthetic organisms (Brown et al., 2018).

Discoba is a eukaryotic supergroup comprising Euglenozoa which gained photosynthetic capabilities via secondary endosymbiosis with green microalgae. Euglenozoa includes euglenophyte microalgae, trypanosomatid parasites, and numerous free-living or parasitic heterotrophic flagellates They display diverse metabolic adaptations, highlighting the plasticity of photosynthesis in eukaryotes (Kostygov et al., 2021). Hemimastigotes are free-living protozoa with two parallel rows of flagella, recognized since the 19th century and assigned a high taxonomic rank based on ultrastructural data (Foissner et al., 1988). As they could not be associated with any known supergroup or orphan lineage, it was proposed to assign hemimastigotes their own supergroup.

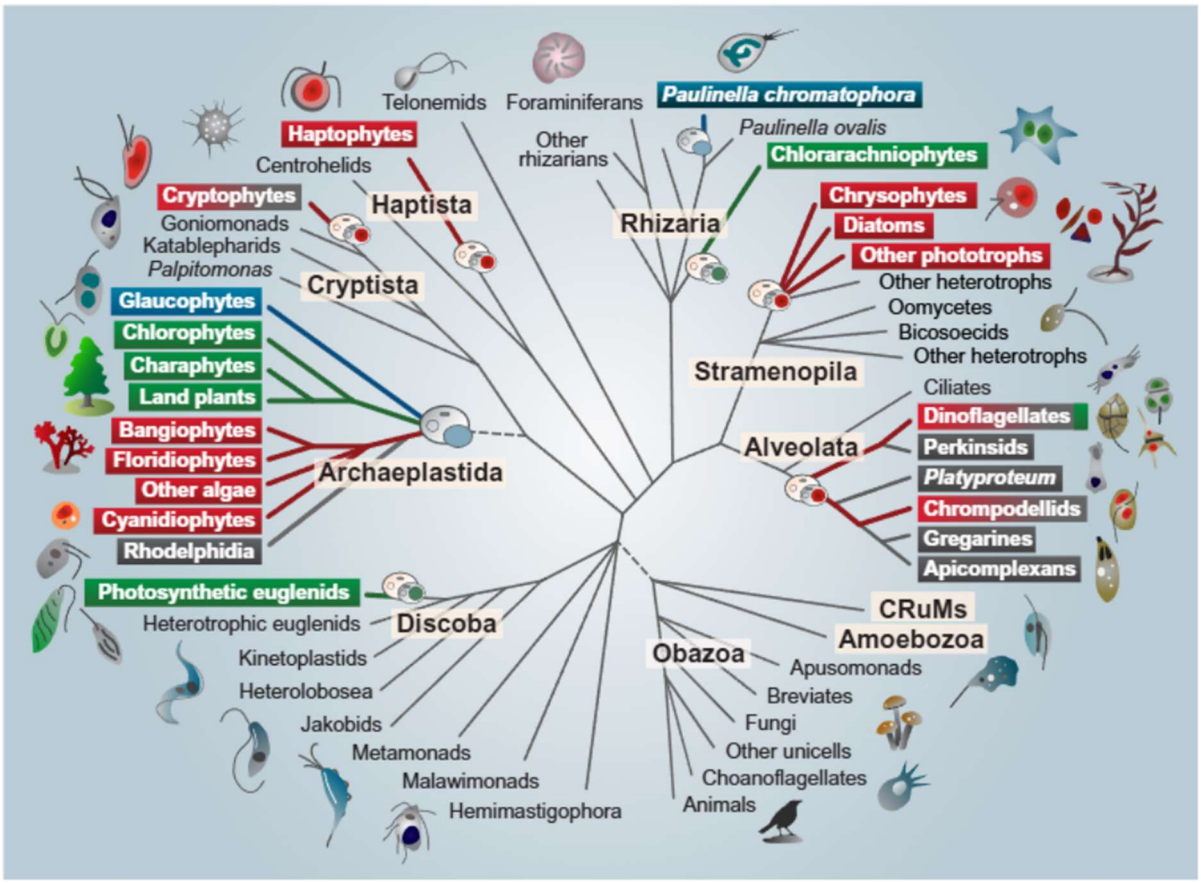

Figure 4. A schematic evolutionary tree of eukaryotes.

The Archaeplastida group contains primary plastids derived directly from cyanobacteria. These primary plastids, originating in red and green microalgae, were later transferred to other eukaryotic groups, including Rhizaria, Discoba, and Stramenopila. In these lineages, the color-coded taxon names indicate whether their plastids originated through secondary or tertiary endosymbiosis involving green or red microalgae. Taxon names shaded in gray denote the presence of one or more members that have secondarily lost photosynthetic capabilities. (Figure from McGrath, 2020)

1.5 Oxygenic photosynthesis :

1.5.1 Basics

Despite the broad morphological and ecological diversity observed among oxygenic photosynthetic organisms—including terrestrial plants, macroalgae, microalgae, and cyanobacteria—the core mechanism of photosynthesis remains remarkably conserved. This essential biological process enables the conversion of solar energy into chemical energy, supporting not only the metabolic needs of photoautotrophs but also sustaining nearly all life on Earth through primary production (Blankenship, 2010). In all these groups, light energy is captured and utilized to drive the transformation of carbon dioxide (CO_2) and water (H_2O) into carbohydrates, oxygen (O_2), and water. This transformation follows a general stoichiometric reaction:

$$6CO_2 + 12H_2O + \text{light energy} \rightarrow C_6H_{12}O_6 + 6O_2 + 6H_2O$$

The photosynthetic apparatus, though subject to organism-specific adaptations in structure and composition, consistently follows a unified organizational scheme composed of several interdependent stages (Figure 5). These include the absorption of light by pigment-protein complexes, the transport of electrons through thylakoid membrane-associated carriers, the synthesis of energy-rich molecules such as ATP and NADPH, and finally the fixation of carbon into organic molecules via the Calvin-Benson Bassham cycle (Nelson & Yocum, 2006; Raven et al., 2017). The integrity of these processes is maintained across lineages through the conservation of key protein complexes, such as the two photosystems (PSI and PSII), and shared metabolic intermediates like ribulose-1,5-bisphosphate (Rochaix, 2011).

Although the ultrastructure of the photosynthetic machinery may differ—for instance, in the arrangement of thylakoid membranes or the spectrum of accessory pigments—the fundamental biochemical logic of photosynthesis is retained (Green & Parson, 2003). Cyanobacteria, often regarded as the evolutionary origin of plastid-containing photosynthetic eukaryotes, exemplify the ancient and robust nature of this system (Sánchez-Baracaldo et al., 2017). They utilize both water as an electron donor and light as an energy source, releasing molecular oxygen as a byproduct—a defining feature of oxygenic photosynthesis. In this regard, the conservation of photosynthesis across diverse taxa highlights its evolutionary optimization and its indispensable role in shaping the Earth's atmosphere and carbon cycle (Falkowski & Raven, 2007)

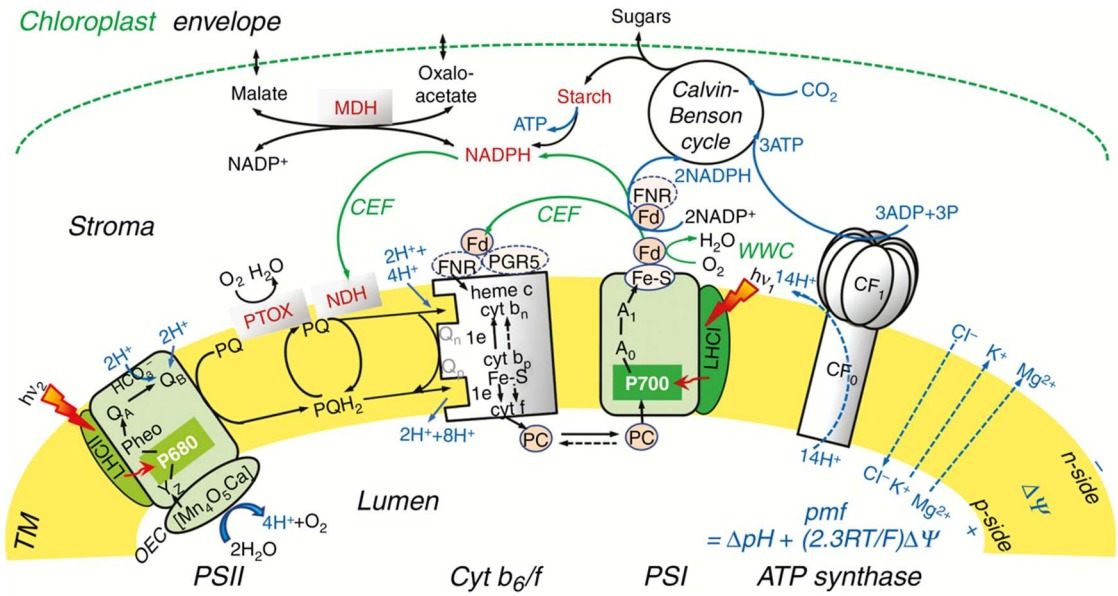

Figure 5. Diagram of the photosynthetic apparatus and electron transport (ET) pathways in plants and algae (Stirbet et al., 2020). The following chapter describes the four main stages of the photosynthesis

1.5.2 Light Harvesting

Light-harvesting is the very first involved systems that capture and transfer solar energy to reaction centers where excitation energy is transferred between chlorophyll molecules through dipole–dipole interactions (Şener et al., 2011).

In cyanobacteria, light is captured through specialized antenna complexes called phycobilisomes (PBS) (Figure 6, left panel), composed of phycobiliproteins such as always phycocyanin and allophycocyanin, and sometimes phycoerythrin (Glazer, 1985; Mullineaux, 2008). These complexes are bound to the surface of thylakoid membranes and efficiently absorb light in the blue-green-orange spectrum, essential for aquatic environments. Cyanobacteria also contain chlorophylls as their primary photosynthetic pigment, accompanied by carotenoids and phycobilins (Scheer, 1991).

Eukaryotic microalgae possess chloroplasts with light-harvesting complexes (LHCs) embedded in their thylakoid membranes (Figure 6, right panel). These complexes include pigments such as chlorophyll a, chlorophyll b (in green microalgae), and carotenoids. The thylakoid

membranes are organized into grana stacks, optimizing light absorption and energy transfer efficiency (Nelson & Yocum, 2006).

Excitation energy transfer (EET) in photosynthesis moves excitation energy from light-absorbing pigments to reaction centers (RCs), enabling charge separation. EET occurs via Förster resonance (in weak coupling) or excitonic transfer (in strong coupling), with rates depending on pigment distance, orientation, and spectral overlap (Forster, 1948; Redfield, 1965). In plants and algae, energy flows through local funnels from high-energy pigments (e.g., Chl b, carotenoids) to Chl a, then to RCs (Croce & van Amerongen, 2011). In cyanobacteria, large phycobilisome complexes composed of phycobilins funnel energy through progressively lower-energy pigments toward both PSII and PSI reaction centers (Liu et al., 2013). Proteins optimize EET by tuning pigment arrangement, energy levels, and coupling, ensuring efficiency despite structural and environmental variability (Liu et al., 2004; Wientjes et al., 2012).

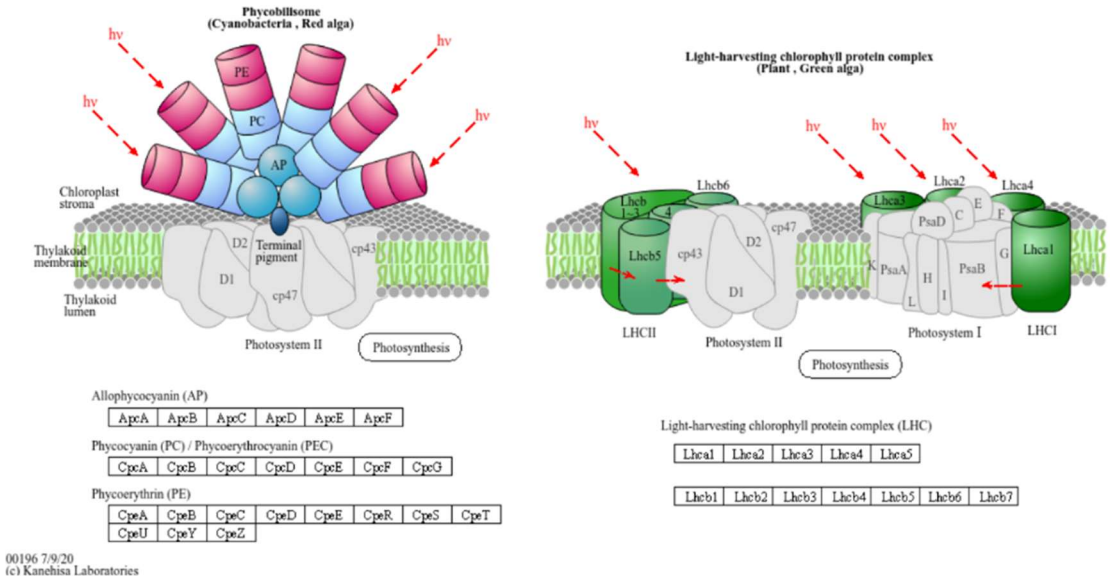

Figure 6. Schematic representation of PBS in cyanobacteria (left) and LHC in eukaryotic organisms (right).

The chlorophyll-binding subunits of photosystems I and II are internal antenna light-harvesting proteins of oxygenic photosynthesis. The antenna proteins that exist in phycobilisomes in cyanobacteria and light-harvesting chlorophyll protein complexes in green plants act as peripheral antenna systems, enabling more efficient absorption of light energy. The diverse protein assemblies constituting these antennae (Bottom) underscore their inherent complexity and interconnection between proteins (Xue et al., 2019).

1.5.3 Electron Transport Chain

After photons harvesting by antenna complexes and further charge separation into the reaction centre, electron are engaged into the photosynthetic chain.. The photosynthetic electron transport chain involves a highly organized series of redox reactions performed by protein complexes embedded within the thylakoid membranes of cyanobacteria and microalgae. This sequence begins in Photosystem II (PSII), where photons excite chlorophyll molecules, resulting in the photolysis of water. This reaction produces oxygen, protons, and high-energy electrons (Ott et al., 1999). The electrons are then transferred to plastoquinone (PQ), a mobile electron carrier, which shuttles them to the cytochrome b_6f complex. The energy released during electron transfer within the cytochrome b_6f complex is utilized to pump protons from the stroma into the thylakoid lumen, contributing to the proton motive force across the membrane (Cramer & Kallas, 2016).

The electrons is then transferred to plastocyanin (PC) or cytochrome c6, which are mobile electron carriers that give electrons to PSI. In PSI, absorbed light energy leads to the excitation of the P700 reaction center chlorophylls, and ejection of an electron that travels through a chain of cofactors—including A_0, A_1, and three iron–sulfur clusters (F_x, F_A, F_B)—ultimately reducing ferredoxin (Fd), a stromal electron carrier. The oxidized $P700^+$ is subsequently reduced by electrons delivered via plastocyanin (PC) or cytochrome c_6, thereby completing the cycle (Nelson & Junge, 2015; Fromme et al., 2001). Subsequently, ferredoxin-NADP+ reductase catalyzes the reduction of NADP+ to NADPH (Nelson & Junge, 2015). Concurrently, the proton gradient established across the thylakoid membrane drives the synthesis of ATP via ATP synthase, a process known as chemiosmotic photophosphorylation (Jagendorf, 2002).

1.5.4 Synthesis of ATP and NADPH

The coordinated action of Photosystem II (PSII) and Photosystem I (PSI) underpins the efficient synthesis of ATP and NADPH, which are crucial for downstream processes such as the Calvin–Benson–Bassham cycle. Both cyanobacteria and eukaryotic microalgae rely on photophosphorylation to generate these energy carriers. However, structural and organizational differences between these organisms have significant implications for the regulation and efficiency of their photosynthetic apparatus.

A key distinction lies in the architecture of the thylakoid membranes. Cyanobacteria possess unstacked thylakoids that are in direct contact with the cytoplasmic environment, facilitating proton diffusion across the membrane. While this arrangement enhances interaction with the surrounding cellular environment, it also results in less efficient proton retention, potentially diminishing the capacity to maintain a steep proton gradient for ATP synthesis (Nelson & Yocum, 2006; Blankenship, 2021). In contrast, the thylakoids of eukaryotic microalgae are organized into stacked grana, creating a more enclosed lumen. This structural confinement improves the retention of protons and supports more robust proton gradient formation, thereby enhancing ATP synthesis (Blankenship, 2021).

Additionally, cyanobacteria and eukaryotic microalgae differ in their strategies to modulate the ATP/NADPH ratio in response to environmental and metabolic demands. While both regulate the relative activities of PSI and PSII, eukaryotic algae also employ sophisticated mechanisms such as cyclic electron flow around PSI to fine-tune the energy balance under varying light and nutrient conditions (Nelson & Junge, 2015; Larkum et al., 2017). Furthermore, the absence of internal compartmentalization in cyanobacteria renders them more susceptible to external fluctuations in pH and ion concentrations, directly impacting electron transport and ATP production (Mullineaux, 2014). In contrast, the compartmentalized chloroplasts of eukaryotic microalgae buffer against such variations, offering enhanced stability in diverse environments (Blankenship, 2021). Notably, exceptions exist, such as *Gloeobacter*, a basal cyanobacterium lacking thylakoid membranes altogether, where photosystems are embedded directly in the plasma membrane (Raven & Sánchez-Baracaldo, 2021).

1.5.5 Carbon Fixation

Oxygenic photosynthesis is commonly divided into two stages: (1) the light-dependent reactions, which generate ATP and NADPH using light energy and water, and (2) the Calvin cycle, which fixes CO_2 into organic molecules using RuBisCO . While the Calvin cycle does not require light directly, it depends on the ATP and NADPH produced by the light reactions. RuBisCO is sensitive to oxygen due to its oxygenase activity, leading to photorespiration, a process that reduces carbon fixation efficiency. In some bacteria and cyanobacteria, RuBisCO is encapsulated in carboxysomes to enhance CO_2 concentration and minimize oxygen interference. Some cyanobacteria can adapt their light-harvesting complexes to environmental changes and have carbon-concentration mechanism (CCM), further improving efficiency (Sato et al., 2024).

In eukaryotic microalgae, carbon fixation takes place in the stroma of chloroplasts. Mechanisms like CCMs and, in some cases, C4 pathways help optimize CO2 fixation under varying environmental conditions. RuBisCO catalyzes the initial step, incorporating CO2 into ribulose-1,5-bisphosphate (RuBP), ultimately forming glyceraldehyde-3-phosphate (G3P), the precursor for carbohydrate synthesis (Giordano, 2005).

1.5.6 Carbohydrate Production

The end product of the Calvin-Benson Bassham cycle is glyceraldehyde-3-phosphate (G3P), which serves as a precursor for synthesizing complex carbohydrates (Blankenship, 2021). Eukaryotic microalgae typically store energy in the form of starch such as amylopectin-rich starch within their chloroplasts, while cyanobacteria accumulate glycogen in the cytoplasm. This difference reflects their evolutionary divergence and environmental adaptations (Ball & Morell, 2003).

These distinctions illustrate the evolutionary adaptations of cyanobacteria and microalgae to maximize photosynthetic efficiency in diverse environments. Together, they exemplify the versatility of photosynthetic mechanisms in capturing solar energy for life on Earth.

1.6 Light response and acclimation

Algae possess highly sophisticated mechanisms to adjust their photosynthetic activity in response to changing light conditions. These mechanisms, spanning short- and long-term responses, optimize energy capture, prevent photodamage, and ensure the sustained efficiency of the photosynthetic apparatus.

1.6.1 Short-Term Regulatory Mechanisms

1.6.1.1 State transitions

One of the first mechanism that occur to prevent photodamage is state transitions. It is a crucial photoprotective mechanism that optimizes photosynthetic efficiency by balancing light energy distribution between photosystem I (PSI) and photosystem II (PSII) (Figure 7). In microalgae, this process involves the reversible phosphorylation and migration of light-harvesting complex II (LHCII) proteins between the photosystems, regulated by the redox state of the plastoquinone pool. The Stt7/STN7 protein kinase plays a key role in this process, phosphorylating LHCII and triggering its movement. State transitions occur on a timescale of minutes, while longer-term acclimation responses adjust photosystem stoichiometry over hours to days. Both short-term state transitions and long-term responses are mediated by the STN7 kinase, which acts as a common redox sensor and signal transducer. This adaptive mechanism allows plants to maintain optimal photosynthetic activity under fluctuating light conditions (Lemeille et al., 2009; Pesaresi et al., 2010;Tikkanen et al., 2011).

In cyanobacteria, state transitions are mediated by the physical redistribution of phycobilisomes, which shift their energy transfer from PSII to PSI under state 2 conditions. This process occurs without phosphorylation, relying instead on membrane reorganization and dynamic interactions between phycobilisomes and photosystems (Joshua & Mullineaux, 2004; Mullineaux & Emlyn-Jones, 2005).

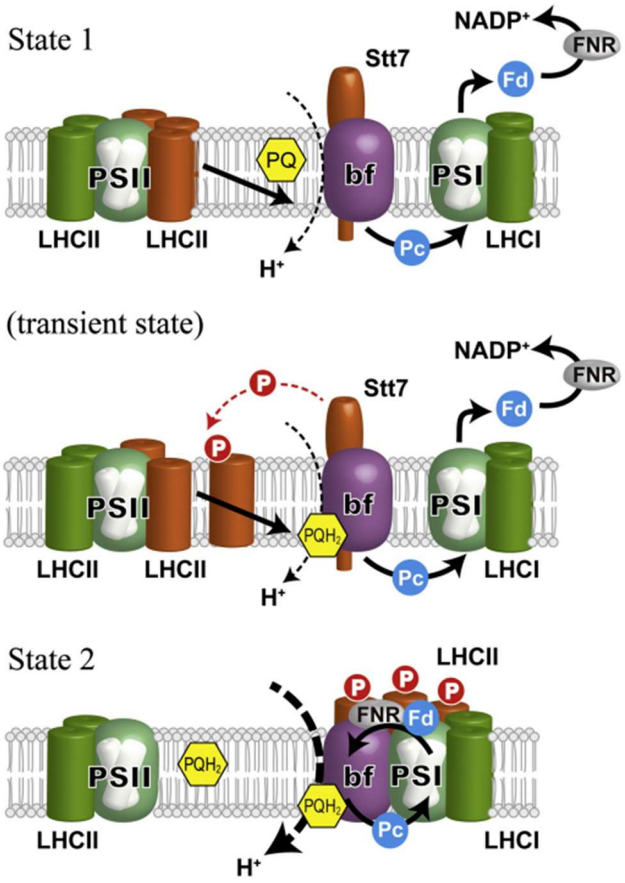

Figure 7. A schematic overview of state transition regulation.

In State 1, when Photosystem I (PSI) is preferentially excited, the plastoquinone (PQ) pool remains in its oxidized form. Under these conditions, the LHCII complexes are associated with Photosystem II (PSII), and the photosynthetic electron transport predominantly follows a linear electron flow (LEF) pathway. This process generates both a trans-thylakoid proton gradient—driving ATP synthesis—and NADPH.

During the transient phase, which is initiated when PSII becomes preferentially excited, the PQ pool transitions to a reduced state. The docking of reduced PQ (PQH_2) at the Qo site of the cytochrome b_6f (Cyt bf) complex activates the Stt7 kinase. This kinase phosphorylates the mobile LHCII complexes (shown in orange), prompting their dissociation from PSII.

In State 2, the now mobile LHCIIs reattach to the PsaH subunit on the opposite side of the main LHC belt of PSI. Furthermore, Cyt bf and ferredoxin–$NADP^+$ reductase (FNR) bind to PSI, forming a "super-supercomplex" (often referred to as a cyclic electron flow or CEF supercomplex). This complex is crucial for establishing cyclic electron flow between PSI and the PQ pool, a process that primarily supports ATP production. Figure and interpretation from Minagawa J., 2011

1.6.1.2 Non-Photochemical Quenching (NPQ)

Non-photochemical quenching (NPQ) is one of the main photoprotective mechanisms in photosynthetic organisms, dissipating excess light energy as heat, safely diverting it away from the photosynthetic reaction centers, preventing the formation of harmful reactive oxygen species and there is several ways to do it.(Goss & Lepetit, 2015). NPQ involves structural changes in light-harvesting complexes, altering energy transfer pathways (Schiphorst & Bassi, 2020). The molecular machinery for NPQ varies across species: land plants rely on PSBS, while most microalgae use light harvesting stress-related (LHCSR), allowing rapid adjustment to changing light intensities. In green microalgae, NPQ comprises rapid (qE) and slower (qT) components, with the latter being more prominent compared to vascular plants (Finazzi & Minagawa, 2014). Furthermore, a proton gradient across the thylakoid membrane induces conformational changes in light-harvesting complexes, increasing their capacity for energy dissipation (Horton et al., 1996; Niyogi & Truong, 2013).

Microalgae dynamically alter the size and distribution of their antenna complexes. For example, pigment density increases under low light to maximize energy capture and decreases under high light to prevent photodamage. This flexibility ensures efficient energy use across varying light conditions. Studies in *Chlamydomonas reinhardtii* have shown extensive reorganization of LHCII and PSI-PSII complexes during light changes (Drop et al., 2014).

Energy Spillover enable excess excitation energy from PSII to be transferred to PSI, particularly under high light, to prevent over-reduction of the electron transport chain and reduce the risk of photodamage and reactive oxygen species (ROS) formation. This mechanism has been observed in red microalgae like *Porphyridium cruentum* (Kowalczyk et al., 2013).

Carotenoïds exhibit significant diversity and play a crucial role in photoprotection. Chlorophytes use the xanthophyll cycle to dissipate excess energy as heat (Figure 8). It involves the interconversion of violaxanthin and zeaxanthin and plays a crucial role in regulating NPQ. This process is controlled by two enzymes: violaxanthin de-epoxidase and zeaxanthin epoxidase. Zeaxanthin formation enhances NPQ and energy dissipation, while violaxanthin promotes light harvesting (Niyogi et al., 1998). The xanthophyll cycle pool size influences NPQ kinetics, with zeaxanthin and violaxanthin antagonistically regulating the switch between light harvesting and photoprotection (Johnson et al., 2008). However, exceptions to this regulatory mechanism exist, as demonstrated in Phaeomonas sp., where zeaxanthin epoxidase activity primarily controls NPQ, challenging the conventional xanthophyll cycle model (Berne et al.,

2018). In diatoms, Violaxanthin is replaced by diadinoxanthin and zeaxanthin is replaced by diatoxanthin but have the same regulatory system (Schaller-Laudel et al., 2015).

Dinoflagellates also use the diadinoxanthin–diatoxanthin cycle, though they possess additional peridinin-based antennae complexes. Although primarily a light-harvesting pigment, it may indirectly participate in NPQ by influencing antenna structure and excitation dynamics (Šišková et al., 2019)

Cyanobacteria use xanthophyll cycle with myxoxanthophyll, zeaxanthin, and B-carotene. They also produce orange carotenoid protein (OCP), which binds to phycobilisomes and quenches excess energy via excited-state interactions, dissipating energy as heat (Wilson et al., 2006) Under high light, it photoactivates ($OCP^{orange} \rightarrow OCP^{red}$), binds to PBS, and quenches excess excitation before it reaches the photosystems (Kirilovsky & Kerfeld, 2016).

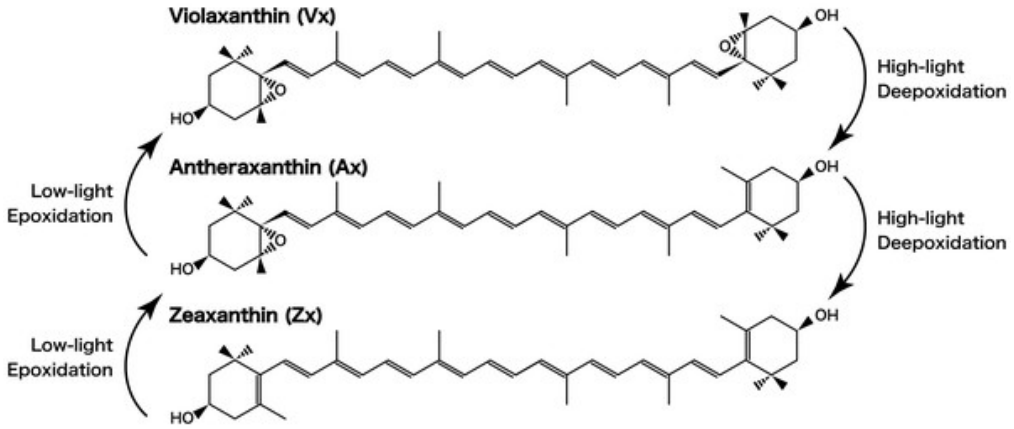

Figure 8. Molecular structures of the xanthophyll cycle pigments.

Arrows between pigments denote enzymatic conversions caused by xanthophyll cycling (picture from Tanabe et al.,2011)

1.6.2 Reactive Oxygen Species (ROS) Management

If light is too strong to be compensated by theses mechanisms, one of the main damaging effects is the production of ROS including superoxide radicals and hydroxyl radicals, can disrupt vital cellular processes in microalgae by attacking proteins, membrane lipids, and nucleic acids (Apel & Hirt, 2004). The production of these ROS is a natural consequence of photosynthesis, particularly under high light but microalgae employ antioxidant systems such as the Mehler-Ascorbate Peroxidase pathway, which redirects excess electrons to oxygen to minimize ROS accumulation (Schmitt et al., 2014).

To maintain photosynthetic efficiency, microalgae actively repair and replace damaged proteins. The D1 protein of PSII, which is highly susceptible to light damage, undergoes continuous degradation and replacement, ensuring sustained photosystem function (Babu et al., 1999).

In certain cyanobacteria, the orange carotenoid protein (OCP) dissipates excess energy as heat and neutralizes singlet oxygen, providing an effective photoprotective mechanism under high light stress (Kirilovsky & Kerfeld, 2012).

1.6.3 Long-Term Acclimation Mechanisms

Under extended periods of excessive or insufficient irradiance, microalgae engage a range of long-term adaptive strategies to safeguard and optimize their photosynthetic apparatus. The most common is the modification of their pigment composition to optimize light capture. For instance, carotenoids like fucoxanthin, peridinin, and phycobiliproteins expand light absorption into the green and blue regions of the spectrum, enabling efficient energy capture in diverse environments (Goss & Jakob, 2010). But also by altering the ratios of chlorophylls and accessory pigments, they refine light absorption profiles and mitigate photoinhibitory damage, ultimately preserving metabolic efficiency (Raven & Geider, 2003).

Structural modifications, such as changes in the organization and composition of photosynthetic complexes, occur to adapt to varying light conditions. Diatoms, for instance, utilize fucoxanthin-chlorophyll protein complexes (FCPs) that are optimized for light adaptation (Gundermann & Büchel, 2014). Microalgae also modify the balance between PSII and PSI, increasing PSII under low light to boost photochemical efficiency, and favoring PSI under high light to prevent over-reduction of the electron transport chain (Rochaix, 2014). Cyanobacteria rely on phycobilisomes, water-soluble light-harvesting complexes that efficiently channel energy to photosystems under low-light or fluctuating conditions. These structures undergo functional reorganization, particularly through interactions with the OCP, which modulates energy flow under high light stress (Kirilovsky & Kerfeld, 2016). Chlororespiration also helps microalgae to maintain redox balance by generating a proton gradient even in the absence of light. This process, observed in *Euglena*, ensures flexibility in managing photosynthetic activity under dynamic conditions (Doege et al., 2000).

These regulatory mechanisms highlight the remarkable adaptability of microalgae to their dynamic light environments. Through biochemical, structural, and molecular strategies, microalgae optimize their photosynthetic efficiency while protecting themselves from light-induced damage. This balance is crucial for their survival and ecological success across diverse habitats.

1.7 Acclimation to shaded environments

Chromatic adaptation exemplifies evolutionary ingenuity, enabling cyanobacteria, microalgae and other photosynthetic eukaryotes to thrive in diverse and often extreme light conditions. By leveraging pigment diversity, sophisticated light-harvesting systems, and dynamic regulatory mechanisms, these organisms optimize their photosynthetic efficiency and maintain ecological balance in marine and terrestrial ecosystems where light can be rare. In this chapter, four different mechanisms of photoacclimation will be described.

1.7.1 Red shifted chlorophylls in eukaryotic microalgae

Chlorophylls (Chl) are pigments that efficiently capture light and transfer the excitation energy toward photosynthetic centers where specialized Chl drive initial step of charge separation and energy transduction.

In oxygenic photosynthetic eukaryotes, three distinct forms of Chl have been identified; Chls *a*, *b*, and *c*. These pigments are integral components of light-harvesting complexes (LHC), although only Chl *a* is essential for energy transduction in photosystem reaction centers (Scheer, 2006; Björn et al .,2009;). Chl *a* exhibits absorption peaks at 430 and 665 nm in methanol, for effective light harvesting and photochemical reactions, making it a crucial pigment. (Oba et al., 1997). When associated with LHC proteins from most organisms, Chl *a* can absorb light up to 685 nm. (Wientjes et al., 2012). However, some eukaryotic phototrophs have developed mechanisms to harvest far-red light, extending absorption up to 710 nm, by modifying pigment-protein interactions within specialized LHC (Croce et al., 2007).

This unusual inducible interaction has been observed in diverse lineages, including green microalgae such as *Ostreobium* sp. (Koehne et al., 1999; Wilhelm and Jakob, 2006) and *Prasiola crispa* (Kosugi et al., 2020), various stramenopiles, such as *Phaeodactylum tricornutum* (Fujita and Ohki, 2004), *Trachydiscus minutus* (Litvín et al., 2019), *Eustigmatophyceae* sp. FP5 (Wolf et al., 2018), and the alveolata *Chromera velia* (Bína et al., 2014; Kotabová et al., 2014). Additionally, this phenomenon has been identified in bryophytes (Alboresi et al., 2008), and flowering plants (Jansson, 1994; Ihalainen et al., 2000).

For instance, *Ostreobium* sp., which inhabits coral reefs under extremely low-light conditions, produces a 22 kDa red LHC that binds chlorophyll *a,* displaying an absorption shoulder at 710

nm (Koehne et al., 1999; Wilhelm and Jakob, 2006). Similarly, the diatom *P. tricornutum* when cultured under red-light conditions, has red Chl *a*-binding LHC with an absorbance maximum at 703 nm, in addition to its standard peak at 680 nm (Fujita and Ohki, 2004). In the alveolate *C. velia*, a red-shifted absorbance peak (ca. 705 nm) appears under red-light conditions, attributed to a red LHC composed of 17 kDa fucoxanthin–chlorophyll a/c protein complex binding Chl *a* (Bína et al., 2014; Kotabová et al., 2014). Meanwhile, the xanthophyte *T. minutus* contains a red–violaxanthin–Chl *a* protein (rVCP) that incorporates violaxanthin, non-esterified vaucheriaxanthin, and Chl *a*, with one of its low-energy Chl *a* molecules likely absorbing at or beyond 700 nm (Bína et al., 2019). Lastly, in *Eustigmatophyceae* sp. FP5, cultivation under far-red light conditions induces a strong absorbance maximum at 705 nm, confirmed by native PAGE analysis, which reveals multiple far-red-absorbing LHCs that bind Chl *a* (Wolf et al., 2017).

In flowering plants and green microalgae, red-shifted Chls are frequently associated with Lhca4, a primary PSI LHC. The red Chls are thought to arise from strong excitonic interactions within closely associated Chl clusters (Morosinotto et al., 2005, Wientjes et al., 2012). These red-shifted pigments, which are almost ubiquitously present in photosystem I, are considered crucial for regulating energy transfer from bulk chlorophylls to P700, as well as dissipating excess excitation energy as heat (Carbonera et al., 2005, Romero et al., 2009). Under low-light conditions, an uphill energy transfer mechanism enables red Chls to efficiently transmit excitation energy to the PSI reaction center (Pålsson et al., 1998; Şener & Schulten, 2005; Schlodder et al., 2014).

Red-shifted Chls associated with photosystem II have also been reported in certain flowering plants, bryophytes, and eukaryotic microalgae such as *Chormera velia*, albeit at a lower frequency and with significantly weaker contribution compared to PSI-associated red-Chls. Studies on flowering plants and green algae suggest a limited excitation transfer to P680 from Red Light harvesting complex (RLHC) (Pettai et al., 2005, Thapper et al., 2009, Kosugi et al., 2020).

1.7.2 Chromatic adaptation of Cyanobacteria

Cyanobacteria employ several specific photoacclimation strategies to modify their pigment composition and photosystem-antenna structure. These strategies include adjusting the component of the photosynthetic system, by modifying the PSI:PSII ratio in response to light changes (Raps et al., 1983; Fujita et al., 1994), redistributing energy between PBS and the photosystems during state transitions (Dong et al., 2009; Liu et al., 2013), dissipating excess light energy at the antenna level with specialized orange carotenoid proteins, or using flavodiiron proteins to alleviate the reducing power in the electron transport chain (Allahverdiyeva et al., 2013; Bersanini et al., 2014). Cyanobacteria also employ additional photoacclimation strategies called complementary chromatic acclimation (CCA) (Kehoe & Grossman, 1994), low-light photoacclimation (LoLiP), and far-red light photoacclimation (FaRLiP) to modify their pigment composition and photosystem structure (Gan & Bryant, 2015).

1.7.2.1 Complementary chromatic adaptation (CCA)

The chromatic acclimation of cyanobacteria is categorized into several groups (Figure 9) (Tandeau de Marsac, 1977; Sanfilippo et al., 2019). CA1 includes cyanobacteria like *Synechocystis* sp. PCC 6803 maintain a consistent PBS structure but changes rod-core linker (Kondo et al., 2005). CA2 consists of cyanobacteria that adjust PE levels while keeping PC levels unchanged, as shown in *Nostoc punctiforme* sp. PCC 73102 (Hirose et al., 2010). CA3, known as complementary chromatic acclimation (CCA), involves cyanobacteria that synthesize a new PBS by altering the rod composition, becoming PE-rich under white or green light and PC-rich under red light (Federspiel and Scott, 1992). Later, CA4 was introduced following the identification of *Synechococcus marinus*, which exhibits chromophore changes in certain peripheral PBPs (Everroad et al., 2006). CA5 was identified with *Acaryochloris marina*, which features chlorophyll *d*-based light-harvesting complexes along with unique rod-shaped antennae that contain phycobiliproteins. These antennae include phycocyanin and have allophycocyanin located at their base (Chen et al., 2009). CA6, also known as FaRLiP, reorganizes the whole harvesting system due to a cluster coding for specific proteins (Gan et al., 2014). Recently, the Hirose group identified CA7 in *Leptolyngbya* sp. PCC 6406, describing a regulation of phycoerythrocyanin (PEC) which maximizes yellow-green light harvesting capacity and CA0 with rod-shaped phycobilisome that balances the excitation of photosystems (Hirose et al., 2019).

Complementary chromatic adaptation (CCA or CA3) is a process that enables to modulate the relative amounts of phycoerythrin (PE) and phycocyanin (PC) in PBS in response to light quality changes (Marsac & Houmard, 1988). Red light promotes PC synthesis, while green light promotes PE synthesis, resulting in blue-green or red coloration, respectively (Kehoe & Grossman, 1994). CCA significantly increases light-use efficiency in *Calothrix* PCC 7601, which is crucial in light-limited environments (Campbell, 1996). CCA is primarily controlled by a two-component signal transduction pathway involving a phytochrome-class photoreceptor and response regulators(Kehoe & Gutu, 2006) that binds to specific promoter regions, simultaneously activating and repressing transcription of different operons in response to red light, as shown in *Fremyella diplosiphon* (Li et al., 2008). CCA also affects energy transfer between photosystems, with cells in red light favoring state I where PSI is preferentially excited and cells in green light favoring state II where PSII is preferentially excited (Campbell, 1996).

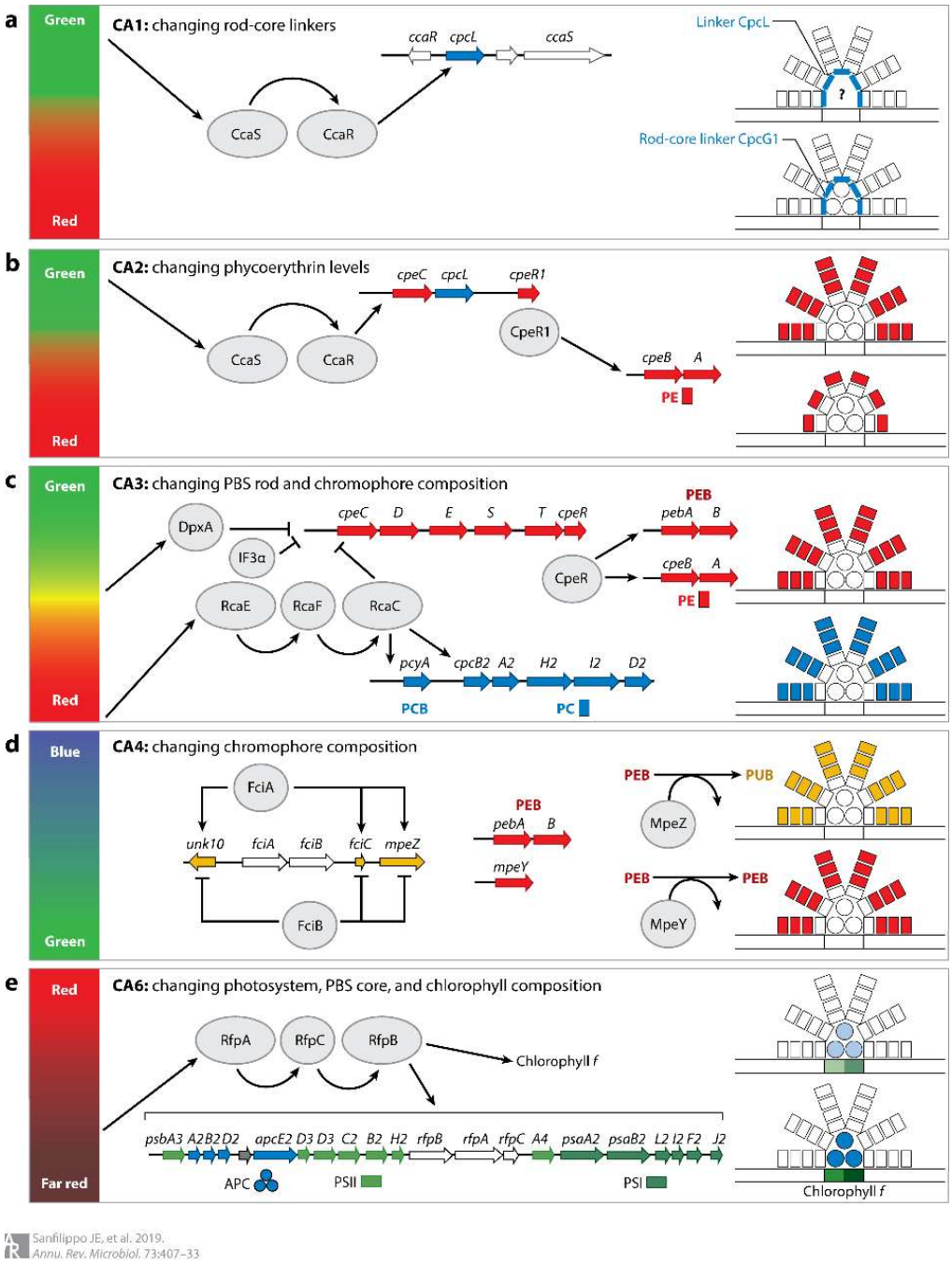

Sanfilippo JE, et al. 2019.
Annu. Rev. Microbiol. 73:407–33

Figure 9. Different types of Chromatic adaptation in cyanobacteria.

(a) CA1 group: Modifies rod-core linker proteins in the phycobilisome to enable acclimation to green and red light. (b) CA2 group: Alters phycoerythrin abundance to adjust light absorption between green and red light. (c) CA3 group: Modulates both PBS rod structure and chromophore composition, allowing adaptation to green, yellow, and red light. (d) CA4 group: Adjusts chromophore composition to facilitate acclimation to green and blue light. (e) CA6 group: Modifies photosystem organization, PBS core, and chlorophyll composition to enable adaptation to far-red light (Sanfilippo et al.,2019).

1.7.2.2 Low light Photoacclimation (LoLiP)

Low-light photoacclimation (LoLiP) that relies on the expression of specialized allophycocyanin (AP) protein subunits (Gan & Bryant, 2015) was first discovered in *Synechococcus* strains (Becraft et al., 2011). The APs are coded by a gene cluster, *apcD4-apcB3-isiX*, which is not present in the genomes of the strains that are only adapted to high light conditions. ApcD4 and ApcB3 contribute to far-red light absorption, while IsiX is expected to create a Chl a-binding protein analogous to IsiA (Olsen et al., 2015) wich is expressed in response to iron stress (Straus, 1994) or high light stress (Havaux et al., 2005). However, it has been demonstrated that proteins of the LoLiP cluster are co-transcribed and functionally interconnected; the regulation of LoLiP genes remains unclear. LoLiP-producing cells exhibit enhanced FRL harvesting, but FRL alone is insufficient to activate the transcription of LoLiP genes, which requires additional environmental factors such as oxygen concentration and irradiance level (Soulier et al.,2022)

1.7.2.3 Far-Red Light Potoacclimation (FarLiP)

Under Far-Red Light (FRL) conditions which often result from canopy shading or soil scattering, certain cyanobacteria display a sophisticated photoacclimation mechanism known as Far-Red Light Photoacclimation (FaRLiP). This process enables these organisms to use FRL for photosynthesis and growth (Gan et al., 2014). First identified in Leptolyngbya sp. JSC-1, FaRLiP has once been detected across at least six cyanobacterial orders, including *Synechococcales*, *Nostocales*, *Chroococcales*, *Chroococcidiopsidales*, *Coleofasciculales*, and *Leptolyngbyales* (Gan et al., 2014; Antonaru et al., 2020) which supports the hypothesis that this acclimation strategy either evolved early and was retained across lineages, or has been subject to horizontal gene transfer in response to selective pressure from FRL-enriched environments (Antonaru et al.,2020). This distribution spans morphologically and physiologically diverse forms, from unicellular planktonic strains (*Synechococcus sp.* PCC 7335) to filamentous, nitrogen-fixing genera (*Nostoc punctiforme*), and living a wide range of ecological niches including microbial mats, freshwater lakes, caves, and endolithic environments such as *Chroococcidiopsis thermalis* PCC 7203 (Gan and Bryant, 2015; Billi et al., 2022). Notably, strains such as *Synechococcus sp*. PCC 7335, *C. thermal*is PCC 7203, *C. fritschii* PCC 9212, and *C. fritschii* PCC 6912 demonstrate the ability to perform both LoLiP and FaRLiP (Gan and Bryant, 2015). This broad taxonomic distribution highlights the adaptive success and ecological relevance of FaRLiP in light-limited ecosystems.

Comparative genomic analyses such as sequence data mining, metagenomic assembly, and phylogenetic tree networks have revealed a conserved FaRLiP cluster comprising approximately 20 genes, depending the species, albeit exhibiting synteny variability among cyanobacteria taxa (Antonaru et al., 2024).This cluster includes *psbA4* gene, a paralog of *psbA* coding for Chl *f* synthase (Ho et al.,2016), along with several paralogous core subunits of PSI, PSII, and PBS, and transcriptional regulators such as RfpA, RfpB, and RfpC, (Ho et al 2017). FaRLiP APCs, including ApcD4 and ApcB3, along with their LoLiP counterparts, exhibit FRL absorption properties (Gan and Bryant 2015; Soulier et al., 2020). Among these, *apcE*2 is widely used as a molecular marker for Chlorophyll *f* (Antonaru et al., 2020).

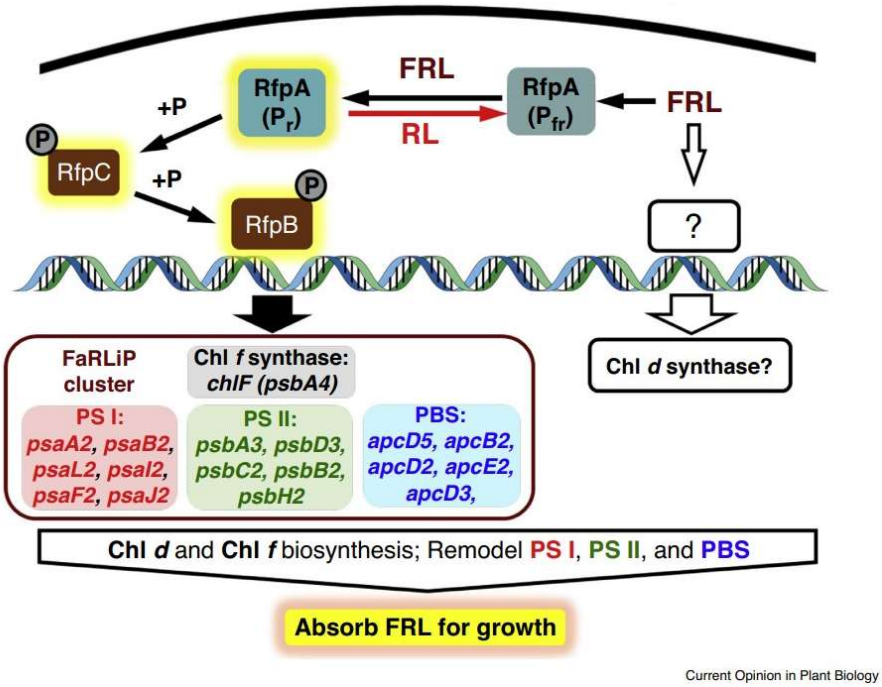

Figure 10. Schematic representation of chlorophyll *f* biosynthesis and the restructuring of the photosynthetic apparatus under far-red light (FRL) which involves a series of regulatory events. When exposed to FRL, the photoreceptor RfpA transitions from its far-red form (Pfr) to the red form (Pr), activating its histidine kinase activity. This leads to the phosphorylation of RfpC, which serves as a phosphate shuttle to phosphorylate the response regulator and transcription activator RfpB. The activation of RfpB induces the expression of genes responsible for chlorophyll biosynthesis and the reorganization of components such as Photosystem I (PSI), Photosystem II (PSII), and phycobilisomes (PBS). These regulatory pathways operate both through RfpABC-dependent mechanisms (indicated by black arrows) and RfpABC-independent routes (white arrows). It is noteworthy that while the phosphorylated form of RfpB is depicted as active, the dephosphorylated states of these proteins may also play active roles in this regulatory network. Picture and interpretation from Ho et al., 2017.

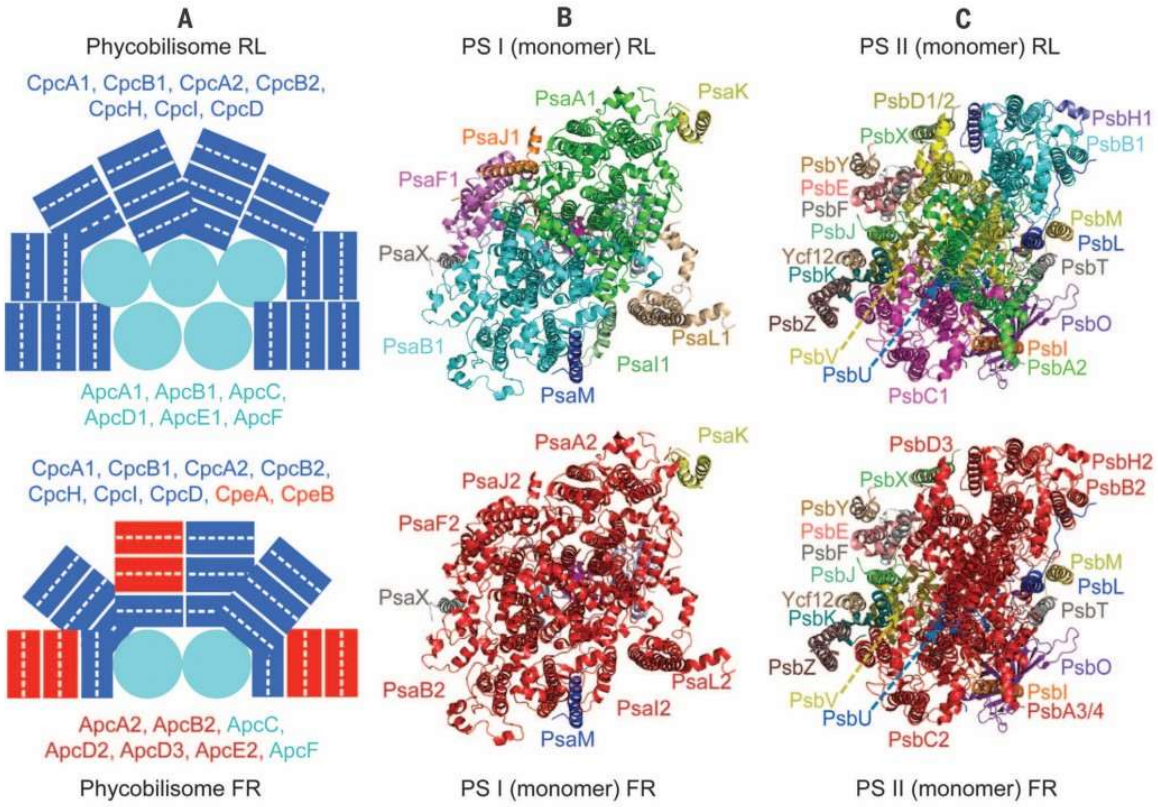

Figure 11. Remodeling of PBS core in Far red Light.

(A) Under far-red conditions, significant changes occur in PBS core substructures. Most allophycocyanin-related (shown in cyan) components of the PBS core are replaced, except for ApcF and ApcC. The linker protein ApcE1, which normally has four REP (linker) domains and assembles a pentacylindrical substructure under white, green, or red light, is replaced by ApcE2, which has only two REP domains and assembles a bicylindrical structure under FRL. Additionally, phycobilisomes in FRL environments incorporate some phycoerythrin components (represented as red disks; phycocyanin is shown in blue), although the photoconversion of the CCA photoreceptor to its green-absorbing form is inefficient under FRL (Hirose et al., 2013).

(B-C) Structural adaptations of PSI and PSII, respectively, under FRL are illustrated using their x-ray crystallographic structures. For PSI, components such as PsaC, PsaD, and PsaE (viewed from the luminal side) remain unchanged, while subunits specific to far-red conditions are modified or replaced. In PSII, viewed from the cytoplasmic side, several subunits, including Ycf12, are absent under far-red conditions. Picture and interpretation from Gan et al., 2014.

1.7.2.4 Chlorophyll f

Chlorophyll *d* and *f*, absorb light at longer wavelengths than the conventional chlorophyll a (Chen et al., 2010), with its Q-band absorption peak shifted from 665 nm to 688 and 698 nm, respectively, in 100% acetone (Figure 12). In chlorophyll f, this red-shift arises from the substitution of a 2-formyl group, replacing the 2-methyl group found in chlorophyll a (Averina et al., 2019; Pinevich & Averina, 2022). This extended absorption spectrum enables cyanobacteria to thrive in FRL-dominated environments, such as beneath dense vegetation or within microbial mats. (Gan & Bryant, 2015).

While chlorophyll d can function as the dominant pigment and act as the primary electron donor in the reaction center of *Acaryochloris* photosystems, chlorophyll *f* primarily operates as an accessory pigment (Loughlin et al., 2013). Incorporation of Chl *f* induces significant changes in energy transfer dynamics and structural organization of both photosystems. Oxidation of Chl *a* into Chl *f* seems to be triggered by PbsA4, a paralogue of D1 subunit in PSII. Although it was not evidenced *in vitro*, this paralogue of D1 subunit may be involved in the formation of "a super-rogue PSII complex" in *Chroococcidiopsis thermalis* PCC7203, which emits at 718 nm when expressed and isolated (Trinugroho et al., 2020). Chl *f* molecules act as linkers between shorter-wavelength and longer-wavelength antenna pigments in *Chroococcidiopsis thermalis* (Nürnberg et al, 2018). As shown in *Halomicronema hongdechloris* PSI, Chl *f* molecules localize at the periphery, rather than in the core, facilitating uphill energy transfer (Kato et al., 2020). Studies on *Cyanobacterium* KC1 have shown that both PSI and PSII maintain distinct reservoirs of Chl *f* molecules, which transfer energy to Chl *a* through mechanisms such as the prolonged excited state duration of Chl *f*, close spatial proximity between Chl *f* and Chl *a*, and specific binding of chlorophylls *f* to apoproteins in *H. hongdechloris* (Itoh et al., 2015; Niedzwiedzki et al., 2014).

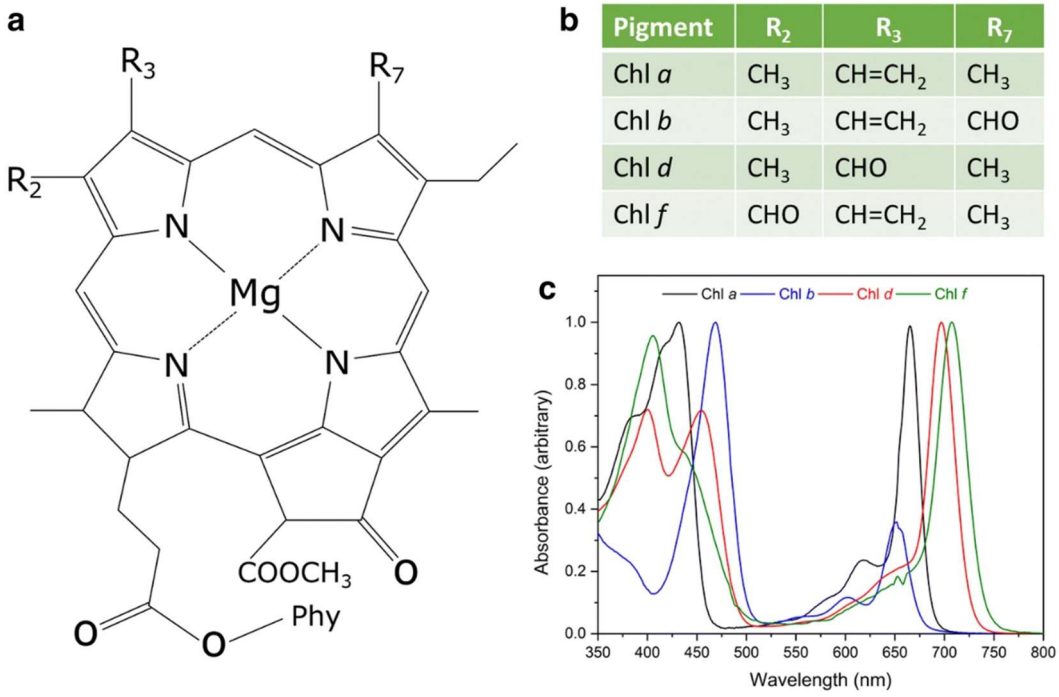

Figure 12. Structural differences of chlorophylls reflect their unique absorption signature.

The structural diversity and absorption spectra of chlorophyll molecules provide critical insights into their roles in photosynthesis. The schematic representation highlights the macrocyclic framework of chlorophyll, with labeled R groups indicating variations across different types. The specific substitutions of these R groups distinguish chlorophylls a, b, c, and d, influencing their absorption properties. Additionally, the absorption spectra of these chlorophylls, measured in pure methanol and purified using high-performance liquid chromatography (HPLC), reveal distinct peaks that correspond to their unique roles in capturing light energy. Picture from Wolf and Blankenship (2019).

1.8 Objectives

The central aim of this doctoral research is to contribute elucidating the molecular, physiological, and evolutionary mechanisms underpinning the adaptation of phototrophic organisms to far-red light (FRL, 700–750 nm). This main objective is embedded within the broader scope of the PORTAL project, which seeks to assess the potential for infrared phototrophy on exoplanets orbiting M-dwarf stars, where photon flux is dominated by infrared radiation.

The specific objectives of this thesis are as follows:

1. **To determine the extent and distribution of far-red photoacclimation across the taxonomic diversity of phototrophic eukaryotes.**

Despite detailed characterization of FaRLiP in a limited number of cyanobacterial species, little is known about whether similar adaptive responses are present in eukaryotic algae. To address this gap, a large-scale physiological screening of microalgal strains spanning diverse phylogenetic lineages was undertaken. This approach seeks to evaluate whether FRL acclimation is a widespread capability or restricted to a few lineages, and to identify novel model systems for deeper investigation.

2. **To dissect the genomic and regulatory architecture of FaRLiP systems in cyanobacteria.**

Previous work has identified gene clusters associated with FRL-induced photosystem remodeling in a few model strains. However, the evolutionary diversity of these genetic modules and the potential existence of uncharacterized variants remain unresolved. A detailed molecular analysis of selected cyanobacterial strain was designed to elucidate the structure, conservation, and regulation of FaRLiP-associated genes. This objective addresses the need to understand the diversity of strategies cyanobacteria have evolved to harvest FRL, and how these might differ in basal or morphologically distinct taxa.

3. **To investigate the molecular basis of far-red light harvesting in eukaryotic phototrophs, with a focus on light -harvesting antenna complexes**.

While FaRLiP has been studied in cyanobacteria, analogous mechanisms in eukaryotic algae remain largely unexplored. Some eukaryotic taxa exhibit pigment compositions or antenna organizations suggestive of adaptations to extended light spectra. Through targeted genetic manipulation, spectroscopic characterization, pigment profiling, and proteomic analyses of selected eukaryotic species, this research aims to identify the molecular innovations that efficient energy capture under FRL. These insights could reveal alternative evolutionary solutions to the challenges of low-energy photon utilization.

Collectively, these objectives aim to expand current knowledge on the diversity and adaptability of photosynthetic systems under far-red light, and to uncover the underlying genetic and biochemical innovations that support life under extended light regimes.

Results

2 Screening of Microalgae for Far-Red Light Acclimation.

2.1 Introduction

Far-red light adaptation has been documented in multiple species, including *Chromera velia*, *Phaeodactylum tricornutum*, and *Trachydiscus minutus*, suggesting that this trait is not confined to a single phylum (Kotabová et al.,2014; Herbstova et al., 2015; Litvín, et al., 2019). Given its ecological advantages across diverse environments, this study hypothesizes that far-red acclimation is a widespread trait among eukaryotic microalgae, possibly evolving through convergent or divergent mechanisms.

To test this, we conducted a broad screening of microalgae spanning multiple evolutionary lineages, addressing the following key questions:

- How prevalent is far-red light acclimation among eukaryotic microalgae?
- Do microalgae from related evolutionary lineages exhibit distinct spectral adaptations?
- What criteria can be used to select model organisms for further characterization of far-red light adaptation?

The results of this screening will provide a foundation for future characterization of far-red acclimation in microalgae.

2.2 Materials and Methods

2.2.1 Sample Selection and Cultivation

With access to the extensive microalgal resources of the Laboratory of Genetics and Physiology of Microalgae at the University of Liège and collaborators, we screened approximately 120 microalgae strains from diverse phylogenetic backgrounds. Strains were obtained from the Roscoff Culture Collection (RCC), Sammlung von Algenkulturen (SAG), and the Culture Collection of Autotrophic Organism (CCALA). These strains spanned 14 different orders from all the phylla, ensuring a broad taxonomic representation.

Each strain has its own specific culture medium, optimal temperature, and irradiance level, reported by their culture collection, as detailed in Table 1. However, applying the precise optimal temperature and irradiance was not always possible due to technical issues.

2.2.2 Experimental Conditions

Microalgae were cultivated under three light conditions for 10 days at 23°C : Far-red light (700–720 nm), Full-spectrum light (control) and Darkness (to distinguish light-dependent effects). Full-spectrum and far-red light intensities were set at 25 µmol photon. $m^{-2}.s^{-1}$. Emission spectra on supplementary figure 1 from chapter 2.

2.2.3 Spectrofluorometry**

In vivo absorbance spectra were acquired from cell suspensions at room temperature using a BLUE-Wave Miniature Spectrometer (StellarNet Inc., Tampa, FL, USA) in conjunction with a tungsten halogen lamp SL1 with a broad spectral range of 350-2500 nm and an SL1-BLUE lamp with a blue LED (470 nm).In vivo fluorescence spectra were obtained at room temperature (23°C) and 77 K with an excitation wavelength of 470 nm using a USB2000+ Ocean Optics spectrometer (Ocean Optics Inc., Dunedin, FL, USA) coupled with a LightBox CCD (Beambio, France).

2.3 Results and Discussion

2.3.1 Absorbance Spectra Analysis

A total of 120 microalgal strains were cultivated, though not all achieved sufficient growth to yield adequate and reliable spectral data. Strains that were acclimated under far-red light, full-spectrum light, and darkness for approximately 10 days. Strains with absorbance spectra similar to those under full-spectrum light were considered non-responsive to far-red light, while those resembling the dark condition were classified as showing no specific far-red response.

Of the 120 strains, 80 produced satisfying absorbance spectra. Among them, thirteen exhibited a distinct shoulder in the 700–720 nm range under far-red light. Difference spectra were calculated by subtracting the far-red light spectrum from the full-spectrum light spectrum.

Notably, *Phaeodactylum tricornutum* exhibited a pronounced shift around 710 nm, consistent with its known, red-shifted chlorophyll antennae (Herbstova et al., 2015). *Chromera velia*, another previously documented far-red light adapter, displayed a distinct shoulder around 700 nm (Kotabová et al.,2014). These two positive controls, *Phaeodactylum tricornutum* and *Chromera velia*, confirmed the reliability of the spectral analysis in detecting red-shifted chlorophyll antennae.

Additionally, *Phaeomonas sp.* and *N. salinosa* displayed a similar to the positive controls but less pronounced shift. The cyanobacterium *Cyanophyceae sp. RCC 5179* exhibited a constitutive shoulder, likely due to the presence of chlorophyll d or f. Other strains, including *Porphyridium sp.*, *Thalassiosira pseudonana*, *Micromonas salina*, *F. pinata*, *Chlamydomonas reinhardtii*, *Tribonema aequale*, and *Euglena gracilis*, showed smaller shifts around 700 nm.

Interestingly, *Vitrella brassicaformis* exhibited a constitutive shoulder around 700 nm, making it the only eukaryotic organism with this trait, previously documented only in cyanobacteria.

Absorbance Screening :

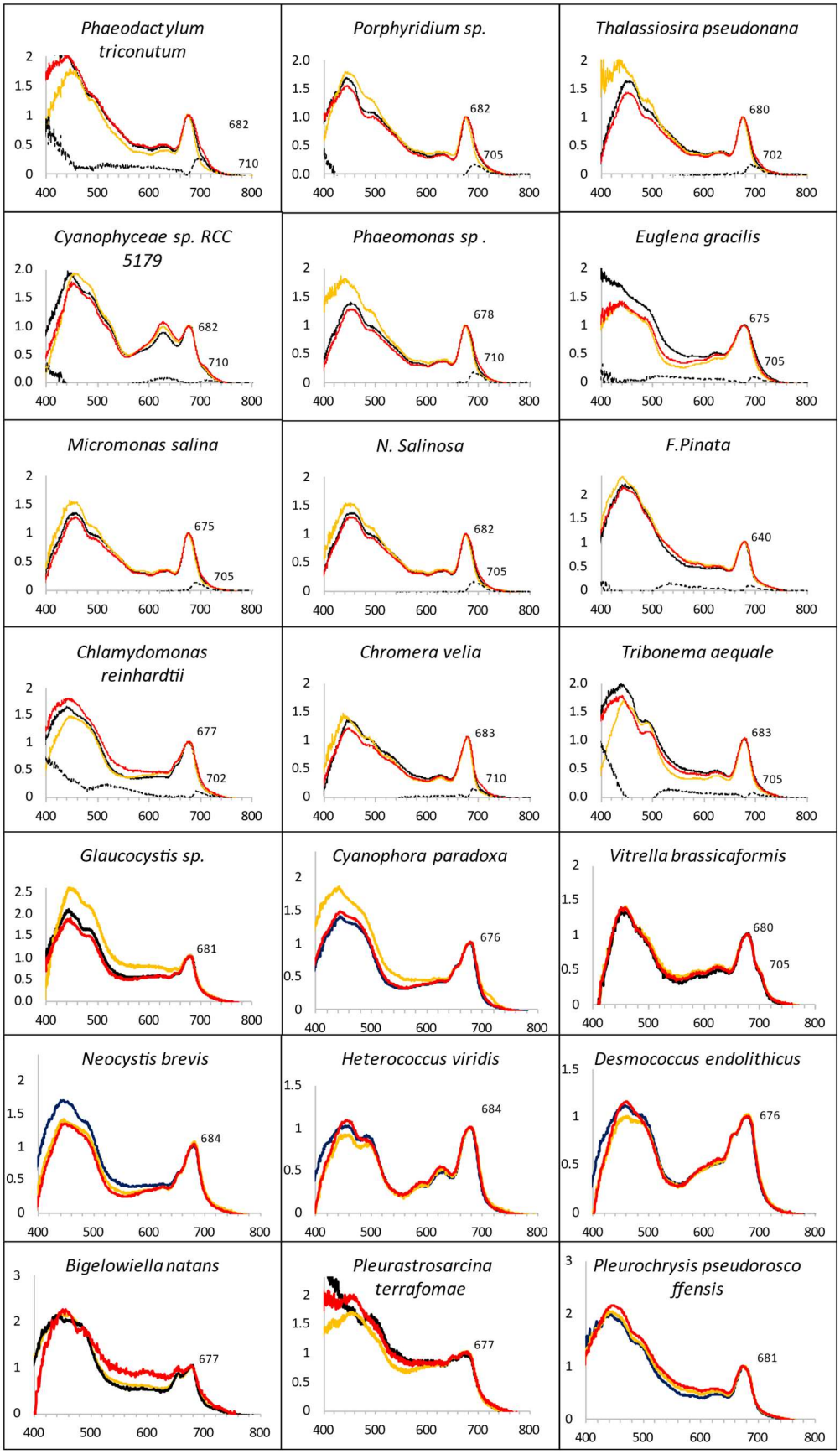

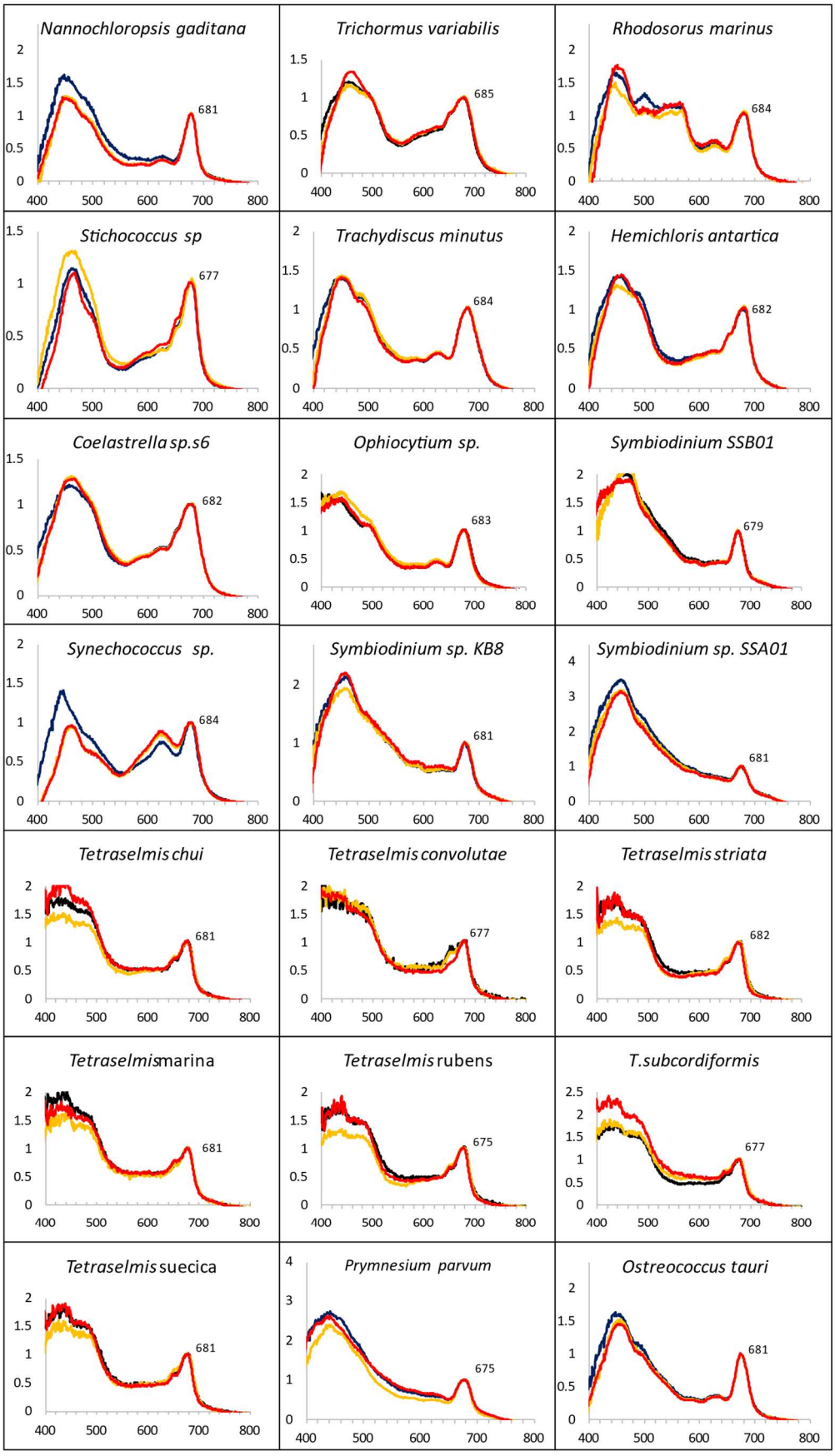
Nannochloropsis gaditana
681
Trichormus variabilis
685
Rhodosorus marinus
684
Stichococcus sp
677
Trachydiscus minutus
684
Hemichloris antartica
682
Coelastrella sp.s6
682
Ophiocytium sp.
683
Symbiodinium SSB01
679
Synechococcus sp.
684
Symbiodinium sp. KB8
681
Symbiodinium sp. SSA01
681
Tetraselmis chui
681
Tetraselmis convolutae
677
Tetraselmis striata
682
Tetraselmis marina
681
Tetraselmis rubens
675
T.subcordiformis
677
Tetraselmis suecica
681
Prymnesium parvum
675
Ostreococcus tauri
681

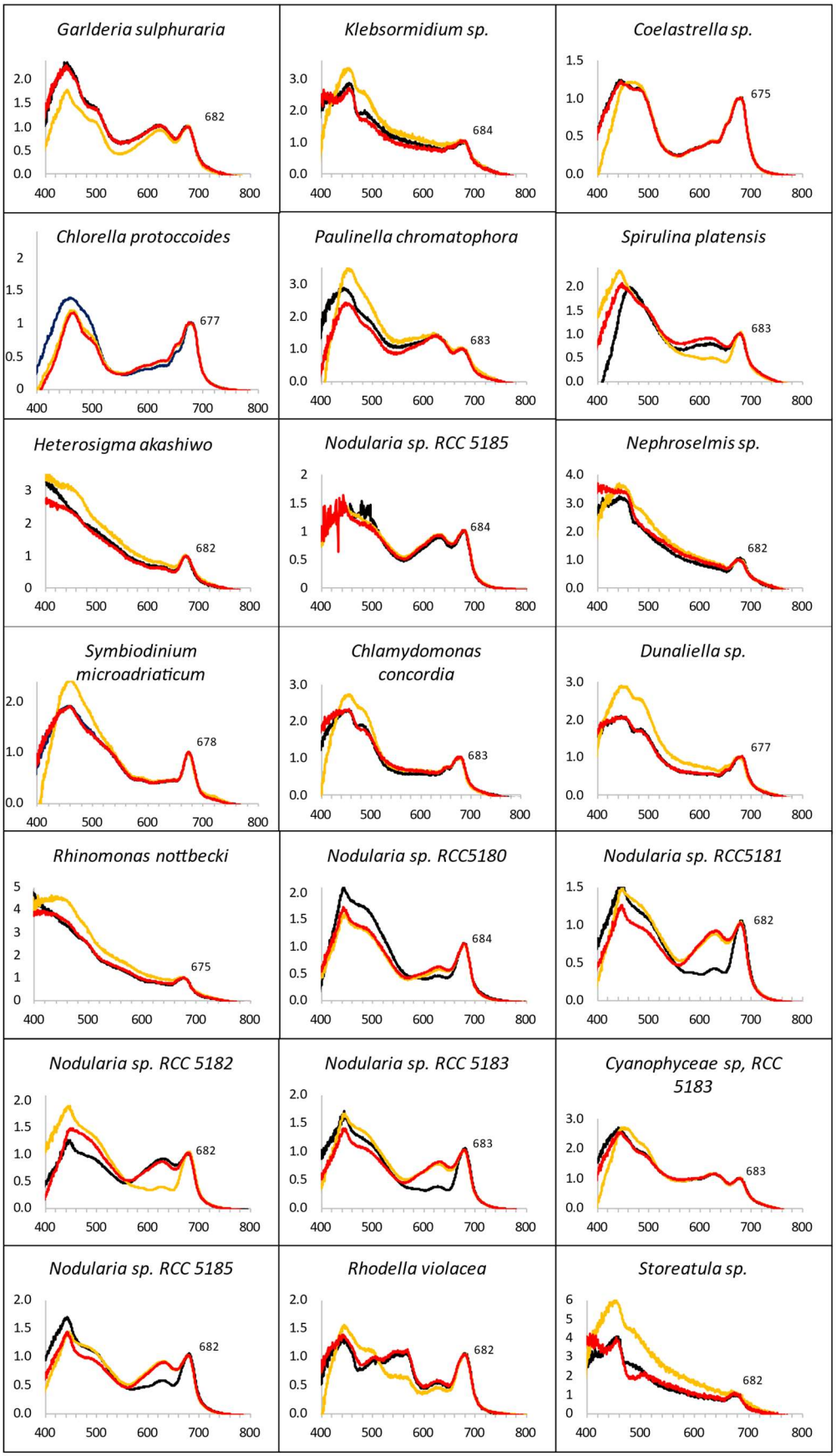
Garlderia sulphuraria
682
Klebsormidium sp.
684
Coelastrella sp.
675
Chlorella protoccoides
677
Paulinella chromatophora
683
Spirulina platensis
683
Heterosigma akashiwo
682
Nodularia sp. RCC 5185
684
Nephroselmis sp.
682
Symbiodinium microadriaticum
678
Chlamydomonas concordia
683
Dunaliella sp.
677
Rhinomonas nottbecki
675
Nodularia sp. RCC5180
684
Nodularia sp. RCC5181
682
Nodularia sp. RCC 5182
682
Nodularia sp. RCC 5183
683
Cyanophyceae sp, RCC 5183
683
Nodularia sp. RCC 5185
682
Rhodella violacea
682
Storeatula sp.
682

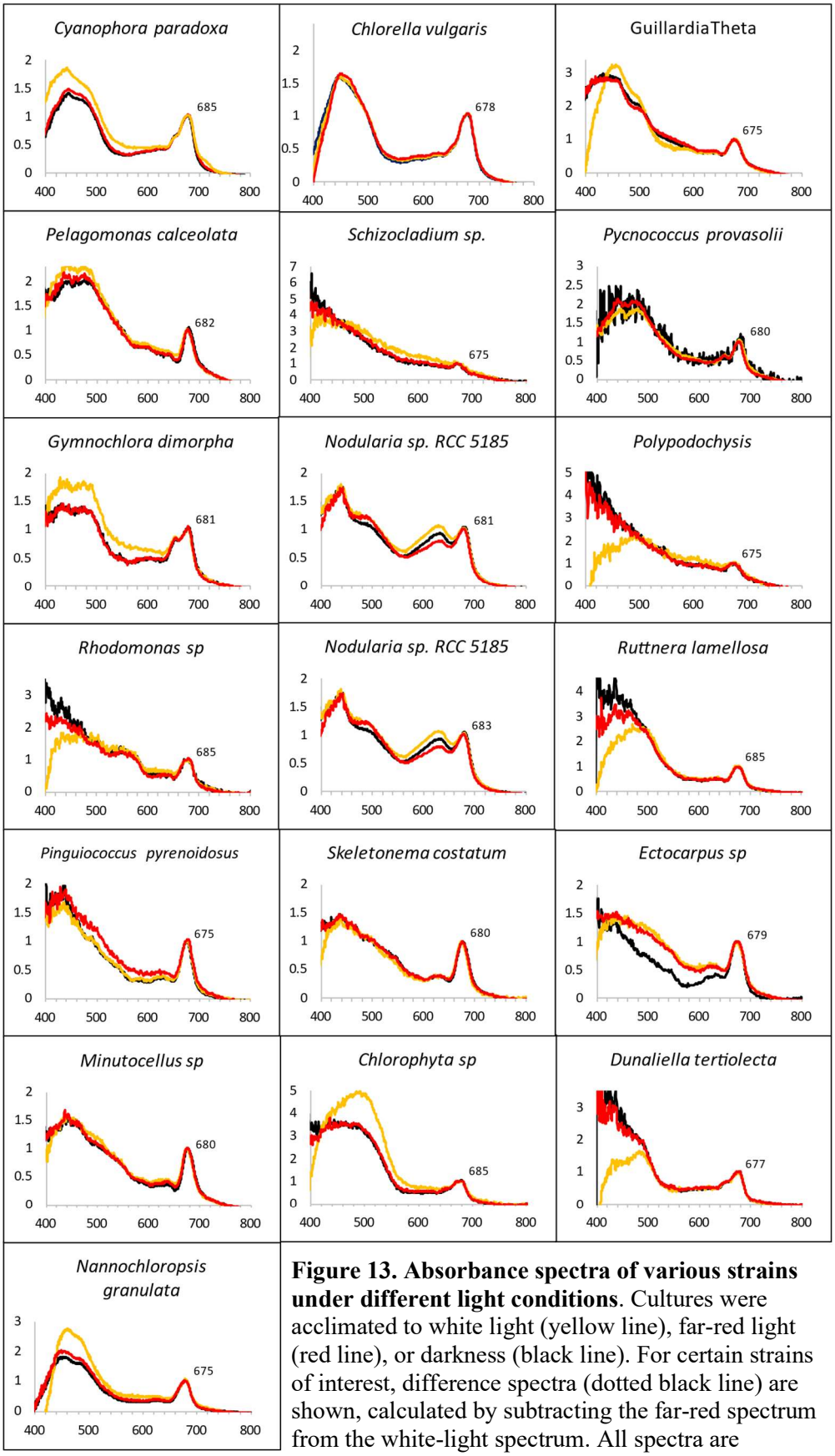

Figure 13. Absorbance spectra of various strains under different light conditions. Cultures were acclimated to white light (yellow line), far-red light (red line), or darkness (black line). For certain strains of interest, difference spectra (dotted black line) are shown, calculated by subtracting the far-red spectrum from the white-light spectrum. All spectra are normalized to their maximum within 660–690 nm, and absorbance is plotted against wavelength

2.3.2 Fluorescence Spectroscopy

67 of the 82 strains produced sufficient biomass for analysis room-temperature fluorescence. Most of them did not shown any differences but five exhibited an additional shifted fluorescence peak compared to the WL peak. As anticipated, *Chromera velia* and *Phaeodactylum tricornutum* displayed a secondary fluorescence emission around 715 nm. Interestingly, *Glaucocystis sp.* also presented a secondary peak, despite showing no pronounced difference in its absorbance spectrum.

While *Euglena gracilis* and *Vitrella brassicaformis* did not show major spectral differences, their principal fluorescence peak appeared around 710 nm, alongside another peak near 685 nm.

Low-temperature (77K) fluorescence measurements were performed on 59 strains, revealing notable emission changes in seven strains. Consistent with previous observations, *Chromera velia* and *Phaeodactylum tricornutum* displayed an additional fluorescence peak at about 715 nm (Kotabová et al.,2014; Herbstova et al., 2015). Surprisingly, several microalgae (including *Phaeomonas sp.*, *Ostreococcus tauri*, *Thalassiosira pseudonana*, *N. salinosa*, and *Microchloropsis salina* etc.) exhibited a comparable fluorescence shift from approximately 685 nm to 715 nm. In darkness, these strains exhibited shifts similar to those observed under FRL conditions; however, their interpretation remains complex and requires further investigation. Modulation of the PSI:PSII stoichiometry, resulting from changes in perceived light intensity, could induce this shift (Chow et al., 1990; Palombi et al., 2011). Alternatively, it may be attributed to the transfer of excitation energy from Photosystem II (PSII) to Photosystem I (PSI), a phenomenon known as spillover (Akhtar et al., 2024). Fluorescence emission around 715nm could also be the result of the presence of a red form of chlorophyll *a* (Kotabova et al., 2014).

Room Temperature Fluorescence Screening :

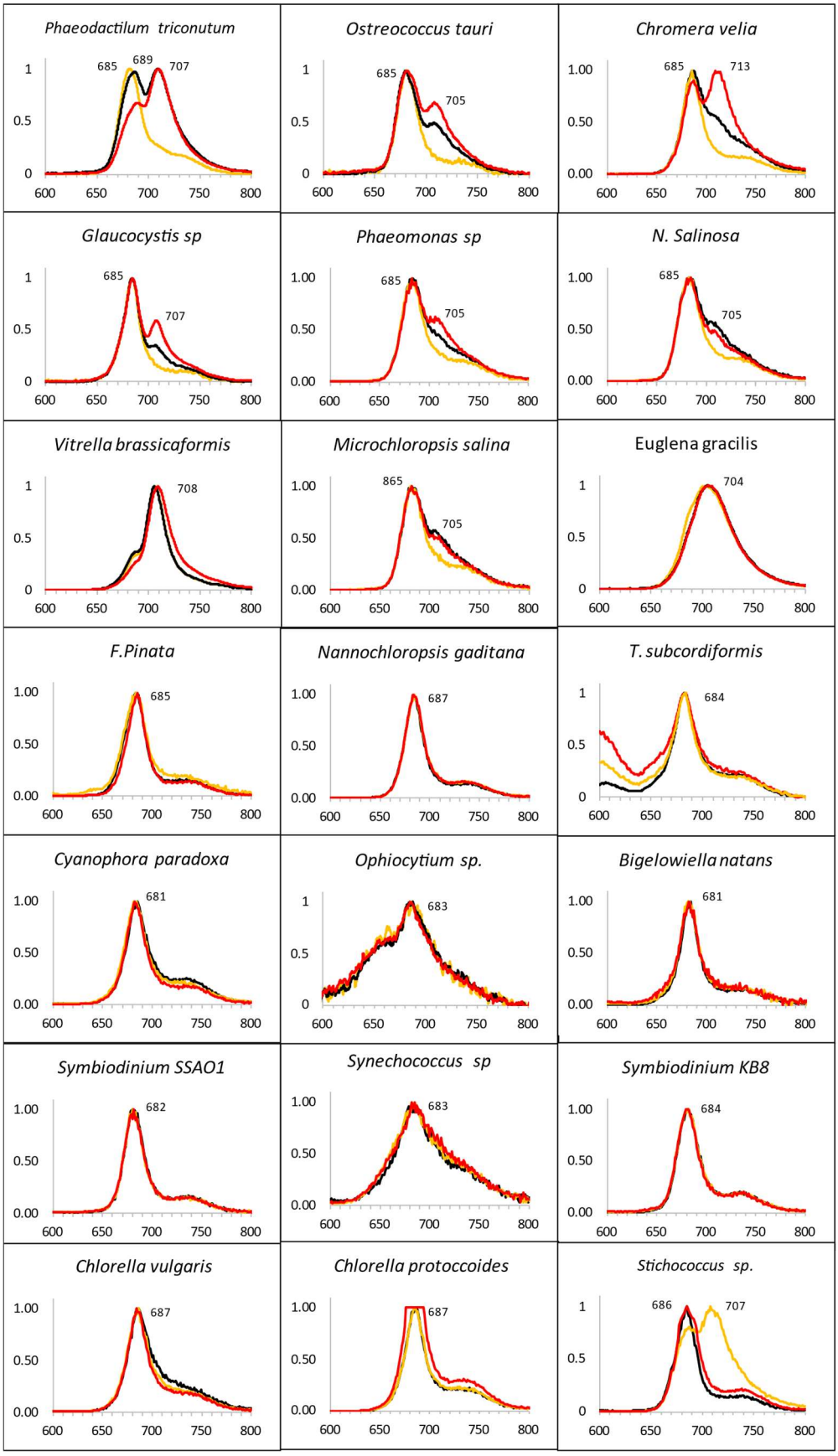

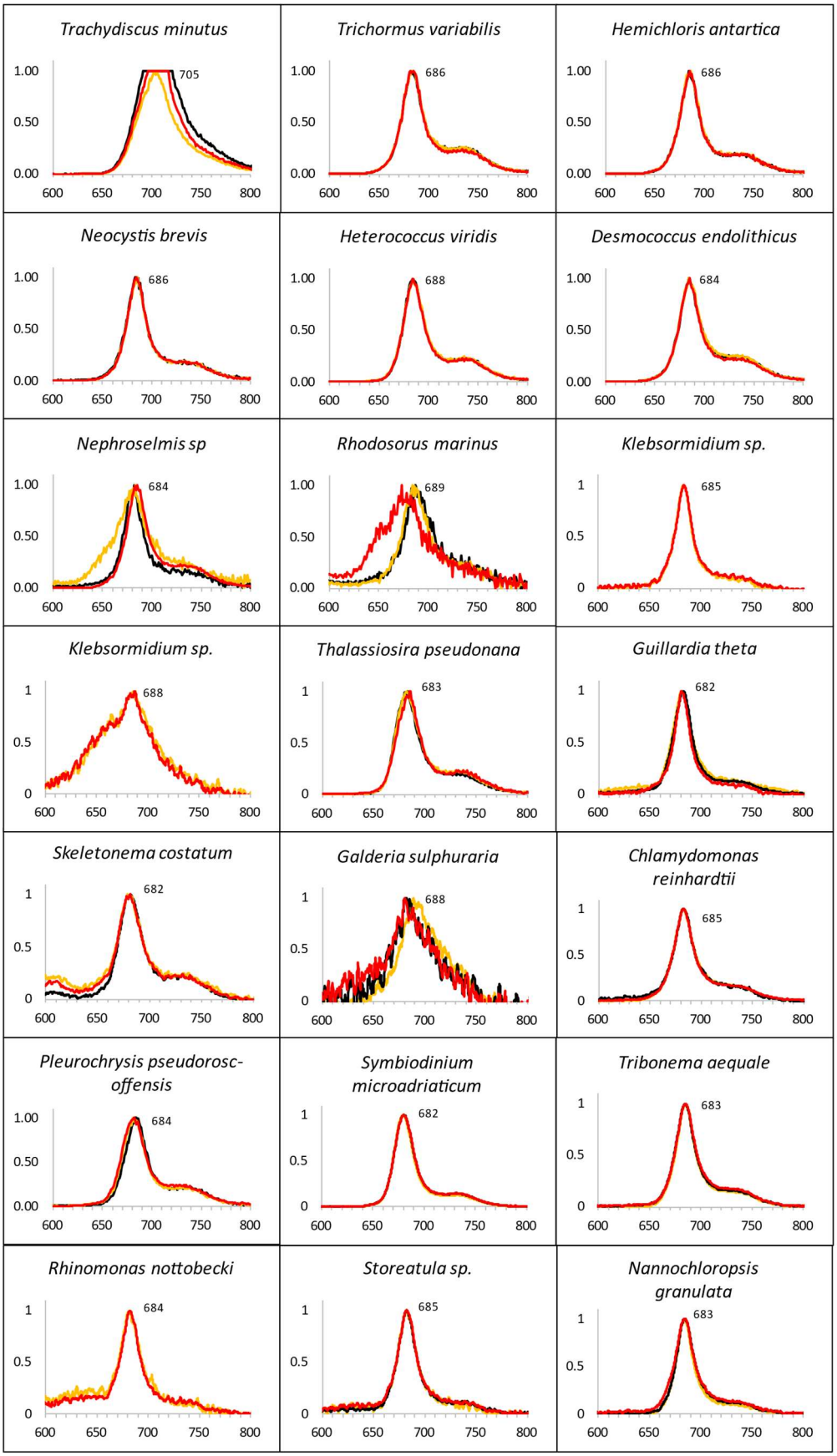
Trachydiscus minutus
705
Trichormus variabilis
686
Hemichloris antartica
686
Neocystis brevis
686
Heterococcus viridis
688
Desmococcus endolithicus
684
Nephroselmis sp
684
Rhodosorus marinus
689
Klebsormidium sp.
685
Klebsormidium sp.
688
Thalassiosira pseudonana
683
Guillardia theta
682
Skeletonema costatum
682
Galderia sulphuraria
688
Chlamydomonas reinhardtii
685
Pleurochrysis pseudorosc-offensis
684
Symbiodinium microadriaticum
682
Tribonema aequale
683
Rhinomonas nottobecki
684
Storeatula sp.
685
Nannochloropsis granulata
683

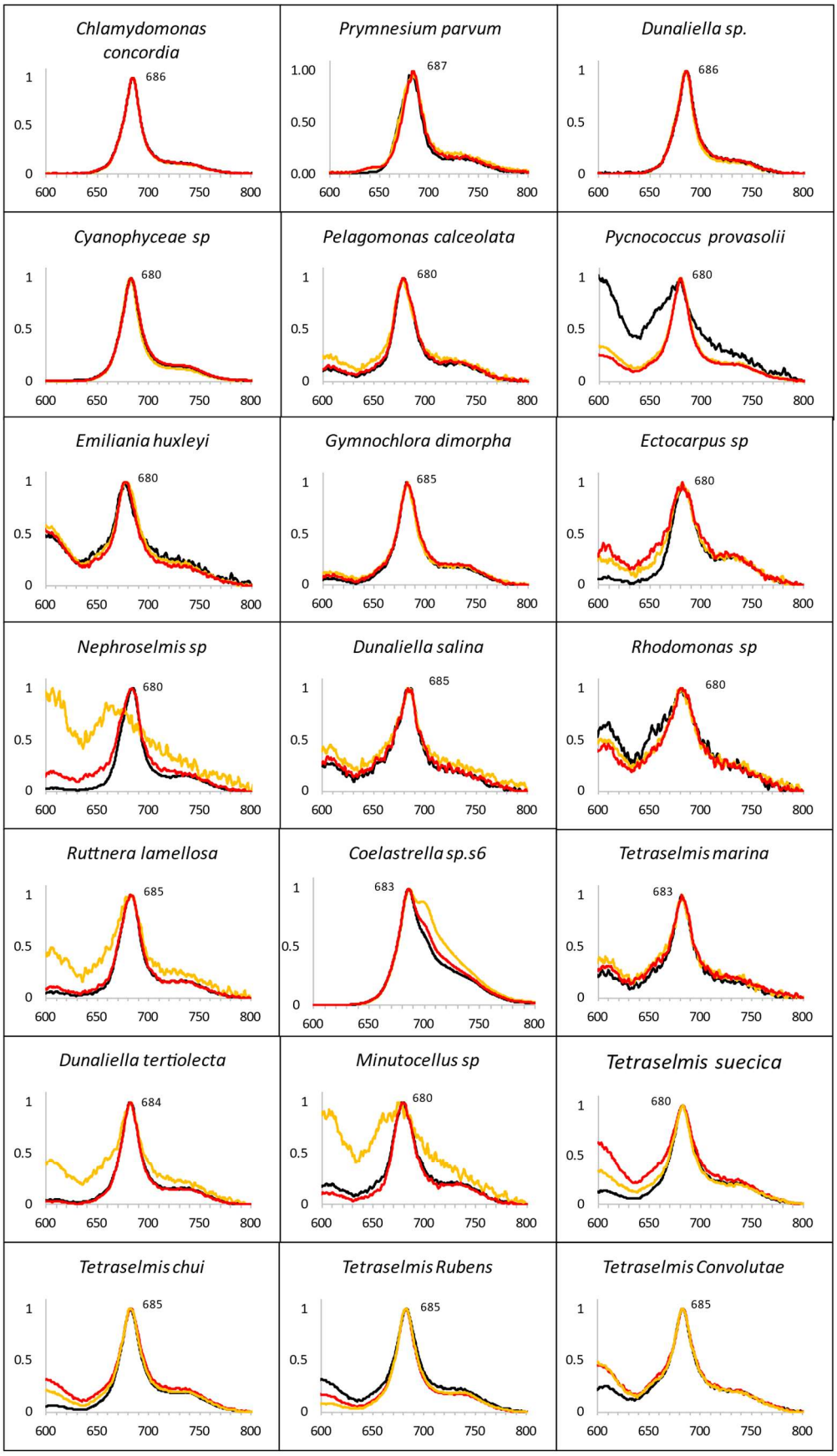
Chlamydomonas concordia
686
Prymnesium parvum
687
Dunaliella sp.
686
Cyanophyceae sp
680
Pelagomonas calceolata
680
Pycnococcus provasolii
680
Emiliania huxleyi
680
Gymnochlora dimorpha
685
Ectocarpus sp
680
Nephroselmis sp
680
Dunaliella salina
685
Rhodomonas sp
680
Ruttnera lamellosa
685
Coelastrella sp.s6
683
Tetraselmis marina
683
Dunaliella tertiolecta
684
Minutocellus sp
680
Tetraselmis suecica
680
Tetraselmis chui
685
Tetraselmis Rubens
685
Tetraselmis Convolutae
685

77K Fluorescence Screening :

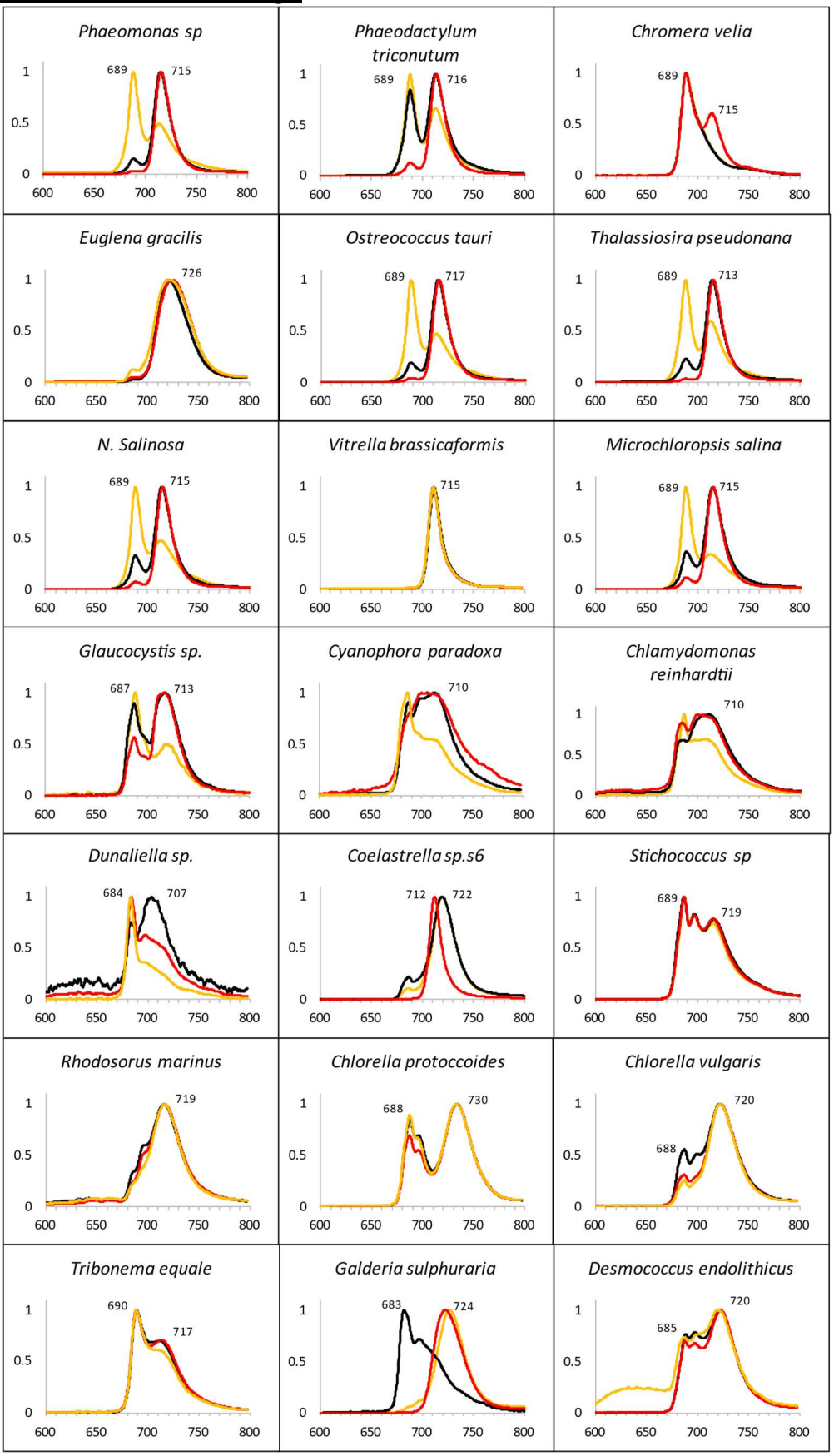

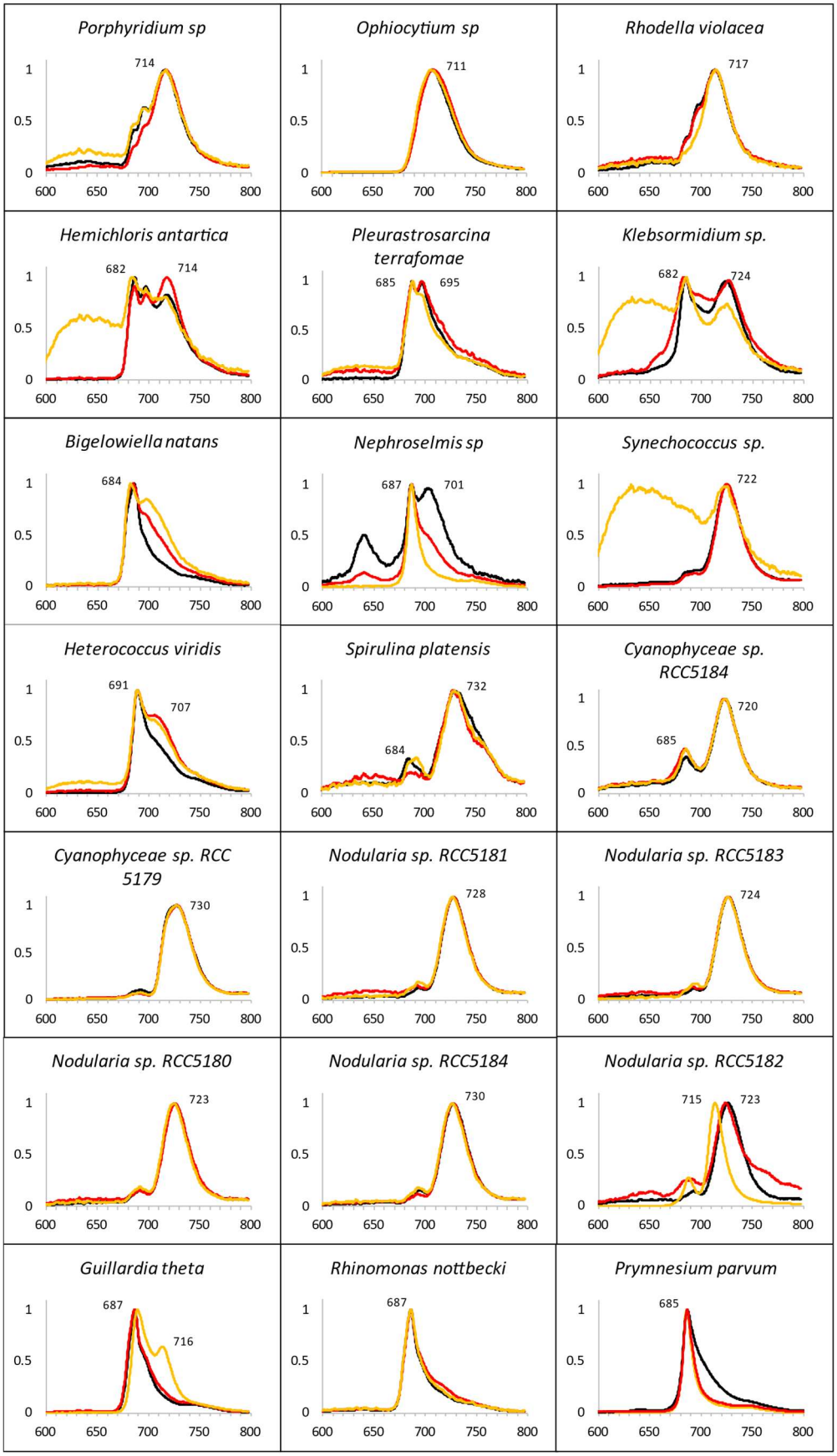
Porphyridium sp
714
Ophiocytium sp
711
Rhodella violacea
717
Hemichloris antartica
682
714
Pleurastrosarcina terrafomae
685
695
Klebsormidium sp.
682
724
Bigelowiella natans
684
Nephroselmis sp
687
701
Synechococcus sp.
722
Heterococcus viridis
691
707
Spirulina platensis
684
732
Cyanophyceae sp. RCC5184
685
720
Cyanophyceae sp. RCC 5179
730
Nodularia sp. RCC5181
728
Nodularia sp. RCC5183
724
Nodularia sp. RCC5180
723
Nodularia sp. RCC5184
730
Nodularia sp. RCC5182
715
723
Guillardia theta
687
716
Rhinomonas nottbecki
687
Prymnesium parvum
685
1
0.5
0
600
650
700
750
800

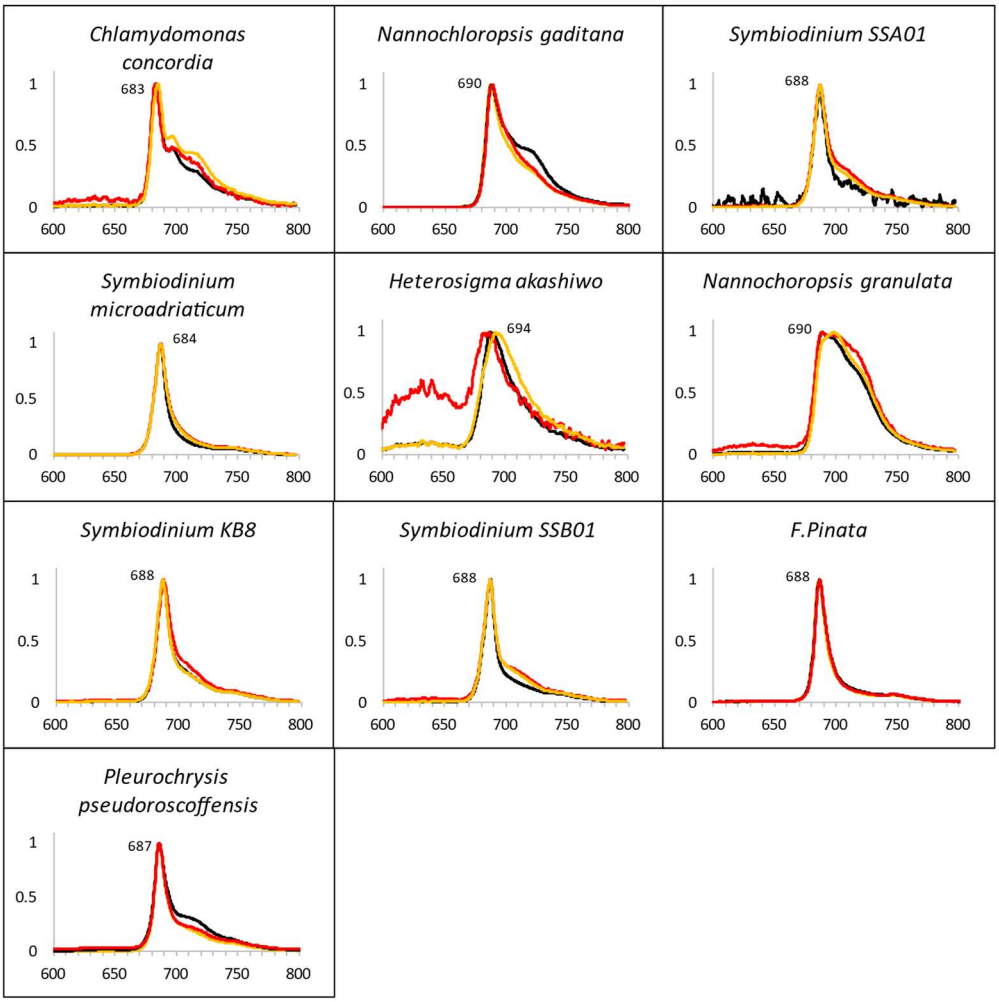

Figure 14. Fluorescence spectra of various strains under different light conditions.

(A) Room-temperature (R.T.) fluorescence and (B) 77K fluorescence spectra for cultures acclimated to white light (yellow line), far-red light (red line), and darkness (black line). Each spectrum is normalized to its maximum intensity, with fluorescence plotted against wavelength (nm).

2.3.3 Selection of Organisms of Interest

Selecting microalgae for further study was challenging due to the large number of microalgae that exhibited interesting spectral characteristics. To maximize the exploration of diverse far-red acclimation strategies, well-studied species were deprioritized in favor of less-characterized candidates.

Previous findings suggest that *Euglena gracilis* may possess an adaptation to far-red light, making it a valuable candidate for refining experimental approaches.

Despite its slow growth rate and tendency to form aggregates, *Vitrella brassicaformis* is remarkable, due to its constitutive absorption of wavelengths up to 700 nm, a trait previously only in cyanobacteria. This makes *Vitrella brassicaformis* the only known eukaryote to have evolved or retained this capability. Given the phylogenetic relationship between *Chromera velia* and *Vitrella brassicaformis*, the two strains will be studied in parallel to facilitate comparisons.

Due to time constraints, selecting more than three organisms was not feasible. To broaden the comparative framework, a cyanobacterium was included. *Stranieria cyanosphaera* SAG 33.87 was chosen for its absorbance shoulder developpement at 710 nm, which was absent in darkness, minor under standard light, and most pronounced under far-red light. This characteristic makes it a compelling subject for further analysis.

2.4 Conclusion

This study provides strong evidence that far-red acclimation is not confined to a single phylogenetic group but rather manifests in species across different taxa. The screening results indicate that while some species exhibit regulated responses to far-red light, others, such as *Vitrella brassicaformis*, possess constitutive mechanisms for absorbing these wavelengths. This screening shows that increase of absorbance above 700 nm combined with emission of fluorescence above 700 nm is relevant to detect acclimation of microalgae and cyanobacteria.

Further characterization will combine in vivo biophysical and physiological approaches to assess functional acclimation to far-red light. Additionally, in vitro characterization of isolated pigment-protein complexes will be conducted to determine which specific complexes are involved in far-red adaptation. These complementary approaches will offer deeper insight into the mechanisms underlying far-red light utilization in eukaryotic microalgae. By selecting *Vitrella brassicaformis*, *Euglena gracilis*, and *Stranieria cyanosphera* as model organisms, this study lays the foundation for detailed physiological and genetic investigations into the mechanisms driving far-red acclimation in microalgae.

List of Strains:

Accession n°	Genre Espèce	Medium	Temperature	Light (µE)	Gowth	Absorbance	R.T. Fluo	77K Fluo
RCC337	*Bigelowiella natans*							
RCC 1	*Chlamydomonas concordia*	K	20	100				
SAG 11-31	*Chlamydomonas reinhardtii*	TMP		50				
SAG 211-10a	*Chlorella protoccoides*	TMP	23					
SAG 211-8b	*Chlorella pyrenoidosa*	TMP						
SAG 2606	*Chlorella vulgaris*	TMP	23					
RCC 6704	*chlorophyta x*							
P18-065	*Chloropican sp.*							
CCMP 2878	*Chromera velia*	F/2	23					
RCC 6336	*Chromera velia*	K/2:ES	22	50				
RCC 1504	*Chroomonas sp*	K/2-L1	17-20	25-100				
RCC 3436	*Chroomonas sp*	K/2	17	50				
RCC 656	*Chrysochromulina sp*	K	20	100				
RCC 6172	*Chrysocystis fragilis*	K/2:ES	22	50				
SAG 2123	*coelastrella sp*	BBM	23					
SAG2123	*Coelastrella sp.s6*							
RCC 6731	*Cyanophora paradoxa*	BG11						
SAG29.80	*Cyanophora paradoxa*	MN						
RCC 5177	*Cyanophyceae XXX sp.*	BG11	22	100				
RCC 5179	*Cyanophyceae XXX sp.*	BG11	22	100				
RCC 5184	*Cyanophyceae XXX sp.*	BG11	22	100				
RCC 6386	*Cyanophyceae XXX sp.*							
SAG4	*Desmococcus endolithicus*	3NBBM +v						
RCC 3579	*Dunaliella salina*	K/2	17	25				
RCC 5172	*Dunaliella sp*	L1	22	100				
RCC 6687	*Dunaliella tertiolecta*	K	17	100				
RCC 2963	*Ectocarpus sp*	K	20	100				
RCC 1216	*Emiliania huxleyi*	K/2	17					
SAG 1224-4/25	*Euglena gracilis*	TMP						
RCC 6327	*Eutreptiella braarudii*		20	25				
CCAP 1029/2	*F.Pinnata*	F/2	18					
SAG 107.79	*Galderia sulphuraria*	Allen						
SAG 45.88	*Glaucocystis*	F/2	26					
CCMP2712	*Guillardia theta*							
RCC 1935	*Gymnochlora dimorpha*	k	20	100				
SAG3	*Hemichloris antartica*	ESP Ag / TOM Ag	<20°					
RCC 3575	*Hemiselmis cf virescens*	K/2	17	25				
RCC 3596	*Heterocapsa triquetra*	K/2 -F/2	15					
SAG1	*Heterococcus viridis*	3NBBM + v Ag	antartica					
RCC 1502	*Heterosigma akashiwo*	K/2	17	25				
SAG 2107	*Klebsormidium sp.*	TMP						
SAG 40.85	*Microchloropsis salina*	F/2	18					
RCC 703	*Minutocellus sp*	K+si	20	4				
RCC 6168	*Mougeotia sp*	BG11	15	25				
SAG 4085	*N. Salinosa*	F/2	18					
SAG 2.99	*Nannochloropsis gaditana*	F/2	18					
RCC 8	*Nannochoropsis granulata*	F/2	20	100				
CCALA 393	*Neocystis brevis*	BBM	Soil					
RCC 1503	*Nephroselmis sp*	K/2	17	25				
RCC 1805	*Nephroselmis sp*	K/2	20					
RCC 6847	*Nephroselmis sp*	L1	15	40				
RCC 5180	*Nodularia sp.*	BG11	atacama desert	100				
RCC 5181	*Nodularia sp.*	BG11	atacama desert	100				
RCC 5182	*Nodularia sp.*	BG11	atacama desert	100				
RCC 5183	*Nodularia sp.*	BG11	atacama desert	100				
RCC 5185	*Nodularia sp.*	BG10	atacama desert	100				
RCC 21	*Ochromonas triangulata*	F/2	20	100				
RCC 6193	*Ophiocytium sp*	BG11	15	25				
RCC 1115	*Ostreococcus tauri*	F/2	18					
RCC 745	*Ostreococcus tauri*	K	20	100				
CCAC 0185B	*paulinella chromatophora*	walish						

RCC 3430	*Pavlomulina ranunculiformis*	K/2:ET	15	50				
RCC 437	*Pavlova sp*	ES	20	100				
RCC 100	*Pelagomonas calceolata*	K	20	4				
RCC 940	*Phaeocystis globosa*	K/2:ET	15	50				
RCC 69	*Phaeodactilum triconutum*	F/2						
RCC 69	*Phaeodactylum tricornutum*	K+si	20	100				
RCC 6335	*Phaeomonas parva*	K/2	20	25				
RCC4482	*Phaeomonas sp*	F/2	18					
RCC 621	*Pinguiococcus pyrenoidosus*	F/20	22	50				
SAG2	*Pleurastrosarcina terrafomae*	3NBBM + v Ag	atacama desert					
RCC 6315	*Pleurochrysis pseudoroscoffensis*	F/2	18					
NiES3941	*Polypodochysis*							
RCC 2962	*Porphiridium sp*							
RCC 2962	*Porphyridium sp*	K	20	100				
P18-098	*Prasinococcus*	k	22					
RCC 137	*Prasinoderma coloniale*	K	20	100				
CCALA 1053	*Prasiola crispa*	BBM	terrestre					
RCC 1505	*Proteomonas sulcata*	K/2	17	25				
RCC 3574	*Proteomonas sulcata*	K/2	17	25				
SAG 127.79	*Prymnesium parvum*	F/2	18					
RCC 135	*Pycnococcus provasolii*	K	20	100				
RCC 6444	*Rhinomonas nottbecki*							
RCC 6310	*Rhodella violacea*	k/2	15	25				
RCC 1506	*Rhodomonas salina*	K/2	17	25				
RCC 1507	*Rhodomonas salina*	K/2	17	25				
RCC 20	*Rhodomonas salina*	K	20	100				
RCC 6434	*Rhodomonas salina*							
RCC 4444	*Rhodomonas sp*	K	22	100				
RCC 6297	*Rhodomonas sp*		22	50				
RCC 6691	*Rhodosorus marinus*	K/2	15	25				
RCC 6196	*Ruttnera lamellosa*	ES	17	25				
NIES1044	*Schizocladium sp.*	k	20					
RCC 70	*Skeletonema cf costatum*	K+si	20	100				
SP2	*Spirulina platensis*							
CCALA 809	*Stichococcus sp*	BBM	snow					
RCC 6329	*Storeatula sp*	K/2	22	50				
CCMP 832	*Symbiodinium KB8*	F/2	26					
RCC 4020	*Symbiodinium microadriaticum*	F/2	22	100				
CCMP 3757	*Symbiodinium SSA01*	F/3	26					
CCMP 3573	*Symbiodinium SSB01*	F/2	26					
SAG 1402-1	*Synechococcus sp.*	BG11	23 ?					
RCC 6441	*Teleaulax acuta*		15					
RCC 128	*Tetraselmis chui*	F/2	18					
RCC 1563	*Tetraselmis Convolutae*	F/2	18					
RCC 156 KO	*Tetraselmis convolutae (ACKS)*	F/2	18					
RCC 6681	*Tetraselmis marina*	F/2	17					
SAG 202.80	*Tetraselmis marina*	F/2	18					
RCC 132	*Tetraselmis rubens*	F/2	18					
RCC 6689	*Tetraselmis rubens*	F/2						
RCC130	*Tetraselmis striata*	F/2	18					
SAG 26.82	*Tetraselmis subcordiformis*	F/2	18					
RCC 6737	*Tetraselmis suecica*	F/2	18					
CCAP1085/12	*Thalassiosira pseudonana*	F/2 +si						
CCALA 931	*Trachydiscus minutus*	BBM						
RCC 6311	*Tribonema aequale*	BG11	14	25				
CLA 0204	*Trichormus variabilis*							
RCC 205	*Triparma pacifica*	K	20	100				
CCMP 3155	*Vitrella brassicaformis*	F/2	26	20				

Table 1. List of Strains

A table listing all strains along with their accession numbers, cultivation media, optimal temperatures, and PPFD. Strains that exhibited successful growth, decline, or mortality are labeled in green, orange, and grey, respectively. Strains successfully analyzed by absorbance, room-temperature (R.T.) fluorescence, or 77K fluorescence are also labeled in green, while those demonstrating a signature of acclimation to the far-red or presence of red form of chlorophyll are marked in red. Strains for which the analysis was unsatisfactory or not feasible are labeled in grey.

3 Light Adaptation Strategies in "Stanieria cyanosphaera" involve Complementary Chromatic Acclimation, Low-light and Far-Red Light Photoacclimations

Short Title

CCA, LoLiP, and FaRLiP in cyanobacteria SAG33.87

Author list

Feller Tom[1], Lara Yannick J.[2], Javaux Emmanuelle J.[2], Cardol Pierre[1*]

Affiliations

1. Genetics and physiology of microalgae, UR InBioS, University of Liège, 4000 Liège, Belgium
2. Early Life Traces & Evolution-Astrobiology, UR Astrobiology, University of Liège, 4000 Liège, Belgium

*Corresponding author : pierre.cardol@uliege.be

Funding

This research was supported by BELSPO (BRAIN project B2/212/PI/PORTAL) in the frame of the PORTAL project, the Belgian Fonds de la Recherche Scientifique projects "GALOP" (F.R.S.-FNRS, PDR T.0032) and "Life in Archean coastal environments" (FRS-FNRS PDR T.037.20), and the ULiege SRA-STEMA project UnLOC.

3.1 Abstract

Cyanobacteria are an ancient clade that developed remarkable adaptability to diverse light conditions through photoacclimation strategies, including low-light photoacclimation (LoLiP), far-red light photoacclimation (FaRLiP), and complementary chromatic acclimation (CCA). This study investigates these mechanisms in *Stanieria cyanosphaera* SAG 33.87, a cyanobacterium isolated from the reed beds of Neusiedler See, Austria. Using a combination of spectroscopic, biochemical, genomic, and fluorescence lifetime imaging analyses, we demonstrate that *S. cyanosphaera* employs CCA, LoLiP and FaRLiP to modulate its photosynthetic apparatus in response to low and far-red light environments. Genomic analysis revealed the presence of canonical LoLiP and FaRLiP clusters, including genes encoding specialized subunits of photosystems and phycobilisomes. Under far-red light, significant structural remodeling of photosystems was observed, with incorporation of chlorophyll *f* in PSII, a pigment enabling light absorption beyond 700 nm, accounting for ~4% of total chlorophyll. In low-light conditions, *S. cyanosphaera* utilized LoLiP to enhance far-red light absorption. High-light stress responses were characterized by increased carotenoid production, though accompanied by reduced photosynthetic efficiency. Fluorescence lifetime analyses revealed longer lifetimes in far-red-acclimated cells, indicative of altered energy transfer dynamics in photosynthetic complexes. Together, these findings highlight the ecological versatility of *S. cyanosphaera*, its dependence on far-red and low-light niches, and the evolutionary importance of FaRLiP and LoLiP in cyanobacterial success in light-limited environments.

3.2 Introduction

Cyanobacteria stand out among chlorophototrophs due to their ability to perform photo-oxidation of water and produce oxygen, a reaction with far-reaching global implications. This oxygenic photosynthesis, which began at least 2.4 billion years ago, played a critical role in oxygenating Earth's atmosphere and ocean, significantly impacting the evolution of the early Earth and life (Hohmann-Marriott and Blankenship, 2011; Lyons et al., 2014, 2021; Demoulin et al 2019). Carbon fixation and subsequent production of oxygen by cyanobacterial photosynthesis significantly contribute to modern ocean biogeochemical fluxes (Flombaum et al., 2013). Modern cyanobacteria occupy diverse habitats and are nearly ubiquitous in the photic zone (Sanchez-Baracaldo et al., 2022). This success is partly explained by their ability to modulate their photosynthetic apparatus in response to light availability.

Information concerning CCA, LoLiP, FarLip and Chl *f* can be found in the Introduction at section 1.7.2. Chromatic adaptation of cyanobacteria

The cyanobacterium "*Stanieria cyanosphaera*" SAG 33.87 was originally isolated in 1963 as *Chroococcidiopsis gigantea* from a reed bed in Neusiedler See at Illmitz, Austria, by Kusel-Fetzmann. Neusiedler See, a large steppe lake, providing a unique habitat characterized by fluctuating light conditions, nutrient availability, and salinity, making it an ideal site for the study of cyanobacterial diversity and photoacclimation strategies. Stanieria genera belong to the ordrer Pleurocapsales, which members are characterized by the production of small cells called baeocytes that result of multiple cell division of a mother cell (Waterbury and Stanier, 1978). Members of this order include other reference Stanieria strains, from which "S. cyanosphaera" SAG 33.87 is not directly related (Shalygin et al., 2019, Brinkman et al., 2015). Members of this order include other reference *Stanieria* strains such as PCC7437, from which the sequence of the 16S rRNA "*Stanieria cyanosphaera*" SAG 33.87 differ (Shalygin et al., 2019, Brinkman et al., 2015). This underline the need of a taxonomic revision.

This study aims to elucidate the light adaptation mechanisms employed by "*Stanieria cyanosphaera*" SAG 33.87 to thrive under various light conditions. Using absorbance and fluorescence analyses, we first explored how the strain adjusts its light-harvesting apparatus. Native separation of photosynthetic complexes revealed the presence of two distinct phenotypes, FaRLiP and LoLiP, which play pivotal roles in light acclimation. The expression of these clusters significantly enhances the ability of "*Stanieria cyanosphaera*" SAG 33.87 to grow efficiently under far-red and low-light conditions.

More broadly, by exploring the strategies of phototrophic life to adapt to various light conditions, this study also contributes to the understanding of their early evolution on the early Earth and to the testing the possibility and signatures of phototrophic life on possible habitable exoplanets around red dwarf stars such as TRAPPIST-1 emitting mostly in the infra-red range.

3.3 Materials and methods

3.3.1 Strain and growth conditions.

"Stanieria cyanosphaera" SAG 33.87 was obtained from the Georg-August Universitat Göttingen Department Experimental Phycology and Culture Collection of Algae (EPSAG). Cells were cultivated in BG11 medium in 30 mL flask under 135 rpm on orbital Unimax *shaker* (Heidolph, Germany, Schwabach) at 23°C. A custom-built algal growth system was designed (AGEM, ULiege). It comprises nine individual chambers, each accommodating a single flask, and equipped with its own LED composition panel, comprising four LEDs: 730 nm, 840 nm, 940 nm, and white light provided by a full spectrum LED. Photosynthetically photon flux density (PPFD) was independently adjusted for each chamber and each LED. Low light (LL) and High Light (HL) were set at PPFD of 15 and 100 µmol photons. m^{-2} s^{-1}, respectively, with the full spectrum LED. The far-red light (FRL) condition was established at 15, 30, and 60 µmol photons. m^{-2} s^{-1}, with 730, 840, and 940 nm LEDs respectively, emulating the emission of the TRAPPIST-1 star in wavelength proportion (Wilson et al., 2021) (Supplementary figure 1).

3.3.2 Spectrofluorometry.

In vivo absorbance spectra were acquired from cell suspensions at room temperature using a BLUE-Wave Miniature Spectrometer (StellarNet Inc., Tampa, FL, USA) in conjunction with a tungsten halogen lamp SL1 with a broad spectral range of 350-2500 nm and an SL1-BLUE lamp with a blue LED (470 nm). *In vivo* fluorescence spectra were obtained at room temperature (23°C) and 77 K with an excitation wavelength of 470 nm using a USB2000+ Ocean Optics spectrometer (Ocean Optics Inc., Dunedin, FL, USA) coupled with a LightBox CCD (Beambio, France).

Absorbance or fluorescence spectra at room temperature and 77 K (excitation $\lambda = 470$ nm) from manually excised bands of the CN gel were acquired using the same equipment. After analysis, the bands were stored at -80°C. *In vivo* chlorophyll fluorescence rise measurements were performed at room temperature on cell suspensions using a JBeamP spectrofluorometer (BeamBio/API, France). Upon the onset of actinic illumination, the fluorescence increased from a baseline value (F_0) to a stable value (F_s) in approximately 1 s. After approximately 3 s of continuous illumination, a saturating pulse (> 3000 µmol photons· m^{-2} s^{-1}, 660 nm) was

applied to reach the maximum fluorescence value (F_m). Based on the collected fluorescence values, the maximum quantum yield and the quantum yield of PSII were calculated using the following equations: $F_v/F_m' = (F_m' - F_0)/F_m'$ and $\Phi II = (F_m' - F_s)/F_m'$. The F_0 parameter reflects the minimal fluorescence intensity for cells dark-adapted for 5 minutes. For light-acclimated cells, F_s and F_m' represent the steady-state and maximum fluorescence intensities, respectively (Gently et al., 1989). Different sources of actinic light were used, consisting of LEDs emitting at 655, 695, and 725 nm. Their PPFD (I) ranged from 0.5 to 751 µmol photons· m^{-2} s^{-1}, 1 to 448 µmol photons· m-2 s-1; 0.1 to 1385 µmol photons· m^{-2} s^{-1}; 0.5 to 75.4 µmol photons· m^{-2} s^{-1}; and 4.5 to 2737 µmol photons· m^{-2} s^{-1}, respectively.

To determine the PSII antenna size, a final concentration of 50 µM 3-(3,4-dichlorophenyl)-1,1-dimethylurea (DCMU) was added to the cell suspension. The antenna size at a given light intensity (expressed in s^{-1}) was calculated using the formula $\ln(2)/t_{1/2}$, where $t_{1/2}$ represents the time required to reach 50% of $F_m - F_0$. The calculated antenna sizes were then plotted against light intensity, and the slope of the resulting linear regression (σ) was determined. The electron transport rate of PSII (ETRII) at a specific light intensity was calculated using the formula $\Phi II \times I \times \sigma$, where ΦII is the quantum yield, I is the light intensity, and σ is the slope obtained from the linear regression.

3.3.3 Fluorescent Lifetime Imaging Microscopy (FLIM).

LL and FRL acclimated cells were incubated in the dark for at least 30 min and inoculated onto 3% BG11 agarose plugs placed on microscopic slides before FLI acquisition. Fluorescent lifetime images were acquired with a Leica Stellaris 8 confocal microscope (Leica, Wetzlar, Germany) using the TauContrast from the TauSense technology at the GIGA-Cell imaging platform (Liège, Belgium). Cells were imaged using a 63 x water immersion objective. PBS excitation was performed by a pulsed laser at 577 nm with a frequency of 80 MHz and a laser power of 0.01 µW. PBS fluorescence emission was captured using a Hyd S detector (Leica, Wetzlar, Germany) set from 601 to 752 nm. Chl *a* and Chl *f* were both excited at 440 nm with a laser pulsed at 80 MHz frequency and a laser power of 0.025 µW. Fluorescence emission was captured with a Hyd S detector (Leica, Wetzlar, Germany) covering from 675 to 685 nm for the Chl *a,* and a Hyd X detector that covered from 730 to 740 nm for the Chl *f.* All acquisition were obtained with 16-line accumulation. In this experiment fluorescence lifetime is estimated as the Average Arrival Time (AAT) of photon detected during the pixel dwell.

3.3.4 Oxymetry.

A JTS-10 spectrophotometer (Bio-Logic Science Instruments, France, Seyssinet-Pariset) was coupled with a Firesting oxygen sensor (PyroScience GmbH, Germany, Aachen). Oxygen evolution was recorded using 4 mL of culture. The same actinic light used for ETR measurements was applied during the experiment. Inside the sealed cuvette, the cells were exposed to 5 min of darkness, followed by three consecutive 5-min light steps at 50, 100, and 300 µmol photons· m^{-2} s^{-1},, and then 5 min of darkness. The results were normalized to the chlorophyll content and expressed as pmol O2. µg Chla-1. s-1

3.3.5 HPLC Analysis.

One mL of culture was harvested and centrifuged, and the resulting pellet was resuspended in 1 mL of HPLC-grade methanol. Glass beads (0.5 mL, 0.2 to 0.5 mm, Qiagen, Germany) were then added. The cells were disrupted using a BeadBeater (FastPrep-24, MP, USA) at 8 m/s for five 10-second intervals, with 2 min of cooling on ice. The cells were subsequently incubated at 4°C for 30 min and centrifuged at 20,000g for 10 min (5424R centrifuge, Eppendorf, Germany, Hambourg). The pellet was kept for PBS analysis (see below), while the supernatant was utilized for HPLC analysis. HPLC analysis was conducted as described in Bern et al.,2018. Briefly, a 70 µL pigment extract was analyzed by reverse-phase HPLC using a Prominence UFLC system (Shimadzu, Kyoto, Japan). Pigments were first eluted with a first step of 100% eluent A (80% methanol, 100 mM ammonium acetate) for 0.5 min. Eluent B (90% acetonitrile) was then used. Next, a mixture of 90% eluent B and 10% eluent C (100% ethyl acetate) was applied for 5 min, followed by 65% eluent B and 35% eluent C for 5.4 min. The gradient continued with 40% eluent B and 60% eluent C for 3.5 min. Finally, 100% eluent C was used for 2 min, and the separation was completed within 8 min with 100% eluent A. Pigment quantities were calculated as the ratio of the area under their respective peaks to the total area of all peaks in the chromatogram at 430 nm. The quantification of chlorophyll f was performed using the extinction coefficient reported by Li et al. (2012).

3.3.6 Protein analyses.

For spectroscopic analyses of phycobillisomes, cell pellets were washed four times with 100% methanol and resuspended in 1 mL of 0.25M M HEPES with protease inhibitor (cOmplete, EDTA-free, Roche, Switzerland). The pellets were disrupted using the BeadBeater at 10 m/s for three 40-second intervals at room temperature. After a centrifugation step at 20,000g for 10 min, the supernatant containing phycoerythrin and phycocyanin was collected.

For native protein analyses, cells were collected and centrifuged at 500 g to obtain a 1 mL pellet. The pellets were resuspended in SHE buffer containing 250 mM sucrose, 1 mM EDTA, 10 mM HEPES, and a protease inhibitor cocktail. Cell lysis was performed using a French press (Hydrobel CLF IP55 IEC34) at 150 bar and 4°C. The lysate was then diluted threefold in SHE buffer containing the protease inhibitor cocktail and centrifuged at 600 g for 10 min at 4°C. The supernatant was collected and recentrifuged at 4°C for 15 min at 17,000 g. The final pellets were resuspended in a sucrose buffer containing 300 mM sucrose, 4 mM EDTA, 20 mM Tris, and the protease inhibitor cocktail at pH 7.2. Protein quantification was performed using the Bradford method with 5 µL of sample, 50 µL of NaOH Triton X-100 solution, and 500 µL of protein assay dye reagent diluted 5x (BioRad, USA). Absorbance at 595 nm was measured using a Lambda 265 UV/VIS spectrofluorometer (PerkinElmer, USA). Proteins from the total membrane preparations were solubilized in a buffer containing 50 mM Tris-HCl, 1.5 mM MgSO4, 100 mM NaCl, 10% glycerol, and a protease inhibitor cocktail (pH 8.4), along with 2 g of n-dodecyl-α-D-maltoside (α-DDM) per g of protein. The mixture was incubated at 4°C with gentle agitation for 30 min, followed by 30 min of rest, and then centrifuged at 21,000 g for 20 min. Supernatants with equal protein concentration were subjected to high-resolution clear-native polyacrylamide gel electrophoresis (hrCN-PAGE) using 4-12% acrylamide gradient gels. The hrCN-PAGE gel was placed in an anode buffer containing 5 mM Bis-Tris (pH 7). The cathode buffer, comprising 5 mM Tricine and 1.5 mM Bis-Tris (pH 7) (Witting et al., 2007), also included 0.05% sodium deoxycholate and 0.02% α-DDM. Protein separation was carried on under a constant voltage of 60 V for 14 hours. Following protein migration, bands were promptly excised and transferred to cuvettes maintained on ice for absorbance and fluorescence measurements and subsequently maintained at -80°C prior mass spectrometry analyses.

3.3.7 Genome sequencing and reconstruction.

Genomic DNA was extracted and purified from a non-axenic culture of SAG 33.87 using the GenElute^{TM} Bacterial Genomic DNA kit (Sigma-Aldrich). Two individual batches of extracted DNA were sent to the GIGA-Genomics platform (Liège, Belgium) for illumina MiSeq v3 sequencing. Both sequencing runs generated 600 bp short reads libraries which were trimmed and corrected using Trimmomatic (0.39) (Bolger et al., 2014) and metaSPAdes(3.13.0) (Nurk et al., 2017). All resulting libraries were then used for a metagenome assembly using Spades (3.13.0). Obtained contigs were implemented into Anvi'o 7.1 platform for metagenomic binning, gene calling (Prodigal v2.6.3), and annotation processes (Eren et al., 2015; Eren et al., 2021; Veseli et al., 2023). Binning consisted of first automatic binning step using metabat2 (2.2.15) and a second step binning manual refinement and taxonomy assignment using Anvi'o interactive interface based on plotting of reads coverage, taxonomic affiliations via taxonomic assignment by Centrifuge (1.0.4) program, and taxonomic affiliations using anvi-run-scg-taxonomy and anvi-estimate-scg-taxonomy programs based on information contained in Genome Taxonomy Database (GTDB). Gene calls were annotated by comparing HMM profiles against the KOfam database (Aramaki et al., 2019).

3.3.8 Protein identification by LC-ESI-MS/MS

Proteins bands were digested overnight trypsin at 37°C, peptides were extracted from the gel and dried by SpeedVac and resuspended in 3% (v/v) acetonitrile with 0.1% (v/v) TFA.

Peptides were directly loaded onto reversed-phase pre-column (Acclaim PepMap 100, Thermo Scientific) and eluted in backflush mode. Peptide separation was performed using a reversed-phase analytical column (Acclaim EasySpray RSLC, 0.075 x 250 mm,Thermo Scientific) with a linear gradient of 4%-27.5% solvent B (0.1% FA in 98% ACN) for 60 min, 27.5%-40% solvent B for 10 min, 40%-95% solvent B for 1 min and holding at 95% for the last 10 min at a constant flow rate of 300 nl/min on an Vanquish Neo system. The peptides were analyzed by an Orbitrap Fusion Lumos tribrid mass spectrometer (ThermoFisher Scientific). The peptides were subjected to NSI source followed by tandem mass spectrometry (MS/MS) in Fusion Lumos coupled online to the nano-LC. Intact peptides were detected in the Orbitrap at a resolution of 120,000. Peptides were selected for MS/MS using HCD setting at 30; ion fragments were detected in the Ion Trap. A data-dependent procedure that alternated between one MS scan followed by MS/MS scans was applied for 3 seconds for ions above a threshold

ion count of 2.0E4 in the MS survey scan with 40.0s dynamic exclusion. The electrospray voltage applied was 2.1 kV. MS1 spectra were obtained with an AGC target of 4E5 ions and a maximum injection time of 50ms, MS2 spectra were acquired with an AGC target of 5E4 ions and a maximum injection time set to dynamic. For MS scans, the m/z scan range was 375 to 1800.

The resulting MS/MS data was processed using Sequest HT search engine within Proteome Discoverer 2.5 SP1 against a *Stanieria cyanosphaera* protein database obtained from Uniprot. Trypsin was specified as cleavage enzyme allowing up to 2 missed cleavages, 4 modifications per peptide and up to 5 charges. Mass error was set to 10 ppm for precursor ions and 0.1 Da for-fragment ions. Oxidation on Met (+15.995 Da), conversion of Gln (-17.027 Da) or Glu (-18.011 Da) to pyro-Glu at the peptide N-term were considered as variable modifications. False discovery rate (FDR) was assessed using Percolator and thresholds for protein, peptide and modification site were specified at 1%.

3.3.9 Statistical Analyses.

Experiments were reproduced at least three times using different populations. Representative values are presented as means, with variation expressed as standard deviation. Homoscedasticity or heteroscedasticity of variances was assessed, and a t-test was performed to evaluate similarities or differences between samples. Results were considered statistically significant if the p-value was <0.05 and labeled with a single asterisk (*), while highly significant results (p-value <0.01) were labeled with two asterisks (**). Non-significant differences were indicated as "N.S."

3.4 Results

3.4.1 Light Acclimation and Pigment Adaptation in "*Stanieria cyanosphaera*" Under Varied Illumination Conditions

"Stanieria cyanosphaera" SAG 33.87 cells were exposed to low white light (LL), high white light (HL), and far-red light (FRL) for 17 days. LL cells exhibited a deep dark green coloration, FRL cells displayed a distinctly brighter green hue, and HL cells appeared yellow brown with a lower biomass (Figure 15, B).

The absorption spectra of whole cells revealed key differences. First, the 625/570 nm ratio was lower in LL and HL cells (0.95±0.05 and 0.87±0.08, respectively) than in FRL cells (1.32±0.04) (Figure 15A). This suggested that the relative abundance of phycocyanin (PC) in relation to phycoerythrin (PE) was lower under LL and HL conditions than under FRL. Absorption spectrum of the soluble fraction of cell pellets, after methanol extraction, confirmed a high PC:PE content in FRL cells compared to LL cells (Figure 15C-D).

Additionally, both LL and FRL cells showed an absorption band beyond 700 nm that was absent in HL cells. Difference spectra (LL minus –HL, and FRL minus LL) further indicated that this peak shifted to a longer wavelength in FRL cells (717 nm) than in LL cells (711 nm) (Figure 15A). Only the methanol extract from FRL cells exhibited a distinct peak at 707 nm (Figure 15E-F). These features may indicate the presence of red-shifted chlorophyll in FRL cells (Li et al., 2012). Finally, the absorption spectra of methanol-extracted pigments revealed notable differences in the 480 nm:440 nm ratio, indicative of the carotenoid-to-chlorophyll *a* ratio. This ratio was highest in HL cells (0.88+-0.09) and lowest in LL cells (LL 0.45 +-0.05) (Figure 15E).

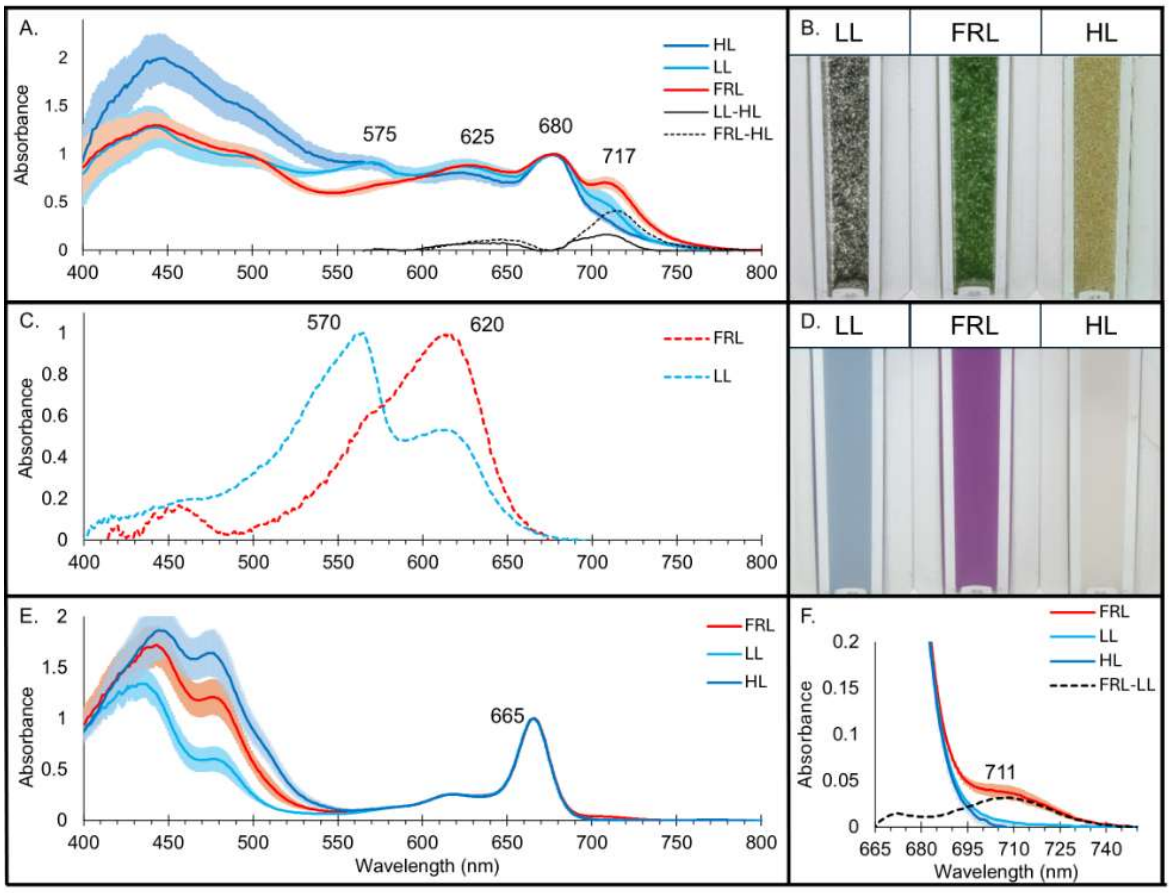

Figure 15. Absorbance Spectra of "Stanieria cyanosphaera" SAG 33.87 under different light conditions.

(A) Average Absorbance spectra of cultures acclimated to low light (LL, light blue line), high light (HL, dark blue line), and far-red light (FRL, red line), following 17 days of exposure. Each spectrum is normalized to the peak at 675 nm (Error bars represent standard deviation for LL (light blue), and FRL (light red), with n=10). The difference spectra between LL and HL, and between FRL and HL are represented by solid and dotted black lines, respectively. (B) Representative photograph of *in vivo* cultures under different light conditions. (C-D) Absorbance spectra and photograph, respectively, of membranes in HEPES mixture after methanol extraction. Spectra are normalized to their maximum absorption. (E-F) Absorbance spectra of methanol extracts from previous cultures. Spectra are normalized to the peak at 665nm, with n = 8 for LL and FRL, and n = 4 for HL.

Pigment compositions were then determined by HPLC analysis (Table 2). Chlorophyll *f* was detected exclusively in FRL cells. Incidentally, this finding confirms that the increase in absorbance at 711 nm observed in LL (see Figure 15A) is due to low-light photoacclimation (LoLiP).

Using extinction coefficients determined by Li et al., (2012) for both chl *a* and chl *f*, the chl *f* : chl *a* ratio was 0.026 ± 0.002 in FRL cells. A similar value (0.035 ± 0.002) was determined from the absorption spectra shown in Figure 1E. In contrast with LL and FRL cells, HL cells exhibited a high amount of myxoxanthophyll, zeaxanthin, and β-carotene, compared to chlorophyll a.

N = 6	LL	FR	HL
Myxoxantophyll	0.3 ± 0.1	0.7 ± 0.1	**7.7 ± 2.5**
Zeaxanthin	4.5 ± 1	5.3 ± 1	**14.1 ± 3.3**
Chlorophyll f	NF	**1.4 ± 0.1**	NF
Chlorophyll a	**86.3 ± 2.6**	79.2 ± 2.5	55.9 ± 3.3
Echinenone	5.6 ± 1.3	**9.2 ± 1**	7.5 ± 1.4
β-Carotene	3.3 ± 0.8	4.3 ± 1.4	**14.7 ± 1.9**

Table 2. Relative Pigment Composition of "Stanieria cyanosphaera" SAG 33.87 Under Different Light Conditions.

Relative amounts of pigments in *"Stanieria cyanosphaera"* SAG 33.87 cells acclimated to low white light (LL), far-red light (FRL), and high white light (HL) conditions (mean ± SD; LL and FRL, *n* = 6; HL, *n*=3). Pigments include Myxoxanthophyll, Zeaxanthin, Chlorophyll *f* (Chl *f*), Chlorophyll *a* (Chl *a*), Echinenone, and β-Carotene. Pigment quantities are expressed as the ratio of the area under their respective peaks to the total area of all peaks in the chromatogram at 430 nm. NF indicates that the pigment was not found.

Room-temperature fluorescence emission spectra of intact cells revealed distinct peaks corresponding to key components of the photosynthetic apparatus (Figure 16A). Peaks at 660 nm, 684 nm, 723 nm, and 734 nm were observed, which can be attributed to allophycocyanin (APC), Photosystem II (PSII), Photosystem I (PSI), and a far-red PSII/PSI complex, respectively (Itoh et al., 2015). HL cells exhibited a dominance of PSII fluorescence emission relative to PSI, whereas LL cells displayed higher fluorescence emission from PSI. In FRL cells, the main fluorescence emission peak was shifted to 734 nm, consistent with the incorporation of chlorophyll *f*, as reported in cyanobacterium KC1 in the literature (Itoh et al., 2015).

Similarly, at 77 K, fluorescence emission spectra (Figure 16B) confirmed the presence of peaks corresponding to APC (660 nm), PSII (685/695 nm), PSI (729 nm), and far-red PSI (742 nm) in *Synechocystis sp*. PCC6803 (Battistuzzi et al., 2023). In FRL-grown cultures, a red shift in the main PSI-associated peak was observed, moving from 729 nm in LL cells to 742 nm, indicating adaptation to far-red light. In contrast, HL cells exhibited a slight blue shift of the PSI-associated peak, from 729 nm to 726 nm, reflecting changes in their photosynthetic complexes under high-light conditions. Altogether, these results suggested that *"Stanieria cyanosphaera"* SAG 33.87 performs both LoLiP and CCA to optimize light-harvesting under low white light and FarLiP under Far-red light.

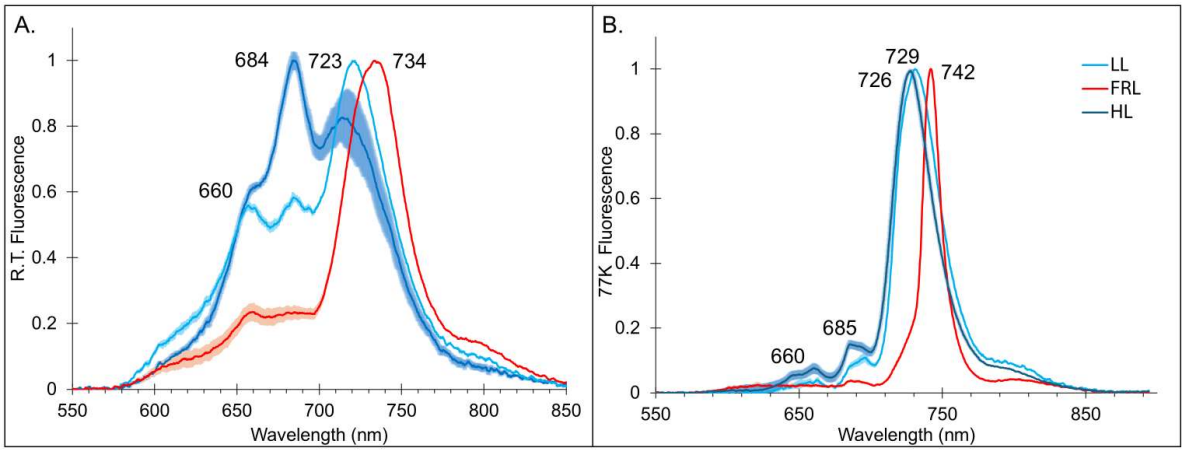

Figure 16. Fluorescence emission spectra of "Stanieria cyanosphaera" SAG 33.87.

Room temperature (A) and 77K (B) fluorescence emission spectra were recorded upon excitation at 470nm. Cells were cultivated under low light (light blue line, LL), high light (dark blue line, HL), and far-red light (red line, FRL). Each spectrum was normalized to its maximum fluorescence peak. (n=3).

3.4.2 Genomic Analysis Reveals the Presence of Canonical LoLiP and FaRLiP Gene Clusters in *"Stanieria cyanosphaera"*.

To investigate whether *"Stanieria cyanosphaera"* SAG 33.87 possesses canonical LoLiP and FaRLiP gene clusters, its genome was sequenced using Illumina technology and subsequently assembled and annotated. The assembled genome has a size of 5.938Mb with 97.2% completeness, consisting of 170 contigs and containing 5449 predicted proteins (see supplementary files available @ https://doi.org/10.58119/ULG/EI9ZII). From this genomic sequence, a continuous 24,404 nt size gene cluster (from nt 2,504 to 26,907) that contained twenty-one FaRLiP canonical genes was characterized (Figure 17). It is divided into four distinct regions coding for core subunits of PSI (*psaJ2/F2/I2/L2/B2/A2*), core subunits of PSII (*psbA3/A4/C2/D3/B2*), core subunits of PBS (*apcD2/B2/D3/E2/D5*), the knotless phytochrome photoreceptor (*rfpA3*) and response regulators *rfpB3* and *rfpC3* and *rfpC4*. All genes belonging to the PSI family are transcribed in the reverse phase. Within the cluster, three hypothetical proteins were also found. Moreover, a LoLiP cluster, spanning nucleotides 181,667 to 184,341 in the genome, comprised two genes encoding core subunits of PBS (*apcD4* and *B3*), and a third gene encoding a Chl *a*-binding protein (*isiX)*.

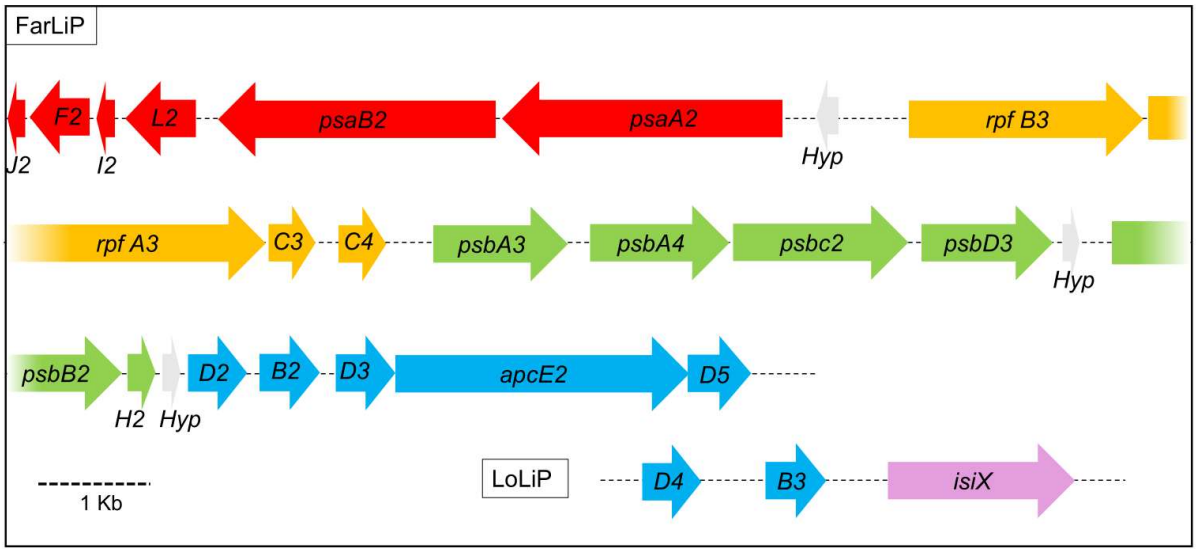

Figure 17. Fluorescence emission spectra of "*Stanieria cyanosphaera*" SAG 33.87.

FarLip: Core subunits of PSI (*psa*, red), core subunits of PSII (*psb*, green), core subunits of PBS (*apc*, blue), knotless phytochrome photoreceptor (*rfpA*), response regulators *rfpB* and *rfpC* (Orange), and hypothetical proteins (grey). LoLiP : core subunits of PBS (*apc*, blue) and Chl *a*-binding protein (*isiX*, pale blue). Relative size of gene and position are represented in nt.

3.4.3 Structural and Spectral Characterization of Photosystems in "*Stanieria cyanosphaera*" Under Low and Far-Red Light.

To gain insight into the composition of photosystems in "*Stanieria cyanosphaera*" SAG 33.87 in LL and FRL cells, the membrane complexes were solubilized in the presence of alpha-dodecyl maltoside and separated by clear-native polyacrylamide gel electrophoresis (CN-PAGE) (Figure 18A). This analysis could not be conducted for HL cells due to insufficient biomass, which aligns with the low maximum quantum yield of PSII (Fv/Fm). Indeed, Fv/Fm was lowest in HL cells (0.24 +/-0.03), highest in FRL cells (0.42±0.03), and intermediate in LL cells (0.3±0.03). Seven main bands (1, 2a, 2b, 3, 3b, 4, 5) were visualized in the extracts of both LL and FRL cells. Due to their proximity within the gel, bands 2a and 2b on the one hand, and bands 3a and 3b on the other hand, were subsequently analyzed as unique bands (2 and 3, respectively). Bands 1-5 were analyzed by mass spectrometry to determine their main components. Bands 4 and 5 were occasionally very faint, resulting in subsequent analyses that were not satisfactorily reproducible. Consequently, only the results from the analyses of bands 1–3 will be described. Bands 1 and 2 comprised mainly PSI and PBS core components, whereas band 3 is dominated by PSII and PSBS core components (Figure 18E). The FRL PS contained many components coded by the FaRLiP cluster: *psaA2, psaB2, psaL2, psaF2, apcB2,* and *apcD2-3* within PSI/PBS complexes, and *psbA3-4, psbB2, psbC2, psbD3, H2, apcB2*, *apcD2-3*, and *isiX* in the PSII/PSBS complex. In contrast, PS of LL cells did not contain components of the FaRLiP cluster but the *apcB3*, *apcD4,* and *isiX* components of the LoLiP cluster in addition to PSI/PSII components. *apcB3*, *apcD4* have been occasionally found associated with FRL PS.

The absorbance spectra of PSI and PSII bands of both LL and FRL cells are virtually identical between 600 and 700 nm, but showed some minor differences in the FR range (Figure 18B). An additional absorption band was present for PSII (bands 3), peaking at ca 710 nm in LL cells and ca 725 nm in FRL cells. These absorption bands are typical of LoLiP and FaRLiP, respectively (Soulier et al., 2020, Gan & Bryant, 2015). These variations in PSII absorption spectra are reflected in the fluorescence emission spectra. For LL-PSII, the emission spectra peaks at 680 nm at both room temperature (RT) and 77K, with a secondary emission peak at 725 nm that is particularly prominent at 77K. In contrast, FRL-PSII emission spectra are dominated by broad peaks centered at 735 nm at RT and 740 nm at 77K (Figure 4C, D). Finally, RT and 77 K fluorescence spectra of both FRL PSI bands are red-shifted compared to their counterparts in LL-cells, both peaking at 735 nm (RT) and 739 nm (77K).

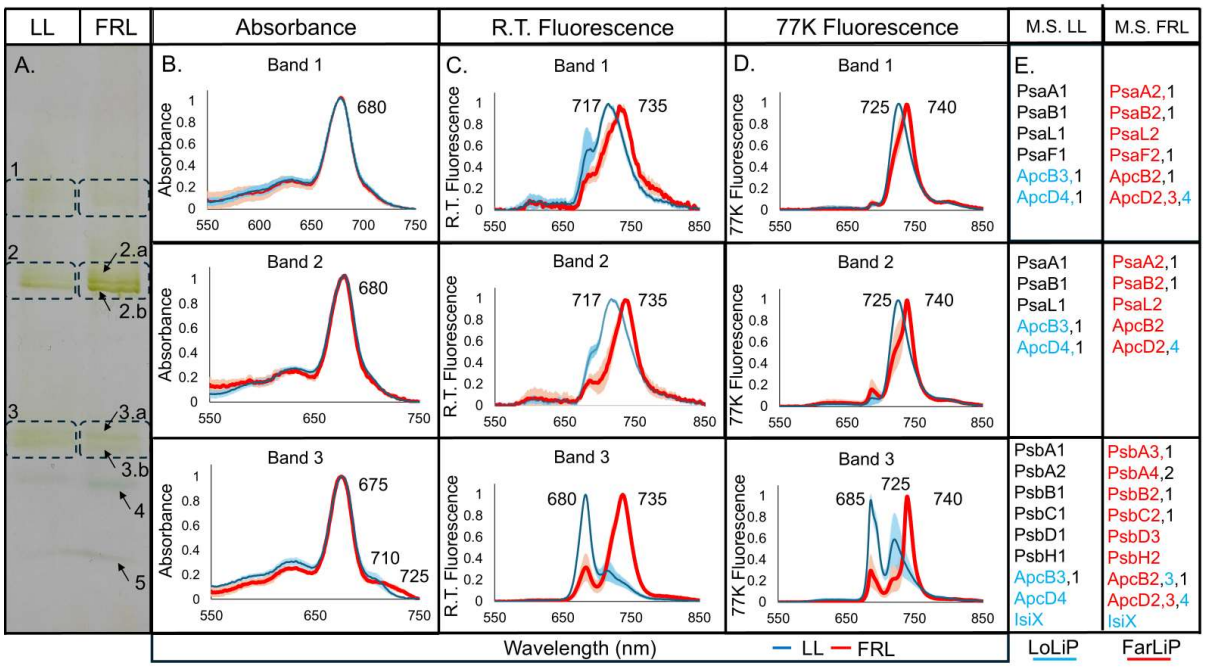

Figure 18. Biochemical and spectroscopic characterization of photosynthetic complexes of "Stanieria cyanosphaera" SAG 33.87.

(a) Clear-Native Polyacrylamide Gel Electrophoresis (CN-PAGE) separation of pigment-protein complexes from total membranes solubilized with 2% n-dodecyl α-D-maltoside. Each lane was loaded with 75 µg of protein (a representative experiment is shown). (b) Average absorption and (c-d) fluorescence emission (R.T. and 77k, excitation at 470 nm) spectra of bands 1-3 (Each spectrum was normalized to its maximum fluorescence peak; error bars are represented in light blue and light red for LL and FRL, respectively; n=3). (e) Main components of the LL and FRL photosynthetic complexes (bands 1-3) determined after mass spectrometry analyses. Proteins specific to the FaRLiP cluster or LoLiP clusters are highlighted in red and blue, respectively. (n=3).

3.4.4 Enhanced Antenna Size and Photosynthetic Performance of PSII in *"Stanieria cyanosphaera"* Under Far-Red Light

The functional antenna size of PSII was assessed by measuring *in vivo* fluorescence increase in the presence of the PSII inhibitor DCMU under red (665 nm) and far-red (725 nm) actinic light. The antenna size at 665 nm was comparable between LL and FRL cells (Figure 19A). However, the 725 nm antenna size was nearly negligible in LL cells (approximately 2% relative to the 665 nm antenna size) but significantly higher in FRL cells (exceeding 30% relative to the 665 nm antenna size) (Figure 5B).

FRL cells demonstrated electron transport rates (ETR) of PSII and net oxygen evolution comparable to those of LL cells under 665 nm actinic illumination. Notably, FRL cells also sustained significant photosynthetic activity under 725 nm actinic light, whereas both ETR and net oxygen evolution in LL cells were substantially lower under these conditions (Figure 19C and 19E).

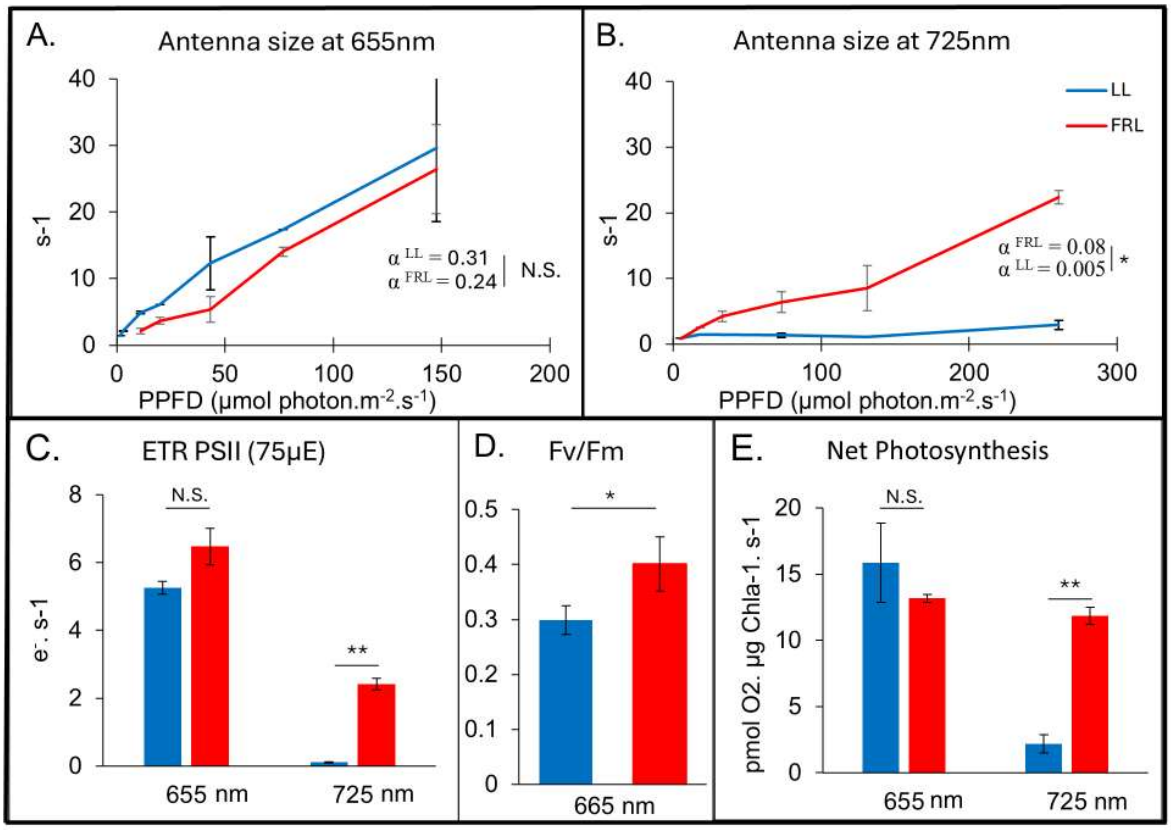

Figure 19. Photosystem II activity.

"Stanieria cyanosphaera" SAG 33.87 **c**ells were grown at 15 µmol photons m^{-2} s^{-1} under white light (LL, blue lines and bars) or Far-red light (FRL, red lines and bars). Actinic lights at 655 nm and 725 nm were used to perform the different biophysical analyses. (A-B) Functional antenna size of PSII (s^{-1}). (C) Electron Transport Rate (ETR) of PSII at 75 µmol photons m^{-2} s^{-1}. (D) Maximum quantum yield of PSII (Fv/Fm). (E) Net photosynthesis calculated by subtracting dark respiration from gross photosynthesis at 100 µmol photons m^{-2} s^{-1}. Values normalized to Chl *a* content (n=3). Statistical analyses were performed using a t-test: "N.S." indicates non-significant differences, $p < 0.05$ (*), and $p < 0.001$ (**).

Finally, the Fluorescence Lifetime Microscopy (FLIM) approach was employed to estimate average long lifetime components of each cell based on the computation of the arrival time by pixel dwell time of each pixel contained in the region of interest. In both conditions, various developmental cell stages were observed, ranging from individual cells to large structures containing small cells (baeocytes) (Figure 20B-G). Large intracellular structures, predominantly observed in some LL cells (Figure 20E-G), likely correspond to cyanophycin granules (Gonzalez-Esquer et al., 2016). In Figure 20A *i),* the long lifetime component of FRL-acclimated Chl *f* - producing cells was 2.3 ± 0.15 ns, while the distribution of mean lifetime values of a subset of cells displayed shorter values (ca 2 ns). *ii-iii)* For Chl *a*, LL-acclimated cells displayed a lifetime of 0.94 ± 0.04 ns, while FRL-acclimated cells exhibited a significantly longer lifetime of 1.13 ± 0.08 ns (p-value <0.001). *iv-v)* When PBS was more specifically excited, FRL-acclimated cells also demonstrated a significantly longer fluorescence lifetime of 0.55 ± 0.15 ns compared to the LL-acclimated cells, which had a shorter lifetime of 0.16 ± 0.33 ns (p-value <0.001).

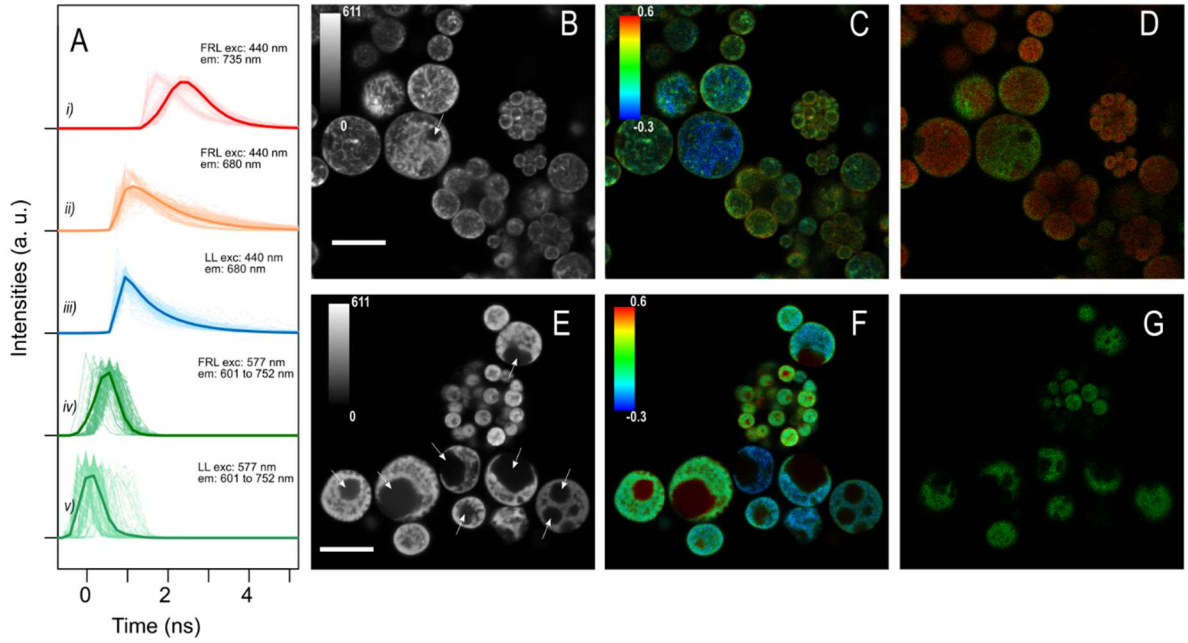

Figure 20. Fluorescence Lifetime Imaging (FLIM) of "Stanieria cyanosphaera" SAG 33.87.

(A) Fluorescence lifetime of *i)* Chl *f* at 730-740 nm upon 440 nm excitation , with 244 replicates; ii-iii) Chl *a* at 675-685 nm using 440 nm excitation from far-red (FR) and low-light (LL) cells with 244 and 299 replicates, respectively, and emission, with ; iv-v) Phycobilisome (PBS) between 601 and 752 nm upon 577 nm excitation from FRL and LL cells, respectively, using, with 240 replicates. All fluorescence lifetime curves were normalized using position normalization as follows (x – median) / sqrt(sum(x-median)^2. All replicates are represented in light color, and the average curve is in dark color. (B,E) Intensity of fluorescence lifetime of PBS from FRL cells (B) and LL cells (E), excited at 577 and measured between 601 and 752nm, with grey intensity scale bar (minimum at 0 and maximum at 611 photons). (C, F) Fluorescence lifetime distribution of PBS from FRL cells (C), and LL cells (F), with rainbow scale bar (minimum in blue at -0.3 ns and maximum in red at 0.6 ns). (D) Overlayed fluorescence lifetime intensity distribution of Chl *a* (in green) and Chl *f* (in red) from FRL cells. (F) Fluorescence lifetime distribution of PBS from LL cells, with rainbow scale bar (Minimum in blue at -0.3 and maximum in red at 0.6 ns). (G) Fluorescence lifetime intensity distribution of Chl *a* (in green) from LL cells. Scale bar is 10 µm.

3.5 Discussion

"Stanieria cyanosphaera" SAG 33.87 demonstrates remarkable flexibility in adapting its photosynthetic apparatus to diverse light conditions through a combination of low-light photoacclimation (LoLiP), far-red light photoacclimation (FaRLiP), complementary chromatic acclimation (CCA), and high-light stress responses. These mechanisms enable the strain to thrive in environments with variable light intensities and spectral qualities.

Chromatic Adaptation Strategies in *Stanieria* sp. SAG33.87

The observed changes in the absorbance spectrum at 570 nm and 625 nm of SAG 33.87 indicate dynamic modulation of the phycoerythrin (PE) to phycocyanin (PC) ratio in phycobilisomes (PBS), a signature of complementary chromatic acclimation (CCA) (Bernát et al., 2021). This enables SAG 33.87 to harvest light effectively across the visible spectrum. These results align with findings by Hirose et al. (2019), which showed that cyanobacteria capable of CCA can efficiently modulate PBS composition to optimize photosynthetic performance across a wide range of light intensities and wavelengths. There are three types of CCA. In Group I, synthesis of PE and PC does not depend on the wavelength of light. Group II, characterized as "unidirectional" adaptation, regulates the synthesis of PE based on light wavelength, while PC synthesis remains unaffected. In Group III, referred to as "bidirectional" or complete CCA, the transition of green light-adapted cells to red light results in the downregulation or cessation of PE synthesis accompanied by an upregulation of PC synthesis (De Marsac & Houmard, 1988). In *Stanieria cyanosphaera"* SAG 33.87, the extensive modulation of PC and PE with wavelengths (see supplementary Figure 2), suggests the presence of a type III CCA mechanism.

High-Light Stress Response

Under high-light (HL) conditions, *"S. cyanosphaera"* SAG 33.87 exhibited elevated levels of myxoxanthophyll, a pigment known to stabilize thylakoid membranes (Mohamed et al., 2005), and β-carotene, which facilitates electronic excitation transfers to chlorophyll a in both photosystems (Stamatakis et al., 2014) or involved in thermal dissipation when recruited by the orange protein (Kerfeld et al, 2017). Additionally, HL conditions led to a marked increase in zeaxanthin relative to chlorophyll *a*. Moreover, the significant increase in zeaxanthin relative to chlorophyll *a* suggests a strong photoprotective response, as zeaxanthin plays critical roles in dissipating excess light energy and protecting against oxidative damage (Niyogi et al., 1997, Dall'Osto et al., 2014). Its accumulation in LHCI and PSI reaction centers, as seen in

Cyanidioschyzon merolae (Haniewicz et al., 2018), and its importance in PSII repair and PSI trimer stabilization in *Synechocystis* sp. PCC 6803 (Kusama et al., 2015; Vajravel et al., 2017) further underscores its role in high-light stress mitigation. Despite these pigment adaptations, *"S. cyanosphaera"* SAG 33.87 showed reduced growth and low Fv/Fm values under HL, reflecting compromised photosynthetic efficiency. The slight blue shift (3 nm) in the maximum fluorescence emission band at 77K (from 729 nm to 726 nm) observed in HL cells likely indicates structural changes in PSI, potentially due to the loss of red chlorophylls. Similar shifts have been reported in LHCI-depleted PSI fractions of *C. merolae* (Haniewicz et al., 2018). Together, these observations suggest that *"S. cyanosphaera"* SAG 33.87 is primarily adapted to low-light conditions, with limited tolerance for high-light environments.

FaRLiP and LoLiP Mechanisms in Far-Red and Low-Light Environments

The high-quality 5.9 Mb assembled genome of *"S. cyanosphaera"* SAG 33.87 provided robust insights into its light acclimation strategies, revealing the presence of both LoLiP and FaRLiP clusters. The FarLiP cluster comprises 19 to 24 canonical genes and the LoLiP cluster encompasses 3 to 4 genes, which are known to play key roles in far-red light photoacclimation in cyanobacteria (Antonaru et al.,2024, Soulier et al., 2022). Interestingly, while the presence of the FarLiP cluster is widespread among cyanobacteria, the synteny and orientation of its genes can vary significantly (Antonaru et al., 2024). In the genome of SAG 33.87, the FaRLiP cluster exhibits conserved synteny of the genetic region with strains such as *Pleurocapsa* sp. PCC 7327 (Gan et al., 2014) and *Hydrococcus rivularis* (Antonaru et al., 2024), suggesting evolutionary stability in this genetic region. This conservation supports the recent proposal to reunite the Chroococcales and Pleurocapsales orders into a single taxonomic group (Bonthond et al., 2021; Strunecký et al., 2023) even though their division modes differ.

The induction of the FaRLiP cluster exclusively under far-red light (FRL) conditions in SAG 33.87 suggests a tightly regulated response to spectral shifts. Clear-native PAGE coupled with mass spectrometry revealed significant remodeling of photosystems in FRL-adapted cells. The presence of FaRLiP-specific subunits in PSII (*e.g.*, *psbA3*, *psbD3*) and PSI (*e.g., psaA2*, *psaB2*), along with PBS components (*apcB2*, *apcD2-3*), highlights the organism's capacity to reconfigure its photosynthetic machinery for far-red light absorption. These structural changes align with observations in *Synechococcus* PCC 7335, where FarLiP components are critical for assembling far-red-adapted photosystems (Gan et al., 2015).

The LoLiP cluster encodes key components, such as *apcB3* and *apcD4*, which are associated with PSI and PSII under low-light conditions. The cluster also encodes an IsiX-like protein, known to bind chlorophyll *a* and enhance low-light harvesting (Soulier et al.,2022). IsiX was exclusively associated with the PSII fraction of *"S. cyanosphaera"* SAG 33.87. Interestingly, proteins from the LoLiP cluster were also present in FRL conditions, suggesting overlapping roles in acclimation stages. In contrast, LL-adapted cells relied only on LoLiP. This dual strategy suggests that LoLiP acts as a response to declining light intensity, while FarLiP is deployed for sustained adaptation in far-red light environments, likely under the control of FarLiP-specific phytochrome photoreceptors, consistent with findings of Gan & Bryant (2015).

Chlorophyll *f* and Photosystem Remodeling in FRL Conditions

The production of chlorophyll *f* in FRL-acclimated cells of *"Stanieria cyanosphaera"* SAG 33.87, accounting for ~4% of total chlorophyll, extends the photosynthetically active radiation range into the far-red region. This ratio is consistent with *Chlorogloeopsis* sp., where chlorophyll *f* represents ~6% of total chlorophyll under FRL (Airs et al., 2014). The remodeling of PS under FRL is also reflected in the fluorescence emission and absorption spectra, with a clear red shift in FRL-adapted cells, a hallmark of FaRLiP-driven acclimation (Gan & Bryant, 2015). The incorporation of chlorophyll *f* into PSII complexes was particularly evident from the 725 nm absorption shoulder. In contrast, PSI, while showing fluorescence red shifts, may incorporate minimal chlorophyll *f*, suggesting a different type of FRL adaptation. Fluorescence emission spectra provided further evidence of adaptive shifts in the photosystems. LL cells exhibited typical PSI fluorescence peaking at 729 nm, while FRL cells showed red-shifted peaks at 734–742 nm, indicative of chlorophyll *f* incorporation. These findings are consistent with previous studies on *Fischerella thermalis*, where far-red-acclimated cells displayed fluorescence emission peaks at similar wavelengths, highlighting a conserved mechanism of spectral adjustment (Itoh et al., 2015).

FRL-adapted cells retained over 30% of their PSII antenna size at 725 nm actinic light, compared to 665 nm, whereas LL-adapted cells showed negligible activity. This robust far-red light utilization mirrors observations in *Chlorogloeopsis fritschii*, where FarLiP adaptations sustain PSII functionality under far-red light (Ho et al., 2019). Additionally, the maintenance of electron transport rates (ETR) and oxygen evolution in FRL cells, despite spectral shifts, highlights their efficiency in energy transfer. In contrast, LL cells showed a ~90% reduction in oxygen evolution at 725 nm, reflecting reliance on less efficient LoLiP pathways under far-red light.

In our FLIM setup, long average fluorescence lifetime (>100 ps) components were analyzed. Since PSI fluorescence lifetimes are much shorter (e.g., 15–25 ps; Krumova et al., 2020), the lifetimes observed here primarily reflect contributions from PSII and PBS (phycobilisomes) (Krumova et al., 2020).

For comparison, in *Synechococcus elongatus* PCC 7942, multiple lifetime components have been reported upon chl *a* excitation. The longest component (0.75–1 ns) corresponds to slow PSII decay and fluorescence decay from some disconnected PBS (Bhatti et al., 2021). Under chl *a* excitation at 440 nm, the fluorescence lifetime at 680 nm in *S. cyanosphaera* cells was within a similar range (0.95–1.1 ns). Notably, FRL-acclimated cells displayed a mean lifetime ~150 ps longer than LL-acclimated cells. Interestingly, in contrast, chl *f*-accumulating cells of *C. thermalis* exhibit shorter fluorescence lifetimes compared to cells lacking chl *f* (Macgregor-Chatwin et al., 2022). Although FRL cells of *S. cyanosphaera* showed higher Fv/FM values (indicative of better photochemical efficiency), the longer lifetimes observed suggest less-efficient trapping by FaRLiP-PSII, a phenomenon also observed in *C. fritschii* PCC 6912, where the photochemical efficiency of FRL-PSII is significantly lower than that of white-light PSII (Mascoli et al., 2020). The far-red mean fluorescence lifetime of FRL-acclimated *S. cyanosphaera* cells was approximately 2.3 ns, closely matching the fluorescence lifetime at 740 nm for closed isolated PSII in the FaRLiP strain *Chlorogloeopsis fritschii* PCC 6912 (Mascoli et al., 2020).

To probe interactions between PBS and photosystems, excitation at 577 nm was employed. FRL cells exhibited significantly longer average fluorescence lifetimes (550 ps) compared to LL cells (160 ps). For comparison, in *Synechocystis* PCC 6803, PBS fluorescence lifetimes associated with connected photosystems decay with lifetimes of 120 ± 20 ps (Krumova et al., 2020). Additionally, FLIM studies on PBS excitation in *S. elongatus* cells reported average lifetimes ranging from 165 to 320 ps (Bhatti et al., 2021). The longer fluorescence lifetimes observed in FRL-PBS of *S. cyanosphaera* suggest the presence of free or partially disconnected PBS. However, we propose that this difference is at least partly attributable to the presence of the FaRLiP-APC (allophycocyanin) protein and the higher phycocyanin:phycoerythrin ratio in FRL PBS. These factors likely contribute to the observed lifetimes, in conjunction with less-efficient energy trapping by FRL-PSII.

3.6 Conclusion (Ecophysiological and Phylogenetic Implications)

Cyanobacteria utilizing LoLiP and FarLiP strategies are often found in light-limited environments, such as microbial mats, stromatolites, endolithic systems and shaded aquatic systems (Behrendt et al., 2015; Chen et al., 2012; Ramírez-Reinat and Garcia-Pichel, 2012). The isolation of *"Stanieria cyanosphaera"* SAG 33.87 from a reed bed in Neusiedler See, Austria, aligns with this ecological niche. This study highlights the remarkable adaptability of *"Stanieria cyanosphaera"* SAG 33.87, employing LoLiP, FaRLiP, and CCA mechanisms to optimize light harvesting. These strategies enable extensive structural remodeling of photosynthetic complexes, incorporation of chlorophyll *f*, and modulation of PBS composition, facilitating efficient energy capture under varying light conditions. Still, this confines organisms to specific niches where far-red light predominates, preventing them from competing effectively in environments with more white or intense light (Mascoli et al., 2020). The evolutionary conservation of FarLiP among cyanobacteria further emphasizes its critical role in far-red light adaptation and the ecological success of cyanobacteria in light-limited environments.

Author contributions

P.C., E.J, and Y.L conceived the study. T.F, Y.L performed the experiments. All authors discussed the results and contributed to the final manuscript.

Acknowledgements

This research was supported by BELSPO (BRAIN project B2/212/PI/PORTAL) in the frame of the PORTAL project, the Belgian Fonds de la Recherche Scientifique projects "GALOP" (F.R.S.-FNRS, PDR T.0032) and "Life in Archean coastal environments" (FRS-FNRS PDR T.037.20), and the ULiege SRA-STEMA project UnLOC. We would like to thank Gaetan Lefèvre from ULiege GIGA-Cell imaging platform for his technical support with FLIM experiments, Alexandre Lambion (ULiege Early Life) for technical help in cell cultures.

Data availability statement

Genomic datasets used for the identification of the LoLiP and FarLiP gene cluster and the protein dataset used for the identification of peptides sequenced by LC-ESI MS/MS are available in the ULiege Open data Repository https://doi.org/10.58119/ULG/EI9ZII. Other data that support the findings of this study are available from the corresponding author upon reasonable request.

3.7 Supplementary Data

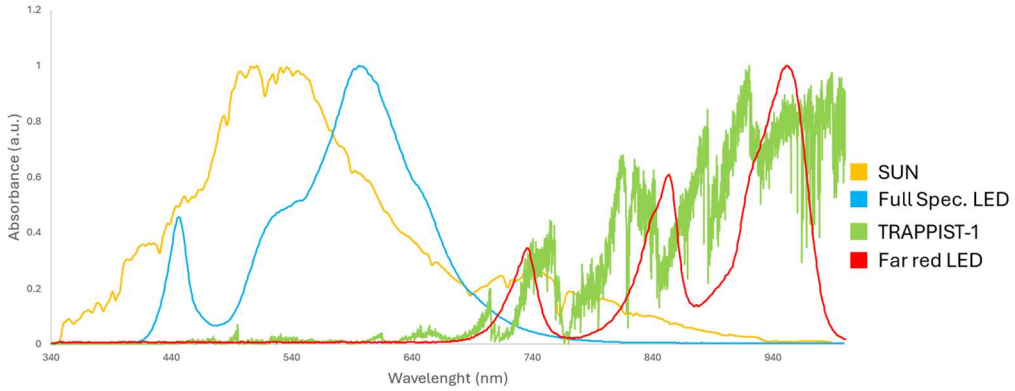

Supplementary Figure 1: Transmittance spectrum.

Solar radiation (obtained under partial shade) in orange, full spectrum and far-red chamber in blue and red, respectively, obtained with Blue-Wave Mignature Spectrometer. TRAPPIST-1 stellar emission in green, from Wilson et al., 2021. All spectra were normalized to their maximum emission values between 340 and 1000nm.

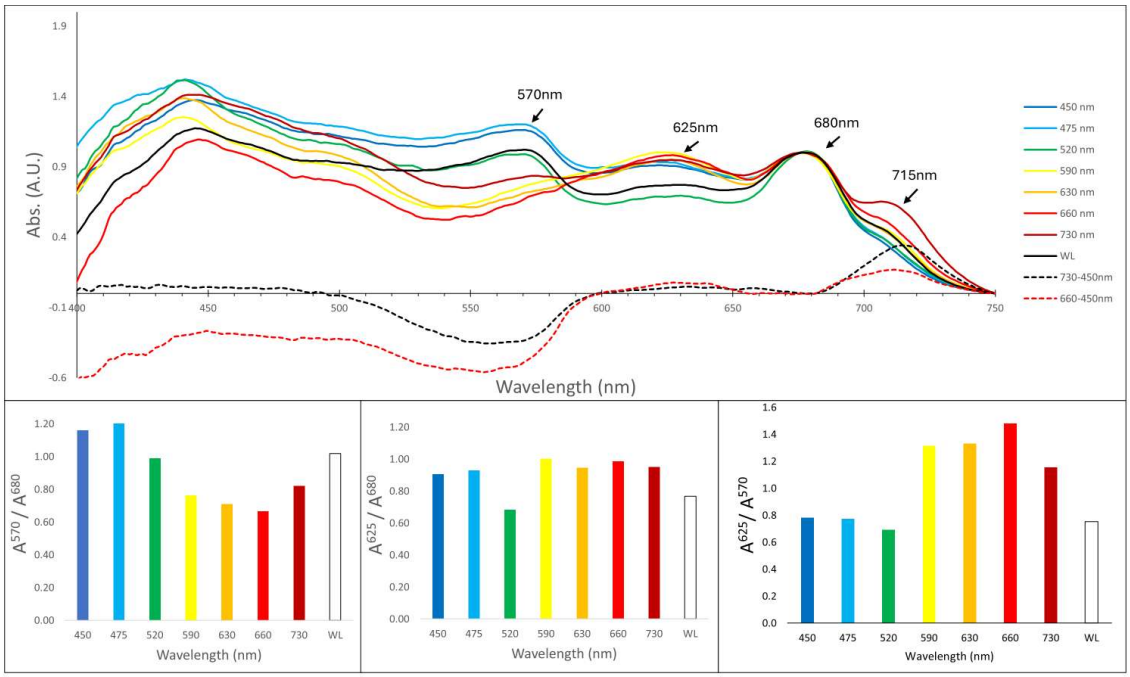

Supplementary Figure 2 Absorbance Spectra of "*Stanieria cyanosphaera*" SAG 33.87 with acclimation to different light conditions.

Absorbance spectra of cultures acclimated to various light conditions, including white light (WL), as well as wavelengths of 450 nm (Dark blue), 475 nm (Light Blue), 520 nm (Green), 590 nm (Yellow), 630 nm (Orange), 660 nm (Red), and 730 nm (Dark Red) following 17 days of acclimation. Dotted lines represent the difference between 730nm and 450nm (Black dotted line) and between 660 and 450nm (Red dotted line).

Based on 625/570 nm ratio, reflecting phycocyanin (PC): Phycoerythrin (PE) ratio, PE production was notably induced under 450 nm, 470 nm, 520 nm, and WL conditions. In contrast, at other wavelengths, from 590 to 730nm, phycocyanin (PC) production was upregulated, accompanied by a downregulation of PE synthesis. These regulations of PC:PE content support the CCA third group, as shown by Kehoe in 2010.

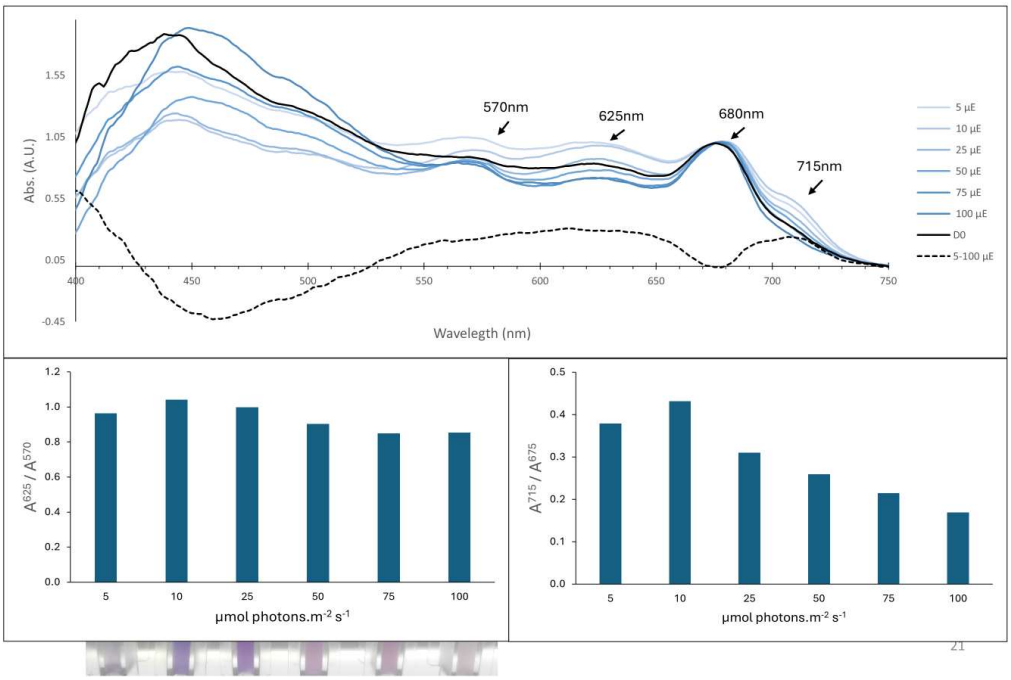

Supplementary Figure 3 Absorbance Spectra of "*Stanieria cyanosphaera*" SAG 33.87 with acclimation to different light intensity.

Absorbance spectra of cultures acclimated to various light intensity from low light to high light, including 5, 10, 25, 50, 75, 100 µmol photons.m^-2 s^-1 (in light blue to dark blue, respectively), following 17 days of acclimation. Dotted line represent difference between 5 and 100µmol photons.m^-2 s^-1.

Absorbance spectra were measured for cultures exposed to white light at intensities of 5, 10, 25, 50, 75, and 100 µmol photons m^-2 s^-1, normalized at 750 nm. No changes were observed in the ratio... suggesting that PC/PE ratio is not affected by light intensity exposure. In contrast, an increase in absorbance at 710 nm was directly correlated with a decrease in light intensity, suggesting that *Stanieria* sp. SAG33.87 performs low-light photoacclimation (LoLiP).

Based on 625/570 nm ratio, reflecting a phycocyanin (PC): Phycoerythrin (PE) ratio, no drastic changes were observed, reflecting a stable balance of PC and PC when exposed to the same light spectrum. On the other hand, 715/675 nm ratio demonstrates an increase in absorbance at 715nm, proportional to the decrease in light intensity.

4 Constitutive Far Red light harvesting in *Vitrella brassicaformis*

Short Title

Far Red acclimation of Vitrella brassicaformis

Author list

Feller Tom[1], Forêt Hadrien[1], Javaux Emmanuelle J.[2], Cardol Pierre[1*]

Affiliations

1. Genetics and physiology of microalgae, UR InBioS, University of Liège, 4000 Liège, Belgium
2. Early Life Traces & Evolution-Astrobiology, UR Astrobiology, University of Liège, 4000 Liège, Belgium

*Corresponding author: pierre.cardol@uliege.be

Funding

This research was supported by BELSPO (BRAIN project B2/212/PI/PORTAL) in the frame of the PORTAL project, the Belgian Fonds de la Recherche Scientifique projects “GALOP” (F.R.S.-FNRS, PDR T.0032) and “Life in Archean coastal environments” (FRS-FNRS PDR T.037.20), and the ULiege SRA-STEMA project UnLOC.

4.1 Abstract :

The ability to harvest far-red light (FRL) is a rare and specialized adaptation in photosynthetic eukaryotes, typically linked to acclimation processes. Here, we describe the constitutive presence of a far-red light-harvesting complex (FR-LHC) in the unicellular alga *Vitrella brassicaformis*, a close relative of *Chromera velia*. While *C. velia* exhibits inducible FRL adaptation, *V. brassicaformis* demonstrates a stable spectral shoulder at 700 nm across all light conditions tested, suggesting a novel, constitutively active FRL antenna system. Spectroscopic, fluorescence, and biochemical analyses confirm that this signature is not attributable to a novel pigment but rather to specific protein-chlorophyll *a* interactions.

HPLC pigment profiling revealed no qualitative differences under far-red light conditions but identified a highly efficient xanthophyll cycle, contributing to photoprotection under high light. Functional analyses demonstrated that *V. brassicaformis* maintains robust PSII efficiency, oxygen production, and electron transport rates under FRL.

Clear-native PAGE coupled with mass spectrometry identified FR-LHC complexes associated with PSII, further supporting their role in efficient far-red light harvesting. Our findings suggest that the constitutive adaptation of *V. brassicaformis* to FRL represents an evolutionary strategy to thrive in its niche within stony coral habitats.

4.2 Introduction

Unusual Colpodellid members

One of the distinguishing characteristics of colpodellids is their predatory activity, which involves consuming bacteria and other microscopic organic debris. However, within this group, the families Vitrellaceae and Chromeraceae are of particular interest to researchers, as they do not exhibit predatory behavior but instead perform photosynthesis.

The Chromeraceae family consists of photoautotrophic alveolates that to date, have been isolated exclusively from the stony coral *Plesiastrea versipora* in Sydney Harbor. Members of this group possess secondary plastids and exhibit molecular and morphological characteristics that closely resemble those of Dinophyta and Apicomplexa. Despite these shared traits, Chromeraceae currently contains only a single described representative: *Chromera velia* (Obornik et al, 2012).

The second family, Vitrellaceae, is represented by the algal symbiont *Vitrella brassicaformis*, which was first isolated in Australia by R. A. Andersen and R. B. Moore from the stony coral *Leptastrea purpurea* at One Tree Island. The life cycle of *V. brassicaformis* exhibits similarities to certain heterokont microalgae (Obornik et al .,2012). Santos (1996) described its vegetative cells as featuring a stigma-like red globule, which closely resembles to members of Eustigmatophyceae. Molecular studies have also demonstrated a close phylogenetic relationship between Vitrella and Apicomplexa (Janouškovec et al. 2010). The life stage under investigation in studies shares morphological features with the heterokont alga *Phaeoschizochlamys mucosa* (Phaeothamniophyceae), which is characterized by a laminated, multilayered cell wall (Obornik et al. 2012).

Initially, *Chromera velia* and *Vitrella brassicaformis* were collectively referred to as chromerids, based on their shared photosynthetic capacity, metabolic traits, and molecular phylogeny (Oborník & Lukeš, 2015). However, Obornik et al. (2012) later identified key distinctions between these taxa. For instance, *V. brassicaformis* is significantly larger, reaching a length of 40 µm , while *C. velia* only attains 10 µm. Moreover, *V. brassicaformis* lacks the finger-like projections found on the shorter flagellum of *C. velia* correct, possesses multiple laminated thick cell walls, and features a prominent pyrenoid. Unlike *C. velia, V. brassicaformis* does not produce four-celled sporangia; instead, its sporangia contain dozens of cells. Furthermore, its plastid genome differs in structure, existing as a highly compact circular genome of 85 kb, compared to 120kb for *C. Velia*. Another notable distinction is the absence of a non-canonical tryptophan codon in the plastid genome of *V. brassicaformis* (Janouškovec et al., 2010). Based on these observations, Obornik et al. (2012) reclassified these organisms into two distinct families: Chromeraceae and Vitrellaceae.

Red-shifted Light Harvesting Complex

Information concerning Red-shifted Light Harvesting Complex was moved to the introduction at section 1.7.1. Red-shifted chlorophylls in eukaryotic microalgae.

Despite extensive research efforts, many aspects of the far-red light-harvesting antennas remain poorly understood. This study reports the constitutive presence of a RLHC in *Vitrella brassicaformis*. Given its close phylogenetic relationship to *Chromera velia*, parallel comparative experiments have been conducted with *C. velia.* Spectroscopic and fluorescence analyses revealed notable similarities between these two species, further supporting the constitutive nature of this antenna. Additional biophysical analyses and native separation of photosynthetic complexes provided deeper insight into its functional role and physiological significance.

4.3 Materials and Methods

Some methods used in this chapter are the same as those used in the section dedicated to *Stanieria cyanosphaera*. For the sake of clarity and completeness, these methods are mentioned again in full and are preceded by **.

4.3.1 Strain and growth conditions

Vitrella brassicaformis CCMP3155 and *Chromera velia* CCMP 2878 were obtained from the Bigelow collection at the National Center for Marine Algae and Microbiot (NCMA). Cultures were grown in L1 medium in 500mL flasks at 26°C under PPFD of 20 µmol photons .m-2.s-1, under both white light (LL) and far-red light (FRL) conditions. The high light (HL) condition was set at 100 µmol photons $m^{-2}.s^{-1}$. For monochromatic experiments, PPFD of 20 µmol photons .m-2.s-1 was used for 450 nm, 475 nm, 520 nm, 590 nm, 630 nm, 660 nm, and 730nm.

4.3.2 Spectrofluorometry**

In vivo absorbance spectra were acquired from cell suspensions at room temperature using a BLUE-Wave Miniature Spectrometer (StellarNet Inc., Tampa, FL, USA) in conjunction with a tungsten halogen lamp SL1 with a broad spectral range of 350-2500 nm and an SL1-BLUE lamp with a blue LED (470 nm).*In vivo* fluorescence spectra were obtained at room temperature (23°C) and 77 K with an excitation wavelength of 470 nm using a USB2000+ Ocean Optics spectrometer (Ocean Optics Inc., Dunedin, FL, USA) coupled with a LightBox CCD (Beambio, France).

Absorbance or fluorescence spectra at room temperature and 77 K (excitation λ = 470 nm) from manually excised bands of the CN gel were acquired using the same equipment. After analysis, the bands were stored at -80°C. *In vivo* chlorophyll fluorescence rise measurements were performed at room temperature on cell suspensions in the presence of Ficol (20% V/V) using a JBeamP spectrofluorometer (BeamBio/API, France), with agitation to decrease the noise background. Upon the onset of actinic illumination, the fluorescence increased from a baseline value (F_0) to a stable value (F_s) in approximately 1 s. After approximately 3 s of continuous illumination, a saturating pulse (> 3000 µmol photons· m^{-2} s^{-1}, 660 nm) was applied to reaching the maximum fluorescence value (F_m). Based on the collected fluorescence values, the maximum quantum yield and the quantum yield of PSII were calculated using the following equations: $F_v/F_m' = (F_m' - F_0)/F_m'$ and $\Phi II = (F_m' - F_s)/F_m'$. The F_0 parameter reflects the minimal fluorescence intensity for cells dark-adapted for 5 minutes. For light-acclimated cells, F_s and F_m' represent the steady-state and maximum fluorescence intensities, respectively (Genty et al., 1989).

Different sources of actinic light were used, consisting of LEDs emitting at 655, 695, and 725 nm. Their PPFD (I) ranged from 0.5 to 751 µmol photons· m^{-2} s^{-1}, 1 to 448 µmol photons· m-2 s-1; 0.1 to 1385 µmol photons· m^{-2} s^{-1}; 0.5 to 75.4 µmol photons· m^{-2} s^{-1}; and 4.5 to 2737 µmol photons· m^{-2} s^{-1}, respectively.

To determine the PSII antenna size, a final concentration of 50 µM 3-(3,4-dichlorophenyl)-1,1-dimethylurea (DCMU) was added to the cell suspension. The functional antenna size at a given light intensity (expressed in s^{-1}) was calculated using the formula $\ln(2)/t_{1/2}$, where $t_{1/2}$ represents the time required to reach 50% of $F_m - F_0$. The calculated antenna sizes were then plotted against light intensity, and the slope of the resulting linear regression (σ) was determined. The electron transport rate of PSII (ETRII) at a specific light intensity was calculated using the formula $\Phi II \times I \times \sigma$, where ΦII is the quantum yield, I is the light intensity, and σ is the slope obtained from the linear regression.

4.3.3 Oxymetry**

A JTS-10 spectrophotometer (Bio-Logic Science Instruments, France, Seyssinet-Pariset) was coupled with a Firesting oxygen sensor (PyroScience GmbH, Germany, Aachen). Oxygen evolution was recorded using 4 mL of culture. The same actinic light used for ETR measurements was applied during the experiment. Inside the sealed cuvette, the cells were exposed to 5 min of darkness, followed by three consecutive 5-min light steps at 50, 100, and 300 µmol photons· m^{-2} s^{-1}, and then 5 min of darkness. The results were normalized to the chlorophyll content and expressed as pmol O2. µg Chl*a*$^{-1}$. s^{-1}

4.3.4 HPLC Analysis.**

One mL of culture was harvested and centrifuged, and the resulting pellet was resuspended in 1 mL of HPLC-grade methanol. Glass beads (0.5 mL, 0.2 to 0.5 mm, Qiagen, Germany) was then added. The cells were disrupted using a BeadBeater (FastPrep-24, MP, USA) at 8 m/s for five 10-second intervals, with 2min of cooling on ice. The cells were subsequently incubated at 4°C for 30 min and centrifuged at 20,000g for 10 min (5424R centrifuge, Eppendorf, Germany, Hambourg). The pellet was kept for PBS analysis (see below), while the supernatant was utilized for HPLC analysis. HPLC analysis was conducted as described in Berne et al., 2018. Briefly, a 70 µL pigment extract was analyzed by reverse-phase HPLC using a Prominence UFLC system (Shimadzu, Kyoto, Japan). Pigments were first eluted with a first step of 100% eluent A (80% methanol, 100 mM ammonium acetate) for 0.5 min. Eluent B (90% acetonitrile) was then used. Next a mixture of 90% eluent B and 10% eluent C (100% ethyl acetate) was applied for 5 min, followed by65% eluent B and 35% eluent C for 5.4 min. The gradient continued with 40% eluent B and 60% eluent C for 3.5 min. Finally, 100% eluent C was used for 2 min, and the separation was completed with 8 min with 100% eluent A. Pigment quantities were calculated as the ratio of the area under their respective peaks to the total area of all peaks in the chromatogram at 430 nm.

4.3.5 Protein analyses

Cells were collected and centrifuged at 500 g to obtain a 1 mL pellet. The pellets were resuspended in SHE buffer containing 250 mM sucrose, 1 mM EDTA, 10 mM HEPES, and a protease inhibitor cocktail. Cell lysis was performed using a French press (Hydrobel CLF IP55 IEC34) at 150 bar and 4°C. The lysate was then diluted threefold in SHE buffer containing the protease inhibitor cocktail and centrifuged at 600 g for 10 min at 4°C. The supernatant was collected and recentrifuged at 4°C for 15 min at 17,000 g. The final pellets were resuspended in a sucrose buffer containing 300 mM sucrose, 4 mM EDTA, 20 mM Tris, and the protease inhibitor cocktail at pH 7.2. Protein quantification was performed using the Bradford method with 5 µL of sample, 50 µL of NaOH Triton X-100 solution, and 500 µL of protein assay dye reagent diluted 5x (BioRad, USA). Absorbance at 595 nm was measured using a Lambda 265 UV/VIS spectrofluorometer (PerkinElmer, USA). Proteins from the total membrane preparations were solubilized in a buffer containing 50 mM Tris-HCl, 1.5 mM MgSO4, 100 mM NaCl, 10% glycerol, and a protease inhibitor cocktail (pH 8.4), along with 2 g of n-dodecyl-α-D-maltoside (α-DDM) per g of protein. The mixture was incubated at 4°C with gentle agitation for 30 min, followed by 30 min of rest, and then centrifuged at 21,000 g for 20 min. Supernatants with equal protein concentration were subjected to high-resolution clear-native polyacrylamide gel electrophoresis (hrCN-PAGE) using 4-12% acrylamide gradient gels. The hrCN-PAGE gel was placed in an anode buffer containing 5 mM Bis-Tris (pH 7). The cathode buffer, comprising 5 mM Tricine and 1.5 mM Bis-Tris (pH 7) (Witting et al., 2007), also included 0.05% sodium deoxycholate and 0.02% α-DDM. Protein separation was carried on under a constant voltage of 60 V for 14 hours. Following protein migration, bands were promptly excised and transferred to cuvettes maintained on ice for absorbance and fluorescence measurements and subsequently maintained at -80°C prior mass spectrometry analyses as described in section 3.3.8.

4.4 Results & Discussions

4.4.1 Spectral Signature of a Constitutive Far Red Acclimation.

Vitrella brassicaformis and *Chromera velia* were cultivated under different monochromatic light conditions at 450 nm, 475 nm, 520 nm, 590 nm, 630 nm, 660 nm, and 730 nm for 17 days. Consistently with previous findings (Kotabová et al., 2014), *C. velia* underwent chromatic acclimation, developing a peak at 706nm under red and far-red light conditions (Figure 24B).

V.brassicaformis also exhibited a absorption shoulder at 700nm, and, unexpectedly, under all light conditions (Figure 24A), or even extended periods (unreported data). Spectral analysis of methanol extracts only revealed a chlorophyll *a* absorption peak at 665nm (Figure 24A). Another notable difference was observed between the major absorption peaks of both species, *V. brassicaformis* showing a peak at 675, while *C. velia* exhibited a slightly red-shifted peak at 680nm. This FRL phenotype was maintained even after more than two years of continuous growth under WL conditions.

When the difference spectra were compared (Figure 24C), the far-red shoulders exhibited distinct absorption profiles. *Vitrella brassicaformis* had a maximum peak at 700 nm, whereas *Chromera velia* had its peak at 707 nm.

In *C. velia*, the absorption peak at 707 nm has been attributed to the formation of a specialized Red-shifted Chromera LHC. Conversely, the persistent far-red absorption shoulder observed in *V. brassicaformis* represents the first documented case of an alga exhibiting constitutive far-red light harvesting. Methanol extract analysis confirmed that this spectral feature was not caused by the synthesis of a novel pigment but is instead likely attributable to a stable LHC, which may remain across different light acclimation conditions.

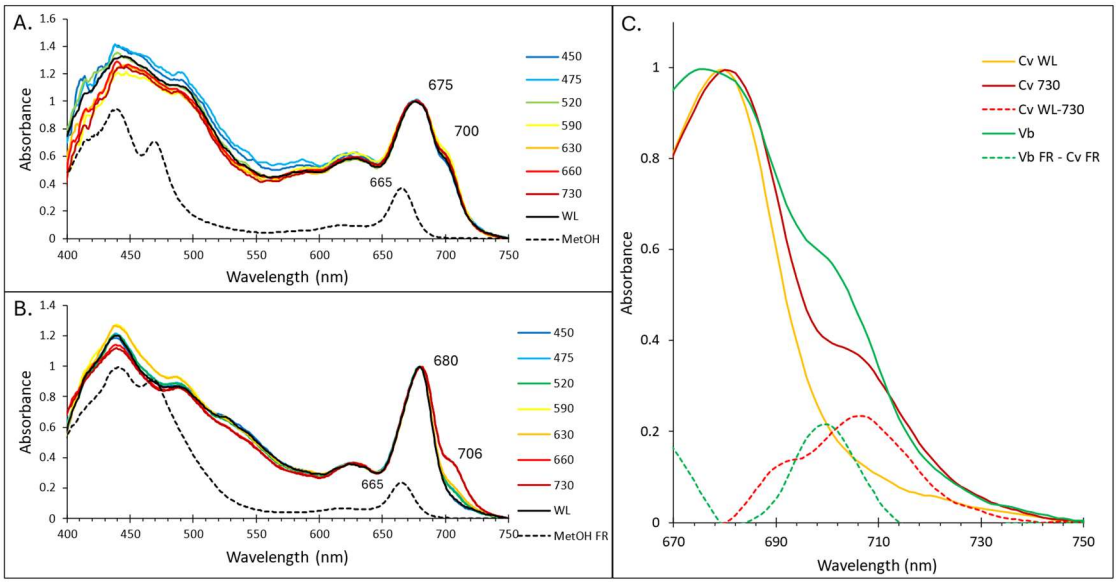

Figure 24. Absorbance Spectra of *Vitrella brassicaformis* and *Chromera velia* under different light conditions.

Absorbance spectra of (A) *V. brassicaformis* cultures and (B) *C. velia* cultures after 17 days of acclimation to different light conditions, including white light (WL, solid black line), and monochromatic light at 450 nm (dark blue), 475 nm (light Blue), 520 nm (green), 590 nm (yellow), 630 nm (orange), 660 nm (red), and 730 nm (dark red). Each spectrum is normalized to the peak at 675 nm. The difference spectra between 730nm and WL are shown as grey dotted lines. Representative absorbance spectra of methanol extract from 730 nm acclimated cells are represented by the black dotted line. (C) Absorbance spectra *of C. velia* acclimated to WL (yellow), 730 nm (red), and *V. brassicaformis* (green). Difference spectra in dotted line between *C. velia* WL vs. 730 nm (dotted red) and *V. brassicaformis* vs. *C. velia* (dotted green).

4.4.2 Fluorescence signature

Fluorescence emission spectroscopy revealed that *Vitrella brassicaformis* exhibited a single, stable peak at 708nm under room temperature conditions (Figure 25A). This emission remained stable across all acclimation conditions. In contrast, *Chromera Velia* displayed a more complex fluorescence emission profile (Figure 25B). At room temperature fluorescence, it exhibited distinct peaks at 687nm and 712nm. When exposed to white light (WL) and monochromatic wavelengths of 450, 475, 520, and 590nm, cultures displayed a single peak at 687nm. However, exposure to longer wavelengths (630nm, 660nm, and 730nm) induced a gradual red shift, resulting in a peak at 711nm. The 712/685nm ratio increased progressively from 1 to 1.1, 1.3, and 2.9 for cells acclimated to 630nm, 660nm, and 730 nm , respectively. When cells were acclimated to 730nm, a minor shift from 711 to 713nm was noted.

A similar phenomenon was observed at 77K. While *V. brassicaformis* cells consistently emitted a single fluorescence peak, *C. velia* exhibited a progressive emission shift from 690 to 718nm. Cultures adapted to 475 nm and 520 nm exhibited a single peak at 690nm. Those exposed to WL, 450 nm, and 590nm, displayed dual emission peaks at 690 and 715nm. Meanwhile, cells exposed to reddish wavelengths (630 and 660nm), exhibited a major emission peak at 717nm, which shifted to 718nm for cells acclimated to 730 nm light.

Chromera velia exhibits a pronounced chromatic adaptation (CA), as evidenced by its strong fluorescence response to blue/green and red light, suggesting an efficient regulatory mechanism involving photoreceptors. CA is a light-quality-dependent mechanism extensively studied in cyanobacteria. However, its occurrence in eukaryotic microalgae remains poorly understood (Kotabová et al. 2014).

Changes in fluorescence emission reflect the complexity and flexibility of the photosynthetic apparatus. The shift from 681 to 713 nm at room temperature has been attributed to the induction of fucoxanthin chlorophyll a/c binding protein production in *Phaeodactylum tricornutum* (Herbstová et al., 2015). This observation aligns with findings regarding Red-CLH from *C. velia* by Kotabová et al. (2014). Interestingly, *C. velia*'s red-light response is initiated within the first three days of acclimation. Cells exposed to 630 nm and 655 nm reached acclimation stability within 7 days, while acclimation to 720 nm continues progressing up to 17 days (see Supplementary Figure 1). These findings suggest that *C. Velia*'s photoacclimation is not exclusive to far-red light, although far-red remains the optimal condition for this response.

In contrast to *C. velia*, *V. brassicaformis* exhibits a consistently red-shifted fluorescence emission, regardless of light conditions. This suggests the constitutive presence of specific antenna complexes, potentially responsible for far-red light harvesting.

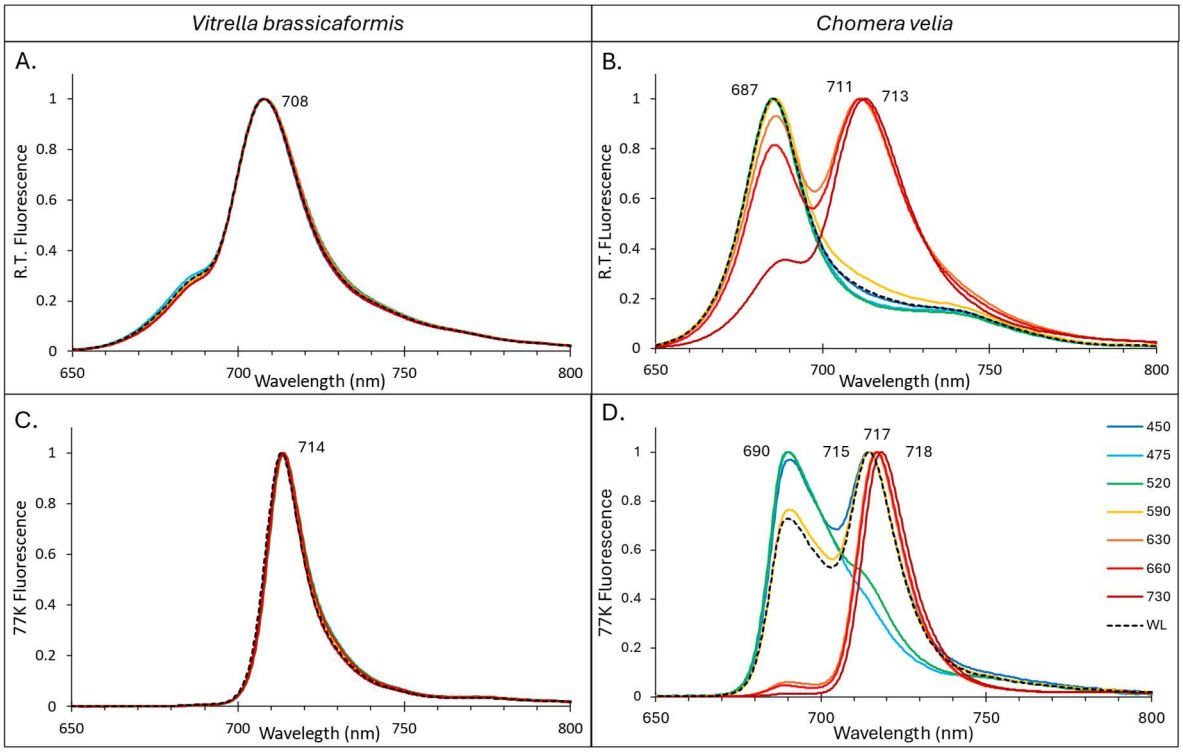

Figure 25. Fluorescence emission spectra of *Vitrella brassicaformis* and *Chromera velia* at Room temperature and 77K.

(A-B) Room temperature and (C-D) 77K fluorescence emission spectra recorded upon excitation at 470nm. Cells were cultured under various light conditions, including white light (WL, dotted black line), and monochromatic wavelengths of 450 nm (dark blue), 475 nm (light Blue), 520 nm (green), 590 nm (yellow), 630 nm (orange), 660 nm (red), and 730 nm (dark red) following 17 days of acclimation. Each spectrum was normalized to its maximum fluorescence peak.

4.4.3 Impact on the photosynthesis efficiency

Vitrella brassicaformis maintains a stable maximum quantum yield of PSII (Fv/Fm; between 0.4 and 0.5) across all light acclimation conditions (Figure 26A). In contrast, *C. velia* exhibits a higher Fv/Fm, reaching up to 0.57 in cells cultured in white light (WL), or exposed to monochromatic lights at 450 nm, 470 nm, 520 nm, and 590 nm. However, this value gradually declines to 0.3 in cultures exposed to longer wavelengths (630 -730 nm) (Figure 26B).

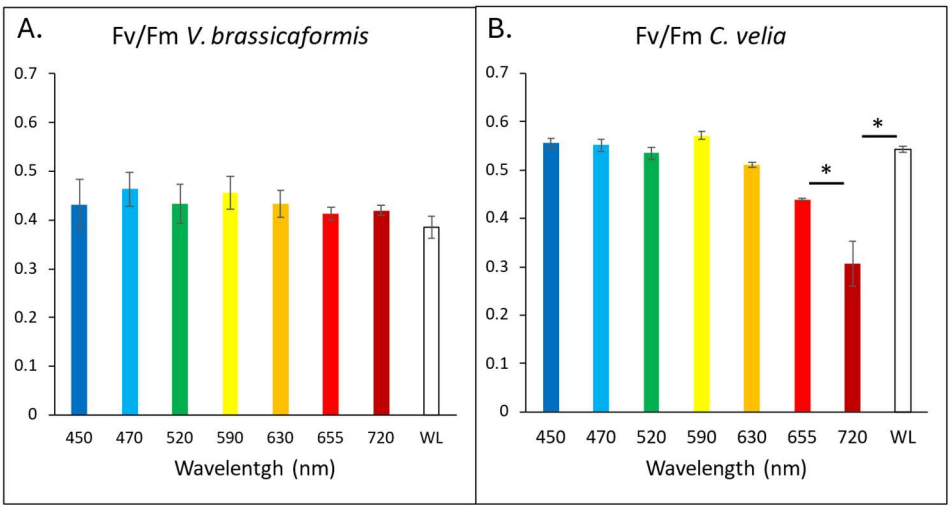

Figure 26. Maximum quantum yield of PSII (Fv/Fm) of cells cultured under

(A) Cells of *V. brassicaformis* and (B) *C. velia* were cultured under various light conditions, including white light (WL in white), as well as wavelengths of 450 nm (dark blue), 475 nm (light blue), 520 nm (green), 590 nm (yellow), 630 nm (orange), 660 nm red), and 730 nm (dark red). (n=3). Statistical analyses were performed using a t-test: , $p < 0.05$ (*).

4.4.4 Biophysics analysis.

Given the markedly pronounced spectral signature of cells acclimated to far-red light, these cells will be compared to those acclimated to white light, serving as the control. Regardless of the acclimation conditions, which showed no variations, *Vitrella brassicaformis* exhibited a significant reduction in its functional antenna size of PSII at wavelengths beyond 700 nm (Figure 27A). Interestingly, *V. brassicaformis* demonstrates greater antenna size at 700 nm than at 660 nm when acclimated to white light.

In contrast, *Chromera velia* adapted to FRL displayed a smaller PSII functional antenna size at 655m but a larger one at 715m (Figure 27B). Both acclimation conditions show a decrease in antenna size at 725m compared to 655nm.

No significant variations in the functional antenna size of PSI were observed between LL- and FRL-acclimated cells of *Vitrella brassicaformis* or *Chromera velia* (Figure 27C-D). In both species, the functional antenna size of PSI decreased drastically beyond 700 nm.

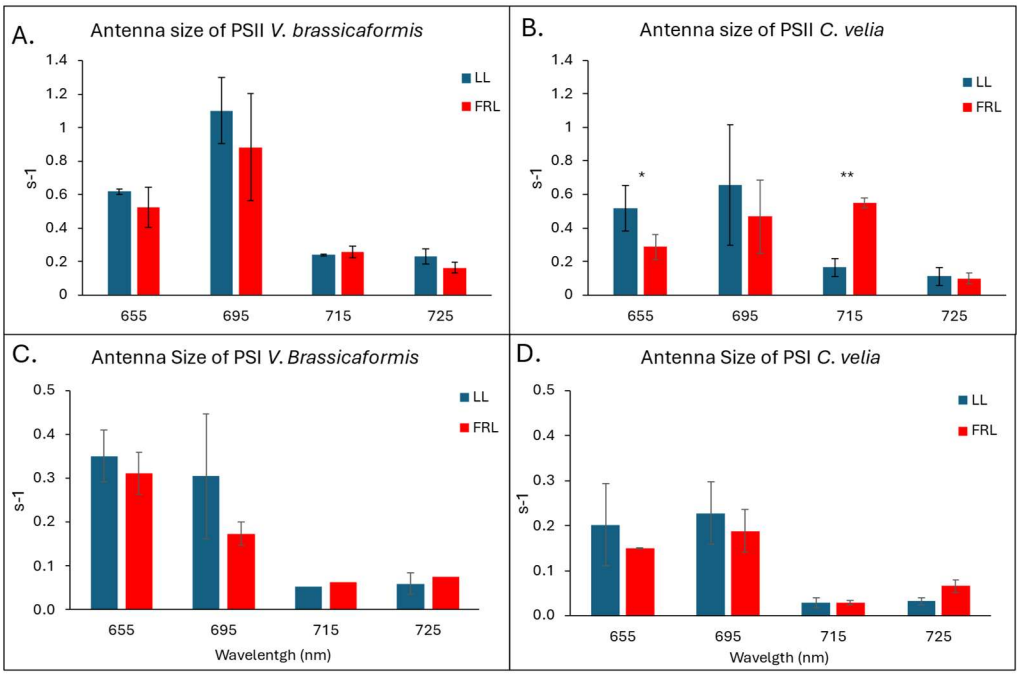

Figure 27. Functional antenna size of Photosystems.

(A-C) *Vitrella brassicaformis* and (B-D) *Chromera velia* were grown at 20 µmolphotons m^{-2} s^{-1} under white light (LL, blue bars) or Far-red light (FRL, red bars). Four different actinic lights were used to perform functional antenna size of (A-B) PSII and (C-D) PSI; 655 nm, 695 nm, 715 nm, and 725 nm, represented in s^{-1} (n=3). Statistical analyses were performed using a t-test, $p < 0.05$ (*), and $p < 0.001$ (**).

Although biophysical analyses on *Vitrella brassicaformis* and *Chromera velia* were challenging due to their tendency to aggregate and raise background noise, the application of Ficoll combined with agitation was employed to mitigate these adverse effects. *V. brassicaformis* exhibited no notable differences in electron transport rate across light conditions (Figure 28A).

Chromera velia grown under Far-red light exhibits no significant difference in electron transfer rates compared to those cultivated in white light conditions when exposed to wavelengths of 655, 695, and 725nm (Figure 28B). However, when subjected to 715 nm light, the PSII of Far-red adapted *C. velia* significantly enhances its electron transfer capabilities.

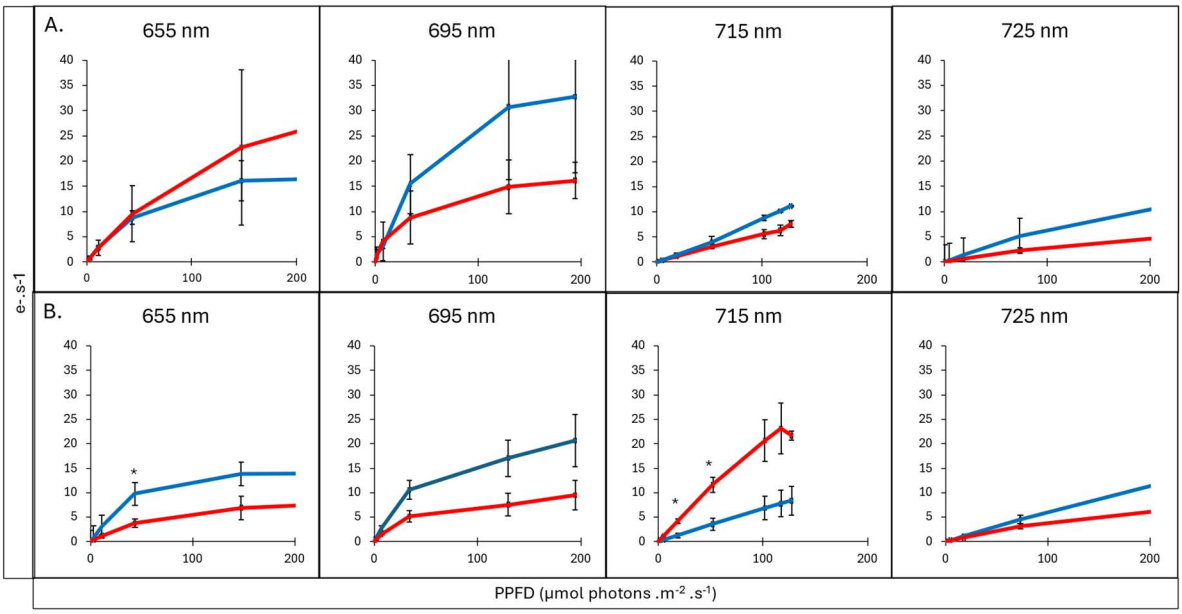

Figure 28. Electron Transport Rate (ETR) of PSII.

(A) *Vitrella brassicaformis* and (B) *Chromera Velia*, respectively were grown at 20 µmol photons m^{-2} s^{-1} under white light (LL, blue lines) or Far-red light (FRL, red lines). Four different actinic lights were used to perform the ETR of PSII; 655 nm, 695 nm, 715 nm, and 725 nm, represented in e^{-}. s^{-1}. (n=3) Statistical analyses were performed using a t-test: , $p < 0.05$ (*).

Vitrella brassicaformis maintains a constant oxygen production up to 700 nm, then drops to 50% at 725 nm (Figure 29A). No differences were observed between WL and FRL (FRL acclimated cells showed a higher oxygen production than WL acclimated cells). *Chromera velia* appears to have a slightly lower, though not statistically significant, oxygen production at 655 and 695 nm when adapted to far-red light (Figure 29B). However, at 725 nm, it shows higher production compared to low-light adaptation. Nevertheless, oxygen levels decreased to 75% and 50% for LL and FR, respectively, when illuminated from 655 nm to 725 nm.

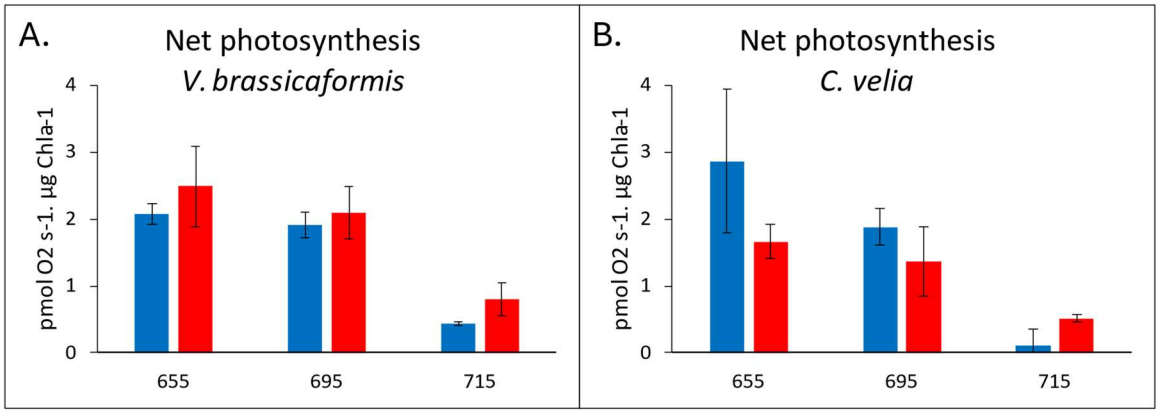

Figure 29. Oxygen production.

Vitrella brassicaformis (A) and *Chromera velia* (B) were grown under WL (Blue) and FRL (Red). Net photosynthesis was calculated by subtracting dark respiration from gross photosynthesis under 50 µmol photons m^{-2} $.s^{-1}$. Values was then normalized to Chl *a* content (n=3)

Discussion Biophysics

In *Vitrella brassicaformis*, the maximum quantum yield of PSII is stable regardless the light condition. This indicates the light variation does not affect PSII, neither its antenna state nor dark redox state of the plastoquinone pool. A stable Fv/Fm ratio has previously been reported in the diatom *Haslea ostrearia*, which even demonstrates a higher quantum yield under red and far-red light conditions (Mouget et al., 2004). In contrast, the observed decrease in Fv/Fm in *Chromera velia* suggests a limitation in its ability to adapt effectively to far-red light despite the production of Red-LHC, supporting findings by Kotabova et al. (2014). This highlights the robustness of the constitutive antenna of *Vitrella brassicaformis* to cope with light variation.

Notably, *V. brassicaformis* exhibits a larger functional antenna size at 695nm, which aligns with the absorbance shoulder of the hypothesized constitutive far-red absorbing antenna, compared to 655 nm, corresponding to the peak absorbance of traditional LHC. This indicates that PSII functional antennae are more efficient at capturing 695nm photons. Following a 17-day acclimation period to far-red light, *C. velia* demonstrates a threefold increase in functional antenna size of PSII at 725nm, while no changes were observed in PSI. This aligns with findings by Kotabova et al. (2014) that showed a functional connection between CLH and PSII.

However, while *C. velia* increased functional antenna size in the far-red region does not offset the reduction in PSII maximum quantum yield. In Contrast, Vitrella maintains a stable yield despite having a smaller functional antenna size at 725nm.

V. brassicaformis demonstrates enhanced oxygen production when previously acclimated to far-red light and maintains a 0.5-fold production under far-red light, despite no alterations in PSII efficiency across light conditions which rely on finding by Y. Li et al. (2014) that shown a decrease of oxygen production by 50% when the cyanobacteria *Halomicronema hongdechloris* was exposed to far red after acclimation. No significant differences were observed in the visible light spectrum for *Chromera velia*, which maintains low oxygen production under far-red light. *Vitrella brassicaformis* photochemistry efficiency underlines a better adaptation to a far-red light environment. The constitutive presence of the red-light harvesting complex may modify the photosynthetic chain more than expected.

4.4.5 Pigment composition, an effective xanthophyll cycle

HPLC pigment separation identified five major pigments in *V. brassicaformis*: violaxanthin, antheraxanthin, zeaxanthin, chlorophyll a, and β-carotene (Table 3A.). No significant variations were observed between far-red light (FRL) and white low-light (LL) conditions. However, under white high light (HL), a slight decrease in violaxanthin content was detected, accompanied by a notable increase in zeaxanthin levels. Additionally, antheraxanthin, an intermediate pigment in the xanthophyll cycle, also exhibited an increase. In contrast, *Chromera velia* contained four distinct pigments: violaxanthin, Isofucoxanthin-like carotenoid, Chlorophyll *a*, and β-carotene (Table 3B.).

When *C. velia* was acclimated to FRL, an increase in violaxanthin content was observed, while levels of the unidentified pigment decreased compared to LL condition. No significant differences in Chl *a* or β-carotene proportions were observable in both microalgae.

This preliminary analysis suggests that the consistent shoulder at 700 nm observed in Figure 24 in *V. brassicaformis* cells is definitely not caused by the presence of an unusual pigment but rather results from an atypical interaction between proteins and chlorophylls a, carotenoids, or xanthophyll pigments.

Exposure to high-light stress alters the redox state of plastoquinone, thereby inducing an increase in the xanthophyll cycle pool size in Chlorella vulgaris (Wilson & Huner, 2000). The violaxanthin cycle, which involves the reversible conversion of violaxanthin to zeaxanthin, with antheraxanthin as an intermediate, plays a crucial role in photoprotection (Jahns et al., 2009). Findings indicate that, while *Vitrella brassicaformis* does not exhibit significant pigment alterations in response to light quality (Far-red light versus white light), it possesses an efficient photoprotective mechanism when exposed to high-light conditions.

While *V. brassicaformis* demonstrates a classic pigmentation involved in the xanthophyll cycle, *Chromera velia* exhibits a notable alteration in pigmentation, particularly involving violaxanthin and isofucoxanthin-like carotenoid (Moore et al., 2008). The increase in violaxanthin content under FRL suggests that the cells perceive the light intensity as lower compared to LL conditions, potentially explaining the observed photoacclimation response. Although it is assumed that violaxanthin has an active role in photoprotection and light harvesting (Kotabova et al., 2011), the precise nature and function of the isofucoxanthin-like carotenoid remain unresolved., The observed exchange between violaxanthin and isofucoxanthin-like carotenoid under changing light conditions suggests a potential role in the xanthophyll cycle.

A. *Vitrella brassicaformis*

%	LL	FRL	HL
Violaxanthin	24.7 ± 1.9	22.9 ± 1.6	19.14 ± 1.4
Anteraxanthin *	5.4 ± 0.2	4.0 ± 0.2	8.28 ± 0.8
Zeaxanthin *	1.95 ± 0.3	1.54 ± 0.3	6.19 ± 0.4
Chl a *	66.6 ± 3.6	68.85 ± 3.8	64.28 ± 0.3
β-Carotene	1.29 ± 1.44	2.81 ± 0.4	2.11 ± 0.6

B. *Chromera velia*

%	LL	FRL
Violaxanthin *	11.2 ± 2.6	18.4 ± 0.7
Isofucoxanthin *	16.9 ± 0.7	9.1 ± 0.3
Chl a	69.7 ± 3.8	70.2 ± 1.3
β-Carotene	2.1 ± 0.5	2.3 ± 0.3

Table 3. HPLC pigment separation from *Vitrella brassicaformis* and *Chromera velia* under different light conditions.

Relative pigments composition of (A) V. brassicaformis and (B) *C. velia* acclimated to low white light (LL), far-red light (FRL), and high white light (HL) conditions. Pigments in V. brassicaformis include violaxanthin, antheraxanthin, zeaxanthin, chlorophyll a (Chl a), and β-Carotene while. *C. velia* contains violaxanthin, an isofucoxanthin-like carotenoid, Chl a, and β-Carotene. Pigment quantities are expressed as the ratio of the area under their respective peaks to the total chromatographic peak area at 430 nm (n=3). Statistical analyses for V. brassicaformis were performed using an ANOVA test, $p < 0.05$ (*). Statistical analyses for C. velia were performed using a t-test, $p < 0.05$ (*).

4.4.6 Composition and Fluorescence Properties of Photosynthetic Complexes in Vitrella brassicaformis

Considering the constitutive presence of the red-light harvesting complex (RLHC), only *Vitrella brassicaformis* grown under white light was used to investigate the composition of photosynthetic complexes. Membrane-bound complexes were solubilized using the presence of alpha-dodecyl maltoside and separated by clear-native polyacrylamide gel electrophoresis (CN-PAGE) (Fig 30A). Five distinct bands were visualized, and their absorption and fluorescence spectra were recorded and revealed distinct maxima (Figure 30B).

The first band exhibited a peak absorption at 680nm, a signature of PSI (Nagao et al., 2023), and a main room temperature (R.T.) fluorescence emission peak at 680 nm. 77K fluorescence reveals a maximum emission at 710 nm and secondary peaks at 722 and 687nm, suggesting a super complex with PSI, PSII, and LHC.

The second band exhibited the same profile as the first band except the 77K fluorescence that displayed a maximum emission at 722nm, a signature of PSI (Nagao et al., 2025). The thickness of the peak at 710nm is believed to be to the presence of associated LHC (Umetani et al., 2017).

The third band had a maximum of absorbance at 675nm and a similar R.T. fluorescence emission to the first two bands. The maximum 77K fluorescence emission at 687 nm with a secondary peak at 710nm suggested the presence of PSII with associated LHC (Umetani et al., 2017).

The fourth exhibited the presence of the red light harvesting complex (RLHC) with a maximum at 670nm and a secondary peak at 700nm. R.T. fluorescence presented a shifted emission peak compared to the other first. Secondary peak emission at 684 and 687 nm for R.T. and 77K fluorescence, respectively, revealed the presence of PSII associated with the RLHC.

The fifth band presented a similar absorbance spectrum to the fourth. R.T. and 77K fluorescence suggested a full free RLHC composition with its own signature.

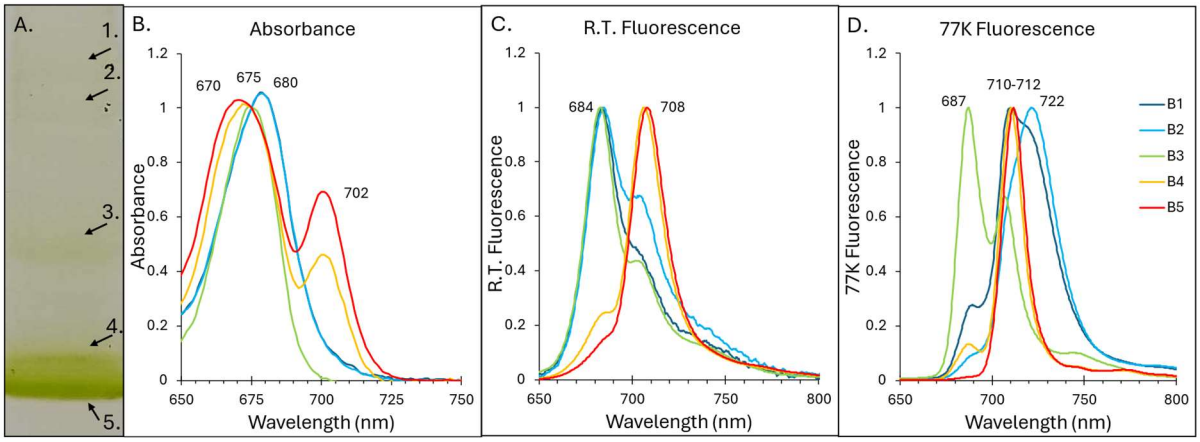

Figure 30. Spectroscopic characterization of photosynthetic complexes of Vitrella brassicaformis.

(A) Clear-Native Polyacrylamide Gel Electrophoresis (CN-PAGE) separation of pigment-protein complexes from total membranes solubilized with 2% n-dodecyl α-D-maltoside. Each lane was loaded with 75 µg of protein (a representative experiment is shown). (B) Absorption and (C-D) fluorescence emission (R.T. and 77k, excitation at 470 nm) spectra of bands. (n=3)

4.4.7 Mass Spectrometry

Consistent with the spectral signatures of PSI, band 1 and 2 contained mainly proteins associated with PSI , while proteins from PSII were detected in bands 3, 4, and 5. Several light-harvesting complex (LHC) proteins were also found in all these bands. In particular, a cluster of two fucoxanthin-chlorophyll-binding proteins (FCP) (accession numbers A0A0G4G849 and A0A0G4G7V1 in positions 99732 and 9733, respectively) was abundant in bands 4 and 5, and was also present in band 3. In contrast, these proteins were absent from bands 1 and 2, suggesting their association with PSII. Interestingly, these proteins are orthologs of *Thalassiosira pseudonana* LhcF7 and Lhcf11 (https://inparanoidb.sbc.su.se/cluster/296877569), that are found in association with all PSII supercomplex in this diatom species (Calvaruso et al, 2020), as FPCII dimers (Feng et al., 2023) No LHC strictly confined to bands 4 and 5 were detected.

4.4.8 Composition and Fluorescence Properties of Photosynthetic Complexes in *Chromera Velia*

The separation of photosynthetic complexes of *Chromera velia* by CN-PAGE revealed five distinct bands (Figure 31A). Absorbance spectra exhibited minor maximal peak variations ranging from 674 to 679 nm for WL and FRL acclimated cells (Figure 31B-C). Bands from FRL acclimated cells displayed a small shoulder at 705 nm. This peak was more pronounced for band 5 and absent in band 4.

Room temperature fluorescence emission spectra of bands from WL cells exhibited identical maximal peaks at 682 nm, with the exception of band 5, which displayed a secondary peak at 705 nm (Figure 31D). Bands from FRL cells demonstrated a consistent shift to 710-712 nm (Figure 31E). Band 4 exhibited a secondary peak at 685 nm.

The 77K fluorescence emission spectra of bands from WL complexes exhibited a predominant absorbance at approximately 690 nm, with the exception of band 1, which demonstrated maximal emission at 712 nm, and band 5, which displayed a secondary peak at 716 nm (Figure 31F). All maximal band emissions from FRL were observed to shift to 716 nm. Band 5 exhibited a secondary peak at 685 nm. The remaining bands, excluding band 1, presented a secondary peak around 690 nm.

CN-PAGE highlighted the importance of the Red-LHC. The fluorescence emission signature of this modified LHC reveals its presence in all the complexes of the photosynthetic chain. Although Red chlorophylls are associated to PSI in cyanobacteria (Brecht, 2009) or plant (Gobets & Van Grondelle, 2001), in eukaryotic microalgae it is often shown their connection to PSII (Kotabova et al., 2014) In *Ostreobium* sp., PSI antenna Lhca1, composed of red chlorophylls, are atypically attached to PSII, wich enable the energy transfer from red chlorophylls to the reaction center of PSII. Although Kotabova et al. (2014) showed a functional connection between Red CLH and PSII, no evidence proves no connection to PSI.

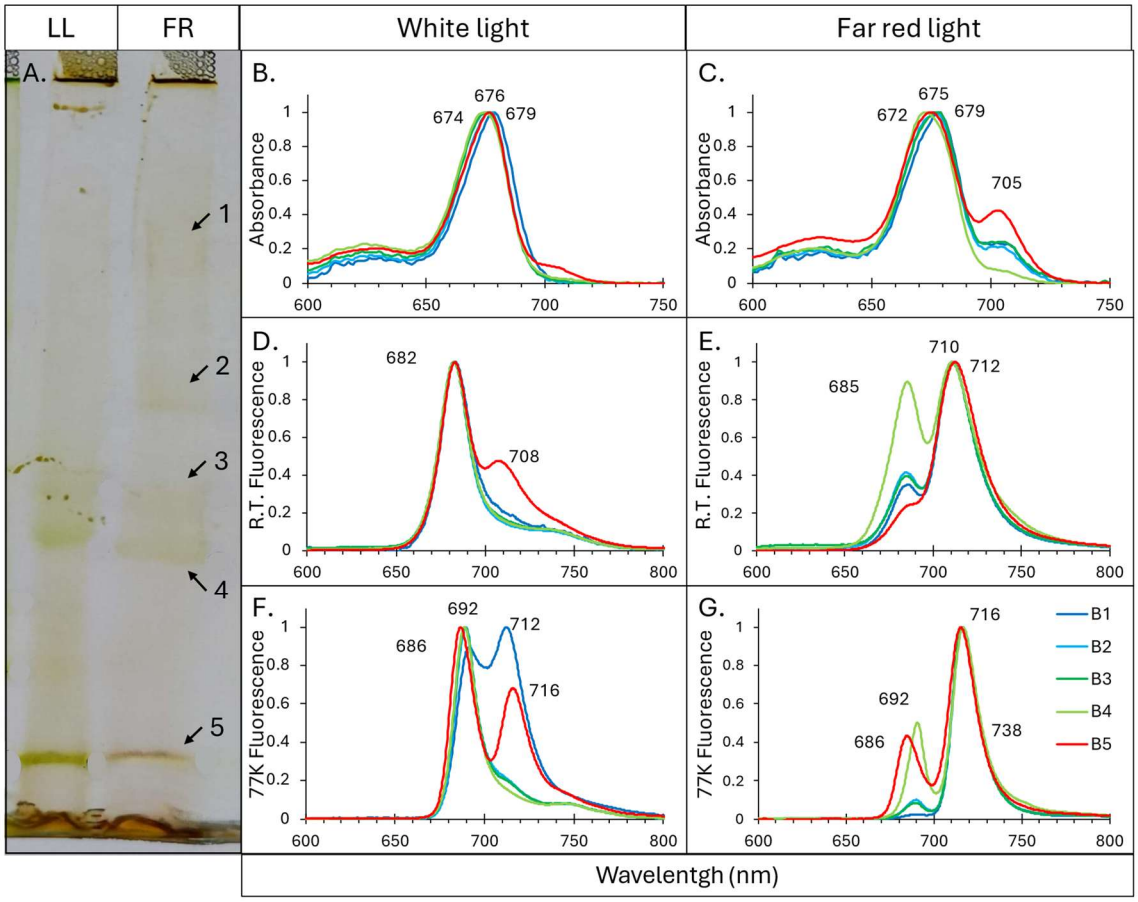

Figure 31. Spectroscopic characterization of photosynthetic complexes of *Chromera velia*.

(A) Clear-Native Polyacrylamide Gel Electrophoresis (CN-PAGE) separation of pigment-protein complexes from total membranes solubilized with 2% n-dodecyl α-D-maltoside. Each lane was loaded with 75 µg of protein. (B-C) Absorption, (D-E) room temperature (R.T.) and (F-G) 77K fluorescence emission spectra of each band upon excitation at 470 nm.

4.5 General Conclusion

Vitrella brassicaformis was originally isolated from a unique habitat within the stony coral *Leptastrea purpurea* along the Australian coast and has not been reported yet outside this specific niche. Although it can be maintained in laboratory flasks, it remains uncertain whether it has a free-living stage, given its limited motility and its close relative to the Apicomplexan, a group typically comprising endoparasitic or symbiotic organisms. Its adaptation to a constrained, low-light environment likely drove the necessity for far-red light adaptation, a capacity that appears to be constitutively expressed. This ability may provide a competitive advantage over other microalgae, reinforcing its role *as* a favored symbiont of *L. purpurea*.

Our findings demonstrate that *V. brassicaformis* maintains stable photosystem II (PSII) efficiency across various wavelengths while preserving both functional antenna size and effective electron transport. Sustained oxygen production under 700 nm light and beyond suggests a high degree of adaptability of *V. brassicaformis*. Separation of the photosynthetic complexes indicates that direct or indirect PSII components underlie this adaptability. However, the exact composition of this potential far-red antenna remains to be determined.

Future research should focus on several key approaches to deepen our understanding of *Vitrella*'s light-harvesting complexes. Phylogenomic analysis could help determine whether a specific LHC family is unique to *Vitrella* or if certain LHCs share evolutionary links with those involved in far-red light (FRL) absorption in other organisms. Additionally, improving purification methods is essential to better distinguish actual components of PSI/PSII from potential contaminants. Finally, cryo-electron microscopy (cryo-EM) could provide valuable structural insights, though it may not identify the specific proteins responsible for light absorption.

4.6 Supplementary figures :

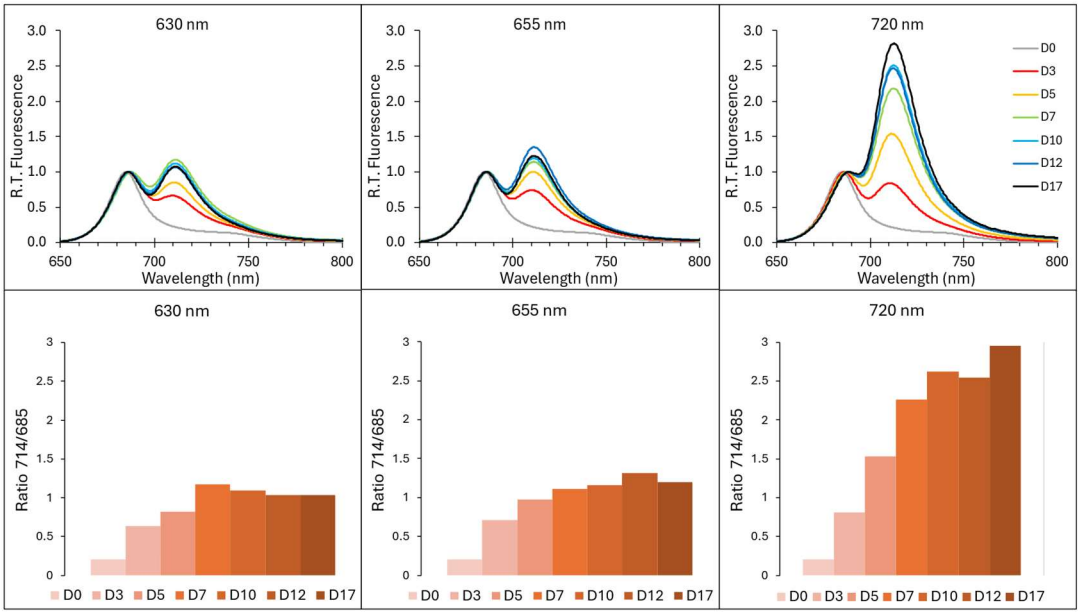

Supplementary Figure 1. Room temperature (R.T.) fluorescence evolution of *Chromera velia* under different wavelength.

(A) R.T. Fluorescence spectra of *C. velia* acclimated to monochromatic light conditions and (B) Ratio between 714 nm and 685 nm. Cells were acclimated to the same wavelength as in Figures 1,2, and 3. Only relevant wavelengths were shown, such as 630nm (left panel), 655nm (center panel), and 720 nm (right panel). Each spectrum was normalized at 685nm.

5 A Unique LHCE Light-Harvesting protein Family is involved in Far-Red Absorption and State Transitions-like mechanism in *Euglena gracilis*

Héctor Miranda-Astudillo[1,2], Rameez Arshad[3], Félix Vega de Luna[1], Zhaida Aguilar-González[2], Tom Feller[1], Hadrien Forêt[1], Wojciech Nawrocki[1,4], Charles Counson[1,5], Pierre Morsomme[6], Hervé Degand[6], Denis Baurain[5], Roman Kouřil[3], Pierre Cardol[1]

[1] Genetics and Physiology of microalgae, InBioS/Phytosystems, University of Liège, Belgium.

[2] Present Address: Departamento de Biología Molecular y Biotecnología, Instituto de Investigaciones Biomédicas, Universidad Nacional Autónoma de México, Mexico City, Mexico.

[3] Faculty of Science, Department of Biophysics, Palacký University Olomouc, Czech Republic.

[4] Institute of Physical and Chemical Biology, French National Centre for Scientific Research, France.

[5] Phylogénomique des Eucaryotes, InBioS/Phytosystems, University of Liège, Belgium.

[6] Institut des Sciences de la Vie, Université Catholique de Louvain, Louvain-la-Neuve, Belgium.

Contribution to the study :

This study was conducted through international collaborations. During my thesis, I contributed to the investigation of LHCE by performing in vivo biophysical analyses, including antenna size measurements, state transitions. Additionally, CN-PAGE was conducted to isolate protein complexes, followed by spectral and fluorescence analysis of the resulting bands. Mass spectrometry, along with related analyses, as well as EM characterization and phylogenetic analysis, were performed by other contributors.

5.1 Abstract

The light-harvesting complexes (LHCs) of land plants and green microalgae play a crucial role in balancing efficient photon capture under low light conditions while mitigating photodamage in high-light environments. The regulatory mechanisms involve modulating the number of LhcbM trimers associated with photosystem II (PSII) and key photoprotection processes, which include heat-dissipation and state transition. *Euglena gracilis,* a secondary green flagellate, has evolved two large Lhc protein families, Lhcb and Lhca, similar to those found in plants and microalgae, although they are not orthologous apart from CP29. Through a combination of phylogenomic, biochemical, and spectroscopic analyses, we reveal that the *Euglena* antenna Lhca protein family is a novel far-red-shifted antenna protein family, now designated as LhcE. Both PSI and PSII in *E. gracilis* retain large antennae regardless of light culture conditions. CP26-less PSII associates with up three LhcbM trimers and one LhcE antenna, while a minimal PSI core composed by PsaA-F, PsaJ, and PsaM is surrounded by an expanded LhcE/LhcbM belt. Additionally, a pentameric LhcE antenna complex preferentially accumulates under low-light and far-red conditions, where it dynamically attaches to or detaches from PSII, functioning in a state transition-like mechanism. These findings provide new insights into alternative photosynthetic adaptation strategies and highlight the evolutionary diversification of light-harvesting mechanisms in secondary plastids.

5.2 Introduction

Photochemical reactions of oxygenic photosynthesis occur in two membrane-embedded complexes: Photosystem II (PSII) and I (PSI). Each photosystem consists of a core complex (CC), which includes a reaction center (RC) and structural subunits, along with an inner antenna system. Additionally, each CC is surrounded by a specific light-harvesting complex (LHC) (Cao et al., 2018; Caspy and Nelson, 2018). The two photosystems absorb different wavelengths of light and function cooperatively during photosynthesis (Emerson, 1957). Excess light primarily damages PSII (Aro et al., 1993), although PSI is also susceptible to photoinhibition, particularly at low temperatures (Sonoike, 1995).

PSI contains a small number of “red” or low-energy chlorophylls, which play a crucial role in regulating energy transfer within its antenna system (Shubin et al., 1992). In plants, most of these “red” chlorophylls are located in the peripheral antenna LHCI (Croce et al., 1998). In contrast, cyanobacteria, which lack the LHCI antenna, incorporate red chlorophylls in their core antenna, with the number varying among species (Karapetyan et al., 2014). Similarly, the *Chlamydomonas reinhardtii* PSI-LHCI complex contains five to six red chlorophylls situated near the RC, likely at the RC-LHCI interface (Gibasiewicz et al., 2005).

While the composition of reaction centers has remained virtually unchanged throughout the evolution of Viridiplantae, LHCs have diversified significantly in photosynthetic eukaryotes (Islam et al., 2020; Koziol et al., 2007; Six et al., 2005). In Viridiplantae, the PSII CC comprises at least 20 subunits, including the dimeric D1/2 RC, inner light-harvesting proteins (CP43 and CP47), over a dozen of low-molecular mass transmembrane subunits (LMM) (PsbE/F/H/I/J/K/L/M/S/Tc/W/X/Z/30/LHCSR), including cytochrome b_{559}, which is not involved in the primary electron transfer pathway in PSII but may participate in secondary electron transfer pathways that protect PSII against photoinhibition (Chu and Chiu, 2016), and the extrinsic subunits of the oxygen-evolving complex (OEC) (PsbO/P/Q). Surrounding PSII CC are located three minor antennas, *i.e.* Lhcb4 (CP29), Lhcb5 (CP26), Lhcb6 (CP24) (Graça et al., 2021; Shen et al., 2019). CP29 and CP26 are essential for non-photochemical quenching (NPQ) in *Chlamydomonas reinhardtii* (Cazzaniga et al., 2020), while CP29, CP26, CP24 are involved on NPQ in plants (Miloslavina et al., 2011). PsbS is a light-stress sensor essential for plant photo protection (Marulanda Valencia and Pandit, 2024) instead of LHCSR, described for green microalgae (Niyogi and Truong, 2013). Viridiplantae PSI CC includes the pseudo-symmetric RC dimer (PsaA/B), ten additional subunits (PsaF/G/H/I/J/K/L/M/N/O) surrounding it, and a stromal cluster composed of PsaC/D/E (Naschberger et al., 2022). PsaG, PsaH, PsaN and PsaO are unique to microalgae and flowering plants. PsaH and PsaO, together with PsaL, are involved in forming a domain in PSI that associates with LHCII to participate in state transition (Yang et al., 2015). Red algal PSI evolved a PsaO subunit at the PsaL/A/K side (Tian et al., 2017) instead of the cyanobacterial PsaX subunit (Chen et al., 2022). PsaA, PsaC, PsaD, PsaE and PsaF are involved on ferredoxin interaction, while PsaF and PsaN interact with plastocyanin to complete the electron flow through plant PSI (Amunts et al., 2007; Caspy et al., 2020).

Euglena gracilis is a photosynthetic flagellate belonging to the Euglenid group, which acquired its chloroplast through a secondary endosymbiosis with a green alga. Unlike primary plastids, *Euglena* chloroplasts possess an additional third envelope membrane, and their thylakoid membranes do not form stacked membrane regions (Klein et al., 1972). The *Euglena* PSII contains PsbA/B/C/D/O/P/Q and the OEC subunits (Suzuki et al., 2004). However, it lacks the minor antennae CP24 (Lhcb6) and CP26 (Lhcb5), and only CP29 (Lhcb4) has been detected (Koziol et al., 2007). Additionally, PsbX/Y, which are associated with PSII susceptibility (Biswas, 2018), were not identified (Sobotka et al., 2017). On the other hand, only five plastid-encoded (PsaA/B/C/J and ycf4) and four nuclear-encoded (PsaD/E/F and ycf3) subunits have been identified in sequence databases so far (Sobotka et al., 2017). Most *Euglena* LHCs are synthesized as large polyproteins precursors from mRNAs, and post-translationally cleaved into individual proteins within the chloroplast. Phylogenetic analyses categorized these LHCs into 8 groups of LhcbM (I-VIII), and at least 5 groups of Lhca proteins (Koziol et al., 2007; Koziol and Durnford, 2008).

Euglena contains the xanthophyll cycle pigments, including diadinoxanthin and diatoxanthin, but lacks lutein, fucoxanthin, and pigments associated with the violaxanthin cycle. Additionally, its chlorophyll *b* content is relatively low (Cunningham and Schiff, 1986). Light-dependent spectral changes have been reported (Brown and French, 1961; Winter and Brandt, 1986; Doege et al., 2000), likely mediated by a shared antenna system used for both photosystems, consisting of LHCI and LHCII proteins (Doege et al., 2000; Winter and Brandt, 1986). The absence of non-photochemical quenching (NPQ) as a photoprotective mechanism has been reported (Winter and Brandt, 1986; Doege et al., 2000) and significant PSII photodamage has been observed in *Euglena* cells exposed to high light intensities (Nagao et al., 2021; Doege et al., 2000).

In this study, we further investigate the structural and functional light mechanisms of adaptation in the photosynthetic machinery of *E. gracilis*, with a particular focus on LHC association with PSI and PSII under far-red and light-limiting growth conditions.

5.3 Material and Methods

5.3.1 Algal strain, Growth conditions, and Total membrane preparation

Euglena gracilis (SAG 1224-5/25) was obtained from the University of Göttingen's Sammlung von Algenkulturen (Germany). Cells were grown in continuous low-light conditions, illuminated with a white, fluorescent lamp at a photosynthetic photon flux density (PPFD) of 50 µmol photons m^{-2} s^{-1} . *Chlamydomonas reinhardtii* cell-wall–less mutant (*cw15 mt+*) strain was grown at 50 µmol photons m^{-2} s^{-1} with 3000K LED illumination as previously described (Rodríguez-Bolaños et al., 2024).

The liquid mineral Tris-minimum-phosphate (TMP) medium (pH 7.0) (Harris et al., 2009) was supplemented with a CO_2 flow (20% in air) and a mix of vitamins (biotin 10^{-7} %, B_{12} vitamin 10^{-7} % and B_1 vitamin 2×10^{-5} % (w/v)).

Cells were harvested at the mid-logarithmic phase by centrifugation at 7000 x *g* for 10 min and stored at -70 °C until use. Cell disruption and total membrane preparation by differential centrifugation were performed as described previously (Yadav et al., 2017), with final centrifugation step adjusted to 17000 x *g*. Membrane fractions were stored at -70 °C until further analysis. Protein concentration was determined by the Bradford method (Bio-rad).

5.3.2 Native electrophoresis

Total membrane fractions were solubilized using n-dodecyl-α-D-maltoside (α-DDM) or n-dodecyl-β-D-maltoside (β-DDM) at a detergent-to-protein ratio of 2.0 g /g in solubilization buffer (SB). The SB contained 50 mM Tris-HCl (pH 8.4), 1.5 mM $MgSO_4$, 50 mM aminocaproic acid, 100 mM NaCl, 10% glycerol, 1 mM phenylmethylsulfonyl fluoride (PMSF), and 50 µg/mL tosyl-lysyl chloromethyl ketone (TLCK). The mixture was incubated at 4 °C with orbital agitation for 2h, and centrifuged at 30,000 x *g* for 30 min.

The resulting supernatants were subjected to high-resolution clear native polyacrylamide gel electrophoresis (*hr*CN-PAGE) (Wittig et al., 2007) using 4%–12% acrylamide gradient gels. To enhance protein resolution, 0.05% sodium deoxycholate and 0.02% α-DM were added to the cathode buffer.

5.3.3 Identification of PS subunits

After electrophoretic separation by *hr*CN-PAGE, bands of interest were manually excised from the gel and subjected to liquid chromatography coupled with electrospray-ionization quadrupole time-of-flight mass spectrometry quantitative analysis (LC-ESI-Q-TOF-MS) as previously described. All the obtained sequences (Suppl. Information) were identified with MASCOT against public protein databases (NRPS/NCBI, UniProt) and our homemade database (available in https://figshare.com/s/57d2ba4ebfbb472ae3de?file=11461148).

5.3.4 Phylogenetic analysis

The conceptual translations of the complete genomes of 272 organisms broadly sampled across the Tree of Life were downloaded from [figshare Life-OF-Mick]. Those protein sequences were submitted to an orthology inference pipeline relying on NCBI-BLAST v2.2.28+ and OrthoFinder v1.1.2 and an inflation parameter set at 1.2. In parallel, reference sequences for PSI/PSII subunits (and a few other proteins) were compiled from the literature for model organisms (C. reinhardtii, Arabidopsis thaliana, Ostreococcus tauri, Synechocystis PCC 6803) [Extended dataset 1 _ Suppl table sheet 0_REF_SEQ]. These reference sequences proteins were then used to fish out the orthogroups of interest through UBLAST (v7.0.959) searches. The script post-processed [process-OGs.pl] was then used so as to identify cases of suboptimal delineation among the orthogroups, i.e., when several reference proteins matched a single (possibly quite large) orthogroup and/or when a single reference protein matched several orthogroups. This step led to the combination of pairs or triplets of orthogroups in order to consolidate families spread over multiple orthogroups [table-that-I-can-build-from-Charles-data-if-needed]. The orthogroups (both single and combined) were then directly aligned with MAFFT v7.273, except for those including ZEP and STK-STN sequences, which were first subsampled based on iterative HMMER (v3.1b2) searches using aligned reference proteins to seed the HMM profiles. Alignments were manually curated using the editor of the MUST software package and then enriched in orthologous sequences using a prerelease version of Forty-Two. This allowed us to mine complete genomes and transcriptomes that were not included in the original taxon sampling [table-to-do]. In particular, we searched four different transcriptome datasets of *Euglena gracilis*, among which the three public datasets analyzed in (Cordoba et al., 2021), to maximize the odds to recover orthologues. For the LHC tree, we specifically used the sequences determined by Koziol (Koziol et al., 2007; Koziol and Durnford, 2008). Enriched alignments were then filtered to discard too partial sequences and to remove

columns containing too many gaps. This was done using ali2phylip.pl (from the Bio-MUST-Core software package) with the corresponding parameters (min and max) set to 0.50 and 0.01, respectively. Phylogenetic inference was carried out using RAxML v8.1.17 under the model PROTGAMMALG4X and 100 rapid bootstrap replicates. The resulting trees were formatted with format-tree.pl, uploaded to iTOL with import-itol.pl and eventually downloaded in their final form with export-itol.pl, all three scripts being also part of Bio-MUST-Core.

For the LHC trees, a number of additional steps were performed. In particular, the 72 LHC sequences identified by Koziol were supplemented by additional sequences recovered from the three transcriptomes analyzed in Cordoba et al. 2021. To this end, the LHC alignment was first stripped out of non-primary green sequences and used in a very sensitive run of Forty-Two (i.e., at a E-value threshold of 1e-05 and with the BRH, trimming, merging and aligning options all disabled). The 160 candidate transcripts were then submitted to the script xlate-and-splice.pl 1) to assemble the sequences using CAP3 (with -p 98 and -o 40), 2) to translate the potential polyproteins in the six possible reading frames and 3) to splice the resulting ORFs based on a PSSM derived from the 44 10-AA linkers described in Koziol 2008. The log L threshold was set to –17 and the minimum ORF/segment length to 24 AA. The 1274 protein fragments were again searched with Forty-Two (setup as above) in order to recover 165 genuine LHC homologues. These new sequences were named as follows: <accession>/<frame>/<orf#>/<segment#>@<length>, e.g., GDJR01029061.1+2/F+2/O1/P1@327, then combined with those of Koziol and dereplicated at an identity threshold of 100% with CD-HIT, eventually resulting into 158 unique LHC sequences Figure S1.

LHC proteins-to-PS core ratios were calculated using averaged values from four major PSII core subunits (PsbA, B, C, and D) or PSI core subunits (PsaA, B, D, and F). Two main factors may influence quantification: (i) differential trypsin digestion efficiency across proteins, and (ii) variation in peptide ionization efficiency. Given the sequence and structure similarities between LHCs (Figure S3, Suppl. Information), we assumed these factors have a negligible impact on LHC quantification. However, variations in abundance of core PSII and PSI subunits (up to a two-fold difference) were observed, prompting us to use averaged values.

5.3.5 Spectrometry

Room temperature absorbance and fluorescence spectra (excitation λ = 470 nm) were obtained using a USB2000+ Ocean Optics spectrometer (Ocean Optics Inc., Dunedin, FL, USA) coupled with a CCD LightBox (Beambio, France). CN gel bands were immediately analyzed after electrophoretic migration.

In vivo chlorophyll *a* fluorescence measurements were evaluated with a Joliot Type Spectrophotometer (JTS-10, Biologic, France). Cells were resuspended in fresh medium at a concentration of 5 µg Chl per ml and maintained under shaking dark conditions. Samples were placed into square cuvettes and continuously stirred using a magnetic stirrer. Before fluorescence recording, dark adaptation was conducted for 10 min. Chlorophyll fluorescence was recorded at regular intervals using 10 µs blue detection light pulses. 200 ms saturating pulses of red light (660 nm) were applied to transiently close the PSII reaction centers, allowing measurement of the maximum fluorescence values (Fm). After dark acclimation inside the spectrofluorometer, a weak far-red light (70 µE m^{-2} s^{-1}) peaking at 720 nm was applied for 15 min. Both dark-acclimated and far-red-acclimated cells were then transferred immediately to a USB2000+ Ocean Optics spectrometer (see above).

The light absorption cross-section of PSII (σ) was determined within the JTS-10 under two different light conditions: red light (25 µE m^{-2} s^{-1}) and far-red light (300 µE m^{-2} s^{-1}). Following dark or far-red light acclimation inside the JTS-10, cells were treated with 10 µM DCMU, an inhibitor of plastoquinone reduction by PSII. After 30 s dark incubation, light was activated, and chlorophyll fluorescence values were recorded. The σ value was calculated as the reciprocal of the time required to reach two-thirds of Fm during fluorescence induction.

5.3.6 Pigment analysis

Bands of interest were manually excised from the CN gel, flash-frozen in liquid nitrogen, and crushed into a fine powder; Pigments were extracted by overnight incubation in 1 mL of 100% methanol under vigorous agitation at 4 °C. Following gel extraction, gel debris was removed by centrifugation at 30,000 x *g* for 60 min, and the supernatant was recovered for high-performance liquid chromatography (HPLC) analysis.

Pigment extraction from whole cells was performed as previously described (Gain et al., 2021), and subsequent analysis of HPLC was carried out as previously described (Berne et al., 2018).

5.3.7 Visualization of the isolated Photosystem supercomplexes and LHCE antenna by transmission electron microscopy.

Both Photosystem supercomplexes (PSI and PSII) and LHCE bands were eluted from native gel bands by diffusion in SB supplemented with 0.01% α-DDM. A 4 µl aliquot of each extracted complex solution was applied on freshly glow-discharged, carbon-coated copper grids. Excess sample was blotted with filter paper and the grids were negatively stained with 2% uranyl acetate to enhance contrast.

Imaging was performed using a Tecnai T20 transmission electron microscope equipped with a Gatan 4000 SP 4K slow-scan CCD camera. Automated data acquisition was conducted to capture images of 2048x2048 pixels, with a magnification of 133,000x magnification and a pixel size of 0.225 nm. A total of 8,034, 7,615 and micrographs were recorded for PSII, PSI and LHCE samples, respectively.

From the selected micrographs, 194,090, 85,435 and 3,840 single particles of PSII, PSI and LHCE complexes, respectively, were independently picked and subjected to reference-free 2D alignment and classification using the image processing framework SCIPION (de la Rosa-Trevín et al., 2016). Structural models were generated by fitting 2D projection maps with high resolution structural models obtained from Protein Data Bank: PSII from *Chlamydomonas reinhardtii* (PDB: 6KAD) (Sheng et al., 2019) and PSI from *Dunaliella salina* (PDB 6RHZ) (Perez-Boerema et al., 2020).

5.4 Results

5.4.1 Expanding the Phylogenetic Landscape of *Euglena gracilis* Light-Harvesting Complex (Lhc) Proteins: Evolutionary Insights and Novel Subfamilies

To investigate the phylogenetic distribution of *Euglena gracilis* light-harvesting complex (Lhc) proteins, we expanded the existing *E. gracilis* Lhc sequence dataset (Koziol and Durnford, 2006; Koziol et al., 2007) by incorporating four recently released *E. gracilis* transcriptomes (Cordoba et al., 2021). This resulted in a final set of 138 Lhc proteins, which were distributed into more than 20 Lhc families (Figure 33A, and Supplementary Figure 1). Two factors likely account for this large number of sequences : the presence of polyproteins and sequence duplication in *E. gracilis* (Koziol et al., 2007), and the possible triploidy of *E. gracilis* nuclear genome (Fields et al., 2024). Using a larger set of reference genomes for Viridiplantae species than in a previous study (Koziol et al., 2007), we constructed a phylogenetic tree of Lhc proteins (Figure 33B and Suppl. Information). LhcbM protein family of *E. gracilis* was previously reported to contain eight main subfamilies (Koziol et al, 2007). In our analysis, most LhcbM sequences form a sister group to the Viridiplantae LhcbM family. This includes additional sequence groups, named LhcbMX1, 2, 3, and 5, that were not previously reported (Koziol et al, 2007). However, three subgroups showed distinct evolutionary trajectories with no homologs in other species. LhcbM2 and LhcbM8 clustered on a basal branch of the Lhcb subtree. LhcbM4 family also formed an independent cluster. Additionally, none of the so-called *E. gracilis* Lhca proteins (Koziol et al., 2007) clustered with either Lhcb or Lhca protein families (Figure 33B). This pattern suggests that this protein family evolved through multiple duplication events from a limited number of Lhc ancestral genes, following a process similar to that observed in the LHCP family from Prasinophyceae (Six et al., 2005) and the Lhcf in diatoms (Islam et al., 2020). Given the distinct evolutionary lineage of this Euglena-specific Lhc group, we propose renaming it LhcE, where “E” denotes Euglena or Euglenozoa (extended dataset 1 - Table of correspondence). Unlike LhcbM proteins, all LhcE lack the trimerization motif WYGP(D)R (Koziol et al., 2007; Koziol and Durnford, 2008). This also applies to the Euglena LhcbM4 protein family, which we renamed here as LhcE13.

Furthermore, our analysis did not identify sequences corresponding to the PSII minor antennae CP26 (Lhcb5) and CP24 (Lhcb6), confirming previous findings (Koziol and Durnford, 2006). Only orthologs of CP29 (Lhcb4) and Lhcb7 minor antenna proteins were detected, highlighting a unique Lhc composition in *E. gracilis*.

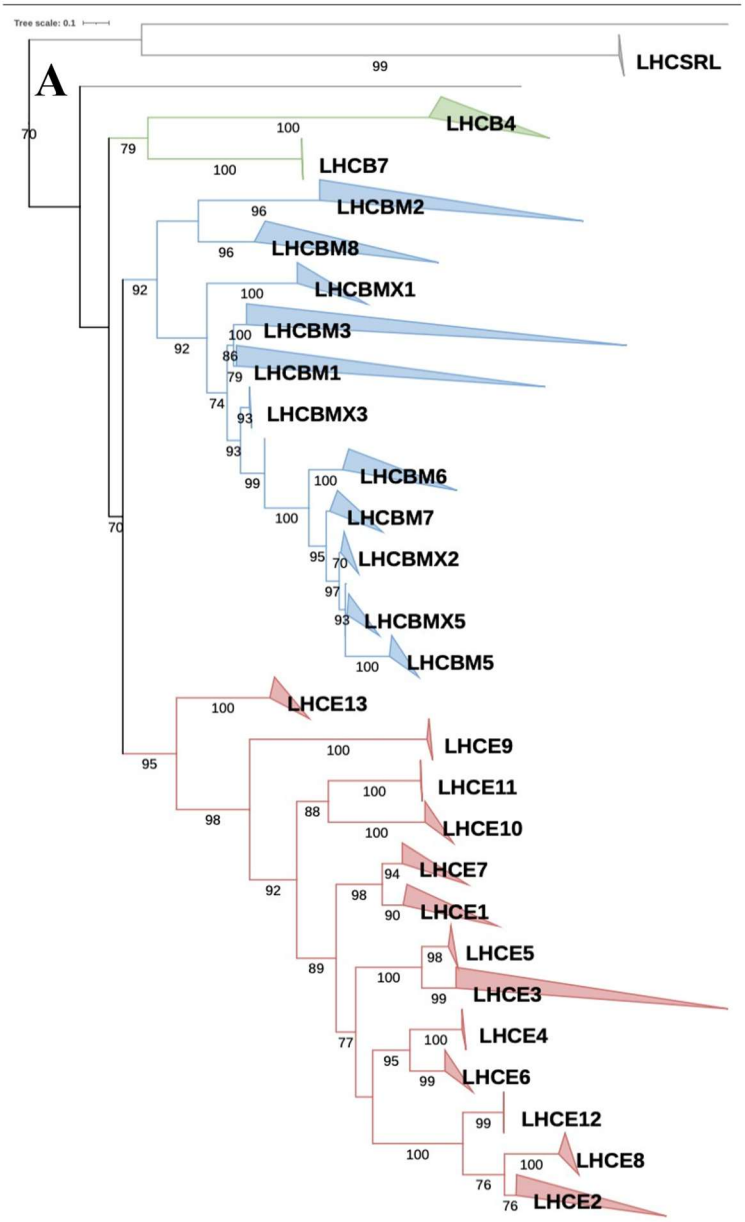
Tree scale: 0.1
A
LHCSRL
LHCB4
LHCB7
LHCBM2
LHCBM8
LHCBMX1
LHCBM3
LHCBM1
LHCBMX3
LHCBM6
LHCBM7
LHCBMX2
LHCBMX5
LHCBM5
LHCE13
LHCE9
LHCE11
LHCE10
LHCE7
LHCE1
LHCE5
LHCE3
LHCE4
LHCE6
LHCE12
LHCE8
LHCE2

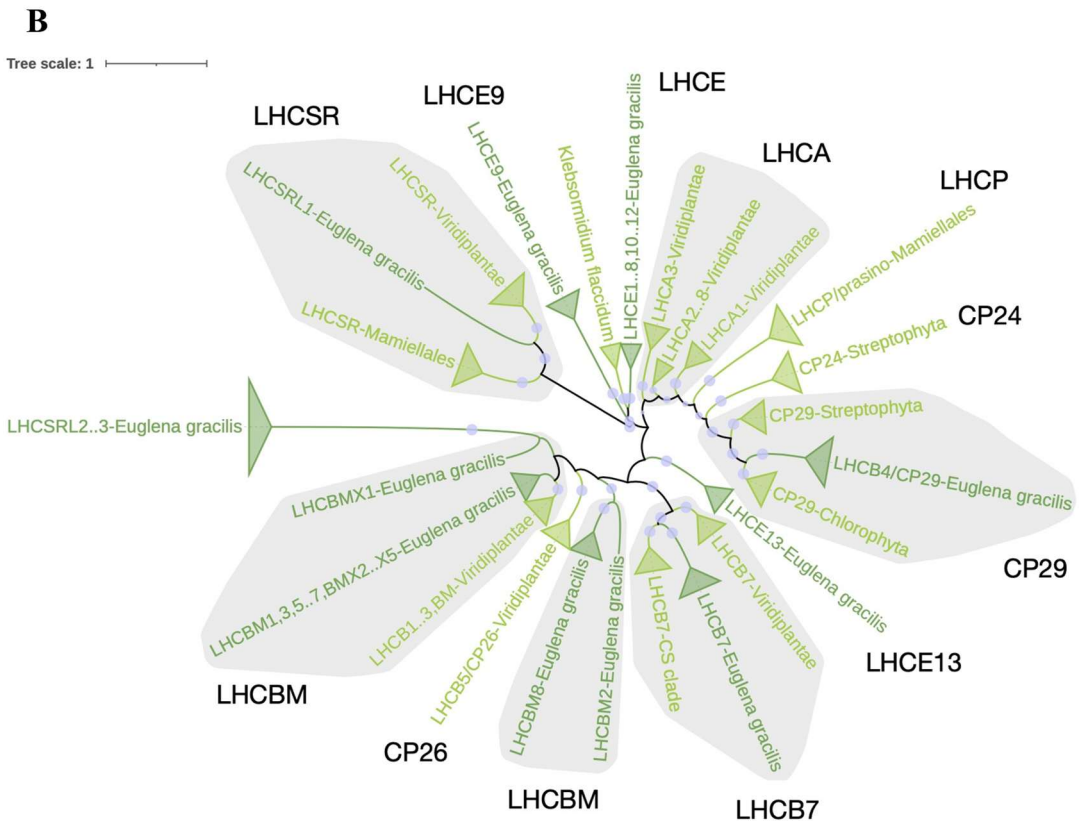

Figure 33. Phylogenetic Analysis of *Euglena gracilis* Light-Harvesting Complex (Lhc) Proteins.

(A) **Phylogenetic tree of Lhc proteins in *Euglena gracilis***: The maximum likelihood phylogenetic tree was constructed using an expanded dataset of *Euglena gracilis* Lhc proteins. Bootstrap values are indicated at key nodes. Lhc proteins are grouped into distinct families, with major clades highlighted in different colors: LhcbM proteins (blue), LhcE proteins (red), Lhcb (green) other Lhc-related families (gray). (B) **Radial phylogenetic tree of Lhc proteins from Euglena gracilis and Viridiplantae**: This tree illustrates the evolutionary relationship between *Euglena gracilis* Lhc proteins and those from other Viridiplantae. Euglena-specific groups, including LhcbM subfamilies (e.g., LhcbMX1-5) and the newly identified LhcE clade, are highlighted. The presence of distinct Euglena-specific clusters supports the hypothesis of multiple gene duplication events, leading to a unique Lhc composition in *Euglena gracilis*.

5.4.2 Identification and Characterization of Photosynthetic Complexes Associated with *Euglena gracilis* Lhc Proteins

To determine the photosynthetic complexes to which these Lhc proteins bind, total membranes from photoautotrophically grown *Euglena* were solubilized using n-dodecyl-α-D-maltoside (α-DDM) or n-dodecyl-β-D-maltoside (β-DDM). The solubilized protein-pigment complexes were subsequently separated by high resolution clear native electrophoresis (*hr*CN). A total of eight and six major green bands, ranging from 110 to 1,500 kDa, were observed for α-DDM and β-DDM, respectively (Figure 34A and Figure S2, *Suppl. Information*). Notably, α-DDM solubilized larger molecular weight complexes compared to β-DDM treatment. Given this, we opted to focus on characterizing α-DDM extracted complexes. Bands from the *hr*CN (Figure 34B) were purified and analyzed using liquid chromatography-electrospray-ionization quadrupole time-of-flight mass spectrometry (LC-ESI-Q-TOF-MS). The results indicate that the 1.5 and 1.3 MDa complexes (bands A1 and A2) primarily contain PSII core subunits and LhcbM proteins. The 930 and 695 kDa complexes (bands A3 and A4) are enriched in PSI core subunits, along with some LhcE proteins, and LhcbMs. The presence of PSII core subunits in the 930 kDa band suggests that PSI and PSII particles of similar size may co-migrate. The 470 and 310 kDa complexes (bands A5 and A6) are mainly composed of PSII core subunits with a limited number of LHCs. Finally, the 180 and 110 kDa complexes (bands A7 and A8) contain only LhcE and LhcbM, respectively. Interestingly, PSII- associated complexes (A1/A2) released the smaller A8 band during purification (Figure 34B, *lanes 2 and 3*). This observation supports the hypothesis that band A8 components are originally integrated within A1 and A2 complexes.

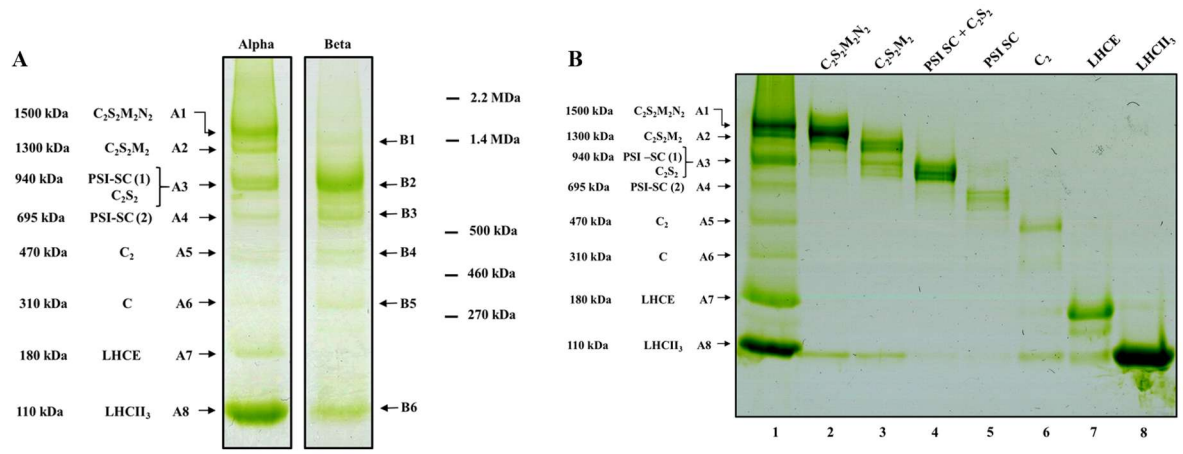

Figure 34. hrCN-PAGE of *Euglena gracilis*

(A) Comparison of pigment-protein complexes extracted using two mild detergents and analyzed by hrCN-PAGE. Total membrane extracts *from Euglena gracilis* were solubilized with n-dodecyl-α-D-maltoside (α-DDM) and n-dodecyl-β-D-maltoside (β-DDM), followed by high-resolution clear native polyacrylamide gel electrophoresis (hrCN-PAGE). α-DDM solubilization yielded eight major chlorophyll-containing bands (A1–A8), ranging from 110 to 1500 kDa. β-DDM solubilization resulted in six major bands (B1–B6), spanning 310 kDa to 2.2 MDa. Identified photosynthetic complexes include PSII-LHC supercomplexes ($C_2S_2M_2N_2$, $C_2S_2M_2$, C_2S_2), PSI supercomplexes (PSI-SC), PSII core (C_2), the LHCE antenna complex, and free $LHCII_3$ trimers. These results highlight differences in extraction efficiency between α-DDM and β-DDM, with α-DDM favoring the solubilization of larger supercomplexes, and LHCE antenna complex stability. **(B) *hr*CN-PAGE of purified photosynthetic pigment-proteins complexes**. Each band from α-DDM extracted membrane samples was manually excised, extracted under liquid nitrogen, and analyzed by liquid chromatography-electrospray-ionization quadrupole time-of-flight mass spectrometry (LC-ESI-Q-TOF-MS) (see Methods 2.3 and 2.5 for details). A sample of each purified complex was reloaded onto lanes 2–8 for validation. Lane 1: Total membrane extract before purification/ Lanes 2–8: Purified complexes corresponding to distinct photosynthetic assemblies. Identified complexes and molecular masses: A1 (1500 kDa): $C_2S_2M_2N_2$; A2 (1300 kDa): $C_2S_2M_2$; A3 (930 kDa): PSI-SC + C_2S_2 ; A4 (695 kDa): PSI-SC ; A5 (470 kDa): C_2 (PSII core) ; A6 (310 kDa): C (PSII monomer) ; A7 (180 kDa): LHCE antenna complex ; A8 (110 kDa): $LHCII_3$ free trimer.

The purified complexes display distinct migration patterns, confirming their identity and integrity after extraction and analysis.

5.4.3 CP26-Less PSII Core Associates Up to Three LHCII Trimers

By integrating phylogenomic and proteomic approaches, we identified orthologues of PsbA-F, PsbH-R, PsbT, PsbW-Z, and Psb27-29/32-33 (Supplementary Table 1), significantly expanding the list of PSII components in *Euglena gracilis* compared to previous surveys (Sobotka et al., 2017). The only PSII subunits not identified were PsbS, a key light-stress sensor involved in photoprotective mechanisms, and PsbU and PsbV, which are predominantly found in cyanobacteria and red microalgae (*Supporting phylogenetic trees can be found here https://drive.google.com/drive/folders/1cJasdU6BRJCYyiyyP0v_ZHc_p-Q7SQIC) Supplemental files*). Thus, the *E. gracilis* PSII core exhibits a subunit composition highly similar to those found in green lineages representatives such as *C. reinhardtii* (Shen et al., 2019) and *A. thaliana* (Graça et al., 2021).

In addition to CP29, LhcbM proteins identified within the PSII-LHC supercomplexes (Figure 34B, *bands A1 and A2*) belong to the types I, V, VI, and VII (Figure 35A). The same LhcbM types are also present in the 110 kDa complex, which likely corresponds to free LhcbM trimers ($LHCII_3$) (Figure 34A, *bands A8 and B6*). Notably, LhcbM proteins were absent in the lower molecular mass PSII complexes (310 & 470 kDa), which are tentatively assigned as C_2 and C_1 PSII core complexes, respectively (Figure 34B, *bands A5 and A6*).

LHC-to-core ratios across bands were further calculated using averaged values from four major PSII core subunits (PsbA/B/C/D). The LhcbM-to-PSII core subunit ratio was found to be 8.5 in the 1.5 Mda complex and 4.4 in the 1.3 MDa complexes. Notably, the proportions of the four LhcbM types in PSII supercomplexes and in the 110 kDa LhcbM complex were identical (Figure 35A and S4), reinforcing the notion that the 110 kDa complex represents detached LHCII trimers from PSII-SC antenna. In addition, the minor antenna protein Lhcb4 (CP29) and the *Euglena* specific LhcE9 were consistently associated with PSII-SC bands in 1:1 stoichiometry (Figure 35A).

PSII-SC Structure and LHCII$_3$ Association

2D projection maps of the largest *E. gracilis* 1.5 MDa PSII-SCs (Figure 34, *band A1*) revealed a dimeric PSII core complex, with each monomer binding up to nine LHCs into three trimers (Figure 35C). This PSII-SC structure closely resembles the $C_2S_2M_2N_2$ (or $C_2S_2M_2L_2$) PSII-SC previously characterized in *C. reinhardtii* under similar solubilization conditions (Burton-Smith et al., 2019; Shen et al., 2019). Based on this structural similarity, the 1.3 MDa complex likely corresponds to $C_2S_2M_2$. The high number of LhcbM in *E. gracilis* 1.5 MDa supercomplex is further supported by chlorophyll *b*/*a* ratios (Supplementary Table 2) and a relative absorption at 480 nm (Soret absorption band), which are higher than those of the PSII core but lower than those of free LHCII trimers (Figure 35B). These changes in the number of LHCII$_3$ associated with the dimeric PSII core were also evident from EM projections of smaller PSII-SCs (Figure S5, *Suppl. information*).

Absence of CP26 and Potential Functional Implications

EM images confirmed that CP29 is consistently associated with the *E. gracilis* PSII core complex, whereas CP26 (Lhcb5), a conserved minor antenna typically positioned adjacent to the S-trimer in *Chlamydomonas* PSII-SC (Burton-Smith et al., 2019; Shen et al., 2019), is absent and not replaced by any other antenna subunit in *Euglena gracilis* (Figure 35C). EM projections also suggest potential PSII heterogeneity, with one N trimer looking incomplete. (Figure 35C *panels B and D*). One possibility is that a single LhcbM from the N-trimer, leaving a dimeric LhcbM antenna instead (Figure S5, *sSuppl. information Figure X*) A similar phenomenon has been observed in *Physcomitrella patens* PSII (Kouřil et al., *manuscript in preparation*). Another possibility is that the N-trimer is exchanged for an LhcE9 monomer (Figure 35C *panels B and D*), consistently found in association with the PSII supercomplex by mass spectrometry (Figure 35A).

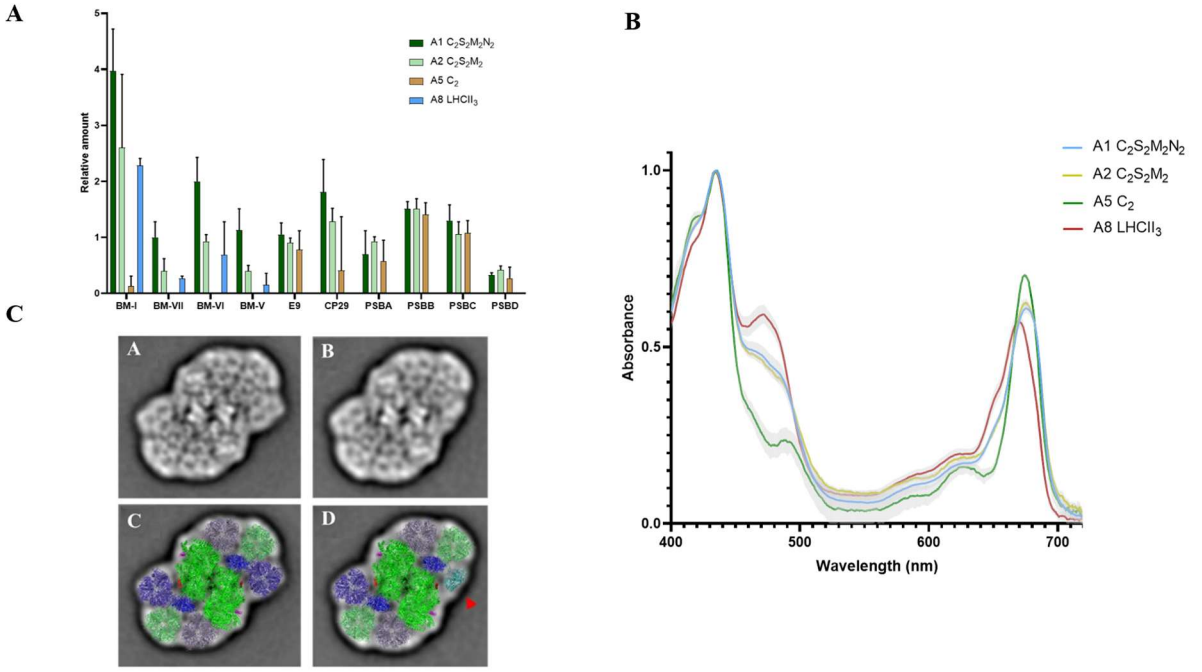

Figure 35. *E. gracilis* photosystem II

(A) Quantification of LHC proteins associated with PSII supercomplexes, PSII core, and free $LHCII_3$. . Relative amounts of different LHCBM subtypes (BM-I, BM-VII, BM-VI, BM-V, CP29) and LhcE9 (E9) were quantified using a proteomic approach across various PSII complexes. The four PSII complexes analyzed include $C_2S_2M_2N_2$ (dark green), $C_2S_2M_2$ (light green), C_2 (brown), and free $LHCII_3$ (blue). Spectral count assigned to each antenna was normalized to the average spectral count assigned to the core complex polypeptides (calculated as (PsbA+PsbB+PsbC+PsbD)/4) in the same band. Relative number of LHCBM in free LHCII trimer is calculated assuming a total of 3 LHCS; LHCBM-I, LHCBM-V, LHCBM-VI, and LHCBM-VII were associated with the PSII-LHC supercomplexes ($C_2S_2M_2N_2$ and $C_2S_2M_2$) but were largely absent from lower molecular weight PSII core complexes. The relative abundance of LHCE9 suggests its integral role in PSII organization and function, differing from the distribution pattern of classical LHCBM proteins. Error bars represent standard deviations from 3 replicates. (**B**) **Absorption spectra of PSII complexes LHCII trimers.** Absorption spectra for bands 1, 2, 5, 7 and 8, normalized to their maximum absorbance. Mean values are represented as solid lines, with standard deviations shown as shaded areas (n=3). The different PSII and antenna complexes are color-coded as follows: $C_2S_2M_2N_2$ (complete PSII-LHC supercomplex) in blue; $C_2S_2M_2$ (PSII-LHC intermediate complex) in light green; C_2 (PSII core complex) in green; LHCE antenna complex in red; $LHCII_3$ free trimer in dark blue. These spectra reveal distinct spectral signatures corresponding to each complex, highlighting

variations in pigment composition and light absorption efficiency across the different photosystem assemblies.

(C) Projection maps and structural models of PSII supercomplexes from *Euglena gracilis* revealed by single particle electron microscopy. (A.) Projection map of a larger type of the PSII supercomplex ($C_2S_2M_2N_2$) and (B., C.) two smaller forms of the PSII $C_2S_2M_2N_2$ supercomplex. (D-F) Structural models of different forms of the PSII supercomplexes obtained by fitting the high resolution structure of the PSII supercomplex from green alga *Chlamydomonas reinhardtii* (PDB: 6AKD (Shen et al., 2019). (D.) The larger form of the PSII supercomplex consists of a dimeric PSII core complex (green), minor antenna proteins CP29 (yellow), and three pairs of LHCII trimers (the S trimer (red), the M trimer (blue), the N trimer (magenta)). (E.-F.) The smaller forms of the PSII supercomplexes lack the N trimer. The reduced density can reflect a PSII heterogeneity (see text for details). The scale bar is 10 nm.

5.4.4 Minimal PSI Core is Surrounded by an LhcE/LhcbM Belt

Our phylogenomic analysis (Supplementary Table 1 and Supplementary Figure 1) confirmed previous findings (Sobotka et al., 2017) regarding the presence of PsaF and PsaJ and the absence of PsaI, PsaK, and PsaL in *E. gracilis*. Expanding our analysis to additional PSI subunits typically found in green lineage (Scheller et al., 2001), we identified PsaM as a chloroplast-encoded subunit, but found no evidence of PsaG, PsaH, PsaN, or PsaO (Supplementary Table 1 and Supplementary Figure 1).

In plants, PsaG and PsaK contribute to Lhca binding (Huang et al., 2021; Ozawa et al., 2018). Their absence in *E. gracilis* raises questions about the structural organization of its PSI-LHC supercomplex. Mass spectrometry quantification provided estimates of LHC numbers per PSI core. In the 930 kDa complex (Figure 34B), an average of 10 Lhc subunits per PSI core was detected, including 7-8 LhcE proteins (types 5, 6, 7, 8, 10, 11, and 13), and 2-3 LhcbM proteins (types II and VIII) (Figure 36A). These LhcbM protein types were absent from PSII-SC and free LHCII trimer (Figure 35A).

In single particle EM projections of the 930 kDa PSI-SC, a larger number of Lhc proteins (11 to 16) could be accommodated around a minimal PSI core composed of Psa, PsaB, PsaC, PsaD, PsaE, PSsaF, PsaJ, and PsaM (Figure 36B). In these fits, a broad row of antennae extends along the PsaM side, forming a structure that reaches the PsaA/B boundaries, creating a variable "flipper" region in the antenna extrinsic part (Figure 36B). On the opposite PsaF side, a more

stable Lhc belt- putatively composed of four Lhc proteins- was observed, resembling the configuration described for the *C. reinhardtii* PSI-LHCI supercomplex (Huang et al., 2021).

Multiple fitting attempts were also made to accommodate a LHCII trimer, given that a ratio of 3 LhcbM proteins per core was determined (Figure 36A). However, no distinct $LHCII_3$ density was observed in PSI-SC projections.

Structural Variability in PSI Antenna

The lower molecular mass PSI complex contains four fewer Lhc proteins (LhcE7, 8, 10, and 13) than the 930 kDa complex (Figure 36A). The presence of smaller PSI-SC classes suggests detachment of several LhcE proteins, particularly near the "flipper" region, indicating that this part of the antenna is less tightly bound. Despite differences in antenna size, both PSI-LHC complexes exhibit a main absorption peak at 677 nm, and a secondary prominent far-red absorption peak at 693 nm, distinguishing them from PSII-LHC supercomplexes (Figure 36C).

A similarly large PSI antenna has been proposed for Prasinophyte (green microalgae), where four lineage-specific LHCPs are attached on the opposite side of the conserved PsaF-side LHCI belt, but without far-red absorption bands (Swingley et al., 2010). In moss (*Physcomitrella patens*), PSI-SC also includes nine LHCI subunits and one $LCHII_3$ surrounding the core, but unlike *Euglena*, this antenna extension occurs in the PsaK side (Iwai et al., 2018).

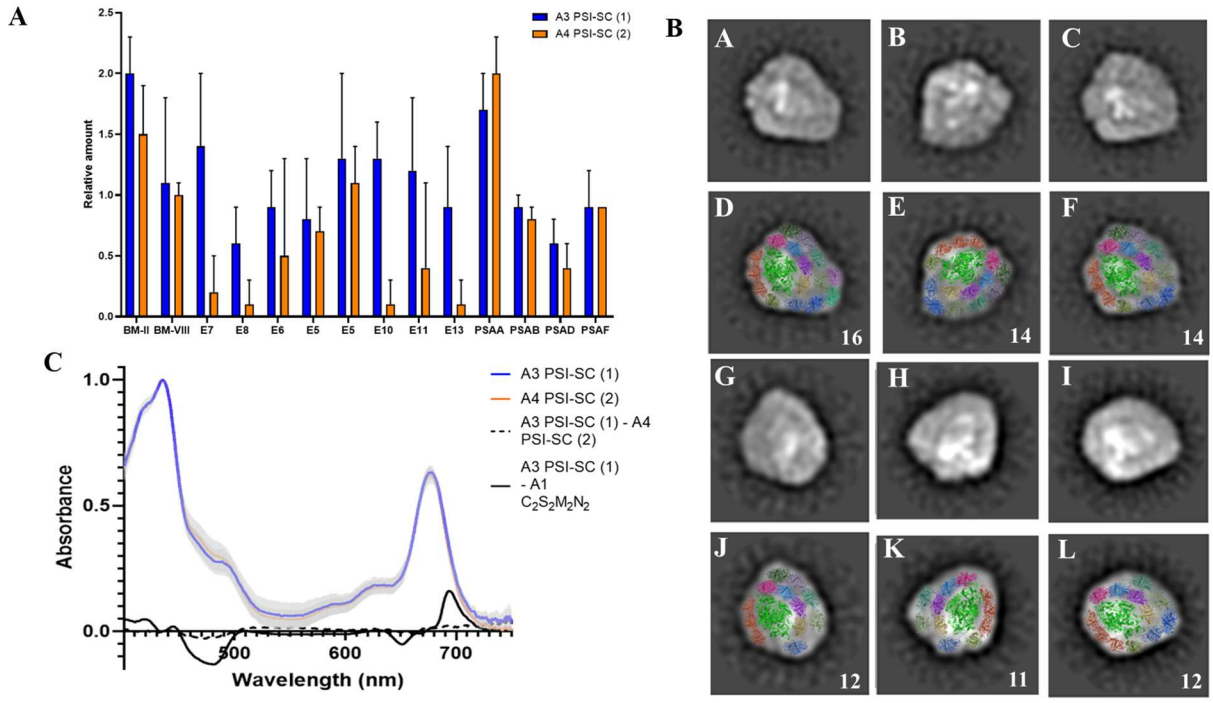

Figure 36. *E. gracilis* Photosystem I supercomplex.

(A) Antenna composition of PSI–LHC supercomplexes determined by MS/MS analysis. LHCs from two different branches are present (see Figure 1C and S1 for details): LHCE antenna proteins of types E5, E6, E7, E8, E10, E11, and LHCBMs of types II, IV, and VIII. (**B) Structural models of PSI-LHCI supercomplexes revealed by single-particle electron microscopy**. Structural models of different PSI-LHCI supercomplex forms obtained through single-particle electron microscopy. Top rows: raw electron density projections. Bottom rows: corresponding fitted models with assigned structural components. Densities were assigned by fitting the high-resolution PSI structure from *Dunaliella salina* (PDB: 6RHZ, Perez-Boerema et al., 2020). Additional antenna proteins were modeled using copies of the Lhca1 subunit from *Dunaliella salina*. PSI core (green); LHC belt at the PsaF side (red); Variable "flipper" region at the PsaM side (multicolored LHC subunits). The structural variability observed highlights differences in antenna organization, providing insights into the dynamic nature of PSI light-harvesting adaptations. The scale bar represents 10 nm. **(C) Absorption spectra of PSI-LHC complexes**. Absorption spectra for bands 3 and 4, corresponding to PSI-LHC complexes, normalized to their maximum absorbance. Mean values are shown as solid lines, with standard deviations represented as shaded areas (n=3). The two PSI-LHC complexes are color-coded as follows PSI-LHC (band A3 in Figure 1A-B) in blue, and PSI-LHC (band A4 in Figure 1-AB) in orange. These spectra highlight the similarity in light absorption profiles between the two PSI-LHC complexes, with distinct peaks in the visible (~440 nm) and far-red (~680 nm) regions, characteristic of PSI-bound antenna systems.

5.4.5 A LHCE Antenna Complex Accounts for Far-Red Absorption in *Euglena gracilis* cells under Low- Light Conditions

The 180 kDa LhcE antenna complex (Figure 34, *band A7*) primarily contains diadinoxanthin and chlorophyll *a* (Supplementary Table 2). Consequently, its absorption spectrum lacks the 480 and 653 nm bands of chlorophyll *b*. While LhcM timers show a maximum absorbance at 672 nm, the LhcE complex exhibits red-shifted absorption peaks at 675 and 692 nm (Figure 37A). At room temperature, its fluorescence emission spectrum is also red shifted, with a maximum at 698 nm, compared to 684 nm for $LCHII_3$ (Figure 37B). Such a red-shifted antenna complex in *E. gracilis* was previously reported (Doege et al., 2000), but no further characterization has been performed.

Based on its molecular mass, the 180 kDa complex is likely composed of five to six LHCE proteins, among which LhcE1, 2, 3, 4 and 12 were identified in various proportions by MS analysis (Figure 37C). None of these LhcE proteins were detected in association with any PSI-LHC or PSII-LHC supercomplexes, suggesting that the LhcE antenna complex is peripheral and readily dissociates upon α-DDM extraction. When β-DDM was used instead of α-DDM, the LhcE antenna complex was destabilized, similar to the largest PSII-LHC supercomplex (Figure 34A), indicating a weaker binding affinity or structural sensitivity to detergent solubilization.

Interestingly, the difference absorption spectrum between LhcbM trimers and the Lhce antenna complex (Figure 37A) closely resembles the difference absorption spectra between PSII-LHC SC and PSI-LHC SC (Figure 36C). Both spectra exhibit negative peaks at 470-480 nm and 650-652 nm, corresponding to the absence of chlorophyll *b*, and a maximum at 692-693 nm, indicative of enhanced far-red absorption by red chlorophylls *a*. This similarity suggests that LhcE proteins are responsible for far-red absorption in PSI-LHC supercomplex, just as they contribute to far-red absorption in the 180 kDa antenna complex.

Structural Insights Into LhcE Antenna Complex Organization

Single particle analyses identified three main projection classes of this antenna (Figure 37D). In the largest projection, five LhcE proteins can be fitted. The two smaller projections likely represent subcomplexes derived from the 180 kDa complex (Figure 34A). Still, the smallest projection may also correspond to contaminations from LhcbM trimers. Given the structural similarity of these projections to $LHCII_3$ in the PSII SCs (Figure 35E), we propose that an LhcE trimer is part of the 180 kDa antenna (Figure 37D). Lower molecular mass subcomplexes are also evident as distinct bands in purified LhcE complex fractions (Figure 34B, *lane 7*).

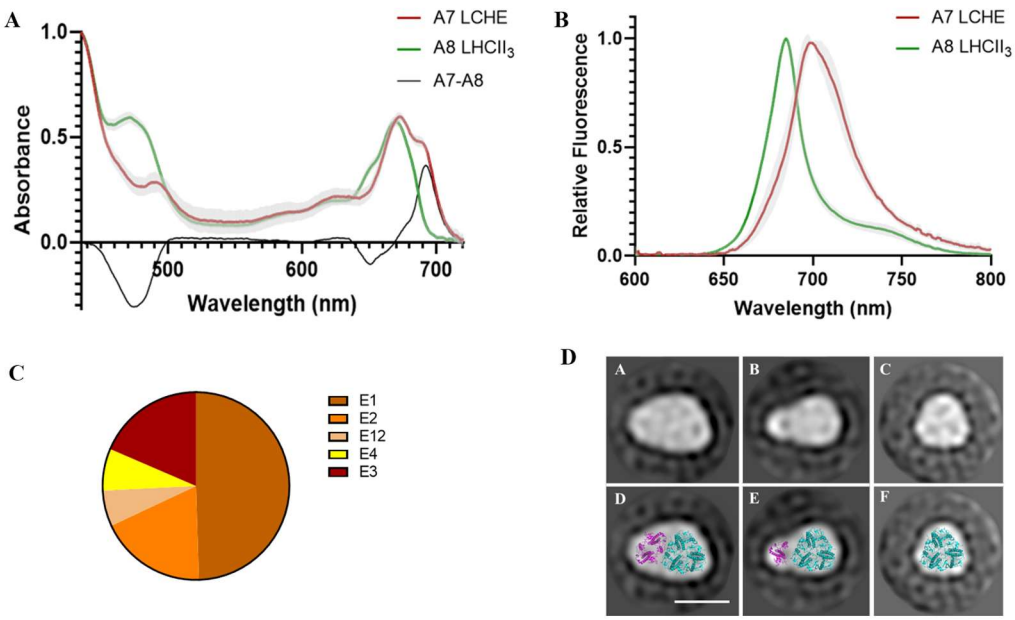

Figure 37. LCHE antenna complex.

A. Absorption spectra of isolated LHCE antenna complex and LHCII trimers. **B.** Room temperature fluorescence spectra of isolated LHCE antenna complex and LHCII trimers. **C.** Relative amounts of LHC proteins in the 110 kDa ($LHCII_3$) and 180 kDa ($LHCE_5$) antenna complexes. **D.** Averaged 2D projections of the LHCE antenna, three major classes were collected with a class sum of 4028, 2907, and 3840 particles, for A, B, and C, respectively. The larger LHCE complex comprises up to 5 LHCE monomers (A and D): 1 trimer (cyan) + 2 monomers (violet). Smaller classes may correspond to LhcE antenna complexes with detached monomers (Panels B, C, E and F). The scale bar is 10 nm.

LhcE Antenna Dynamics Under Different Light Regimes

Comparing the distribution of pigment-proteins complexes under varying light conditions revealed a decrease in the 180 kDa LHCE antenna complex under higher light regimes (Figure 38A). This reduction was accompanied by a decline in far-red absorption capacity in whole cells (Figure 38B). Furthermore, high-light conditions led to (i) decreased fluorescence emission at 705 nm at room temperature (Figure 38C), (ii) an increase in the chlorophyll *b*/*a* ratio (0.16 ± 0.01 in LL, 0.2 ± 0.01 in HL, $p < 0.005$) of whole cells, a unique trait among photosynthetic organisms (Nagao et al., 2021), and (iii) photoinhibition, as indicated by the low value of Fv/Fm (Figures S6, *Suppl. information*). Altogether, these findings suggest that the primary long-term light acclimation strategy in *Euglena gracilis* involves modulating the amount of the LHCE antenna complex.

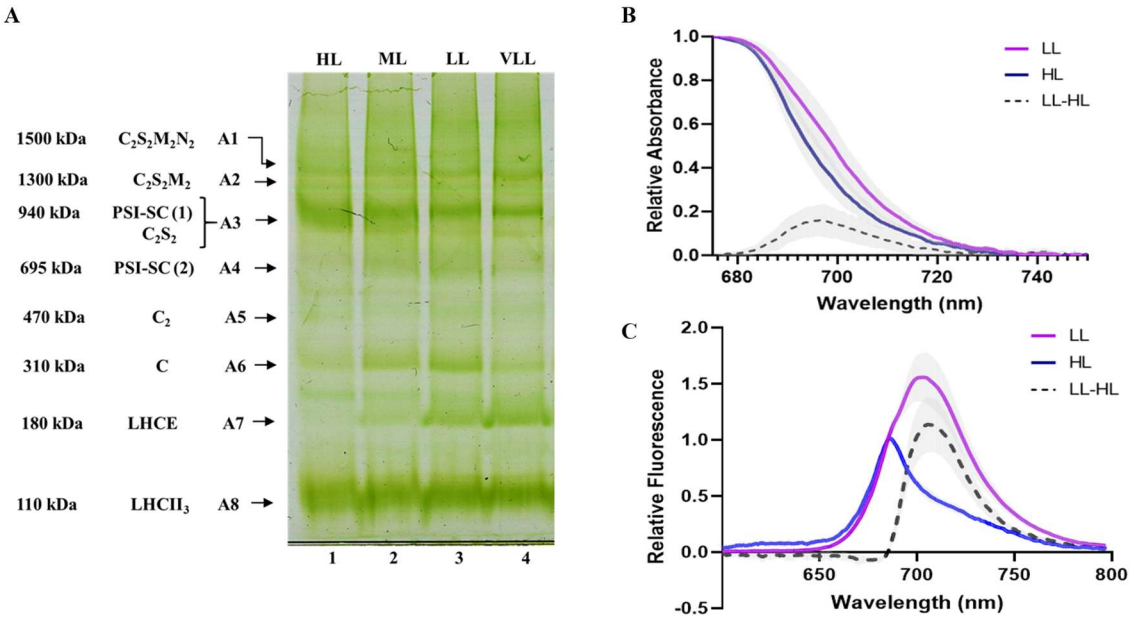

Figure 38. Dynamics of LCHE antenna complex under changing light conditions.

A. *hr*CN-PAGE of photosynthetic pigment-proteins complexes in *E. gracilis* cells grown in different light intensities (high light (HL), medium light (ML), low light (LL), very low light (VLL). **B.** Absorption spectra of whole cells grown in LL and HL. **C.** Room temperature fluorescence spectra of whole cells grown in LL and HL. Values are represented as mean ± s.d. (n=3).

5.4.6 The LhcE Antenna Complex is Involved in a State Transition-like process

In addition to modulating antenna abundance, green plants and cyanobacteria dynamically adjust antenna size through state transitions (Minagawa, 2011). *Euglena* state transitions were evidenced by an increase of PSII maximum fluorescence 146 ± 9 % at room temperature (State I) upon short-term exposure to far-red light (720 nm). This increase returns to its initial value upon dark acclimation (State II) (Figure 39A).

To identify the antenna binding to PSII in State I, we leverage the fact that the LhcbM trimers emit at 684 nm, while the LhcE antenna complex exhibits a red-shifted fluorescence emission peak (Figure 37B). The room-temperature fluorescence emission difference spectrum between State II and State I in *E. gracilis* peaks at 707 nm (Figure 39B) and closely resembles that of the isolated LhcE antenna complex (Figure 37B). This spectral shift is also similar to the difference in fluorescence emission spectra between LL and HL acclimated cells (Figure 38C). As a matter of comparison, the difference fluorescence emission spectra of *Chlamydomonas reinhardtii* cells in State II and State I correspond to the spectra of isolated $LHCII_3$ (Figure S7, suppl. information figure).

This strongly suggests that the far-red-emitting LhcE antenna complex preferentially binds to PSII in State I. Consistently, PSII absorption capacity for far-red (720 nm) increases significantly relative to red light (660 nm) during the transition from State II to State I (Figure 39C). Under these conditions, none of the room-temperature fluorescence emitters were affected by DCMU addition (Figure S8, *Suppl. information*), a well-known inhibitor of plastoquinone reduction by PSII (Bennoun, 1970). This confirms that these emitters are functionally connected to PSII, as previously reported (Doege et al., 2000).

When *Euglena* cells were grown under high-light conditions, where LhcE antenna complex abundance is significantly reduced (Figure 38A), and far-red fluorescence emission (700-710 nm) strongly reduced (Figure 38C), no significant changes in PSII antenna were observed between dark and far-red acclimate cells (Figure 39C and 39D), indicating that state transition did not take place in absence of LhcE antenna complex.

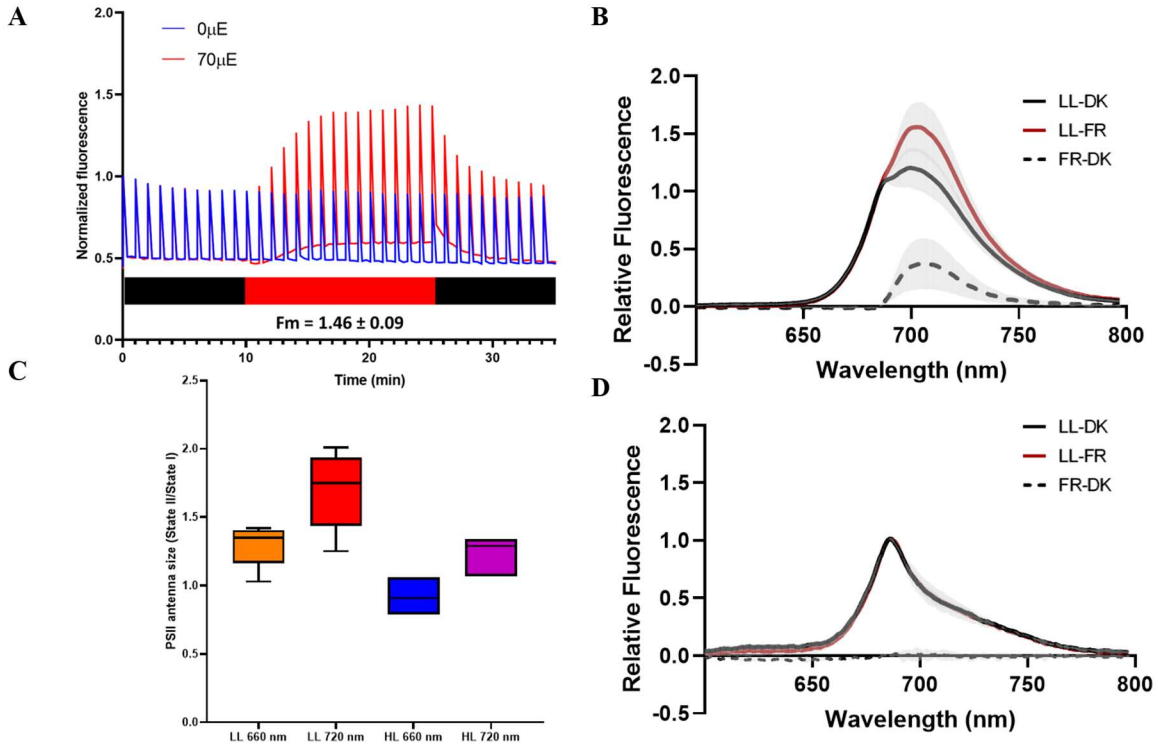

Figure 39. LhcE antenna complex is involved in state transition and connected to PSII.

A. *In vivo* monitoring of maximum chlorophyll a fluorescence was performed on LL-grown cells in darkness (blue line), or during exposure to FR (720 nm) illumination (red line). The red/black bar indicates the period of FR illumination and dark, respectively. **C.** PSII antenna size was estimated upon illumination at 660 nm or 720 nm after exposure of LL and HL cells to darkness (state II) or to FR (state I). **B,D.** Room Temperature fluorescence spectra of cells after exposure to darkness (DK) or far-red illumination (FR) during 15 minutes. LL and HL indicate the light intensity of growing conditions, 50 and 450 PPFD, respectively.

5.5 Discussion

Chlorophyll *a* is common to nearly all oxygenic photosynthetic organisms. In rhodophytes, glaucophytes, and most cyanobacteria, it is the only chlorophyll species functioning in the photosystems (Gould et al., 2008). In land plants and green microalgae, while chlorophyll *a* is essential for photochemistry, chlorophyll *b* plays a crucial role in stabilizing the major light-harvesting complexes (LHCs) (Tanaka and Tanaka, 2011). *Euglena gracilis* underwent independent Lhc diversification (Figure 33), likely driven by lineage-specific adaptations and genome triploidy. The newly proposed LhcE protein family, specific to Euglena, contains only chlorophyll *a* and diadinoxanthin (Supplementary Table 2), which contributes to the low chlorophyll *b* content in *Euglena gracilis* (Cunningham and Schiff, 1986). The Lhce protein family is phylogenetically distinct from Viridiplantae Lhc families (Figure 33B), further supporting an independent evolutionary trajectory within the Euglenozoa lineage (Fields et al., 2024). Members of the LhcE family are primarily associated with PSI-LHC supercomplex and the free 180 kDa antenna complex, but LhcE9 is also found in PSII. The 180-kDa LhcE antenna complex is likely organized as a pentamer comprising LhcE1, LhcE2, LhcE3, LhcE4, LhcE12 (Figure 37), a structure not previously observed in green plastids (Iwai et al., 2024). Interestingly, a tetramer/pentamer of fucoxanthin chlorophyll a/c-binding proteins was recently described in the diatom *Chaetoceros gracilis* (Zhou et al., 2024; Iwai etal., 2024), suggesting potential functional convergence among photosynthetic eukaryotes. Beyond its unique protein-pigment composition, the *E. gracilis* 180-kDa LhcE antenna possesses several other remarkable traits. Its absorption spectrum exhibits a 20 nm red-shifted prominent secondary absorption peak compared to LhcbM trimers (Figure 37A). Finally, it is highly dynamic, with its abundance decreasing under increasing light intensities (Figure 36C), which correlates with an increase in chlorophyll *b/a* ratio. This adaptation may be linked to either the evolution of its light environment (Bag, 2021) or an ancestral origin. The latter hypothesis is supported by the species-specific LhcE branch splitting from the major Lhc tree and the absence of canonical LhcA genes observed in our phylogenomic analysis (Figures 33 and Figure S1, *suppl. informationl S1*).

It has been proposed that the ancestor to all modern algal lineages contained PSI-specific LHC antenna proteins, while PSII absorbance was supplemented by phycobilisomes. Over time, LHC proteins in green microalgae and land plants evolved to be more photosystem-specific, with LHCII antenna primarily associating with PSII (Pan et al., 2020). This PSII specificity aligns with the $C_2S_2M_2N_2$ projections observed for *Euglena* PSII SC (Figure 35C).

In several lineages, the PSI antenna system was reduced in favor of enhanced PSII absorption (Swingley et al., 2010). However, in *Euglena* the opposite trend appears to have occurred. Our structural observations indicate an increased number of Lhc units surrounding a PSI core, including at least LhcbM (LhcbM2 and LhcbM8) and more than 10 LhcE (Figure 36A), compared to other green species (Gorski et al., 2022; Qin et al., 2019). Remarkably, LhcbM2 and LhcbM8 form basal branches in the Lhcb tree of Viridiplantae (Figure 33) and have therefore evolved independently from PSII-associated LhcbM proteins. A similar large PSI antenna system is observed in the diatom *Chaetoceros neogracilis* PSI-FCPI supercomplex (Xu et al., 2020) and in the symbiotic dinoflagellate *Symbiodinium* PSI-LHC supercomplex (Zhao et al., 2024). The large PSI antenna is associated in *E. gracilis* to a minimal PSI core comprising 8 subunits (Supplementary Table 1). Again, the loss of most peripheral PSI core subunits is not unique to *E. gracilis*, but rather appears to be a case of convergent evolution in secondary photosynthetic lineages (Basso et al., 2014; Neilson et al., 2017; Sobotka et al., 2017). These findings suggest that expansion of the PSI antenna concomitant to PSI core reduction is an adaptive mechanism that emerged after the acquisition of the secondary green plastid.

In Viridiplantae, light-harvesting complex regulation is achieved through multiple adaptive mechanisms that balance efficient light capture with photoprotection under fluctuating environmental conditions. These mechanisms include notably dissipation of excess absorbed energy as heat to prevent photodamage, and state transitions, which dynamically redistribute LHCII between PSII and PSI to balance excitation energy (review). State transition is regulated by the redox state of the plastoquinone pool (Virtanen and Tyystjärvi, 2023) , with a key step being the phosphorylation of the mobile $LHCII_3$ antenna (Longoni et al., 2019). This phosphorylation event leads to $LHCII_3$ dissociation from PSII followed by its association with PSI in green microalgae (Huang et al., 2021; Pan et al., 2021).

In contrast, our results indicate that a canonical state transition mechanism involving LhcbM trimers is absent in *E. gracilis*. Instead, a pentameric LhcE antenna complex associates to PSII upon far-red light exposure. In 1961, Brown and French had proposed that *Euglena gracilis* uses a common antenna system, a hypothesis supported by our findings regarding the species-specific $LHCE_5$ red antenna complex (Figures 33C and 36E). In *C. reinhardtii*, CP29 is pivotal in state transition (Tokutsu et al., 2009). While we cannot fully exclude that CP29 also plays a similar role in *Euglena gracilis*, the fact that CP29 is surrounded by LhcbM trimers, which do not detach makes this role unlikely. Instead, we propose that LhcE9, that is bound to all PSII complexes (Figure 35A), could create a novel interface that facilitates the binding of the 180

kD LhcE antenna complex. The minor antenna CP26 is also lacking on *E. gracilis* PSII (Figure 35C and Supplementary Table 1), and its loss is maybe concomitant with the acquisition of the unique pentameric LhcE antenna complex.

Euglena PSI core is surrounded by a belt of LhcbM and LhcE proteins (Figure 36C). This unique arrangement likely influenced Lhc protein interactions with PSI, effectively restricting any canonical state transition mechanism. Additionally, the loss of PsaH, PsaL and PsaO, which are essential for LhcbM trimers binding during state transition in Viridiplantae (Yang et al., 2015), further suggests that *E. gracilis* does not preserve the classical state transition mechanism. The reversible binding of the far-red LhcE antenna complex in *E. gracilis* (Figure 39) appears to be a mechanism for light harvesting optimization under low-light or far-red-light conditions.

5.6 Concluding remarks

Light adaptation mechanisms are important to ensure the survival of photosynthetic organisms against dramatic changes in illumination (Finazzi et al., 1999). As described above, most of the classical mechanisms observed in Viridiplantae have been lost in *Euglena gracilis.* Instead, *E. gracilis* has acquired a species-specific mobile antenna, named here LHCE. This LHCE antenna complex, together with LhcE associated with PS-LHC, are responsible for far red absorption capacity of *E. gracilis* cells, accumulating in low-light and far-red regimes to increase photon absorption capacity. For more than sixty years after the first observation of changes in spectral properties of *E. gracilis* cells in function of light in culture (Brown and French, 1961), we therefore identified the antenna complex responsible for it. Interestingly, this unique LHCE complex, and not the classical $LHCII_3$ antenna, is involved in a state transition-like mechanism in *E. gracilis* as an adaptation in response to light changes.

5.7 Supplementary Figures

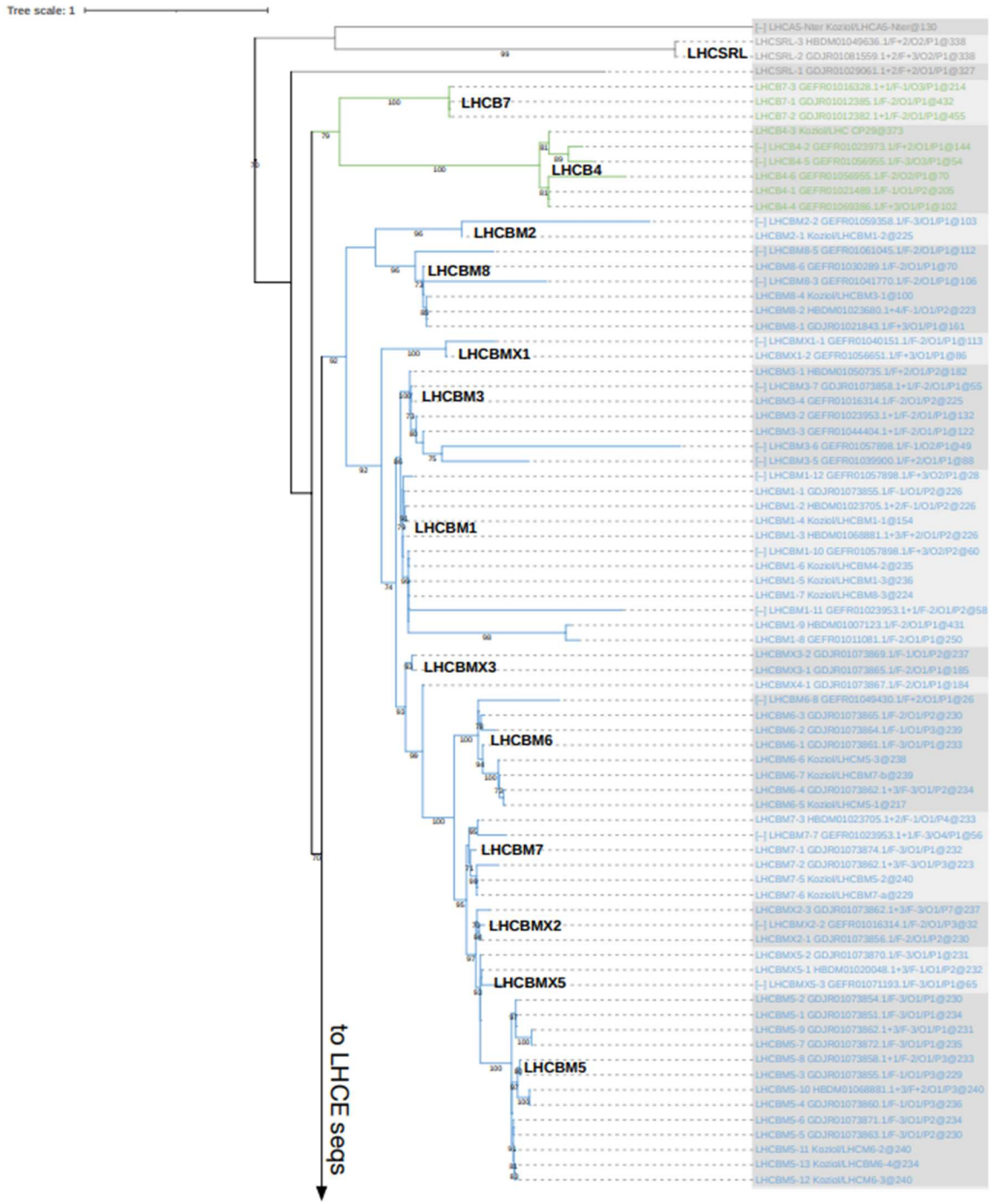

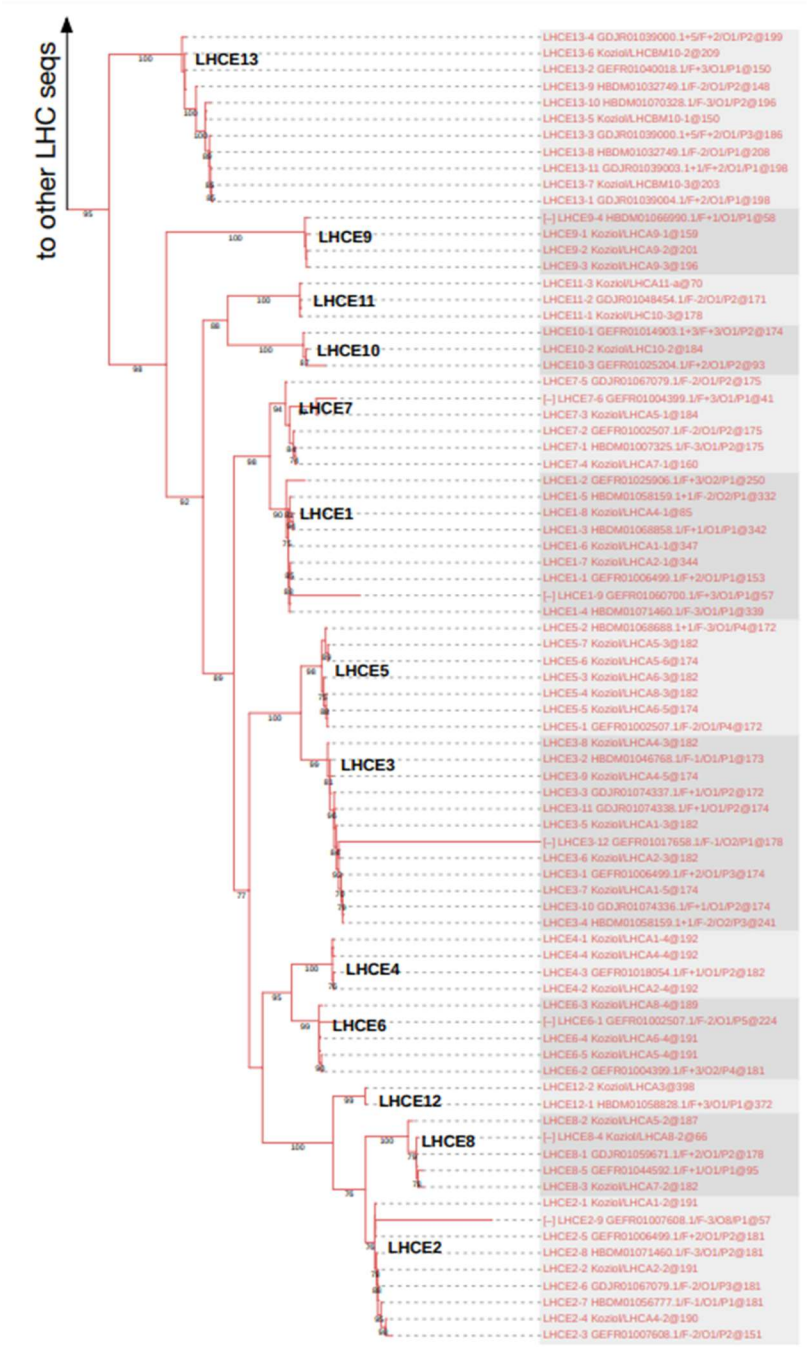

Supplementary Figure 1 : Phylogenetic Analysis of Euglena gracilis Light-Harvesting Complex (Lhc) Proteins.

The maximum likelihood phylogenetic tree was constructed using an expanded dataset of Euglena gracilis Lhc proteins. Bootstrap values are indicated at key nodes. Lhc proteins are grouped into distinct families, with major clades highlighted in different colors: LhcbM proteins (blue), LhcE proteins (red), Lhcb (green) other Lhc-related families (gray).

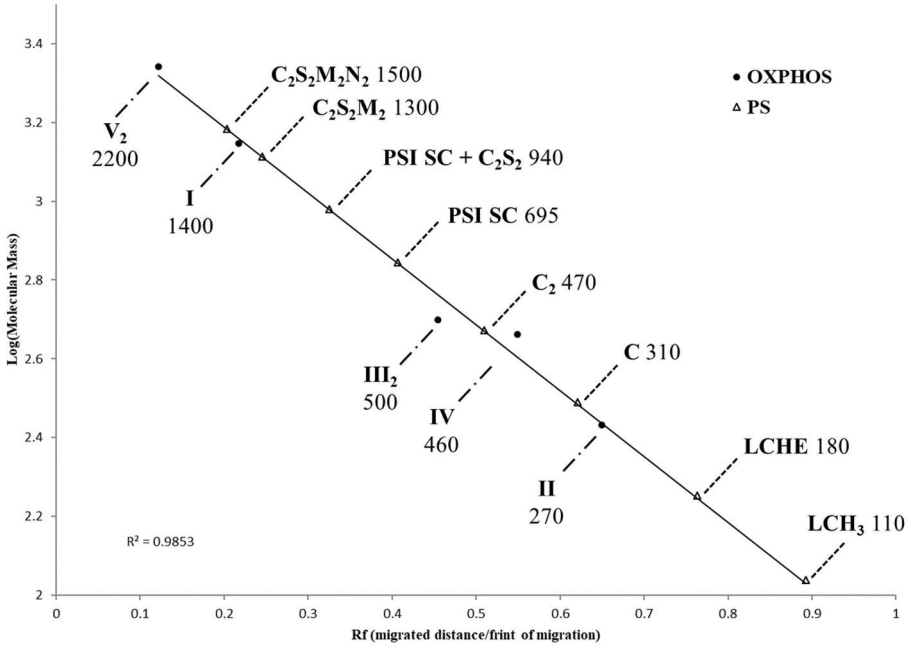

Supplementary Figure 2: Estimated molecular masses for the Euglena gracilis photosynthetic complexes.

The logarithms of the molecular masses of previously characterized mitochondrial complexes (●) (V_2, I, III_2, IV) (Miranda-Astudillo et al., 2018; Yadav et al., 2017) were plotted against their migration distance in *hr*CN-PAGE (R^2 = 0.9755). Then, the migration distances of the *Euglena* photosynthetic complexes (Δ) were interpolated and their corresponding molecular masses inferred.

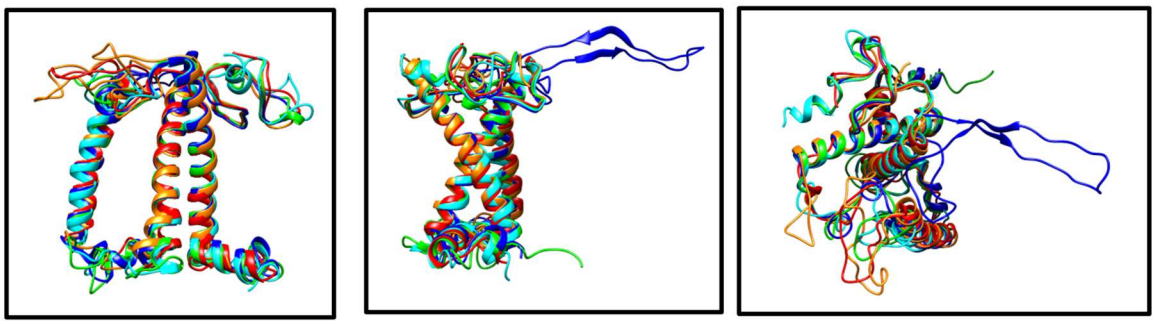

Supplementary Figure 3 . Structural comparison of Light Harvesting Complexes.

Overlap of LHCII (green), CP24 (orange), CP26 (cyan), CP29 (blue), LhcE9 (red) structures. Left panel: side view, center panel: 90° rotation on the same plane view, right panel: upper view. Structures from LHCII, CP24, CP26 and CP29 were obtained from PSII-LHCII supercomplex from Pisum sativum (PDB: 5XNL(Su et al., 2017)). LhcE9 homology model were obtained with SWISS-MODEL (Waterhouse et al., 2018).

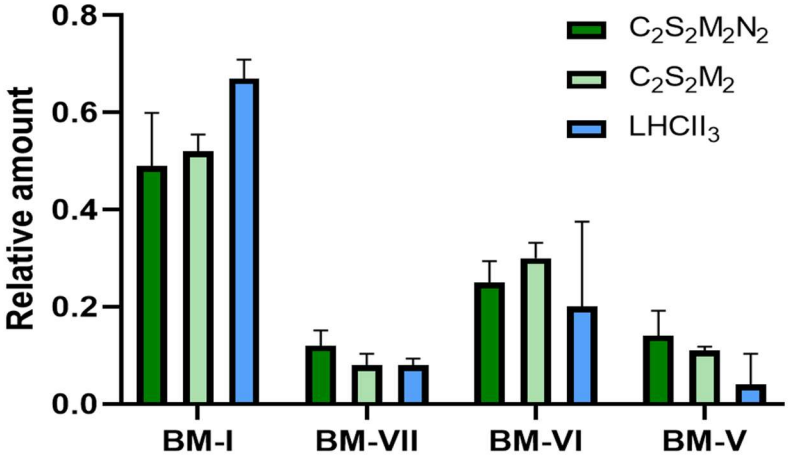

Supplementary Figure 4. Distribution of LhcbM in PSII-SC and Free LHCII Across Different PSII/LHCII Particles.

The bar graph illustrates the relative amounts of LhcbM (BM-I, BM-VII, BM-VI, BM-V). The color-coded bars represent different PSII-LHCII compositions: $C_2S_2M_2N_2$ (dark green), $C_2S_2M_2$ (light green), and free $LHCII_3$ (blue). Error bars represent standard deviations.

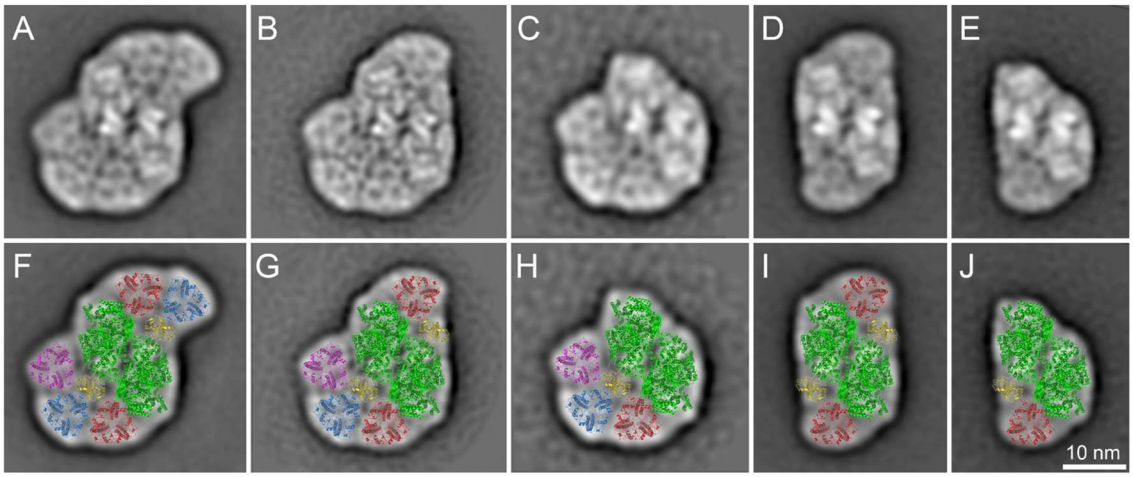

Supplementary Figure 5. Smaller PSII classes

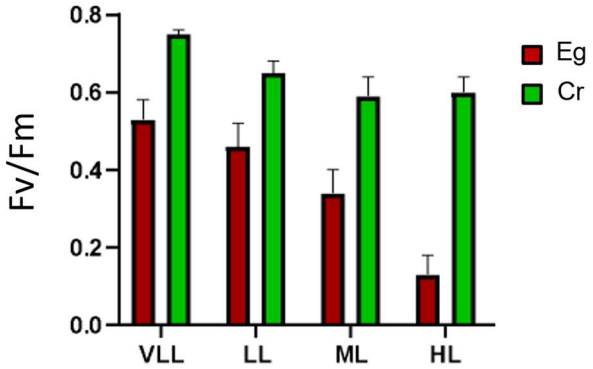

Supplementary Figure 6. Maximum Quantum Yield of Photosystem II (Fv/Fm) in Euglena and Chlamydomonas Under Different Light Conditions.

The bar graph represents the maximum quantum yield of Photosystem II (Fv/Fm) in ***Euglena gracilis*** **(red bars)** and ***Chlamydomonas reinhardtii*** **(green bars)** grown under different light regimes: **very low light (VLL), low light (LL), medium light (ML), and high light (HL)**. Fv/Fm values indicate the photochemical efficiency of photosystem II, with higher values reflecting better photosynthetic performance. Chlamydomonas consistently exhibits higher Fv/Fm values across all light conditions compared to Euglena. The decrease in Fv/Fm with increasing light intensity is more pronounced in Euglena, suggesting a higher sensitivity to high-light stress. Error bars represent standard deviations.

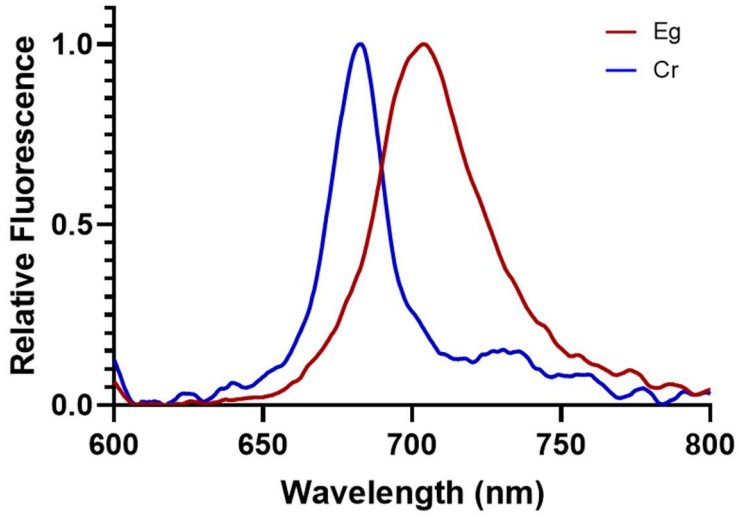

Supplementary Figure 7. Difference Fluorescence Emission Spectra between State I and State II at Room Temperature.

Room temperature fluorescence emission spectra of Euglena gracilis (Eg, red) and Chlamydomonas reinhardtii (Cr, blue) were recorded at room temperature under State I and State II conditions. The difference spectra (State I - State II) are displayed.

Protein	Identified by	E: Score/Identified Peptides	S: Score/Identified Peptides	Accession	References
Photosystem I					
PsaA	E/S/P	153/16	250/12	comp64894_c0_seq1	(Sobotka et al., 2017); This work
PsaB	E/S/P	142/15	29/3	comp64709_c0_seq3	(Sobotka et al., 2017); This work
PsaC	E/S/P	15/4	14/5	comp40626_c0_seq1	(Sobotka et al., 2017); This work
PsaD	E/S/P	199/18	44/4	comp63474_c0_seq1	(Sobotka et al., 2017); This work
PsaE	E/P	82/9	—	comp52439_c0_seq2	(Sobotka et al., 2017); This work

PsaF	E/P	76/12	—	comp59715_c0_seq1	(Sobotka et al., 2017); This work
PsaJ	P	—	—	AKL82384.1	(Sobotka et al., 2017); (Bennett and Triemer, 2015); This work
PsaM	P	—	—	CAA50083.1	(Schlunegger and Stutz, 1984); This work
Photosystem II					
PsbA (D1)	E/P	123/20	—	comp53636_c0_seq2	(Sobotka et al., 2017); This work
PsbB(CP47)	E/S/P	309/58	378/19	comp59418_c0_seq1	(Sobotka et al., 2017); This work
PsbC (CP43) (VII) (34kDa)	E/S/P	212/29	415/19	comp61278_c0_seq2	(Sobotka et al., 2017); This work
PsbD (D2)	E/S/P	140/16	274/14	comp59248_c0_seq2	(Sobotka et al., 2017); This work
PsbE (cyt559α)	E/S/P	14/4	122/8	CAA30108.1	(Cushman et al., 1988); This work
PsbF (cyt559β)	S	—	25/2	P05334.1	(Cushman et al., 1988); This work
PsbH (10kDa)	E/P	16/2	—	comp45461_c0_seq1	(Sobotka et al., 2017); This work
PsbI	E/S/P	14/2	43/3	comp16326_c0_seq1	(Sobotka et al., 2017); This work
PsbJ	PGenomic	—	—	CAA50098.1	(Jenkins et al., 1995); This work

PsbK	PGenomic	—	—	CAA50085.1	(Jenkins et al., 1995); This work
PsbL	PGenomic	—	—	CAA50097.1	(Jenkins et al., 1995); This work
PsbM	E/S/P	86/8	68/3	comp52703_c0_seq1	This work
PsbN	PGenomic	—	—	807511	(Hallick et al., 1993); This work
PsbO (OEE1)	E/P	12/2	—	comp61990_c0_seq1	(Sobotka et al., 2017); This work
PsbP (OEE2)	E/P	88/10	—	comp51350_c0_seq1	(Sobotka et al., 2017); This work
PsbQ (OEE3)	E/P	146/24	—	comp55004_c0_seq2	(Sobotka et al., 2017); This work
PsbR	P	—	—	*********	This work
PsbT (PsbTc) (ycf8)	PGenomic	—	—	CAA50132.1	(Jenkins et al., 1995); This work
PsbW	E/P	16/5	—	comp49777_c0_seq3	This work
PsbX					This work
PsbY	P	—	—	comp51240_c0_seq2	This work
PsbZ (ycf9)	S	—	15/2	comp32647_c0_seq2	(Sobotka et al., 2017); This work
Psb27	E/P	42/5	—	comp56040_c0_seq1	(Sobotka et al., 2017); This work
Psb28	P	—	—	*********	This work
Psb29	P	—	—	*********	This work
Psb30 (ycf12)	PGenomic	—	—	AKL 82351.1	(Bennett and Triemer, 2015)

Psb32	P	—	—	*********	This work
Psb33	P	—	—	*********	This work
Ycf48	Genomic	—	—	ELL00007923	(Sobotka et al., 2017)

Supplementary Table 1. Composition of the photosystem I and II cores complex in *Euglena gracilis*.

E: Liquid chromatography-Electrospray-ionisation quadrupole time-of-flight mass spectrometry from complete band from CN-PAGE. S: Tandem mass spectrometry from isolated spots from the 3D gels. P: Phylogenomic approach for conserved subunits.

Pigment	**$C_2S_2M_2N_2$**	**$C_2S_2M_2$**	**PSI-SC**	**PSI-SC**	**C_2**	**LHCE**	**$LHCII_3$**
Neoxanthin	1.4 ± 0.02	2.0 ± 0.06	0.7 ± 0.04	0.8 ± 0.05	3.0 ± 0.2	0.5 ± 0.01	9.1 ± 0.1
Diadinoxanthin	10.9 ± 0.3	8.3 ± 0.2	13.0 ± 0.8	10.9 ± 0.8	15.6 ± 1.2	18.1 ± 0.4	20.2 ± 0.3
Diatoxanthin	0.8 ± 0.03	0.9 ± 0.02	1.1 ± 0.1	0.6 ± 0.03	0.8 ± 0.2	0.8 ± 0.1	1.7 ± 0.03
Chlorophyll *b*	20.8 ± 0.6	18.9 ± 0.5	7.4 ± 0.4	5.4 ± 0.3	13.1 ± 1.6	2.6 ± 0.13	27.7 ± 0.3
Chlorophyll *a*	65.3 ± 1.6	69.2 ± 1.8	77.2 ± 5.2	81.7 ± 5.7	66.6 ± 5.1	77.2 ± 1.5	40.6 ± 0.5
Beta-carotene	0.8 ± 0.14	0.67 ± 0.02	0.65 ± 0.06	0.61 ± 0.03	0.84 ± 0.02	0.75 ± 0.27	0.64 ± 0.01
***a*/*b* ratio**	3.1	3.7	10.4	15.2	5.1	29.8	1.5

Supplementary Table 2 . Pigment composition of pigment-protein complexes of E gracilis.

Mean ± s.d. of the relative mass of each pigment (n=3).

6 Functional Analysis of the LHCE12 Knockout in *Euglena gracilis*

6.1 Introduction

The light-harvesting complexes (LHCs) of *Euglena gracilis* originate from large messenger RNA (mRNA) transcripts that give rise to over 50 polyprotein precursors (Koziol & Durnford, 2008). These precursors are subsequently directed to the chloroplast, where the mRNAs undergo cleavage to produce individual proteins. The LHCE complex, with an estimated molecular weight of 180-250 kDa, is believed to consist of five to six LHCE-type proteins, including LHC E1, E2, E3, E4, and E12 (unpublished data). Among these, LHCE12—previously identified as LHCA3 in the analysis by Koziol et al. (2007)—is the only member not encoded as a polyprotein, (identified as Transcript_11021 or HBDM01058828.1/F+3/O1/P1).

A key challenge in studying *Euglena gracilis* at the genetic level is its polyploid genome, which consists of an unknown number of chromosomes (Zoltner & Field 2022). This genomic redundancy complicates gene deletion approaches such as CRISPR-Cas9, particularly for genes encoded as polyproteins. In cases where multiple gene copies exist, the inactivation of a target gene on certain chromosomes may be compensated by functional copies present elsewhere in the genome. This redundancy presents a significant obstacle for generating null mutants and assessing the phenotypic consequences of gene knock-outs. Given that most LHCE-type proteins, including LHC-E1, E2, E3, and E4, are derived from polyproteins, their genetic manipulation is inherently complex. In contrast, LHCE12, being encoded by a single gene rather than a polyprotein, may represent a more feasible target for functional studies.

6.2 Material and Methods

CrispR-Cas9 was following Nomura et al., (2020).

Strain cultivation, Spectrofluorometry, biophysical analysis and N-PAGE were conducted following the Material and Methods from the previous chapter (section 5.3).

6.3 Results

Four knockout mutants targeting this gene were generated using the wild-type *E. gracilis* strain CCAP 1224/5Z (hereafter referred to as the "Japanese strain") following Nomura et al., 2020 protocols. Another wild-type *E. gracilis* strain. SAG 1224-5/25 is referred to as the "Liège strain."

To verify the effect of the LHCE12 gene knockout. a reverse transcription PCR (RT-PCR) was performed on Transcript_11021 in various clones (Figure 47). Four mutant lines—LHCE12-18, LHCE12-26, LHCE12-27, and LHCE12-31—produce a short transcript (~543 and 234 bp. depending on the primers used: 20Fw&943Rv vs. 316Fw&943Rv) compared to the wild-type strain. This indicates that the LHCE12-specific transcript is effectively altered in these knockout mutants. The following analysis will discuss the impact of this mutation on *E. gracilis* cells and their photosynthetic complexes.

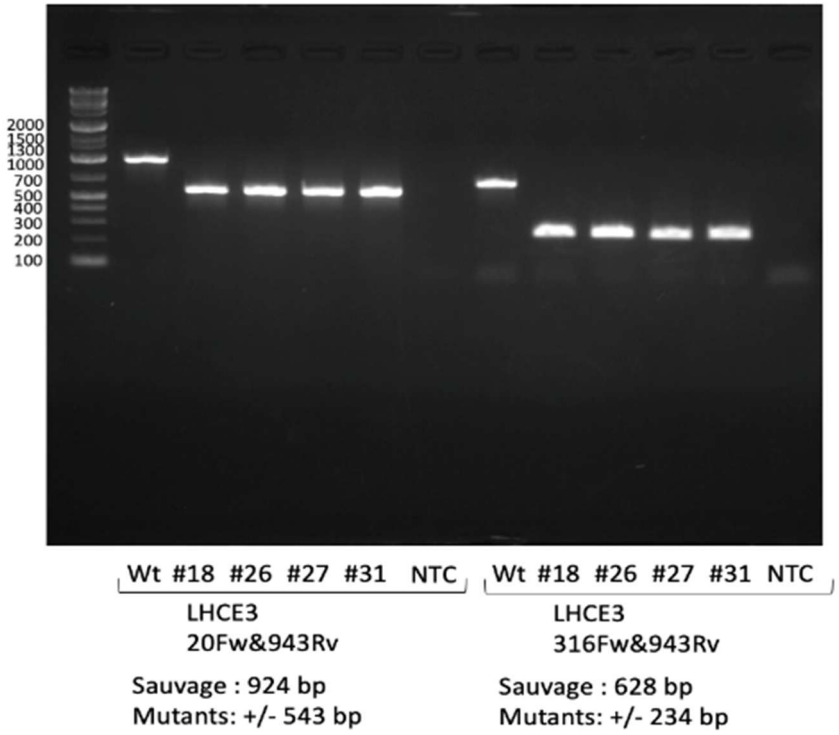

Figure 47. RT-PCR performed on mRNA from mixotrophic cultures of wild-type Euglena gracilis and LHCE12 mutants.

RT-PCR was conducted using two primers (20Fw & 943Rv and 316Fw & 943Rv) on the LHCE12-18, LHCE12-26, LHCE12-27, and LHCE12-31 mutants. The molecular weight marker used was the Gene Ladder Wide1.

6.3.1 Spectral signature

In vivo optical spectrometry and room-temperature spectrofluorimetry measurements of the various cultures using revealed no significant differences in the recorded spectra (Figures 48B and 48B). A slight blue-shift (i.e.. toward higher-energy wavelengths) was observed in the room-temperature fluorescence of the “Liège” wild-type strain (Figure 48B). However. this shift does not appear to be statistically significant and is likely attributable to experimental variability.

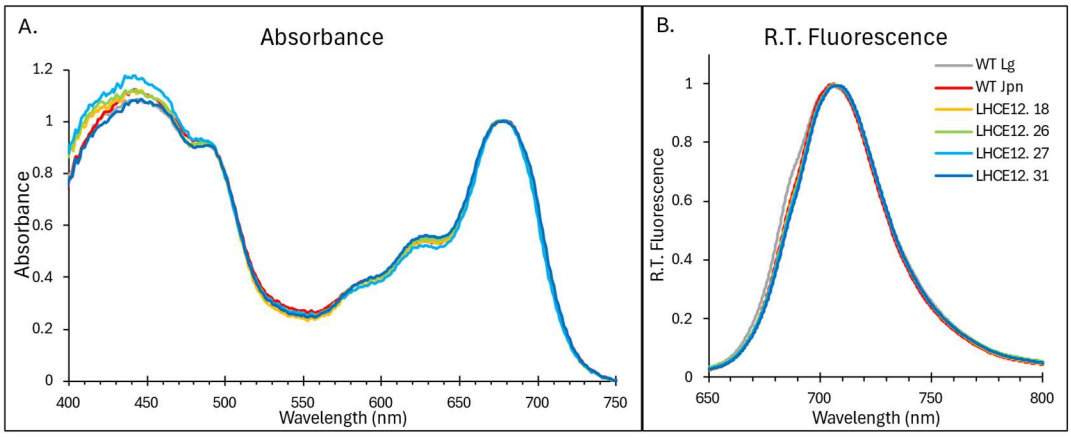

Figure 48. Absorbance and room-temperature fluorescence (R.T.) spectra of wild-type and LHCE12 mutants Euglena gracilis.

(A) Absorbance and (B) R.T. Fluorescence spectra for the wild-type "Liège" (gray line) and "Japanese“ (red line) strains. as well as the LHCE12-18 (yellow line). LHCE12-26 (green line). LHCE12-27 (light blue). and LHCE12-31 (dark blue) mutants. Each spectrum was normalized to a maximum fluorescence intensity. The standard deviation for each spectrum is highlighted in the same color (n = 3).

6.3.2 Biophysical analysis

The photosystem II (PSII) functional antenna sizes of wild-type and mutant *Euglena gracilis* cultures were assessed under actinic light conditions identical to those used for ETR measurements (655, 959, 715, and 725 nm) After a 5min dark acclimation period.

The functional antenna size decreases sharply by about 60% at 695 nm relative to 655 nm, falling from 1.2 to 0.5 s^{-1} (Figure 49A). Under far-red illumination at 715 and 725 nm, this reduction becomes even more pronounced, leaving only about 14% of the optimal functional size (approximately 0.17 s^{-1}). Notably, the LHCE12 mutations did not have any significant influence on PSII antenna size under any of the actinic lighting conditions tested.

Although the functional antenna size decreases at wavelengths longer than 655 nm, the maximum electron transfer rate at 100 µmol photons·m^{-2}·s^{-1} remains comparable at 695 nm (Figure 49B). No significant differences were detected between the wild-type (WT) and mutant strains.

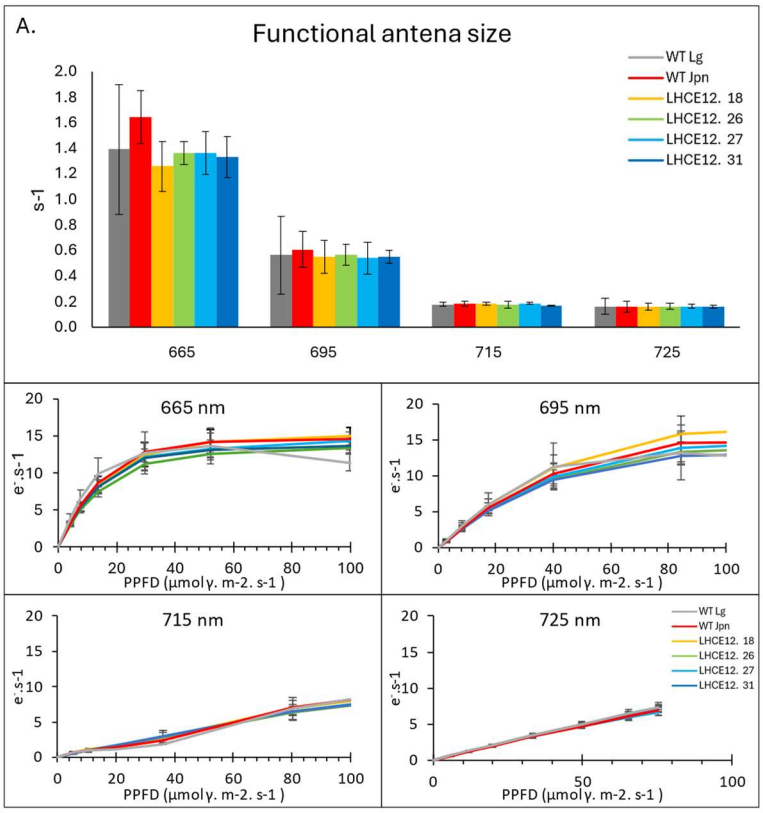

Figure 49. Functional Antenna Size and Electron transfer rate (ETR) of wild-type and LHCE12 mutants Euglena gracilis.

(A) Functional antenna size (s^{-1}), and (B) ETR for the wild-type "Liège" (gray line) and "Japanese“ (red line) strains, as well as the LHCE12-18 (yellow line). LHCE12-26 (green line). LHCE12-27 (light blue). and LHCE12-31 (dark blue) mutants. Statistical analysis was performed using t.test with $p < 0{,}005$ (*) (n = 3).

6.3.3 LHCE Isolation and Analysis

The migration patterns of photosynthetic complexes from the “Japanese” wild-type strain and the LHCE12 mutant strains each revealed eight distinct bands per sample (Figure 50). Band 7, which corresponds to the LHCE antenna complex, was present in every mutant extract as well as in the “Liège” wild-type strain. However, in extracts from the “Liège” strain, the LHCE complex band did not align with that observed in the “Japanese” wild-type strain and its mutants (i.e.. band 7). Instead, it appeared at a lower molecular weight—referred to as band 7* (Figure xb). The difference in migration patterns between band 7* (Japanese strain) and band 7 (Liège strain) could arises from a combination of post-translational modifications, differences in protein complex assembly, structural variations, pigment binding differences, or underlying genetic divergence. Additional biochemical, spectroscopic, and genetic analyses would be required to determine the exact mechanism.

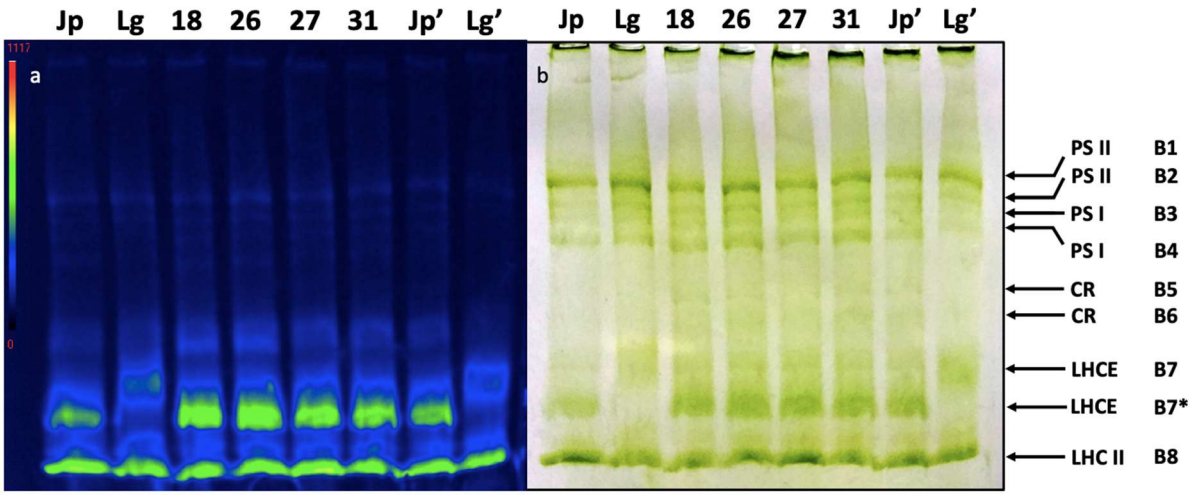

Figure 50. Spectroscopic characterization of photosynthetic complexes of wild-type and LHCE12 mutants Euglena gracilis.

(a) Clear-Native Polyacrylamide Gel Electrophoresis (CN-PAGE) separation of pigment-protein complexes from total membranes solubilized with 2% n-dodecyl α-D-maltoside. Each lane was loaded with 75 µg of protein (a representative experiment is shown). (b) Fluorescence picture of the gel upon 470nm excitation.

The corresponding bands (B7 and B7*) were analyzed using spectroscopy. In the “Liège” wild-type strain, band 7 showed the characteristic LHCE absorption pattern, with two distinct peaks at 675 and 690 nm (Figure 51A). However, in the same strain, band 7* lacked the 690 nm peak. By contrast, the “Japanese” wild-type strain and its mutants did not display an LHCE-specific pattern in band 7 but both 675 and 690 nm peaks were present in band 7* (Figure 51B). These findings imply that the LHCE complexes in the “Japanese” strain have lower molecular weight than those in the “Liège” strain. Consistent with earlier observations, the other bands on the gel displayed similar absorption profiles. typically centered around 675 nm (673–677 nm).

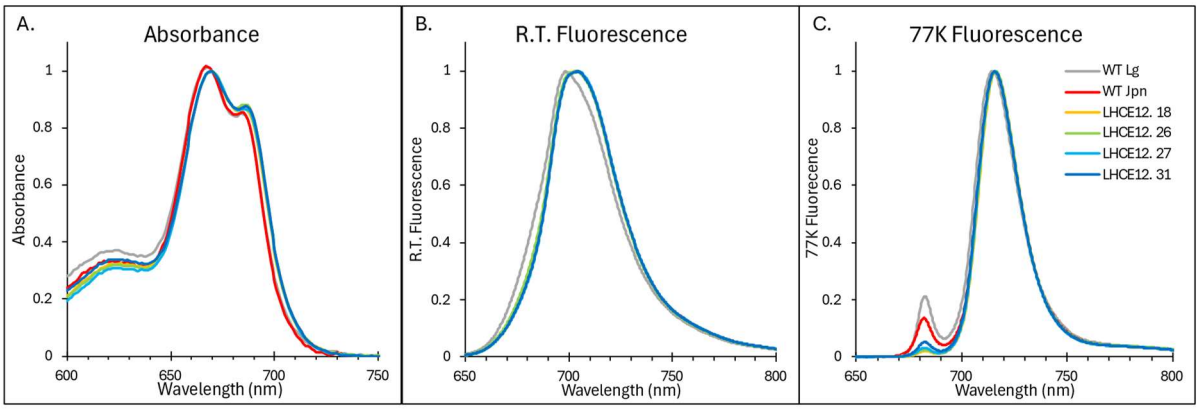

Figure 51. Spectrometric signature of isolated LHCE12.

(A) Absorbance (B) R.T. Fluorescence, and (C) 77K Fluorescence spectra for the wild-type "Liège" (gray line) and "Japanese“ (red line) strains, as well as the LHCE12-18 (yellow line), LHCE12-26 (green line), LHCE12-27 (light blue), and LHCE12-31 (dark blue) mutants. Each spectrum was normalized to a maximum fluorescence intensity. The standard deviation for each spectrum is highlighted in the same color (n = 3).

To assess the impact of the LHCE12 mutation on the pigment composition of the complexes, each band from the hrCN-PAGE gel (Figure 50) was pulverized, extracted, and then analyzed via reversed-phase high-performance liquid chromatography (HPLC). The results showed that all bands had comparable pigment concentrations, regardless of their source (Table 6). This finding indicates that the LHCE12 mutation does not seem to influence the pigment content within the photosynthetic pigment–protein complexes.

(%)	Neoxanthin	Diadinoxanthin	Chl b	Chl a	B-carotene
Band 1 (SC-PS II)	3.40 ± 0.20	16.31 ± 0.27	8.70 ± 0.57	69.13 ± 0.53	2.47 ± 0.22
Band 2 (SC-PS II)	2.31 ± 0.31	15.91 ±0.36	6.07 ±0.74	72.48 ±1.04	3.24 ± 0.55
Band 3 (SC-PS I)	1.38 ± 0.12	15.62 ± 0.25	4.01 ±0.39	76.06 ±1.4	2.93 ±0.09
Band 4 (SC-PS I)	0.89 ± 0.11	15.66 ±0.61	2.80 ±0.35	77.15 ±1.52	3.50 ±0.95
Band 5 (CR-PS II)	0.69 ±0.45	12.61 ±1.47	1.87 ±0.73	78.66 ±1.86	6.49 ±1.5
Band 6 (CR-PS II)	0.35 ±0.08	14.85 ±0.79	1.39 ±0.16	79.36 ±0.69	4.05 ±0.73
Band 7 (LHCE)	0.00	19.83	0.04	80.12	0.00
Band 7* (LHCE)	0.40 ± 0.30	19.17 ±0.21	1.17 ±0.79	79.21 ±1.84	0.06 ±0.12
Band 8 (LHCBM)	6.75 ±0.35	15.35 ±0.14	11.23 ±0.62	66.67 ±0.66	0.00 ±0.01

Table 6. HPLC pigment separation of isolated complexes from CN-PAGE.

Pigment quantities are expressed as the ratio of the area under their respective peaks to the total area of all peaks in the chromatogram at 430 nm. Considering no differences were detected between the wild-type and mutant strains. The mean and standard deviations were calculated across the entire set of samples.

6.3.4 Protein composition of LHCE :

Analyses were conducted on the LHCE antenna complex bands from the “Liège” and “Japanese” wild-type strains using LC-ESI-Q-TOF-MS to examine the peptide composition of the LHCE antenna complex. As expected, LHCE12 was not detected in the LHCE complexes of the knockout mutants LHCE12-18, LHCE12-26, LHCE12-27, and LHCE12-31. Although LHCE12 was present in both wild-type strains, it accounted for less than 0.3% of the detected peptides. The mutant strains showed no difference in LHCE antenna major composition compared to the wild type. The three most abundant proteins identified were LHCE4A, LHC1B, and LHC2C/3A, collectively accounting for more than 75% of the detected peptides. The remaining peptides, which varied between strains and mutants, included proteins such as LHCBM, PSBD, CP47, PSBP1, PSB0, PSB1, LHCB4, PSBQ, each detected in varying proportions.

6.4 Conclusion :

The results of this study demonstrate that the knockout of *LHCE12* in *Euglena gracilis* leads to a complete loss of its full-lenght transcript in all mutant strains, confirming the efficiency of the CRISPR-Cas9 gene disruption approach. Despite this genetic modification, our analyses indicate that the structural and functional integrity of the LHCE antenna complex remains largely unaffected. Spectroscopic characterization, pigment composition profiling, and proteomic analyses collectively reveal that the loss of *LHCE12* does not lead to significant alterations in the composition or function of the photosynthetic machinery.

The electrophoretic differences between the “Japanese” and “Liège” wild-type strains highlight potential variations in protein assembly, post-translational modifications, or pigment-binding properties, warranting further investigation. Given the genetic complexity of *Euglena gracilis*, where key LHC proteins are encoded as polyproteins, future studies should focus on alternative gene silencing approaches, such as RNA interference (RNAi) or CRISPR interference (CRISPRi), to selectively target other LHCE subunits like LHCE1, LHCE2, LHCE3, and LHCE4. These strategies could overcome the challenges posed by polyprotein organization and reveal the specific roles of individual LHC components in photosynthetic function. By refining genetic tools for *Euglena*, this research opens new avenues to dissect the molecular mechanisms underlying light harvesting in this unique organism.

7 General conclusion

This thesis contributes to the growing understanding of the remarkable diversity and evolutionary plasticity of far-red light (FRL) adaptation strategies among oxygenic phototrophs. Through a multidisciplinary approach—combining physiology, genomics, biophysics, and spectroscopy—we add new insights into how both prokaryotic and eukaryotic photosynthetic organisms have evolved distinct mechanisms to harvest light beyond the visible spectrum. These findings complement existing research on phototrophic adaptation and address ongoing questions in microbial ecology, evolutionary biology, and astrobiology.

Far-red light acclimation, while relatively rare, offers a critical advantage to phototrophs in shaded or photon-limited environments (Gan et al., 2014; Smith, 1994). Our initial screening of 120 microalgal strains across diverse taxonomic groups contributes to the evidence that FRL adaptation is not confined to a single lineage but is distributed across phylogenetically distant groups. This supports the idea of convergent evolutionary solutions to spectral constraints. In cyanobacteria, the canonical Far-red Light Photoacclimation (FaRLiP) system is known to remodel the photosynthetic apparatus—including PSI, PSII, PBS subunits, chlorophyll *f* biosynthesis, and photoreceptors (Elias et al., 2024). Our observations in *Stanieria cyanosphaera* SAG 33.87 align with this, revealing transcriptional and structural adjustments under FRL consistent with FaRLiP-regulated adaptation.

Beyond FaRLiP, cyanobacteria also display complementary light-acclimation strategies. Type III Complementary Chromatic Adaptation (CCA) modulates the phycobilisome composition, while Low-Light Photoacclimation (LoLiP) enhances allophycocyanin expression for improved light harvesting. Our work adds detail to these mechanisms by examining excitation lifetimes in FaRLiP-induced PSII in *S. cyanosphaera*, where longer lifetimes suggest potential trade-offs with charge separation efficiency. Despite this, the strain maintains high PSII efficiency, preserved antenna size, and stable oxygen production under far-red light, further illustrating the effectiveness of its acclimation strategy.

While our research focused primarily on low-light adaptation, we recognize the need for future studies exploring whether *S. cyanosphaera* also retains high-light protective mechanisms, such as those mediated by the Orange Carotenoid Protein (OCP), crucial for non-photochemical quenching (Kirilovsky, 2007). Additionally, we acknowledge methodological challenges,

including CN-PAGE variability and fluorescence heterogeneity in aggregated cells, which require careful interpretation of biophysical data. Comparative genomics holds promise for uncovering whether *S. cyanosphaera* employs an as-yet-uncharacterized acclimation system distinct from known FaRLiP, CCA, or LoLiP clusters.

This thesis also contributes to the relatively underexplored area of far-red light adaptation in eukaryotic phototrophs. In *Vitrella brassicaformis*, we characterized a constitutive far-red absorbing photosystem, maintaining a stable spectral shoulder at 700 nm under all tested conditions. Spectroscopic and biochemical analyses suggest that this adaptation results not from novel pigments, but from persistent pigment-protein interactions within PSII. These findings build upon existing knowledge, indicating that such a constitutive mechanism may confer ecological advantages in dimly lit, coral-associated habitats where spectral filtering favors long-wavelength light.

In contrast, *Chromera velia*, a close relative of *Vitrella*, exhibited a dynamic acclimatory response, increasing antenna size at 715 nm and adjusting fluorescence peaks under far-red conditions. *Vitrella*, by comparison, displayed a higher functional antenna size at 695 nm, consistent with its spectral signature and indicative of a distinct strategy for far-red adaptation.

Euglena gracilis presented yet another adaptation model. Rather than synthesizing new pigments, it dynamically reorganizes its antenna complexes, enhancing state transitions and improving energy distribution between photosystems. This flexibility ensures balanced PSI/PSII excitation pressure under varying spectral conditions. Our fluorescence and biophysical analyses complement previous studies, confirming that *Euglena* maintains effective photosynthesis in the far-red spectrum through dynamic regulation of LHCII-PSII connectivity.

Collectively, these observations contribute to the understanding of divergent strategies among eukaryotic phototrophs: stable optimization in *Vitrella*, dynamic tuning in *Euglena*, and intermediate plasticity in *Chromera*. Notably, all three species extend photosynthetic activity into the far-red range without synthesizing new pigments, underscoring the versatility of chlorophyll *a* and its interaction matrix.

The evolutionary and ecological implications of these findings are significant. The phylogenetic breadth of FaRLiP-bearing cyanobacteria—including Nostocales, Chroococcidiopsidales, Leptolyngbyales, and others—supports the idea of repeated selection for far-red photosynthesis in shaded environments (Antonaru et al., 2024). Our observations in *Vitrella* suggest that eukaryotic algae may also evolve stable spectral tuning mechanisms, challenging assumptions about the plasticity of algal photosynthesis. The presence of this trait in an alveolate species closely related to apicomplexans prompts further exploration into the evolutionary history of plastids and phototrophic capabilities in this lineage (Kotabova et al., 2014).

These adaptations likely contribute to ecological differentiation, allowing phototrophs to minimize interspecific competition. *Vitrella's* ability to exploit far-red light likely facilitates coexistence with other phototrophs in coral environments, while *Euglena's* rapid modulation of antenna systems may provide an advantage in highly variable habitats such as turbid waters or canopy-filtered light conditions.

Several future research directions emerge from this work:

- Comparative transcriptomics of *Vitrella*, *Euglena*, and *Chromera* under varied spectra could clarify the regulatory networks governing FRL acclimation.
- Structural resolution of *Vitrella's* far-red light-harvesting complexes using cryo-electron microscopy would illuminate PSII-core and antenna arrangements.
- Proteomic and pigment-binding studies could pinpoint the subunits responsible for red-shifted absorption.
- Phylogenetic analyses are needed to understand the evolutionary emergence of FRL adaptation across lineages.
- Environmental surveys of extreme or symbiotic ecosystems could reveal the natural prevalence and ecological importance of far-red phototrophy.

Beyond ecological and evolutionary significance, these insights contribute to astrobiology and the objectives of the PORTAL project. By investigating phototrophic responses to FRL-rich environments, this research provides empirical data relevant to the potential for oxygenic photosynthesis under M-dwarf starlight (Battistuzzi et al., 2023). While promising, we acknowledge that factors such as stellar variability, UV radiation, and atmospheric composition must be considered before drawing conclusions about exoplanetary habitability.

In conclusion, this thesis adds to the growing body of evidence that far-red light adaptation is an evolutionarily widespread and functionally versatile trait. By integrating molecular, physiological, and ecological perspectives, we contribute to a deeper understanding of how phototrophs optimize energy capture across environmental gradients. These findings provide a conceptual and methodological foundation for future studies on photosynthesis in extreme environments, the evolution of plastids, coral symbiosis, and the search for life on planets orbiting red-shifted stars.

8 References

- Agostini, A., Bína, D., Barcytė, D., Bortolus, M., Eliáš, M., Carbonera, D., & Litvín, R. (2024). Eustigmatophyte model of red-shifted chlorophyll a absorption in light-harvesting complexes. *Communications Biology*, *7*(1), 1406.
- Akhtar, P., Balog-Vig, F., Han, W., Li, X., Han, G., Shen, J. R., & Lambrev, P. H. (2024). Quantifying the energy spillover between photosystems II and I in cyanobacterial thylakoid membranes and cells. *Plant and Cell Physiology*, *65*(1), 95-106.
- Albanese, P., Melero, R., Engel, B.D., Grinzato, A., Berto, P., Manfredi, M., Chiodoni, A., Vargas, J., Sorzano, C.Ó.S., Marengo, E., Saracco, G., Zanotti, G., Carazo, J.M., Pagliano, C., 2017. Pea PSII-LHCII supercomplexes form pairs by making connections across the stromal gap. Sci. Rep. 7, 1–16.
- Albanese, P., Tamara, S., Saracco, G., Scheltema, R.A., Pagliano, C., 2020. How paired PSII–LHCII supercomplexes mediate the stacking of plant thylakoid membranes unveiled by structural mass-spectrometry. Nat. Commun. 11, 1–14.
- Alboresi, A., Caffarri, S., Nogue, F., Bassi, R., & Morosinotto, T. (2008). In Silico and Biochemical Analysis of Physcomitrella patens Photosynthetic Antenna: Identification of Subunits which Evolved upon Land Adaptation. PLoS ONE, 3(4), e2033.
- Allahverdiyeva, Y., Mustila, H., Ermakova, M., Bersanini, L., Richaud, P., Ajlani, G., Battchikova, N., Cournac, L., & Aro, E. (2013). Flavodiiron proteins Flv1 and Flv3 enable cyanobacterial growth and photosynthesis under fluctuating light. *Proceedings of the National Academy of Sciences*, *110*(10), 4111–4116.
- Allen, J. F., & Martin, W. (2007). Out of thin air. *Nature*, *445*(7128), 610-612.
- Allen, J.F., Bennett, J., Steinback, K.E., Arntzen, C.J., 1981. Chloroplast protein phosphorylation couples plastoquinone redox state to distribution of excitation energy between photosystems. Nature 291, 25–29.
- Amunts, A., Drory, O., Nelson, N., 2007. The structure of a plant photosystem I supercomplex at 3.4 Å resolution. Nature 447, 58–63.
- Antonaru, L. A., Cardona, T., Larkum, A. W., & Nürnberg, D. J. (2020). Global distribution of a chlorophyll f cyanobacterial marker. *The ISME journal*, *14*(9), 2275-2287.
- Antonaru, L. A., Rad-Menéndez, C., Mbedi, S., Sparmann, S., Pope, M., Oliver, T., Wu, S., Green, D., Gugger, M., & Nürnberg, D. J. (2024). The ancient evolution of far-red light

photoacclimation in cyanobacteria. Biorxiv. [Preprint] Available from : https://www.biorxiv.org/content/10.1101/2024.05.15.594131v1

- Apel, K., & Hirt, H. (2004). Reactive oxygen species: metabolism, oxidative stress, and signal transduction. *Annu. Rev. Plant Biol.*, *55*(1), 373-399.
- Archibald, J. M. (2009). The origin and spread of eukaryotic photosynthesis: evolving views in light of genomics.
- Archibald, J. M. (2015). Endosymbiosis and eukaryotic cell evolution. *Current Biology*, *25*(19), R911-R921.
- Aro, E.M., Virgin, I., Andersson, B., 1993. Photoinhibition of Photosystem II. Inactivation, protein damage and turnover. BBA - Bioenerg. 1143, 113–134.
- Averina, S., Velichko, N., Pinevich, A., Senatskaya, E., & Pinevich, A. (2019). Non-a chlorophylls in cyanobacteria. *Photosynthetica*, *57*(4), 1109–1118.
- Babu, T. S., Jansen, M. A., Greenberg, B. M., Gaba, V., Malkin, S., Mattoo, A. K., & Edelman, M. (1999). Amplified degradation of photosystem II D1 and D2 proteins under a mixture of photosynthetically active radiation and UVB radiation: dependence on redox status of photosystem II. *Photochemistry and Photobiology*, *69*(5), 553-559.
- Bag, P., 2021. Light harvesting in fluctuating environments: Evolution and function of antenna proteins across photosynthetic lineage. Plants 10.
- Ball, S. G., & Morell, M. K. (2003). From bacterial glycogen to starch: understanding the biogenesis of the plant starch granule. *Annual review of plant biology*, *54*(1), 207-233.
- Basso, S., Simionato, D., Gerotto, C., Segalla, A., Giacometti, G.M., Morosinotto, T., 2014. Characterization of the photosynthetic apparatus of the Eustigmatophycean Nannochloropsis gaditana: Evidence of convergent evolution in the supramolecular organization of photosystem i. Biochim. Biophys. Acta - Bioenerg. 1837, 306–314.
- Battistuzzi, M., Cocola, L., Claudi, R., Pozzer, A. C., Segalla, A., Simionato, D., Morosinotto, T., Poletto, L., & La Rocca, N. (2023). Oxygenic photosynthetic responses of cyanobacteria exposed under an M-dwarf starlight simulator: Implications for exoplanet's habitability. *Frontiers in Plant Science*, *14*.
- Becraft, E. D., Cohan, F. M., Kühl, M., Jensen, S. I., & Ward, D. M. (2011). Fine-Scale Distribution Patterns of Synechococcus Ecological Diversity in Microbial Mats of Mushroom Spring, Yellowstone National Park. *Applied and Environmental Microbiology*, *77*(21), 7689–7697.

- Behrendt, L., Brejnrod, A., Schliep, M., Sørensen, S. J., Larkum, A. W. D., & Kühl, M. (2015). Chlorophyll f-driven photosynthesis in a cavernous cyanobacterium. *The ISME Journal*, *9*(9), 2108–2111.
- Belgio, E., Kapitonova, E., Chmeliov, J., Duffy, C.D.P., Ungerer, P., Valkunas, L., Ruban, A. V., 2014. Economic photoprotection in photosystem II that retains a complete light-harvesting system with slow energy traps. Nat. Commun. 5.
- Bennett, M.S., Triemer, R.E., 2015. Chloroplast Genome Evolution in the Euglenaceae. J. Eukaryot. Microbiol. 62, 773–785.
- Bennoun, P., 1970. Réoxydation du quencher de fluorescence "Q" en présence de 3-(3,4-dichlorophényl)-1,1-diméthylurée. BBA - Bioenerg. 216, 357–363.
- Bernát, G., Zavřel, T., Kotabová, E., Kovács, L., Steinbach, G., Vörös, L., Prášil, O., Somogyi, B., & Tóth, V. R. (2021). Photomorphogenesis in the Picocyanobacterium Cyanobium gracile Includes Increased Phycobilisome Abundance Under Blue Light, Phycobilisome Decoupling Under Near Far-Red Light, and Wavelength-Specific Photoprotective Strategies. *Frontiers in Plant Science*, *12*.
- Berne, N., Fabryova, T., Istaz, B., Cardol, P., & Bailleul, B. (2018). The peculiar NPQ regulation in the stramenopile Phaeomonas sp. challenges the xanthophyll cycle dogma. *Biochimica Et Biophysica Acta (BBA) - Bioenergetics*, *1859*(7), 491–500.
- Bersanini, L., Battchikova, N., Jokel, M., Rehman, A., Vass, I., Allahverdiyeva, Y., & Aro, E. (2013). Flavodiiron Protein Flv2/Flv4-Related Photoprotective Mechanism Dissipates Excitation Pressure of PSII in Cooperation with Phycobilisomes in Cyanobacteria. *PLANT PHYSIOLOGY*, *164*(2), 805–818.
- Bhattacharya, D., Price, D. C., Chan, C. X., Gross, J., Steiner, J. M., & Löffelhardt, W. (2014). Analysis of the genome of Cyanophora paradoxa: an algal model for understanding primary endosymbiosis. *Endosymbiosis*, 135-148.
- Bhatti, A. F., Kirilovsky, D., van Amerongen, H., & Wientjes, E. (2021). State transitions and photosystems spatially resolved in individual cells of the cyanobacterium Synechococcus elongatus. *Plant physiology*, *186*(1), 569-580.
- Billi, D., Napoli, A., Mosca, C., Fagliarone, C., de Carolis, R., Balbi, A., ... & Nürnberg, D. J. (2022). Identification of far-red light acclimation in an endolithic Chroococcidiopsis strain and associated genomic features: Implications for oxygenic photosynthesis on exoplanets. *Frontiers in Microbiology*, *13*, 933404.

- Bína, D., Durchan, M., Kuznetsova, V., Vácha, F., Litvín, R., & Polívka, T. (2019). Energy transfer dynamics in a red-shifted violaxanthin-chlorophyll a light-harvesting complex. Biochimica Et Biophysica Acta (BBA) - Bioenergetics, 1860(2), 111–120.
- Bína, D., Gardian, Z., Herbstová, M., Kotabová, E., Koník, P., Litvín, R., Prášil, O., Tichý, J., & Vácha, F. (2014). Novel type of red-shifted chlorophyll a antenna complex from Chromera velia: II. Biochemistry and spectroscopy. *Biochimica Et Biophysica Acta (BBA) - Bioenergetics*, *1837*(6), 802–810.
- Biswas, S., 2018. The role of PsbX and PsbY in Photosystem II of Synechocystis sp. PCC 6803. University of Otago, Dunedin. New Zealand.
- Björn, L. O., Papageorgiou, G. C., Blankenship, R. E., & Govindjee, N. (2009). A viewpoint: Why chlorophyll a? *Photosynthesis Research*, *99*(2), 85–98.
- Blankenship, R. E. (2010). Early evolution of photosynthesis. *Plant physiology*, *154*(2), 434-438.
- Blankenship, R. E. (2021). *Molecular mechanisms of photosynthesis*. John Wiley & Sons.
- Bonthond, G., Shalygin, S., Bayer, T., & Weinberger, F. (2021). Draft genome and description of Waterburya agarophytonicola gen. nov. sp. nov. (Pleurocapsales, Cyanobacteria): a seaweed symbiont. *Antonie Van Leeuwenhoek*, *114*(12), 2189–2203.
- Brecht, M. (2009). Spectroscopic characterization of photosystem I at the single-molecule level. *Molecular Physics*, *107*(18), 1955–1974.
- Brinkmann, H., Göker, M., Koblížek, M., Wagner-Döbler, I., & Petersen, J. (2018). Horizontal operon transfer, plasmids, and the evolution of photosynthesis in Rhodobacteraceae. *The ISME journal*, *12*(8), 1994-2010.
- Brinkmann, N., Hodač, L., Mohr, K. I., Hodačová, A., Jahn, R., Ramm, J., Hallmann, C., Arp, G., & Friedl, T. (2015). Cyanobacteria and Diatoms in Biofilms of Two Karstic Streams in Germany and Changes of Their Communities Along Calcite Saturation Gradients. *Geomicrobiology Journal*, *32*(3–4), 255–274.
- Brown, J.S., French, C.S., 1961. The Long Wave Length Forms of Chlorophyll a. Biophys. J. 1, 539–550.
- Brown, M. W., Heiss, A. A., Kamikawa, R., Inagaki, Y., Yabuki, A., Tice, A. K., ... & Roger, A. J. (2018). Phylogenomics places orphan protistan lineages in a novel eukaryotic super-group. *Genome biology and evolution*, *10*(2), 427-433.
- Büdel, B. (1999). Ecology and diversity of rock-inhabiting cyanobacteria in tropical regions. *European Journal of Phycology*, *34*(4), 361-370.

- Burki, F., Kaplan, M., Tikhonenkov, D. V., Zlatogursky, V., Minh, B. Q., Radaykina, L. V., ... & Keeling, P. J. (2016). Untangling the early diversification of eukaryotes: a phylogenomic study of the evolutionary origins of Centrohelida, Haptophyta and Cryptista. *Proceedings of the Royal Society B: Biological Sciences*, *283*(1823), 20152802.
- Burki, F., Okamoto, N., Pombert, J. F., & Keeling, P. J. (2012). The evolutionary history of haptophytes and cryptophytes: phylogenomic evidence for separate origins. *Proceedings of the Royal Society B: Biological Sciences*, *279*(1736), 2246-2254.
- Burki, F., Roger, A. J., Brown, M. W., & Simpson, A. G. (2020). The new tree of eukaryotes. *Trends in ecology & evolution*, *35*(1), 43-55.
- Burton-Smith, R.N., Watanabe, A., Tokutsu, R., Song, C., Murata, K., Minagawa, X.J., 2019. Structural determination of the large photosystem II-light-harvesting complex II supercomplex of Chlamydomonas reinhardtii using nonionic amphipol. J. Biol. Chem. 294, 15003–15013.
- Campbell, D. (1996). Complementary chromatic adaptation alters photosynthetic strategies in the cyanobacterium Calothrix. *Microbiology*, *142*(5), 1255–1263.
- Canfield, D. E. (2006). Models of oxic respiration, denitrification and sulfate reduction in zones of coastal upwelling. *Geochimica et Cosmochimica Acta*, *70*(23), 5753-5765.
- Cantonati, M., Komárek, J., & Montejano, G. (2015). Cyanobacteria in ambient springs. *Biodiversity and Conservation*, *24*, 865-888.
- Cao, P., Su, X., Pan, X., Liu, Z., Chang, W., Li, M., 2018. Structure, assembly and energy transfer of plant photosystem II supercomplex. Biochim. Biophys. Acta - Bioenerg. 1859, 633–644.
- Carbonera, D., Agostini, G., Morosinotto, T., & Bassi, R. (2005). Quenching of Chlorophyll Triplet States by Carotenoids in Reconstituted Lhca4 Subunit of Peripheral Light-Harvesting Complex of Photosystem I. Biochemistry, 44(23), 8337–8346.
- Cardona, Tanai. "A fresh look at the evolution and diversification of photochemical reaction centers." *Photosynthesis research* 126 (2015): 111-134.
- Carpenter, E. J. (2002). Marine cyanobacterial symbioses. In *Biology and Environment: Proceedings of the Royal Irish Academy* (Vol. 102, No. 1, pp. 15-18). Royal Irish Academy.
- Caspy, I., Borovikova-Sheinker, A., Klaiman, D., Shkolnisky, Y., Nelson, N., 2020. The structure of a triple complex of plant photosystem I with ferredoxin and plastocyanin. Nat. Plants 6, 1300–1305.
- Caspy, I., Nelson, N., 2018. Structure of the plant photosystem I. Biochem. Soc. Trans. BST20170299.

- Cavalier-Smith, T. (2002). The phagotrophic origin of eukaryotes and phylogenetic classification of Protozoa. *International journal of systematic and evolutionary microbiology*, *52*(2), 297-354.
- Cavalier-Smith, T. (2006). Cell evolution and Earth history: stasis and revolution. *Philosophical Transactions of the Royal Society B: Biological Sciences*, *361*(1470), 969-1006.
- Cazzaniga, S., Kim, M., Bellamoli, F., Jeong, J., Lee, S., Perozeni, F., Pompa, A., Jin, E.S., Ballottari, M., 2020. Photosystem II antenna complexes CP26 and CP29 are essential for nonphotochemical quenching in Chlamydomonas reinhardtii. Plant Cell Environ. 43, 496–509.
- Cazzaniga, S., Kim, M., Bellamoli, F., Jeong, J., Lee, S., Perozeni, F., Pompa, A., Jin, E.S., Ballottari, M., (2020). Photosystem II antenna complexes CP26 and CP29 are essential for nonphotochemical quenching in Chlamydomonas reinhardtii. Plant Cell Environ. 43, 496–509.
- Chen, M., Li, Y., Birch, D., & Willows, R. D. (2012). A cyanobacterium that contains chlorophyll f – a red-absorbing photopigment. *FEBS Letters*, *586*(19), 3249–3254.
- Chen, M., Liu, X., He, Y., Li, N., He, J., Zhang, Y., (2022). Diversity Among Cyanobacterial Photosystem I Oligomers. Front. Microbiol. 12, 1–8.
- Chen, M., Schliep, M., Willows, R. D., Cai, Z., Neilan, B. A., & Scheer, H. (2010). A Red-Shifted Chlorophyll. *Science*, *329*(5997), 1318–1319.
- Chen, Y.E., Ma, J., Wu, N., Su, Y.Q., Zhang, Z.W., Yuan, M., Zhang, H.Y., Zeng, X.Y., Yuan, S., 2018. The roles of Arabidopsis proteins of Lhcb4, Lhcb5 and Lhcb6 in oxidative stress under natural light conditions. Plant Physiol. Biochem. 130, 267–276.
- Chow, W. S., Melis, A., & Anderson, J. (1990). Adjustments of photosystem stoichiometry in chloroplasts improve the quantum efficiency of photosynthesis. *Proceedings of the National Academy of Sciences*, *87*(19), 7502-7506.
- Chu, H.A., Chiu, Y.F., 2016. The roles of cytochrome b559 in assembly and photoprotection of photosystem II revealed by site-directed mutagenesis studies. Front. Plant Sci. 6, 1–7.
- Chukhutsina, V.U., Liu, X., Xu, P., Croce, R., (2020). Light-harvesting complex II is an antenna of photosystem I in dark-adapted plants. Nat. Plants 6, 860–868.
- Cordoba, J., Perez, E., Van Vlierberghe, M., Bertrand, A.R., Lupo, V., Cardol, P., Baurain, D., 2021. De novo transcriptome meta-assembly of the mixotrophic freshwater microalga euglena gracilis. Genes (Basel). 12.

- Cramer, W. A., & Kallas, T. (Eds.). (2016). *Cytochrome complexes: evolution, structures, energy transduction, and signaling* (Vol. 41). Dordrecht: Springer.
- Croce, R., & van Amerongen, H. (2011). Light-harvesting and structural organization of photosystem II: from individual complexes to thylakoid membrane. *Journal of Photochemistry and Photobiology B: Biology*, *104*(1-2), 142-153.
- Croce, R., & van Amerongen, H. (2020). Light harvesting in oxygenic photosynthesis: Structural biology meets spectroscopy. *Science*, *369*(6506), eaay2058.
- Croce, R., Zucchelli, G., Garlaschi, F.M., Jennings, R.C., 1998. A thermal broadening study of the antenna chlorophylls in PSI- 200, LHCI, and PSI core. Biochemistry 37, 17355–17360.
- Cunningham, F., Schiff, J., 1986. Chlorophyll-Protein Complexes from Euglena gracilis and Mutants Deficient in Chlorophyll b. Plant Physiol. 80, 223–230.
- Cushman, C., Christopher, D.A., Little, M.C., Hailick, R.B., Price, C.A., 1988. Organization of the psbE, psbF, off38, and off42 gene loci on the Euglena gracilis chloroplast genome. Curr. Genet. 13, 173–180.
- Daines, S. J., Mills, B. J., & Lenton, T. M. (2017). Atmospheric oxygen regulation at low Proterozoic levels by incomplete oxidative weathering of sedimentary organic carbon. *Nature Communications*, *8*(1), 14379.
- Dall'Osto, L., Bassi, R., & Ruban, A. (2014). Photoprotective Mechanisms: Carotenoids. In *Springer eBooks* (pp. 393–435).
- Dall'Osto, L., Caffarri, S., Bassi, R., 2005. A mechanism of nonphotochemical energy dissipation, independent from PsbS, revealed by a conformational change in the antenna protein CP26. Plant Cell 17, 1217–1232.
- De la Cerda, B., Castielli, O., Durán, R. V., Navarro, J. A., Hervás, M., & De la Rosa, M. A. (2007). A proteomic approach to iron and copper homeostasis in cyanobacteria. *Briefings in Functional Genomics and Proteomics*, *6*(4), 322-329.
- de la Rosa-Trevín, J.M., Quintana, A., del Cano, L., Zaldívar, A., Foche, I., Gutiérrez, J., Gómez-Blanco, J., Burguet-Castell, J., Cuenca-Alba, J., Abrishami, V., Vargas, J., Otón, J., Sharov, G., Vilas, J.L., Navas, J., Conesa, P., Kazemi, M., Marabini, R., Sorzano, C.O.S., Carazo, J.M., 2016. Scipion: A software framework toward integration, reproducibility and validation in 3D electron microscopy. J. Struct. Biol. 195, 93–99.
- De Marsac, N., & Houmard, J. (1988). Complementary chromatic adaptation: Physiological conditions and action spectra. In *Methods in enzymology on CD-ROM/Methods in enzymology* (pp. 318–328).

- Demoulin, C.F., Lara, Y.J., Cornet, L., François, C., Baurain, D., Wilmotte, A. and Javaux, E.J., (2019). Cyanobacteria evolution: Insight from the fossil record. *Free Radical Biology and Medicine*, *140*, pp.206-223.
- Doege, M., Ohmann, E., & Tschiersch, H. (2000). Chlorophyll fluorescence quenching in the alga Euglena gracilis. *Photosynthesis Research*, *63*, 159-170.
- Doege, M., Ohmann, E., Tschiersch, H., 2000. Chlorophyll fluorescence quenching in the alga Euglena gracilis. Photsynth. Res. 63, 159–170.
- Domokos, I., Malec, P., AL, E., 2004. Phosphatidylglycerol Is Essential for Oligomerization of Photosystem I Reaction Center 1. Plant Physiol. 134, 1471–1478.
- Dong, C., Tang, A., Zhao, J., Mullineaux, C. W., Shen, G., & Bryant, D. A. (2009b). ApcD is necessary for efficient energy transfer from phycobilisomes to photosystem I and helps to prevent photoinhibition in the cyanobacterium Synechococcus sp. PCC 7002. *Biochimica Et Biophysica Acta (BBA) - Bioenergetics*, *1787*(9), 1122–1128.
- Drop, B., Webber-Birungi, M., Yadav, S. K., Filipowicz-Szymanska, A., Fusetti, F., Boekema, E. J., & Croce, R. (2014). Light-harvesting complex II (LHCII) and its supramolecular organization in Chlamydomonas reinhardtii. *Biochimica et Biophysica Acta (BBA)-Bioenergetics*, *1837*(1), 63-72.
- Elias, E., Oliver, T. J., & Croce, R. (2024). Oxygenic photosynthesis in far-red light: strategies and mechanisms. *Annual review of physical chemistry*, *75*.
- Emerson, R., 1957. Dependence of Yield of Photosynthesis in Long-Wave Red on Wavelength and Intensity of Supplementary Light. Science (80-.). 125, 746–752.
- Eren, A. M., Esen, Ö. C., Quince, C., Vineis, J. H., Morrison, H. G., Sogin, M. L., & Delmont, T. O. (2015). Anvi'o: an advanced analysis and visualization platform for 'omics data. *PeerJ*, *3*, e1319.
- Eren, A. M., Kiefl, E., Shaiber, A., Veseli, I., Miller, S. E., Schechter, M. S., ... & Willis, A. D. (2021). Community-led, integrated, reproducible multi-omics with anvi'o. *Nature microbiology*, *6*(1), 3-6.
- Everroad, C., Six, C., Partensky, F., Thomas, J. C., Holtzendorff, J., & Wood, A. M. (2006). Biochemical bases of type IV chromatic adaptation in marine Synechococcus spp. *Journal of bacteriology*, *188*(9), 3345-3356.hir
- Falkowski, P. G., & Raven, J. A. (2013). *Aquatic photosynthesis*. Princeton University Press.

- Fan, D.Y., Hope, A.B., Smith, P.J., Jia, H., Pace, R.J., Anderson, J.M., Chow, W.S., 2007. The stoichiometry of the two photosystems in higher plants revisited. Biochim. Biophys. Acta - Bioenerg. 1767, 1064–1072.
- Federspiel, N. A., & Scott, L. (1992). Characterization of a light-regulated gene encoding a new phycoerythrin-associated linker protein from the cyanobacterium Fremyella diplosiphon. *Journal of bacteriology*, *174*(18), 5994-5998.
- Ferroni, L., Baldisserotto, C., Giovanardi, M., Pantaleoni, L., Morosinotto, T., Pancaldi, S., 2011. Revised assignment of room-temperature chlorophyll fluorescence emission bands in single living cells of Chlamydomonas reinhardtii. J. Bioenerg. Biomembr. 43, 163–173.
- Finazzi, G., & Minagawa, J. (2014). High light acclimation in green microalgae. *Non-photochemical quenching and energy dissipation in plants, algae and cyanobacteria*, 445-469.
- Finazzi, G., Furia, A., Barbagallo, R.P., Forti, G., 1999. State transitions, cyclic and linear electron transport and photophosphorylation in Chlamydomonas reinhardtii. Biochim. Biophys. Acta - Bioenerg. 1413, 117–129.
- Flombaum, P., Gallegos, J. L., Gordillo, R. A., Rincón, J., Zabala, L. L., Jiao, N., Karl, D. M., Li, W. K. W., Lomas, M. W., Veneziano, D., Vera, C. S., Vrugt, J. A., & Martiny, A. C. (2013). Present and future global distributions of the marine Cyanobacteria Prochlorococcus and Synechococcus. *Proceedings of the National Academy of Sciences*, *110*(24), 9824–9829.
- Foissner, W., Blatterer, H., & Foissner, I. (1988). The Hemimastigophora (Hemimastix amphikineta nov. gen., nov. spec.), a new protistan phylum from Gondwanian soils. *European journal of protistology*, *23*(4), 361-383.
- Förster, T. (1948). Zwischenmolekulare energiewanderung und fluoreszenz. *Annalen der physik*, *437*(1-2), 55-75.
- Fromme, P., Jordan, P., & Krauß, N. (2001). Structure of photosystem I. *Biochimica et Biophysica Acta (BBA)-Bioenergetics*, *1507*(1-3), 5-31.
- Fujita, Y., & Ohki, K. (2004). On the 710 nm Fluorescence Emitted by the Diatom Phaeodactylum tricornutum at Room Temperature. Plant and Cell Physiology, 45(4), 392–397.
- Fujita, Y., Murakami, A., Aizawa, K., & Ohki, K. (1994). Short-term and Long-term Adaptation of the Photosynthetic Apparatus: Homeostatic Properties of Thylakoids. In *Springer eBooks* (pp. 677–692).

- Gain, G., Vega de Luna, F., Cordoba, J., Perez, E., Degand, H., Morsomme, P., Thiry, M., Baurain, D., Pierangelini, M., Cardol, P., 2021. Trophic state alters the mechanism whereby energetic coupling between photosynthesis and respiration occurs in Euglena gracilis. New Phytol. 232, 1603–1617.
- Gan, F., & Bryant, D. A. (2015). Adaptive and acclimative responses of cyanobacteria to far-red light. *Environmental Microbiology*, *17*(10), 3450–3465.
- Gan, F., Shen, G., & Bryant, D. A. (2014). Occurrence of Far-Red Light Photoacclimation (FaRLiP) in Diverse Cyanobacteria. *Life*, *5*(1), 4–24.
- Gan, F., Zhang, S., Rockwell, N. C., Martin, S. S., Lagarias, J. C., & Bryant, D. A. (2014). Extensive remodeling of a cyanobacterial photosynthetic apparatus in far-red light. *Science*, *345*(6202), 1312–1317.
- Geitler, L. (1932). Cyanophyceae. *Kryptogamen-Flora von Deutschland, Osterreich und der shweiz*, *14*.
- Gentil, J., Hempel, F., Moog, D., Zauner, S., & Maier, U. G. (2017). Origin of complex algae by secondary endosymbiosis: a journey through time. *Protoplasma*, *254*, 1835-1843.
- Genty, B., Briantais, J., & Baker, N. R. (1989). The relationship between the quantum yield of photosynthetic electron transport and quenching of chlorophyll fluorescence. *Biochimica Et Biophysica Acta (BBA) - General Subjects*, *990*(1), 87–92.
- Gibasiewicz, K., Szrajner, A., Ihalainen, J.A., Germano, M., Dekker, J.P., Van Grondelle, R., 2005. Characterization of low-energy chlorophylls in the PSI-LHCI supercomplex from Chlamydomonas reinhardtii. A site-selective fluorescence study. J. Phys. Chem. B 109, 21180–21186.
- Giordano, M., Beardall, J., & Raven, J. A. (2005). CO 2 concentrating mechanisms in algae: mechanisms, environmental modulation, and evolution. *Annu. Rev. Plant Biol.*, *56*(1), 99-131.
- Glazer, A. N. (1985). Light harvesting by phycobilisomes. *Annual review of biophysics and biophysical chemistry*, *14*(1), 47-77.
- Gobets, B., & Van Grondelle, R. (2001). Energy transfer and trapping in photosystem I. *Biochimica Et Biophysica Acta (BBA) - Bioenergetics*, *1507*(1–3), 80–99.
- Gonzalez-Esquer, C. R., Smarda, J., Rippka, R., Axen, S. D., Guglielmi, G., Gugger, M., & Kerfeld, C. A. (2016). Cyanobacterial ultrastructure in light of genomic sequence data. *Photosynthesis Research*, *129*(2), 147–157.

- Gorski, C., Riddle, R., Toporik, H., Da, Z., Dobson, Z., Williams, D., Mazor, Y., 2022. The structure of the Physcomitrium patens photosystem I reveals a unique Lhca2 paralogue replacing Lhca4. Nat. Plants 8, 307–316. 01099-w
- Goss, R., & Jakob, T. (2010). Regulation and function of xanthophyll cycle-dependent photoprotection in algae. Photosynthesis research, 106, 103-122.
- Goss, R., & Lepetit, B. (2015). Biodiversity of NPQ. *Journal of plant physiology*, *172*, 13-32.
- Gould, S.B., Waller, R.F., McFadden, G.I., 2008. Plastid evolution. Annu. Rev. Plant Biol. 59, 491–517.
- Graça, A.T., Hall, M., Persson, K., Schröder, W.P., 2021. High-resolution model of Arabidopsis Photosystem II reveals the structural consequences of digitonin-extraction. Sci. Rep. 11, 1–12.
- Graça, A.T., Hall, M., Persson, K., Schröder, W.P., 2021. High-resolution model of Arabidopsis Photosystem II reveals the structural consequences of digitonin-extraction. Sci. Rep. 11, 1–12.
- Green, B., & Parson, W. W. (Eds.). (2003). *Light-harvesting antennas in photosynthesis* (Vol. 13). Springer Science & Business Media.
- Grotjohann, I., & Fromme, P. (2005). Structure of cyanobacterial Photosystem I. *Photosynthesis Research*, *85*(1), 51–72.
- Gundermann, K., & Büchel, C. (2014). Structure and functional heterogeneity of fucoxanthin-chlorophyll proteins in diatoms. In *The structural basis of biological energy generation* (pp. 21-37). Dordrecht: Springer Netherlands.
- Hackett, J. D., Yoon, H. S., Butterfield, N. J., Sanderson, M. J., & Bhattacharya, D. (2007). Plastid endosymbiosis: sources and timing of the major events. *Evolution of primary producers in the sea*, 109-132.
- Hallick, R.B., Hong, L., Drager, R.G., Favreau, M.R., Monfort, A., Orsat, B., Spielmann, A., Stutz, E., 1993. Complete sequence of Euglena gracilis chloroplast DNA. Nucleic Acids Res. 21, 3537–3544.
- Hallick, R.B., Hong, L., Drager, R.G., Favreau, M.R., Monfort, A., Orsat, B., Spielmann, A., Stutz, E., 1993. Complete sequence of Euglena gracilis chloroplast DNA. Nucleic Acids Res. 21, 3537–3544.
- Haniewicz, P., Abram, M., Nosek, L., Kirkpatrick, J., El-Mohsnawy, E., Olmos, J. D. J., Kouřil, R., & Kargul, J. M. (2017). Molecular Mechanisms of Photoadaptation of

Photosystem I Supercomplex from an Evolutionary Cyanobacterial/Algal Intermediate. *PLANT PHYSIOLOGY*, *176*(2), 1433–1451.

- Harris, E.H., Stern, D.B., Witman, G.B., 2009. Chlamydomonas in the Laboratory, in: Harris, E.H., Stern, D.B., Witman, G.B. (Eds.), The Chlamydomonas Sourcebook. Academic Press, pp. 241–302.
- Havaux, M., Guedeney, G., Hagemann, M., Yeremenko, N., Matthijs, H. C., & Jeanjean, R. (2005b). The chlorophyll-binding protein IsiA is inducible by high light and protects the cyanobacterium Synechocystis PCC6803 from photooxidative stress. *FEBS Letters*, *579*(11), 2289–2293.
- Herbstová, M., Bína, D., Kaňa, R., Vácha, F., & Litvín, R. (2017). Red-light phenotype in a marine diatom involves a specialized oligomeric red-shifted antenna and altered cell morphology. *Scientific Reports*, *7*(1), 11976.
- Herbstová, M., Bína, D., Koník, P., Gardian, Z., Vácha, F., & Litvín, R. (2015). Molecular basis of chromatic adaptation in pennate diatom Phaeodactylum tricornutum. *Biochimica Et Biophysica Acta (BBA) - Bioenergetics*, *1847*(6–7), 534–543.
- Hirose, Y., Chihong, S., Watanabe, M., Yonekawa, C., Murata, K., Ikeuchi, M., & Eki, T. (2019). Diverse Chromatic Acclimation Processes Regulating Phycoerythrocyanin and Rod-Shaped Phycobilisome in Cyanobacteria. *Molecular Plant*, *12*(5), 715–725.
- Hirose, Y., Narikawa, R., Katayama, M., & Ikeuchi, M. (2010). Cyanobacteriochrome CcaS regulates phycoerythrin accumulation in Nostoc punctiforme, a group II chromatic adapter. *Proceedings of the National Academy of Sciences*, *107*(19), 8854-8859.
- Ho, M., & Bryant, D. A. (2019). Global Transcriptional Profiling of the Cyanobacterium Chlorogloeopsis fritschii PCC 9212 in Far-Red Light: Insights Into the Regulation of Chlorophyll d Synthesis. *Frontiers in Microbiology*, *10*.
- Ho, M., Gan, F., Shen, G., & Bryant, D. A. (2016). Far-red light photoacclimation (FaRLiP) in Synechococcus sp. PCC 7335. II.Characterization of phycobiliproteins produced during acclimation to far-red light. *Photosynthesis Research*, *131*(2), 187–202.
- Ho, M., Soulier, N. T., Canniffe, D. P., Shen, G., & Bryant, D. A. (2017). Light regulation of pigment and photosystem biosynthesis in cyanobacteria. *Current Opinion in Plant Biology*, *37*, 24–33.
- Hohmann-Marriott, M. F., & Blankenship, R. E. (2011). Evolution of photosynthesis. Annual review of plant biology, 62(1), 515-548.
- Horton, P., Ruban, A. V., & Walters, R. G. (1996). Regulation of light harvesting in green plants. *Annual review of plant biology*, *47*(1), 655-684.

- Huang, Z., Shen, L., Wang, W., Mao, Z., Yi, X., Kuang, T., Shen, J.-R., Zhang, X., Han, G., 2021. green alga Chlamydomonas reinhardtii in State 2. Nat. Commun. 12, 1–14.
- Ihalainen, J. A., Gobets, B., Sznee, K., Brazzoli, M., Croce, R., Bassi, R., Van Grondelle, R., Korppi-Tommola, J. E. I., & Dekker, J. P. (2000). Evidence for Two Spectroscopically Different Dimers of Light-Harvesting Complex I from Green Plants. Biochemistry, 39(29), 8625–8631.
- Islam, S., Sabharwal, T., Wu, S., Bullock, T.J., Mehdy, M.C., 2020. Early dynamics of photosynthetic Lhcf2 and Lhcf15 transcription and mRNA stabilities in response to herbivory-related decadienal in Phaeodactylum tricornutum. Sci. Rep. 10, 1–12.
- Itoh, S., Ohno, T., Noji, T., Yamakawa, H., Komatsu, H., Wada, K., Kobayashi, M., & Miyashita, H. (2015). Harvesting Far-Red Light by Chlorophyllfin Photosystems I and II of Unicellular Cyanobacterium strain KC1. *Plant and Cell Physiology*, *56*(10), 2024–2034.
- Iwai, M., Grob, P., Iavarone, A.T., Nogales, E., Niyogi, K.K.K., 2018. A unique supramolecular organization of photosystem I in the moss Physcomitrella patens. Nat. Plants 4, 904–909.
- Jagendorf, A. T. (2002). Photophosphorylation and the chemiosmotic perspective. *Photosynthesis Research*, *73*, 233-241.
- Jahns, P., Latowski, D., & Strzalka, K. (2008). Mechanism and regulation of the violaxanthin cycle: The role of antenna proteins and membrane lipids. *Biochimica Et Biophysica Acta (BBA) - Bioenergetics*, *1787*(1), 3–14.
- Janouškovec, J., Horák, A., Oborník, M., Lukeš, J., & Keeling, P. J. (2010). A common red algal origin of the apicomplexan, dinoflagellate, and heterokont plastids. *Proceedings of the National Academy of Sciences*, *107*(24), 10949–10954.
- Jansson, S. (1994). The light-harvesting chlorophyll ab-binding proteins. Biochimica Et Biophysica Acta (BBA) - Bioenergetics, 1184(1), 1–19.
- Jenkins, K.P., Hong, L., Hallick, R.B., 1995. Alternative splicing of the Euglena gracilis chloroplast roaA transcript. RNA 1, 624–633.
- Johnson, M. P., Davison, P. A., Ruban, A. V., & Horton, P. (2008). The xanthophyll cycle pool size controls the kinetics of non-photochemical quenching in Arabidopsis thaliana. *FEBS letters*, *582*(2), 262-266.
- Joshua, S., & Mullineaux, C. W. (2004). Phycobilisome diffusion is required for light-state transitions in cyanobacteria. *Plant physiology*, *135*(4), 2112-2119.

- Karapetyan, N. V., Bolychevtseva, Y. V., Yurina, N.P., Terekhova, I. V., Shubin, V. V., Brecht, M., 2014. Long-wavelength chlorophylls in photosystem i of cyanobacteria: Origin, localization, and functions. Biochem. 79, 213–220.
- Kasting, J. F. (1993). Earth's early atmosphere. *Science*, *259*(5097), 920-926.
- Kato, K., Shinoda, T., Nagao, R., Akimoto, S., Suzuki, T., Dohmae, N., Chen, M., Allakhverdiev, S. I., Shen, J., Akita, F., Miyazaki, N., & Tomo, T. (2020). Structural basis for the adaptation and function of chlorophyll f in photosystem I. *Nature Communications*, *11*(1).
- Kehoe, D. M. (2010). Chromatic adaptation and the evolution of light color sensing in cyanobacteria. *Proceedings of the National Academy of Sciences*, *107*(20), 9029–9030.
- Kehoe, D. M., & Grossman, A. R. (1994). Complementary chromatic adaptation: photoperception to gene regulation. *Seminars in Cell Biology*, *5*(5), 303–313.
- Kehoe, D. M., & Gutu, A. (2006). Responding to Color: The Regulation of Complementary Chromatic Adaptation. *Annual Review of Plant Biology*, *57*(1), 127–150.
- Kerfeld, C. A., Melnicki, M. R., Sutter, M., & Dominguez-Martin, M. A. (2017). Structure, function and evolution of the cyanobacterial orange carotenoid protein and its homologs. *New Phytologist*, *215*(3), 937–951.
- Kiang, N. Y., Segura, A., Tinetti, G., Blankenship, R. E., Cohen, M., Siefert, J., ... & Meadows, V. S. (2007). Spectral signatures of photosynthesis: Coevolution with other stars and the atmosphere on extrasolar worlds. *Astrobiology*, *7*(3), 486-7.
- Kirilovsky, D. (2007). Photoprotection in cyanobacteria: the orange carotenoid protein (OCP)-related non-photochemical-quenching mechanism. *Photosynthesis Research*, *93*, 7-16.
- Kirilovsky, D., & Kerfeld, C. A. (2013). The Orange Carotenoid Protein: a blue-green light photoactive protein. *Photochemical & Photobiological Sciences*, *12*(7), 1135-1143.
- Kirilovsky, D., & Kerfeld, C. A. (2016). Cyanobacterial photoprotection by the orange carotenoid protein. *Nature plants*, *2*(12), 1-7.
- Klein, S., Schiff, J.A., Holowinsky, A.W., 1972. Events surrounding the early development of Euglena chloroplasts. II. Normal development of fine structure and the consequences of preillumination. Dev. Biol. 28, 253–273.
- Knoll, A. H. (2003). The geological consequences of evolution. *Geobiology*, *1*(1), 3-14.
- Koehne, B., Elli, G., Jennings, R. C., Wilhelm, C., & Trissl, H. (1999). Spectroscopic and molecular characterization of a long wavelength absorbing antenna of Ostreobium sp. Biochimica Et Biophysica Acta (BBA) - Bioenergetics, 1412(2), 94–107.

- Komárek, J. (2016). A polyphasic approach for the taxonomy of cyanobacteria: principles and applications. *European Journal of Phycology*, *51*(3), 346-353.
- Kondo, K., Geng, X. X., Katayama, M., & Ikeuchi, M. (2005). Distinct roles of CpcG1 and CpcG2 in phycobilisome assembly in the cyanobacterium Synechocystis sp. PCC 6803. *Photosynthesis research*, *84*, 269-273.
- Kostygov, A. Y., Karnkowska, A., Votýpka, J., Tashyreva, D., Maciszewski, K., Yurchenko, V., & Lukeš, J. (2021). Euglenozoa: taxonomy, diversity and ecology, symbioses and viruses. *Open Biology*, *11*(3), 200407.
- Kosugi, M., Ozawa, S. I., Takahashi, Y., Kamei, Y., Itoh, S., Kudoh, S., Kashino, Y., & Koike, H. (2020). Red-shifted chlorophyll a bands allow uphill energy transfer to photosystem II reaction centers in an aerial green alga, Prasiola crispa, harvested in Antarctica. Biochimica Et Biophysica Acta (BBA) - Bioenergetics, 1861(2), 148139.
- Kotabová, E., Jarešová, J., Kaňa, R., Sobotka, R., Bína, D., & Prášil, O. (2014). Novel type of red-shifted chlorophyll a antenna complex from ***Chromera velia***. I. Physiological relevance and functional connection to photosystems. Biochimica Et Biophysica Acta (BBA) - Bioenergetics, 1837(6), 734–743.
- Kotabová, E., Kaňa, R., Jarešová, J., & Prášil, O. (2011). Non-photochemical fluorescence quenching inChromera veliais enabled by fast violaxanthin de-epoxidation. *FEBS Letters*, *585*(12), 1941–1945.
- Kouřil, R., Nosek, L., Semchonok, D., Boekema, E.J., Ilík, P., 2018. Organization of Plant Photosystem II and Photosystem I Supercomplexes, in: Harris, J.R., Boekema, E.J. (Eds.), Membrane Protein Complexes: Structure and Function. Subcellular Biochemistry. Springer Nature, pp. 259–286.
- Kowalczyk, N., Rappaport, F., Boyen, C., Wollman, F. A., Collén, J., & Joliot, P. (2013). Photosynthesis in Chondrus crispus: the contribution of energy spill-over in the regulation of excitonic flux. *Biochimica et Biophysica Acta (BBA)-Bioenergetics*, *1827*(7), 834-842.
- Koziol, A.G., Borza, T., Ishida, K.-I., Keeling, P., Lee, R.W., Durnford, D.G., 2007. Tracing the Evolution of the Light-Harvesting Antennae in Chlorophyll a/b-Containing Organisms. Plant Physiol. 143, 1802–1816.
- Koziol, A.G., Durnford, D.G., 2008. Euglena light-harvesting complexes are encoded by multifarious polyprotein mRNAs that evolve in concert. Mol. Biol. Evol. 25, 92–100.
- Krumova, S., Laptenok, S., Borst, J., Ughy, B., Gombos, Z., Ajlani, G., & Van Amerongen, H. (2010). Monitoring Photosynthesis in Individual Cells of Synechocystis sp. PCC 6803 on a Picosecond Timescale. *Biophysical Journal*, *99*(6), 2006–2015.

- Kusama, Y., Inoue, S., Jimbo, H., Takaichi, S., Sonoike, K., Hihara, Y., & Nishiyama, Y. (2015). Zeaxanthin and Echinenone Protect the Repair of Photosystem II from Inhibition by Singlet Oxygen in Synechocystis sp. PCC 6803. *Plant and Cell Physiology*, *56*(5), 906–916.
- Kusel-Fetzmann, E., Weidinger, M., 2008. Ultrastructure of five Euglena species positioned in the subdivision Serpentes. Protoplasma 233, 209–222.
- Lara, Y. J., McCann, A., Malherbe, C., François, C., Demoulin, C. F., Sforna, M. C., ... & Javaux, E. J. (2022). Characterization of the halochromic gloeocapsin pigment, a cyanobacterial biosignature for paleobiology and astrobiology. *Astrobiology*, *22*(6), 735-754.
- Larkum, A. W. D., Szabó, M., Fitzpatrick, D., & Raven, J. A. (2018). Cyclic electron flow in cyanobacteria and eukaryotic algae. In *Photosynthesis and bioenergetics* (pp. 305-343).
- Lemeille, S., Willig, A., Depège-Fargeix, N., Delessert, C., Bassi, R., & Rochaix, J. D. (2009). Analysis of the chloroplast protein kinase Stt7 during state transitions. *PLoS biology*, *7*(3), e1000045.
- Li, L., Alvey, R. M., Bezy, R. P., & Kehoe, D. M. (2008). Inverse transcriptional activities during complementary chromatic adaptation are controlled by the response regulator RcaC binding to red and green light-responsive promoters. *Molecular Microbiology*, *68*(2), 286–297.
- Li, Y., & Chen, M. (2015). Novel chlorophylls and new directions in photosynthesis research. *Functional Plant Biology*, *42*(6), 493-501.
- Li, Y., Lin, Y., Loughlin, P. C., & Chen, M. (2014). Optimization and effects of different culture conditions on growth of Halomicronema hongdechloris – a filamentous cyanobacterium containing chlorophyll f. *Frontiers in Plant Science*, *5*.
- Li, Y., Scales, N., Blankenship, R. E., Willows, R. D., & Chen, M. (2012). Extinction coefficient for red-shifted chlorophylls: Chlorophyll d and chlorophyll f. *Biochimica Et Biophysica Acta (BBA) - Bioenergetics*, *1817*(8), 1292–1298.
- Litvín, R., Bína, D., Herbstová, M., Pazderník, M., Kotabová, E., Gardian, Z., Trtílek, M., Prášil, O., & Vácha, F. (2019). Red-shifted light-harvesting system of freshwater eukaryotic alga Trachydiscus minutus (Eustigmatophyta, Stramenopila). *Photosynthesis Research*, *142*(2), 137–151.
- Liu, H., Zhang, H., Niedzwiedzki, D. M., Prado, M., He, G., Gross, M. L., & Blankenship, R. E. (2013). Phycobilisomes Supply Excitations to Both Photosystems in a Megacomplex in Cyanobacteria. *Science*, *342*(6162), 1104–1107.

- Liu, K., Sun, J., Song, Y. G., Liu, B., Xu, Y. K., Zhang, S. X., ... & Liu, Y. (2004). Superoxide, hydrogen peroxide and hydroxyl radical in D1/D2/cytochrome b-559 photosystem II reaction center complex. *Photosynthesis Research*, *81*, 41-47.
- Longoni, P., Samol, I., Goldschmidt-Clermont, M., 2019. The Kinase STATE TRANSITION 8 Phosphorylates Light Harvesting Complex II and Contributes to Light Acclimation in Arabidopsis thaliana. Front. Plant Sci. 10, 1–13.
- Loughlin, P., Lin, Y., & Chen, M. (2013). Chlorophyll d and Acaryochloris marina: current status. *Photosynthesis Research*, *116*, 277-293.
- Lovelock, J. E. (1965). A physical basis for life detection experiments. *Nature*, *207*(4997), 568-570.
- Lyons, T. W., Diamond, C. W., Planavsky, N. J., Reinhard, C. T., & Li, C. (2021). Oxygenation, life, and the planetary system during Earth's middle history: An overview. *Astrobiology*, *21*(8), 906-923.
- Lyons, T. W., Reinhard, C. T., & Planavsky, N. J. (2014). The rise of oxygen in Earth's early ocean and atmosphere. *Nature*, *506*(7488), 307–315.
- Lyons, T. W., Tino, C. J., Fournier, G. P., Anderson, R. E., Leavitt, W. D., Konhauser, K. O., & Stüeken, E. E. (2024). Co-evolution of early Earth environments and microbial life. *Nature Reviews Microbiology*, 1-15.
- MacGregor-Chatwin, C., Nürnberg, D. J., Jackson, P. J., Vasilev, C., Hitchcock, A., Ho, M., Shen, G., Gisriel, C. J., Wood, W. H., Mahbub, M., Selinger, V. M., Johnson, M. P., Dickman, M. J., Rutherford, A. W., Bryant, D. A., & Hunter, C. N. (2022). Changes in supramolecular organization of cyanobacterial thylakoid membrane complexes in response to far-red light photoacclimation. *Science Advances*, *8*(6).
- Makhalanyane, T. P., Valverde, A., Velázquez, D., Gunnigle, E., Van Goethem, M. W., Quesada, A., & Cowan, D. A. (2015). Ecology and biogeochemistry of cyanobacteria in soils, permafrost, aquatic and cryptic polar habitats. *Biodiversity and Conservation*, *24*, 819-840.
- Margulis, L. (1971). Symbiosis and evolution. *Scientific American*, *225*(2), 48-61.
- Martin, W., & Russell, M. J. (2003). On the origin of cells: An hypothesis for the evolutionary transitions from abiotic geochemistry to chemoautotrophic prokaryotes, and from prokaryotes to nucleated cells. *Philosophical Transactions of the Royal Society B: Biological Sciences*, 358(1429), 59–85.
- Marulanda Valencia, W., Pandit, A., 2024. Photosystem II Subunit S (PsbS): A Nano Regulator of Plant Photosynthesis. J. Mol. Biol. 436, 168407.

- Mascoli, V., Bersanini, L., & Croce, R. (2020). Far-red absorption and light-use efficiency trade-offs in chlorophyll f photosynthesis. *Nature plants*, *6*(8), 1044-1053.
- Mathis, P. (1990). Compared structure of plant and bacterial photosynthetic reaction centers. Evolutionary implications. *Biochimica et Biophysica Acta (BBA)-Bioenergetics*, *1018*(2-3), 163-167.
- McGrath, C. (2020b). Highlight: the colorful history of Plastids. *Genome Biology and Evolution*, *12*(7), 991–992.
- Medina, M., Collins, A. G., Taylor, J. W., Valentine, J. W., Lipps, J. H., Amaral-Zettler, L., & Sogin, M. L. (2003). Phylogeny of Opisthokonta and the evolution of multicellularity and complexity in Fungi and Metazoa. *International Journal of Astrobiology*, *2*(3), 203-211.
- Miloslavina, Y., De Bianchi, S., Dall'Osto, L., Bassi, R., Holzwarth, A.R., 2011. Quenching in Arabidopsis thaliana mutants lacking monomeric antenna proteins of photosystem II. J. Biol. Chem. 286, 36830–36840. Minagawa, J. (2011). State transitions—the molecular remodeling of photosynthetic supercomplexes that controls energy flow in the chloroplast. *Biochimica et Biophysica Acta (BBA)-Bioenergetics*, *1807*(8), 897-905.
- Mohamed, H. E., Van De Meene, A. M. L., Roberson, R. W., & Vermaas, W. F. J. (2005). Myxoxanthophyll Is Required for Normal Cell Wall Structure and Thylakoid Organization in the Cyanobacterium Synechocystis sp. Strain PCC 6803. *Journal of Bacteriology*, *187*(20), 6883–6892.
- Moore, R. B., Oborník, M., Janouškovec, J., Chrudimský, T., Vancová, M., Green, D. H., Wright, S. W., Davies, N. W., Bolch, C. J. S., Heimann, K., Šlapeta, J., Hoegh-Guldberg, O., Logsdon, J. M., & Carter, D. A. (2008). A photosynthetic alveolate closely related to apicomplexan parasites. *Nature*, *451*(7181), 959–963.
- Moreira, D., & López-García, P. (2002). The molecular ecology of microbial eukaryotes unveils a hidden world. TRENDS in Microbiology, 10(1), 31-38.
- Morosinotto, T., Mozzo, M., Bassi, R., & Croce, R. (2005). Pigment-Pigment Interactions in Lhca4 Antenna Complex of Higher Plants Photosystem I. Journal of Biological Chemistry, 280(21), 20612–20619.
- Mouget, J., Rosa, P., & Tremblin, G. (2004). Acclimation of Haslea ostrearia to light of different spectral qualities – confirmation of `chromatic adaptation' in diatoms. *Journal of Photochemistry and Photobiology B Biology*, *75*(1–2), 1–11.

- Mulkidjanian, A. Y., Koonin, E. V., Makarova, K. S., Mekhedov, S. L., Sorokin, A., Wolf, Y. I., ... & Galperin, M. Y. (2006). The cyanobacterial genome core and the origin of photosynthesis. *Proceedings of the National Academy of Sciences*, *103*(35), 13126-13131.
- Mullineaux, C. W. (2008). Phycobilisome-reaction centre interaction in cyanobacteria. *Photosynthesis research*, *95*, 175-182.
- Mullineaux, C. W. (2014). Electron transport and light-harvesting switches in cyanobacteria. *Frontiers in plant science*, *5*, 7.
- Mullineaux, C. W., & Emlyn-Jones, D. (2005). State transitions: an example of acclimation to low-light stress. *Journal of experimental botany*, *56*(411), 389-393.
- Nagao, R., Ogawa, H., Suzuki, T., Dohmae, N., Kato, K., Nakajima, Y., & Shen, J. (2025). Biochemical evidence for the diversity of LHCI proteins in PSI-LHCI from the red alga Galdieria sulphuraria NIES-3638. *Photosynthesis Research*, *163*(1).
- Nagao, R., Ueno, Y., Furutani, M., Kato, K., Shen, J., & Akimoto, S. (2023). Biochemical and spectroscopic characterization of PSI-LHCI from the red alga Cyanidium caldarium. *Photosynthesis Research*, *156*(3), 315–323.
- Nagao, R., Yokono, M., Kato, K.H., Ueno, Y., Shen, J.R., Akimoto, S., 2021. High-light modification of excitation-energy-relaxation processes in the green flagellate Euglena gracilis. Photosynth. Res. 149, 303–311.
- Naschberger, A., Mosebach, L., Tobiasson, V., Kuhlgert, S., Scholz, M., Perez-Boerema, A., Ho, T.T.H., Vidal-Meireles, A., Takahashi, Y., Hippler, M., Amunts, A., 2022. Algal photosystem I dimer and high-resolution model of PSI-plastocyanin complex. Nat. Plants 8, 1191–1201.
- Neilson, J.A.D., Rangsrikitphoti, P., Durnford, D.G., 2017. Evolution and regulation of Bigelowiella natans light-harvesting antenna system. J. Plant Physiol. 217, 68–76.
- Nelson, N., & Junge, W. (2015). Structure and energy transfer in photosystems of oxygenic photosynthesis. *Annual review of biochemistry*, *84*(1), 659-683.
- Nelson, N., & Yocum, C. F. (2006). Structure and function of photosystems I and II. *Annu. Rev. Plant Biol.*, *57*(1), 521-565.
- Nikolaev, S. I., Berney, C., Fahrni, J. F., Bolivar, I., Polet, S., Mylnikov, A. P., ... & Pawlowski, J. (2004). The twilight of Heliozoa and rise of Rhizaria, an emerging supergroup of amoeboid eukaryotes. *Proceedings of the National Academy of Sciences*, *101*(21), 8066-8071.

- Nishihara, A., Tsukatani, Y., Azai, C., & Nobu, M. K. (2024). Illuminating the coevolution of photosynthesis and Bacteria. *Proceedings of the National Academy of Sciences*, *121*(25), e2322120121.
- Niyogi, K. K., & Truong, T. B. (2013). Evolution of flexible non-photochemical quenching mechanisms that regulate light harvesting in oxygenic photosynthesis. *Current opinion in plant biology*, *16*(3), 307-314.
- Niyogi, K. K., Grossman, A. R., & Björkman, O. (1998). Arabidopsis mutants define a central role for the xanthophyll cycle in the regulation of photosynthetic energy conversion. *The plant cell*, *10*(7), 1121-1134.
- Nürnberg, D. J., Morton, J., Santabarbara, S., Telfer, A., Joliot, P., Antonaru, L. A., Ruban, A. V., Cardona, T., Krausz, E., Boussac, A., Fantuzzi, A., & Rutherford, A. W. (2018). Photochemistry beyond the red limit in chlorophyll f–containing photosystems. *Science*, *360*(6394), 1210–1213.
- Oba, T., Mimuro, M., Wang, Z., Nozawa, T., Yoshida, S., & Watanabe, T. (1997). Spectral Characteristics and Colloidal Properties of Chlorophyll a‘ in Aqueous Methanol. *The Journal of Physical Chemistry B*, *101*(16), 3261–3268.
- Oborník, M., & Lukeš, J. (2015). The organellar genomes of Chromera and vitrella, the phototrophic relatives of apicomplexan parasites. *Annual Review of Microbiology*, *69*(1), 129–144.
- Oborník, M., Modrý, D., Lukeš, M., Černotíková-Stříbrná, E., Cihlář, J., Tesařová, M., Kotabová, E., Vancová, M., Prášil, O., & Lukeš, J. (2012). Morphology, Ultrastructure and Life Cycle of Vitrella brassicaformis n. sp., n. gen., a Novel Chromerid from the Great Barrier Reef. *Protist*, *163*(2), 306–323.
- Olsen, M. T., Nowack, S., Wood, J. M., Becraft, E. D., LaButti, K., Lipzen, A., Martin, J., Schackwitz, W. S., Rusch, D. B., Cohan, F. M., Bryant, D. A., & Ward, D. M. (2015). The molecular dimension of microbial species: 3. Comparative genomics of Synechococcus strains with different light responses and in situ diel transcription patterns of associated putative ecotypes in the Mushroom Spring microbial mat. *Frontiers in Microbiology*, *6*.
- Olson, J. M., & Pierson, B. K. (1987). Origin and evolution of photosynthetic reaction centers. *Origins of life and evolution of the biosphere*, *17*, 419-430.
- Ott, T., Clarke, J., Birks, K., & Johnson, G. (1999). Regulation of the photosynthetic electron transport chain. *Planta*, *209*, 250-258.

- Ozawa, S.I., Bald, T., Onishi, T., Xue, H., Matsumura, T., Kubo, R., Takahashi, H., Hippler, M., Takahashi, Y., 2018. Configuration of ten light-harvesting chlorophyll a/b complex i subunits in chlamydomonas reinhardtii photosystem I. Plant Physiol. 178, 583–595.
- Palombi, L., Cecchi, G., Lognoli, D., Raimondi, V., Toci, G., & Agati, G. (2011). A retrieval algorithm to evaluate the Photosystem I and Photosystem II spectral contributions to leaf chlorophyll fluorescence at physiological temperatures. *Photosynthesis research*, *108*, 225-239.
- Pålsson, L. O., Flemming, C., Gobets, B., Van Grondelle, R., Dekker, J. P., & Schlodder, E. (1998). Energy Transfer and Charge Separation in Photosystem I: P700 Oxidation Upon Selective Excitation of the Long-Wavelength Antenna Chlorophylls of Synechococcus elongatus. Biophysical Journal, 74(5), 2611–2622.
- Pan, X., Cao, P., Su, X., Liu, Z., Li, M., 2020. Structural analysis and comparison of light-harvesting complexes I and II. Biochim. Biophys. Acta - Bioenerg. 1861, 148038.
- Pan, X., Tokutsu, R., Li, A., Takizawa, K., Song, C., Murata, K., Yamasaki, T., Liu, Z., Minagawa, J., Li, M., 2021. Structural basis of LhcbM5-mediated state transitions in green algae. Nat. Plants 7, 1119–1131.
- Pancaldi, S., Baldisserotto, C., Ferroni, L., Bonora, A., Fasulo, M.P., 2002. Room temperature microspectrofluorimetry as a useful tool for studying the assembly of the PSII chlorophyll-protein complexes in single living cells of etiolated Euglena gracilis Klebs during the greening process. J. Exp. Bot. 53, 1753–1763.
- Parfrey, L. W., Lahr, D. J., Knoll, A. H., & Katz, L. A. (2011). Estimating the timing of early eukaryotic diversification with multigene molecular clocks. *Proceedings of the National Academy of Sciences*, *108*(33), 13624-13629.
- Peers, G., Truong, T.B., Ostendorf, E., Busch, A., Elrad, D., Grossman, A.R., Hippler, M., Niyogi, K.K., 2009. An ancient light-harvesting protein is critical for the regulation of algal photosynthesis. Nature 462, 518–521.
- Perez-Boerema, A., Klaiman, D., Caspy, I., Netzer-El, S.Y., Amunts, A., Nelson, N., 2020. Structure of a minimal photosystem I from the green alga Dunaliella salina. Nat. Plants 6, 321–327.
- Pesaresi, P., Hertle, A., Pribil, M., Schneider, A., Kleine, T., & Leister, D. (2010). Optimizing photosynthesis under fluctuating light: the role of the Arabidopsis STN7 kinase. *Plant signaling & behavior*, *5*(1), 21-25.
- Pettai, H., Oja, V., Freiberg, A., & Laisk, A. (2005). The long-wavelength limit of plant photosynthesis. FEBS Letters, 579(18), 4017–4019.

- Pinevich, A. V., & Averina, S. G. (2022). On the Edge of the Rainbow: Red-Shifted Chlorophylls and Far-Red Light Photoadaptation in Cyanobacteria. *Microbiology*, *91*(6), 631–648.
- Qin, X., Pi, X., Wang, W., Han, G., Zhu, L., Liu, M., Cheng, L., Shen, J.R., Kuang, T., Sui, S.F., 2019. Structure of a green algal photosystem I in complex with a large number of light-harvesting complex I subunits. Nat. Plants 5, 263–272.
- Ramírez-Reinat, E. L., & Garcia-Pichel, F. (2012). CHARACTERIZATION OF A MARINE CYANOBACTERIUM THAT BORES INTO CARBONATES AND THE REDESCRIPTION OF THE GENUS MASTIGOCOLEUS1. *Journal of Phycology*, *48*(3), 740–749.
- Raps, S., Wyman, K., Siegelman, H. W., & Falkowski, P. G. (1983). Adaptation of the Cyanobacterium Microcystis aeruginosa to Light Intensity. *PLANT PHYSIOLOGY*, *72*(3), 829–832.
- Raven, J. A., & Geider, R. J. (2003). Adaptation, acclimation and regulation in algal photosynthesis. In *Photosynthesis in algae* (pp. 385-412). Dordrecht: Springer Netherlands.
- Raven, J. A., & Sánchez-Baracaldo, P. (2021). Gloeobacter and the implications of a freshwater origin of Cyanobacteria. *Phycologia*, *60*(5), 402-418.
- Raven, P. H., Singer, S. R., Johnson, G. B., Mason, K. A., & Losos, J. B. (2017). *Biologie*. De Boeck supérieur.
- Raymond, J., & Blankenship, R. E. (2008). The origin of the oxygen-evolving complex. *Coordination chemistry reviews*, *252*(3-4), 377-383.
- Raymond, J., & Segrè, D. (2006). The effect of oxygen on biochemical networks and the evolution of complex life. *Science*, *311*(5768), 1764-1767.
- Redfield, R., & Radin, P. (1954). The primitive world and its transformations. *Ethics*, *64*(3).
- Reyes-Prieto, A., Weber, A. P., & Bhattacharya, D. (2007). The origin and establishment of the plastid in algae and plants. *Annu. Rev. Genet.*, *41*(1), 147-168.
- Rippka, R., Deruelles, J., Waterbury, J. B., Herdman, M., & Stanier, R. Y. (1979). Generic assignments, strain histories and properties of pure cultures of cyanobacteria. *Microbiology*, *111*(1), 1-61.
- Roberta Croce,*y Agnieszka Chojnicka,z Tomas Morosinotto,§ Janne A. Ihalainen,{ Frank van Mourik,k Jan P. Dekker,§ Roberto Bassi,§k and Rienk van Grondellez (2007) The Low-Energy Forms of Photosystem I Light-Harvesting Complexes: Spectroscopic Properties and Pigment-Pigment Interaction Characteristics Biophysical Journal Volume 93 October 2007 2418–2428

- Rochaix, J. D. (2011). Regulation of photosynthetic electron transport. *Biochimica et Biophysica Acta (BBA)-Bioenergetics*, *1807*(3), 375-383.
- Rochaix, J. D. (2014). Regulation and dynamics of the light-harvesting system. *Annual review of plant biology*, *65*(1), 287-309.
- Rockwell, N. C., Lagarias, J. C., & Bhattacharya, D. (2014). Primary endosymbiosis and the evolution of light and oxygen sensing in photosynthetic eukaryotes. *Frontiers in ecology and evolution*, *2*, 66.
- Rodríguez-Bolaños, M., Vargas-Romero, G., Jaguer-García, G., Aguilar-Gonzalez, Z.I., Lagos-Romero, V., Miranda-Astudillo, H. V., 2024. Antares I: a Modular Photobioreactor Suitable for Photosynthesis and Bioenergetics Research. Appl. Biochem. Biotechnol. 196, 2176–2195.
- Rodríguez-Ezpeleta, N., Brinkmann, H., Burey, S. C., Roure, B., Burger, G., Löffelhardt, W., ... & Lang, B. F. (2005). Monophyly of primary photosynthetic eukaryotes: green plants, red algae, and glaucophytes. *Current biology*, *15*(14), 1325-1330.
- Rojdestvenski, I., Ivanov, A.G., Cottam, M.G., Borodich, A., Huner, N.P.A., Öquist, G., 2002. Segregation of photosystems in thylakoid membranes as a critical phenomenon. Biophys. J. 82, 1719–1730.
- Romero, E., Mozzo, M., Van Stokkum, I. H., Dekker, J. P., Van Grondelle, R., & Croce, R. (2009). The Origin of the Low-Energy Form of Photosystem I Light-Harvesting Complex Lhca4: Mixing of the Lowest Exciton with a Charge-Transfer State. Biophysical Journal, 96(5), L35–L37.
- Sánchez-Baracaldo, P., Bianchini, G., Wilson, J. D., & Knoll, A. H. (2021). Cyanobacteria and biogeochemical cycles through Earth history. *Trends in Microbiology*, *30*(2), 143–157.
- Sánchez-Baracaldo, P., Raven, J. A., Pisani, D., & Knoll, A. H. (2017). Early photosynthetic eukaryotes inhabited low-salinity habitats. *Proceedings of the National Academy of Sciences*, *114*(37), E7737-E7745.
- Sanfilippo, J. E., Garczarek, L., Partensky, F., & Kehoe, D. M. (2019). Chromatic acclimation in cyanobacteria: a diverse and widespread process for optimizing photosynthesis. *Annual review of microbiology*, *73*(1), 407-433.
- Santos, L. M. A. (1996). The Eustigmatophyceae: actual knowledge and research perspectives. *Nova Hedwigia Beiheft*, *112*, 391-406.
- Sato, H., Mizoi, J., Shinozaki, K., & Yamaguchi-Shinozaki, K. (2024). Complex plant responses to drought and heat stress under climate change. *The Plant Journal*, *117*(6), 1873-1892.

- Schaller-Laudel, S., Volke, D., Redlich, M., Kansy, M., Hoffmann, R., Wilhelm, C., & Goss, R. (2015). The diadinoxanthin diatoxanthin cycle induces structural rearrangements of the isolated FCP antenna complexes of the pennate diatom Phaeodactylum tricornutum. *Plant Physiology and Biochemistry*, *96*, 364-376.
- Scheer, H. (1991). Photochemistry and photophysics of biliprotein chromophores: a case of molecular ecology. In *Photobiology: the science and its applications* (pp. 491-495). Boston, MA: Springer US.
- Scheer, H. (2006). An overview of chlorophylls and bacteriochlorophylls: biochemistry, biophysics, functions and applications. In *Springer eBooks* (pp. 1–26).
- Scheller, H.V., Jensen, P.E., Haldrup, A., Lunde, C., Knoetzel, J., 2001. Role of subunits in eukaryotic Photosystem I. Biochim. Biophys. Acta - Bioenerg. 1507, 41–60.
- Schiphorst, C., & Bassi, R. (2020). Chlorophyll-xanthophyll antenna complexes: in between light harvesting and energy dissipation. *Photosynthesis in algae: biochemical and physiological mechanisms*, 27-55.
- Schlodder, E., Lendzian, F., Meyer, J., Çetin, M., Brecht, M., Renger, T., & Karapetyan, N. V. (2014). Long-Wavelength Limit of Photochemical Energy Conversion in Photosystem I. Journal of the American Chemical Society, 136(10), 3904–3918.
- Schmitt, F. J., Renger, G., Friedrich, T., Kreslavski, V. D., Zharmukhamedov, S. K., Los, D. A., ... & Allakhverdiev, S. I. (2014). Reactive oxygen species: re-evaluation of generation, monitoring and role in stress-signaling in phototrophic organisms. *Biochimica et Biophysica Acta (BBA)-Bioenergetics*, *1837*(6), 835-848.
- Şener, M. K., & Schulten, K. (2005). PHYSICAL PRINCIPLES OF EFFICIENT EXCITATION TRANSFER IN LIGHT HARVESTING. In *WORLD SCIENTIFIC eBooks* (pp. 1–26).
- Şener, M., Strümpfer, J., Hsin, J., Chandler, D., Scheuring, S., Hunter, C. N., & Schulten, K. (2011). Förster Energy transfer Theory as reflected in the structures of photosynthetic Light-Harvesting systems. *ChemPhysChem*, *12*(3), 518–531.
- Shalygin, S., Huang, I., Allen, E. H., Burkholder, J. M., & Zimba, P. V. (2019). Odorella benthonica gen. & sp. nov. (Pleurocapsales, Cyanobacteria): an odor and prolific toxin producer isolated from a California aqueduct. *Journal of Phycology*, *55*(3), 509–520.
- Sharma, S., Jaiswal, T., & Singh, S. S. (2024). Photosynthetic Organisms in Extreme Environments. In *Stress Biology in Photosynthetic Organisms: Molecular Insights and Cellular Responses* (pp. 213-248). Singapore: Springer Nature Singapore.

- Shen, L., Huang, Z., Chang, S., Wang, W., Wang, J., Kuang, T., Han, G., Shen, J.R., Zhang, X., 2019. Structure of a C2S2M2N2-type PSII–LHCII supercomplex from the green alga Chlamydomonas reinhardtii. Proc. Natl. Acad. Sci. U. S. A. 116, 21246–21255.
- Sheng, X., Watanabe, A., Li, A., Kim, E., Song, C., Murata, K., Song, D., Minagawa, J., Liu, Z., 2019. Structural insight into light harvesting for photosystem II in green algae. Nat. Plants 5, 1320–1330.
- Shestakov, S. V., & Karbysheva, E. A. (2017). The origin and evolution of cyanobacteria. *Biology Bulletin Reviews*, *7*, 259-272.
- Shubin, V. V, Bezsmertnaya, I.N., Karapetyan, N. V., 1992. Isolation from Spirulina membranes of two photosystem I-type complexes, one of which contains chlorophyll responsible for the 77 K fluorescence band at 760 nm. FEBS J. 309, 340–342.
- Sibbald, S. J., & Archibald, J. M. (2020). Genomic insights into plastid evolution. *Genome biology and evolution*, *12*(7), 978-990.
- Six, C., Worden, A.Z., Rodríguez, F., Moreau, H., Partensky, F., 2005. New insights into the nature and phylogeny of prasinophyte antenna proteins: Ostreococcus tauri, a case study. Mol. Biol. Evol. 22, 2217–2230.
- Smirnov, A. V., Chao, E., Nassonova, E. S., & Cavalier-Smith, T. (2011). A revised classification of naked lobose amoebae (Amoebozoa: Lobosa). *Protist*, *162*(4), 545-570.
- Smith, H. (1994). Sensing the light environment: the functions of the phytochrome family. In *Photomorphogenesis in plants* (pp. 377-416). Dordrecht: Springer Netherlands.
- Sobotka, R., Esson, H.J., Koník, P., Trsková, E., Moravcová, L., Horák, A., Dufková, P., Oborník, M., 2017. Extensive gain and loss of photosystem i subunits in chromerid algae, photosynthetic relatives of apicomplexans. Sci. Rep. 7, 1–13.
- Sonoike, K., 1995. Selective photoinhibition of photosystem I in isolated thylakoid membranes from cucumber and spinach. Plant Cell Physiol. 36, 825–830.
- Soulier, N., Laremore, T. N., & Bryant, D. A. (2020). Characterization of cyanobacterial allophycocyanins absorbing far-red light. *Photosynthesis Research*, *145*(3), 189–207.
- Soulier, N., Walters, K., Laremore, T. N., Shen, G., Golbeck, J. H., & Bryant, D. A. (2022). Acclimation of the photosynthetic apparatus to low light in a thermophilic Synechococcus sp. strain. *Photosynthesis Research*, *153*(1–2), 21–42.
- Stal, L. J. (2007). Cyanobacteria: diversity and versatility, clues to life in extreme environments. In *Algae and cyanobacteria in extreme environments* (pp. 659-680). Dordrecht: Springer Netherlands.

- Stamatakis, K., Tsimilli-Michael, M., & Papageorgiou, G. C. (2014). On the question of the light-harvesting role of β-carotene in photosystem II and photosystem I core complexes. *Plant Physiology and Biochemistry*, *81*, 121–127.
- Stanier, R. Y., Sistrom, W. R., Hansen, T. A., Whitton, B. A., Castenholz, R. W., Pfennig, N., ... & Trüper, H. G. (1978). Proposal to place the nomenclature of the cyanobacteria (blue-green algae) under the rules of the International Code of Nomenclature of Bacteria. *International Journal of Systematic and Evolutionary Microbiology*, *28*(2), 335-336.
- Stirbet, A., Lazár, D., Guo, Y., & Govindjee, G. (2020). Photosynthesis: basics, history and modelling. *Annals of botany*, *126*(4), 511-537.
- Straus, N. A. (1994). Iron Deprivation: Physiology and Gene Regulation. In *Springer eBooks* (pp. 731–750).
- Strunecký, O., Ivanova, A. P., & Mareš, J. (2023). An updated classification of cyanobacterial orders and families based on phylogenomic and polyphasic analysis. *Journal of Phycology*, *59*(1), 12-51.
- Suzuki, T., Tada, O., Makimura, M., Tohri, A., Ohta, H., Yamamoto, Y., Enami, I., 2004. Isolation and Characterization of Oxygen-Evolving Photosystem II Complexes Retaining the PsbO , P and Q Proteins from Euglena gracilis. Plant Cell Physiol. 45, 1168–1175.
- Swingley, W.D., Iwai, M., Chen, Y., Ozawa, S. ichiro, Takizawa, K., Takahashi, Y., Minagawa, J., 2010. Characterization of photosystem I antenna proteins in the prasinophyte Ostreococcus tauri. Biochim. Biophys. Acta - Bioenerg. 1797, 1458–1464. Tanabe, Y., Shitara, T., Kashino, Y., Hara, Y., & Kudoh, S. (2011). Utilizing the effective xanthophyll cycle for blooming of Ochromonas smithii and O. itoi (Chrysophyceae) on the snow surface. *PloS one*, *6*(2), e14690.
- Tanaka, R., Tanaka, A., 2011. Chlorophyll cycle regulates the construction and destruction of the light-harvesting complexes. Biochim. Biophys. Acta - Bioenerg. 1807, 968–976.
- Tandeau de Marsac, N. (1977). Occurrence and nature of chromatic adaptation in cyanobacteria. *Journal of bacteriology*, *130*(1), 82-91.
- Thapper, A., Mamedov, F., Mokvist, F., HammarströM, L., & Styring, S. (2009). Defining the Far-Red Limit of Photosystem II in Spinach. The Plant Cell, 21(8), 2391–2401.
- Tian, L., Liu, Z., Wang, F., Shen, L., Chen, J., Chang, L., Zhao, S., Han, G., Wang, W., Kuang, T., Qin, X., Shen, J.R., 2017. Isolation and characterization of PSI–LHCI super-complex and their sub-complexes from a red alga Cyanidioschyzon merolae. Photosynth.

Res. 133, 201–214. Tice, M. & Lowe, D. Photosynthetic microbial mats in the 3,416-Myr-old ocean.(2004). *Nature* **431**, 549–552

- Tikkanen, M., Grieco, M., & Aro, E. M. (2011). Novel insights into plant light-harvesting complex II phosphorylation and 'state transitions'. *Trends in plant science*, *16*(3), 126-131.
- Tokutsu, R., Iwai, M., Minagawa, J., 2009. CP29, a monomeric light-harvesting complex II protein, is essential for state transitions in Chlamydomonas reinhardtii. J. Biol. Chem. 284, 7777–7782.
- Trinugroho, J. P., Bečková, M., Shao, S., Yu, J., Zhao, Z., Murray, J. W., Sobotka, R., Komenda, J., & Nixon, P. J. (2020b). Chlorophyll f synthesis by a super-rogue photosystem II complex. *Nature Plants*, *6*(3), 238–244.
- Tsuji, Y., & Yoshida, M. (2017). Biology of haptophytes: complicated cellular processes driving the global carbon cycle. In *Advances in botanical research* (Vol. 84, pp. 219-261). Academic Press.
- Umena, Y., Kawakami, K., Shen, J., & Kamiya, N. (2011). Crystal structure of oxygen-evolving photosystem II at a resolution of 1.9 Å. *Nature*, *473*(7345), 55–60.
- Umetani, I., Kunugi, M., Yokono, M., Takabayashi, A., & Tanaka, A. (2017). Evidence of the supercomplex organization of photosystem II and light-harvesting complexes in Nannochloropsis granulata. *Photosynthesis Research*, *136*(1), 49–61.
- Vajravel, S., Kis, M., Kłodawska, K., Laczko-Dobos, H., Malec, P., Kovács, L., Gombos, Z., & Toth, T. N. (2017). Zeaxanthin and echinenone modify the structure of photosystem I trimer in Synechocystis sp. PCC 6803. *Biochimica Et Biophysica Acta (BBA) - Bioenergetics*, *1858*(7), 510–518.
- Veseli, I., Chen, Y. T., Schechter, M. S., Vanni, C., Fogarty, E. C., Watson, A. R., Jabri, B., Blekhman, R., Willis, A. D., Yu, M. K., Fernàndez-Guerra, A., Füssel, J., & Eren, A. M. (2024). Microbes with higher metabolic independence are enriched in human gut microbiomes under stress. *eLife* 12:RP89862.
- Virtanen, O., Tyystjärvi, E., 2023. Plastoquinone pool redox state and control of state transitions in Chlamydomonas reinhardtii in darkness and under illumination. Photosynth. Res. 155, 59–76.
- Waller, R. F., & McFadden, G. I. (2005). The apicoplast: a review of the derived plastid of apicomplexan parasites. *Current issues in molecular biology*, *7*(1), 57-80.
- Warner, M. E., & Berry-Lowe, S. (2006). Differential xanthophyll cycling and photochemical activity in symbiotic dinoflagellates in multiple locations of three species of Caribbean coral. *Journal of experimental marine biology and ecology*, *339*(1), 86-95.

- Waterbury, J. B., & Stanier, R. Y. (1978). Patterns of growth and development in pleurocapsalean cyanobacteria. *Microbiological reviews*, *42*(1), 2-44.
- Wientjes, E., Roest, G., & Croce, R. (2012). From red to blue to far-red in Lhca4: How does the protein modulate the spectral properties of the pigments? Biochimica Et Biophysica Acta (BBA) - Bioenergetics, 1817(5), 711–717.
- Wilhelm, C., & Jakob, T. (2006). Uphill energy transfer from long-wavelength absorbing chlorophylls to PS II in Ostreobium sp. is functional in carbon assimilation. Photosynthesis Research, 87(3).
- Wilson, D. J., Froning, C. S., Duvvuri, G. M., France, K., Youngblood, A., Schneider, P. C., Berta-Thompson, Z., Brown, A., Buccino, A. P., Hawley, S., Irwin, J., Kaltenegger, L., Kowalski, A., Linsky, J., Loyd, R. O. P., Miguel, Y., Pineda, J. S., Redfield, S., Roberge, A., . . . Vieytes, M. (2021). The Mega-MUSCLES Spectral energy distribution of TRAPPIST-1. *The Astrophysical Journal*, *911*(1), 18.
- Wilson, K. E., & Huner, N. P. A. (2000). The role of growth rate, redox-state of the plastoquinone pool and the trans-thylakoid ΔpH in photoacclimation of Chlorella vulgaris to growth irradiance and temperature. *Planta*, *212*(1), 93–102.
- Winter, J., Brandt, P., 1986. Stage-Specific State I-State II Transitions during the Cell Cycle of Euglena gracilis . Plant Physiol. 81, 548–552.
- Wittig, I., Karas, M., & Schägger, H. (2007). High Resolution Clear Native Electrophoresis for In-gel Functional Assays and Fluorescence Studies of Membrane Protein Complexes. *Molecular & Cellular Proteomics*, *6*(7), 1215–1225.
- Wolf, B. M., & Blankenship, R. E. (2019). Far-red light acclimation in diverse oxygenic photosynthetic organisms. *Photosynthesis research*, *142*(3), 349-359.
- Wolf, B. M., Niedzwiedzki, D. M., Magdaong, N. C. M., Roth, R., Goodenough, U., & Blankenship, R. E. (2017). Characterization of a newly isolated freshwater Eustigmatophyte alga capable of utilizing far-red light as its sole light source. Photosynthesis Research, 135(1–3), 177–189.
- Xiong, J., & Bauer, C. E. (2002). Complex evolution of photosynthesis. *Annual Review of Plant Biology*, *53*(1), 503–521.
- Xu, C., Pi, X., Huang, Y., Han, G., Chen, X., Qin, X., Huang, G., Zhao, S., Yang, Y., Kuang, T., Wang, W., Sui, S.F., Shen, J.R., 2020. Structural basis for energy transfer in a huge diatom PSI-FCPI supercomplex. Nat. Commun. 11, 1–12.

- Xue, Y., Ma, J., He, Y., Yu, S., Lin, Z., Xiong, Y., Rafique, F., Jiang, F., Sun, L., Ma, M., Zhou, Y., Li, X., & Huang, Z. (2019). Comparative transcriptomic and proteomic analyses of the green and white parts of chimeric leaves in Ananas comosus var. bracteatus. *PeerJ*, *7*, e7261.
- Yadav, K.N.S., Miranda-Astudillo, H. V., Colina-Tenorio, L., Bouillenne, F., Degand, H., Morsomme, P., González-Halphen, D., Boekema, E.J., Cardol, P., 2017. Atypical composition and structure of the mitochondrial dimeric ATP synthase from Euglena gracilis. Biochim. Biophys. Acta - Bioenerg. 1858, 267–275. Yang, H., Liu, J., Wen, X., Lu, C., 2015. Molecular mechanism of photosystem I assembly in oxygenic organisms. Biochim. Biophys. Acta 1847, 838–848.
- Yokono, M., Akimoto, S., 2018. Energy transfer and distribution in photosystem super/megacomplexes of plants. Curr. Opin. Biotechnol. 54, 50–56.
- Yokono, M., Takabayashi, A., Akimoto, S., Tanaka, A., 2015. A megacomplex composed of both photosystem reaction centres in higher plants. Nat. Commun. 6, 6–11.
- Zhao, L.S., Wang, N., Li, K., Li, C.Y., Guo, J.P., He, F.Y., Liu, G.M., Chen, X.L., Gao, J., Liu, L.N., Zhang, Y.Z., 2024. Architecture of symbiotic dinoflagellate photosystem I–light-harvesting supercomplex in Symbiodinium. Nat. Commun. 15, 1–13.
- Zimorski, V., Rauch, C., van Hellemond, J.J., Tielens, A.G.M., Martin, W.F., 2017. The Mitochondrion of Euglena gracilis, in: Schwartzbach, S.D., Shigeoka, S. (Eds.), Euglena: Biochemistry, Cell and Molecular Biology. Springer International Publishing, Cham, pp. 19–37.

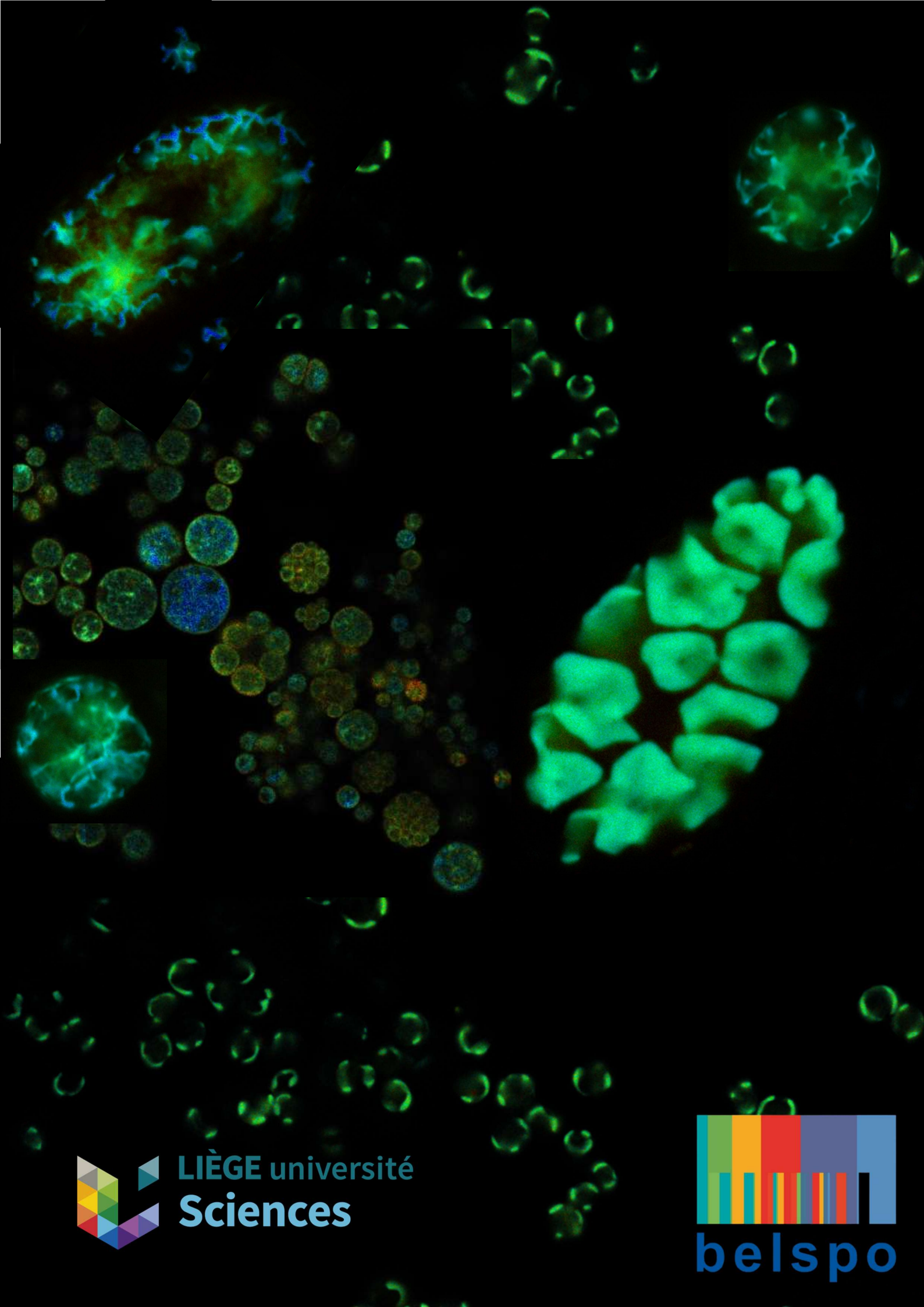

LIÈGE université
Sciences

belspo